Vapor uptake in polymer materials: Simulations and Theory

Guido Ritsema van Eck

Vapor uptake in polymer materials: Simulations and theory

Guido Cornelis Ritsema van Eck

Dutch title:
Opname van dampen in polymeermaterialen: Simulaties en theorie

Vapor uptake in polymer materials: Simulations and theory

Dissertation

to obtain
the degree of doctor at the University of Twente,
on the authority of the rector magnificus,
Prof. Dr. Ir. A. Veldkamp,
on account of the decision of the graduation committee,
to be publicly defended
on Wednesday the 12th of June 2024 at 14:45

by

Guido Cornelis Ritsema van Eck
Born on the 16th of October 1996
in Utrecht, the Netherlands

This dissertation has been approved by the promotors:

Dr. Ir. S.J.A. de Beer

and

Prof. Dr. J.H. Snoeijer

Contents

Chapter 1

Introduction*

1.1   Introduction

Polymer materials are everywhere in the modern world. They are used as packaging materials, they make up the tires of our cars and bicycles, and they are in the clothes we wear every day in the form of natural or synthetic fibers. Polymer coatings are more easily overlooked, but perhaps just as commonplace. They are often found in the form of paints, which provide aesthetics and protect the underlying surface from damage. However, polymer coatings can also be used to change the way a surface interacts with its environment. An example from daily life would be non-stick pans, which often gain their non-stick properties from a fluorinated polymer coating. Advanced polymer coatings, which can provide surfaces with a variety of useful properties, are an active topic of research. [1] In this thesis, the main class of polymer coatings we consider will be polymer brushes.

Figure 1.1: **a)**: Marine organisms growing on ships can cause environmental and economic damage. Anti-fouling brush coatings have been proposed as a solution. Image by Luis Bartolomé Marcos released under CC-BY-SA 4.0 International license **b)**: A microfluidic chip. Responsive polymer brushes can be used as a tool to control the flow of liquid through the channels on such chips. Image by FMN Laboratory, Bauman Moscow State Technical University released under CC-BY-4.0 International license.

A polymer brush is a coating in which the long, chain-like polymer molecules are all chemically bonded to the surface by one end. [2] Since the molecules in the brush are tightly crowded together, they stretch away from the surface for space, [3] and we could imagine them sticking out like the bristles of a brush. These brushes have many interesting properties with potential for technological uses. For example, a hydrophilic polymer brush can strongly bind a thin layer of water to a surface. Other surfaces can easily slide over this water layer, leading to extremely low friction. This use of polymer brushes

was inspired by the layers of hydrophilic proteins that lubricate our synovial joints. [4] A hydrated polymer brush like this also has anti-fouling properties: it prevents molecules and particles from sticking to the surface. [5–7] This is useful in a (bio)medical setting, for example, where surfaces may need to be kept clean of proteins, cells and bacteria. [8] Functional groups or particles with antibacterial properties can also be included in such brushes, creating surfaces that both kill bacteria and prevent dead bacteria from staying on the surface. [9, 10] Uses for anti-fouling are not just limited to the micro-scale, however: as shown in figure 1.1a, shellfish and other sea life can can grow on the hull of ships, increasing drag and reducing fuel efficiency. Brush-based anti-fouling layers are being researched to prevent this marine biofouling. [11] Moreover, polymers are responsive to small changes in their environment, such as temperature, pH, or chemical composition. [12, 13] As a result, the behavior of polymer brushes changes in response to their environment as well: they will extend further in a favorable environment, and collapse into a dense layer on the surface in an unfavorable environment. This responsiveness can be used to create so-called smart materials, whose properties can be switched from one state to another on demand. Responsive polymer brushes have been used to control adhesion and friction, [14, 15] for example by "picking up" particles in a collapsed brush, moving them, and then releasing them by changing the solvent environment to swell the brush. [16] They have also been used for opening or closing channels via the collapse or swelling of a polymer brush in "lab-on-a-chip" applications, [17, 18] microfluidic devices like shown in figure 1.1b which can be used to control and analyze chemical processes. Finally, the use of drug-loaded polymer brushes for the controlled release of medicine is being researched. [19, 20]

The applications mentioned above are mainly understood for polymer brushes in liquid environments, however. While brushes are also very promising for various uses in the gas phase, as will be described in **chapter 2**, the interaction between polymer brushes and vapors remains less studied. In this thesis, we try to develop a deeper theoretical understanding of vapor uptake in brushes to help expand their range of application. Coarse-grained molecular dynamics simulations are used as a primary tool, since they produce generalizable results and provide easy access to microscopic properties of the simulated system. Achieving our goal will first require identifying and testing an appropriate model of brush-vapor thermodynamics. This model can then be used to predict the effect of coating structure and polymer architecture on vapor swelling.

1

1.2   Overview of the Thesis

Chapter 2 extensively reviews the state of the art with respect to polymer brushes in gaseous environments. The first part of the review covers fundamental research into brushes in air, and discusses how existing models for liquid solvation might extend to the gas phase. The second half of the review provides an overview of applications for polymer brushes in air, grouped into common categories.

In **Chapter 3**, molecular dynamics simulations are used to determine whether the absorption of vapors into a polymer brush is well-described by a modified Flory-Huggins theory, which was originally used to describe the swelling of brushes in mixed solvent. Polymers are represented by a generic bead-spring model, and a Lennard-Jones gas at constant chemical potential is used as the vapor. Absorption isotherms for the vapor are compared to those predicted by the model at a range of grafting densities and interaction parameters.

In **Chapter 4**, predictions made by the aforementioned theory are tested by comparing the vapor swelling of polymer brushes to that of physisorbed coatings with the same chain length distribution and composition. The relation between brush height (as a proxy for absorption) and relative humidity is obtained both from molecular dynamics simulations and ellipsometry measurements of real coatings in water vapors.

Chapter 5 covers simulation work on polymer brushes composed of multiple, immiscible polymer species, in order to test whether interfaces between the two polymers enhance the vapor uptake relative to a single-species brush. Brushes of various copolymer architectures and mixtures of homopolymers are compared to identify optimal structures in a two-component brush.

Chapter 6 describes an investigation into Schroeder's paradox, an unusual vapor swelling effect. This apparent paradox manifests in the experimental observation that certain gels swell more in a liquid than they do in the corresponding saturated vapor, in contradiction to conventional thermodynamic predictions. Experiments and simulations are presented with the goal of finding a simple system in which the paradox occurs, and investigating its cause.

1.3 References

[1] W.-L. Chen, R. Cordero, H. Tran, and C. K. Ober, "50th anniversary perspective: Polymer brushes: Novel surfaces for future materials", Macromolecules **50**, 4089–4113 (2017), URL https://doi.org/10.1021/acs.macromol.7b00450.

[2] S. T. Milner, "Polymer brushes", Science **251**, 905–914 (1991), URL https://science.sciencemag.org/content/251/4996/905.

[3] Alexander, S., "Adsorption of chain molecules with a polar head: a scaling description", J. Phys. (Paris) **38**, 983–987 (1977), URL https://doi.org/10.1051/jphys:01977003808098300.

[4] J. Klein, "Hydration lubrication", Friction **1**, 1–23 (2013).

[5] W. Yang and F. Zhou, "Polymer brushes for antibiofouling and lubrication", Biosurface and Biotribology **3**, 97–114 (2017), URL https://www.sciencedirect.com/science/article/pii/S2405451817300181.

[6] C. Leng, H. Huang, K. Zhang, H.-C. Hung, Y. Xu, Y. Li, S. Jiang, and Z. Chen, "Effect of surface hydration on antifouling properties of mixed charged polymers", Langmuir **34**, 6538–6545 (2018).

[7] E. M. Benetti and N. D. Spencer, "Using polymers to impart lubricity and biopassivity to surfaces: Are these properties linked?", Helv. Chim. Acta **102**, e1900071 (2019), URL https://onlinelibrary.wiley.com/doi/abs/10.1002/hlca.201900071.

[8] M. Krishnamoorthy, S. Hakobyan, M. Ramstedt, and J. E. Gautrot, "Surface-initiated polymer brushes in the biomedical field: Applications in membrane science, biosensing, cell culture, regenerative medicine and antibacterial coatings", Chem. Rev. (Washington, DC, U. S.) **114**, 10976–11026 (2014), URL https://doi.org/10.1021/cr500252u, pMID: 25353708.

[9] P. Li, Z. Ding, Y. Yin, X. Yu, Y. Yuan, M. Brió Pérez, S. de Beer, G. J. Vancso, Y. Yu, and S. Zhang, "Cu2+-doping of polyanionic brushes: A facile route to prepare implant coatings with both antifouling and antibacterial properties", Eur. Polym. J. **134**, 109845 (2020), URL https://www.sciencedirect.com/science/article/pii/S0014305719326084.

1

[10] D. Mitra, E.-T. Kang, and K. G. Neoh, "Polymer-based coatings with integrated antifouling and bactericidal properties for targeted biomedical applications", ACS Appl. Polym. Mater. **3**, 2233–2263 (2021), URL `https://doi.org/10.1021/acsapm.1c00125`.

[11] C. Yoshikawa, R. Takagi, T. Nakaji-Hirabayashi, T. Ochi, Y. Kawamura, and H. Thissen, "Marine antifouling coatings based on durable bottlebrush polymers", ACS Applied Materials & Interfaces **14**, 32497–32509 (2022), URL `https://doi.org/10.1021/acsami.2c06647`, pMID: 35816694.

[12] M. Wei, Y. Gao, X. Li, and M. J. Serpe, "Stimuli-responsive polymers and their applications", Polym. Chem. **8**, 127–143 (2017), URL `http://dx.doi.org/10.1039/C6PY01585A`.

[13] D. Mukherji, C. M. Marques, and K. Kremer, "Smart responsive polymers: Fundamentals and design principles", Annu. Rev. Condens. Matter Phys. **11**, 271–299 (2020).

[14] S. Z. Moghaddam and E. Thormann, "Surface forces and friction tuned by thermo-responsive polymer films", Curr. Opin. Colloid Interface Sci. **47**, 27–45 (2020), URL `https://www.sciencedirect.com/science/article/pii/S1359029419300986`, surface Forces.

[15] Y. Yu, M. Brió Pérez, C. Cao, and S. de Beer, "Switching (bio-) adhesion and friction in liquid by stimulus responsive polymer coatings", Eur. Polym. J. **147**, 110298 (2021), URL `https://www.sciencedirect.com/science/article/pii/S001430572100032X`.

[16] Y. Yu, R. A. Lopez de la Cruz, B. D. Kieviet, H. Gojzewski, A. Pons, G. Julius Vancso, and S. de Beer, "Pick up, move and release of nanoparticles utilizing co-non-solvency of pnipam brushes", Nanoscale **9**, 1670–1675 (2017), URL `http://dx.doi.org/10.1039/C6NR09245D`.

[17] B. D. Kieviet, P. M. Schön, and G. J. Vancso, "Stimulus-responsive polymers and other functional polymer surfaces as components in glass microfluidic channels", Lab Chip **14**, 4159–4170 (2014), URL `http://dx.doi.org/10.1039/C4LC00784K`.

[18] T. H. Pial, H. S. Sachar, P. R. Desai, and S. Das, "Overscreening, co-ion-dominated electroosmosis, and electric field strength mediated flow reversal in polyelectrolyte brush functionalized nanochannels", ACS Nano **15**, 6507–6516 (2021).

[19] D. Li, L. Xu, J. Wang, and J. E. Gautrot, "Responsive polymer brush design and emerging applications for nanotheranostics", Adv. Healthcare Mater. **10**, 2000953 (2021), URL `https://onlinelibrary.wiley.com/doi/abs/10.1002/adhm.202000953`.

[20] H. Choi, A. Schulte, M. Müller, M. Park, S. Jo, and H. Schönherr, "Drug release from thermo-responsive polymer brush coatings to control bacterial colonization and biofilm growth on titanium implants", Adv. Healthcare Mater. **10**, 2100069 (2021).

Chapter 2

Fundamentals and Applications of Polymer Brushes in Air*

For several decades, high-density, end-tethered polymers, forming so-called polymer brushes, have inspired scientists to understand their properties and to translate them to applications. While earlier research focused on polymer brushes in liquids, it was recently recognized that these brushes can find application in air as well. In this review, we report on recent progress in unraveling fundamental concepts of brushes in air, such as their vapor-swelling and solvent partitioning. Moreover, we provide an overview of the plethora of applications in air (e.g. in sensing, separations or smart adhesives) where brushes can be key components. To conclude, we provide an outlook by identifying open questions and issues that, when solved, will pave the way for the large scale application of brushes in air.

2.1 Introduction

In recent years, the interaction between polymer brushes and gaseous media has become a subject of research attention. Brushes may swell, similarly to their liquid-solvated state, by capturing vapors of a favorable solvent. As a result, polymer brush functionalization can provide selectivity and enhanced responsiveness in various gas sensor designs, [1, 2] induce the formation of long-ranged superstructures by vapor-annealing brush coated particles [3] or enable the formation of perfectly smooth metal coatings. [4] The same sorption behavior has also been combined with thermoresponsive polymers to create materials with temperature-dependent water sorption, with applications in moisture capture and management. [5, 6] Moreover, previously outlined applications such as antifouling [7] and lubrication [8–10] may also be extended to surfaces in air. However, polymer brushes in air deviate qualitatively from their behavior in liquids, both at interfaces [11] and in the bulk. [12] This has given rise to new scientific questions that need answering to enable and optimize the application of polymer brushes in air.

In this chapter, we aim to provide an overview of the fundamental considerations that are relevant to polymer brush research in air, and of the steps taken towards particular applications in the last two decades. We emphasize generally relevant physical phenomena and chemical effects that are exemplary of broad classes of materials. In section 2.2, we introduce the basic concepts of polymer brush physics, then discuss how vapor sorption isotherms and vertical density profiles arise from the structure of the polymer brush. Furthermore, we qualitatively discuss the more complex mixing effects and phase separations that may occur in the case of vapor mixtures and mixed brushes. In section 2.3, we cover developments in polymer brush research specific to the fields of gas sensing, membrane separations, control of friction and adhesion, and wetting. Here, we include both experimental steps towards these applications and fundamental work of particular relevance to these applications. Finally, we discuss important open questions and issues for the large-scale applicability of brush-based technologies in section 2.4.

2.2 Fundamentals

Introduction to polymer brushes (in air)

In this section, we explain the basic properties and synthesis of polymer brushes. We describe the distinctive height scaling and solvation response of the brush,

explain the main contributions to the free energy, and outline commonly used thermodynamic descriptions of the brush, in particular for brushes in air. Polymer brushes can be composed of negatively charged anionic or positively charged cationic polyelectrolytes, [13, 14] zwitterionic polymers, [15] neutral macromolecules or copolymers containing different types of monomers. [16] Individually, surface-anchored polymers behave comparably to free polymers, assuming conformations that minimize their free energy, which consists of contributions from solvent, substrate and polymer-polymer contacts, and the conformational entropy of the chain. In the simplest case, this is a "mushroom"; a surface-anchored analogue to the coil and globule states found in free polymers. Under poor solvent conditions, however, the most favorable conformation is often a "pancake" state in which the polymer backbone adsorbs to the grafting surface. [17] When the density of polymers on the surface becomes sufficiently high, the polymers start to overlap and volume interactions cause the chains to stretch away from the surface. This structure of "bristles" extending away from the substrate gives the polymer brush its name. The transition from individual chains to a brush is frequently described in terms of the reduced tethering density: [18]

$$\Sigma = \rho_{\mathrm{g}} \pi r_{\mathrm{gyr}}^2,$$

where ρ_{g} is the number of chains per unit area, and r_{gyr} is the radius of gyration of a single grafted chain under the given conditions of solvent and temperature. Hence, Σ represents the number of chains that occupy the surface area covered by a single chain under ideal conditions. While $\Sigma < 1$ leads to non-overlapping mushrooms or pancakes by this definition, $\Sigma > 1$ does not necessarily imply a highly extended polymer brush. The point at which a grafted polymer layer starts to display the characteristic scalings of a brush appears to differ from system to system, but generally occurs for $\Sigma > 5$. [18, 19] An interesting intermediate regime occurs for brushes in the approximate $1 < \Sigma < 5$ range under poor solvent conditions. In this situation the brush may separate into inhomogeneous aggregates on the substrate, sometimes called "octopus micelles" [20], which minimize the free energy of unfavorable solvent interactions at the expense of chain stretching. Curiously, these octopus micelles can only be formed when the grafted polymers collapse rapidly; for a slow decrease in solvent quality, polymers will individually collapse into mushrooms, which can no longer aggregate once the solvent quality has decreased sufficiently to make this favorable. [21]

The methods of synthesizing polymer brushes fall into two broad categories, illustrated in Figure 2.1: grafting-from and grafting-to approaches. In grafting-

2
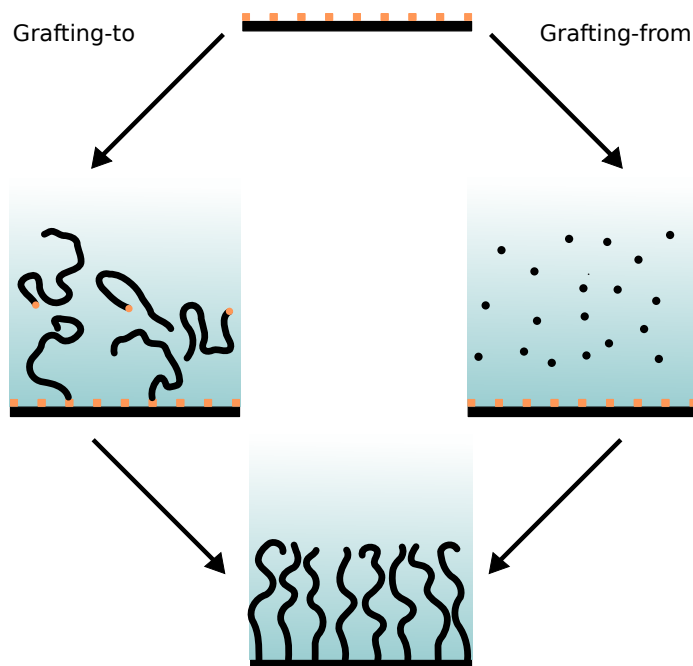
Figure 2.1: A schematic illustration of the two broad strategies for polymer brush synthesis: in grafting-to, polymer chains with reactive end groups are attached to anchoring groups (both represented in orange) at a surface from solution, whereas in grafting-from, polymerization occurs in situ from surface-bound initiators.

from procedures, the substrate is functionalized with initiator moieties and the brush is grown by in-situ polymerization, whereas in grafting-to, fully grown polymer chains are chemically or physically attached to the substrate. [22] Grafting-from typically employs controlled radical polymerization methods (e.g.

Grafting density
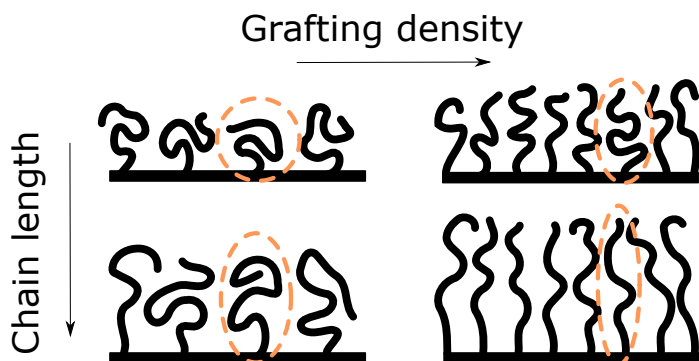
Chain length

Figure 2.2: Illustration of the effects of grafting density and chain length on polymer brush behaviour. In low-density coatings of short polymers, each chain individually takes on an energy-minimizing conformation. As the chain length and grafting density increase, excluded volume interactions cause the chains to extend.

atom transfer radical polymerization, reversible addition-fragmentation chain-transfer, or nitroxide-mediated polymerization) or ring-opening metathesis where applicable. [23, 24] While this restricts the range of available monomers and synthetic conditions, grafting-from strategies nonetheless remain highly relevant due to their ability to produce brushes with a high areal density of chains. On the other hand, the use of pre-fabricated polymers in grafting-to affords much greater control of the architecture, molecular weight and dispersity of the polymer, but steric interactions between chains strongly limit the attainable grafting density.

Polymer brushes under gaseous atmospheres tend to collapse as in poor solvents, since the low density of gases presents them with very few energetically favorable interactions. However, interesting behaviors arise when polymer brushes in air are exposed to good solvents. Solvent droplets placed on brushes may spread or partially evaporate, and conversely solvent vapors may condense in the presence of the brush. The composition of a solvated brush in air therefore depends on the concentration of the solvent vapor. To our knowledge, the first work to describe the swelling of polymer brushes by vapors was presented over two decades ago by Brochard-Wyart and De Gennes, theoretically investigating the capillary rise of a liquid against a brush-covered plate. [25] In experimental work, brush swelling by vapors is often characterized in terms of an effective interaction parameter, by imposing chemical equilibrium between the vapor and a Flory-Huggins (FH) type description of the brush. [26–30]

Notably, some of these works [26, 30] follow Birshtein and Lyatskaya [31] in modifying the FH model to account for the entropic elasticity of the polymer chains. In typical cases, the elastic contribution is small relative to enthalpic terms, as is reflected in experiments where brush swelling is independent of grafting density. [29, 32] However, it is important to include an elasticity term when describing strongly absorbing brushes in vapors near saturation, as it enforces a finite brush height, differentiating the brush from a free polymer melt in the FH description. We discuss the quantitative details of these models in section 2.2.

Isotherms

Vapor sorption is commonly described in terms of a sorption isotherm: the relation between a vapor's pressure relative to saturation (for water: the relative humidity) and the ab- or adsorption of this vapor. This is highly relevant from both theoretical and experimental perspectives, since the pressure of a vapor is an important thermodynamic quantity, as well as a typical experimental variable. In theoretical and simulation works, sorption is generally represented by the solvent volume fraction ϕ_s, whereas in experimental settings the ratio between the swollen height and the dry height of the brush, known as the swelling ratio $\frac{H}{H_0}$, is commonly used due to its ease of measurement. Assuming that the brush does not contain voids and the volume of the polymer and solvent does not change upon mixing, these quantities are related by $\phi_s = 1 - \left(\frac{H}{H_0}\right)^{-1}$. In this section, we quantitatively discuss the absorption isotherms predicted by a modified Flory-Huggins model, and compare with experimentally obtained isotherms.

The shape of the sorption isotherm is dictated by the chemical equilibrium between a bulk vapor reservoir and the solvent sorbed in the brush. Typically, the chemical potential of the bulk solvent vapor phase is assumed to be constant; experimentally, this corresponds to a large reservoir or atmosphere of solvent vapor. Since chemical equilibrium requires the absence of chemical potential gradients, this means the absorption isotherm is determined by the free energy of the solvated brush, of which the derivative w.r.t the number of absorbed solvent particles provides the chemical potential of sorbed solvent. In the extended Flory-Huggins theory by Birshtein and Lyatskaya [31] discussed in section 2.2, the free energy of the brush is given by

$$\frac{F_{\text{mix}}}{k_{\text{B}}T} = n_s \ln \phi_s + \chi n_s \phi_p + n_p \frac{3h^2}{2N}, \tag{2.1}$$

where n and ϕ are the number of particles and the volume fraction of a species, with subscripts s and p denoting solvent and polymer respectively, χ is the Flory-Huggins interaction parameter for polymer-solvent contacts, and N is the degree of polymerization for all chains. This expression deviates from the standard Flory-Huggins model in the omission of a translational entropy term for polymer chains, and the addition of the last addend, which approximates the entropic cost of brush swelling.

The chemical equilibrium condition for this modified model is stated as

$$\ln\left(\frac{P}{P_{\text{sat}}}\right) = \ln(1 - \phi_{\text{p}}) + \phi_{\text{p}} + \chi\phi_{\text{p}}^2 + \frac{3\rho_{\text{g}}^2}{\phi_{\text{p}}}, \tag{2.2}$$

with P the partial pressure of the vapor, P_{sat} the saturation pressure of the vapor, ϕ_{p} the volume fraction of polymer in the brush, and χ the Flory-Huggins interaction parameter between solvent and polymer. The left-hand side of equation 2.2 represents the chemical potential of the solvent vapor, assuming ideal gas conditions. The right-hand side, which is the derivative of equation 2.1 with respect to the amount of absorbed solvent, is the chemical potential of solvent in the brush. This defines the sorption isotherm for fixed χ and ρ_{g}. Further discussion of this model can be found in references 31 and 33. While this description was originally proposed for a brush in a one-component solvent (where the left-hand side of equation 2.2 is always zero), it is equally applicable to gaseous environments, requiring only the assumption that the brush is free of voids. Moreover, this gas-phase scenario can also be compared to a solute or minority component in a background medium that is unfavorable to both the solute and the polymer, although this requires the additional assumption that the background medium interacts equally with the solute and the polymer. This extension to the gas phase does disregard Schroeder's paradox, however. While a liquid and a saturated vapor should solvate the brush identically from a thermodynamic perspective, liquids have been experimentally found to swell polymer materials considerably more than saturated vapors. This result, known as Schroeder's paradox, was found for gelatin by Schroeder in 1903, and has recently attracted renewed attention for its relevance to polymeric membrane materials. [34, 35] However, as no conclusive thermodynamic explanation for this effect exists as of yet, this cannot be accounted for theoretically.

The isotherms described by equation 2.2 take on a concave-upward shape for positive or weakly negative values of χ, whereas strong attractive interactions (large negative χ) shift the isotherm towards a concave-downward shape. In

most experimental systems, the concave-upward shape, shown in black in Figure 2.3, is observed, [27–29, 32, 36, 37] in line with the generally positive χ parameters of real solvent-polymer systems. Although less frequently reported, the concave-downward isotherm, shown in blue in Figure 2.3 is attainable in polyelectrolytic or densely hydrogen-bonding systems in water. [29, 38] The concave-upward case is similar to the type 3 isotherm in the Brunauer-Deming-Deming-Teller (BDDT) classification, [39] in which the vapor's energy of condensation drives adsorption onto a weakly attractive substrate: for positive FH parameters, brush-solvent contacts are enthalpically unfavorable, but sorption is driven by the entropy of vapor molecules entering the volume of the brush. The enthalpic cost per vapor molecule only decreases as the solvent fraction increases, leading to the upward curvature of the isotherm. The concave-downward form of the isotherm loosely resembles the Langmuir (BDDT type 1) isotherm in the sense that sorption is enthalpically driven and limited by the sorption capacity of the substrate, but these limits are different in origin.

Experimental isotherms may display additional features when this lattice model does not fully capture the free energy of the system, however. For instance, the assumption that brush swelling is linearly related to solvent uptake does not always apply to real systems, since polymeric materials often contain free volume that may be filled by solvent. [36, 40] This effect is most pronounced in materials below their glass transition temperature [36] and in "stiff" polymers, i.e. polymers with large persistence lengths [41]. Sorption by void-filling leads to increased solvent uptake at low pressures when compared to the Flory-Huggins-based isotherm, and Laschitsch et al. suggest that the transition from void-filling to a Flory-Huggins regime may be associated with a solvent-induced glass transition. [36] Single-stranded DNA (ssDNA) brushes in water vapor may even collapse with increasing relative humidity. This effect was first described by Wagman et al. in terms of a lattice model incorporating void sites, and later by Zhao et al. based on hydrogen bonding between sorbed water and the ssDNA strands. [12, 42]

A related effect was observed by Galvin et al. in a neutron reflectivity (NR) study of polyelectrolyte brushes: [28] a brush containing zwitterionic sulfobe-taine side groups displayed different sorption behavior in humid air depending on its grafting density, with Flory-Huggins type behavior at moderate grafting densities, but unexpectedly low solvent uptake at both low and high grafting densities (see Figure 2.4). This was attributed to the collapse of the brush by formation of side group complexes within chains at low grafting densities
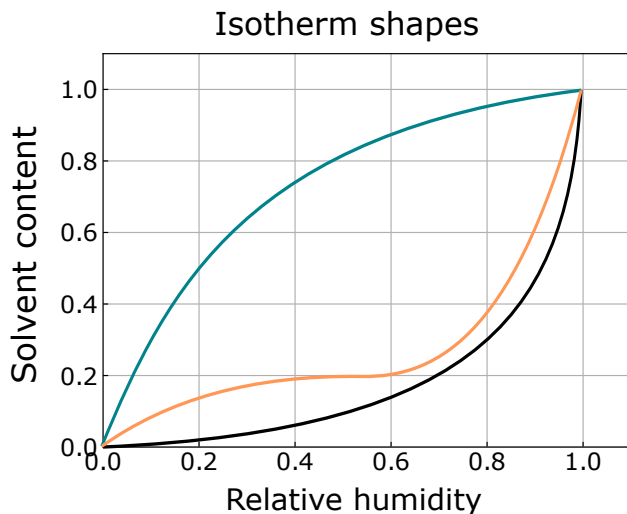
Figure 2.3: Approximate shapes of the different types of sorption isotherms discussed in this section. Black: Typical concave-upward Flory-Huggins isotherm. Blue: Concave-downward Flory-Huggins isotherm, found in extremely strongly interacting systems. Orange: Isotherm with crossover from void-filling regime to Flory-Huggins behavior at higher relative humidities. Vertical axis is normalized by the solvent content at saturation for the given system. The curves shown here are strictly illustrative and should not be used for any quantitative comparison.

(top right Figure 2.4) and between chains at high densities (bottom right Figure 2.4), with the intermediate systems being unable to form a high density of either type of complex (bottom left Figure 2.4). Moreover, these high-density zwitterionic brushes appeared to swell while maintaining or decreasing their solvent content under some conditions. This suggests a long-range restructuring, in which the formation of interchain complexes also increases the free volume within the brush.

Löhmann et al. report that isotherms for polyelectrolyte brush/polyelectrolyte multilayer composites in water vapor can be shifted by modifying the thickness of the multilayer component. [43] Moreover, at high relative humidities, a water-enriched region forms in between the brush and multilayer components. Although these isotherms are reported in terms of the swelling ratio, excluding void-filling effects, they display a regime transition that superficially resembles the one seen in reference 36. The shift from swelling of the individual compo-
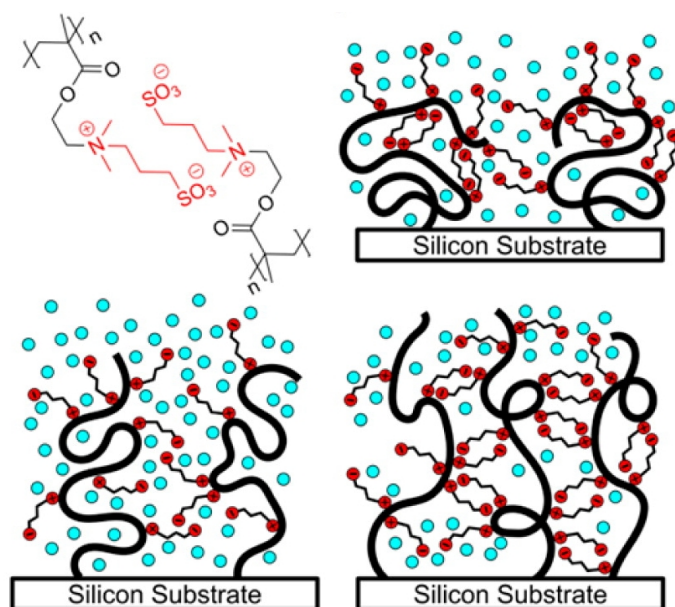
Figure 2.4: The mechanism proposed for non-monotonous swelling of polyzwitterionic brushes by Galvin et al. [28] Top left: Structure of the sulfobetaine side chain complex; top right: intramolecular association of ionic groups in low-density brushes; bottom left: minimal association of ionic groups in brushes of moderate density; bottom right: intermolecular association of ionic groups in dense brushes. Reproduced from ref. 28. Copyright 2014 American Chemical Society.

nents at low relative humidity to accumulation of solvent in the intermediate region at high relative humidity appears to be the cause of this two-regime isotherm.

Outlook on Isotherm Modelling

Since the shape of the isotherm follows from a chemical equilibrium condition, improving upon the model discussed here primarily requires a more exact free energy description for the brush. Accounting for the distribution of chain end positions and differences in composition over the brush height may quantitatively improve on equation 2.2, but will typically not alter the scaling. [44] However, various further adjustments may improve the results for specific systems. In the case of hydrogen bonding or complexation between polymer and

solvent, a composition-dependent expression for χ could be used to account for saturation of the relevant functional groups. Nevertheless, the most broadly relevant open issue for brushes in air specifically is the effect of free volume. While the energetic effect of free volume can be reasonably well described within a lattice model, we are not aware of a predictive theory relating the free volume fraction in a brush to the solvation state of the brush and the persistence length of the polymer. This would close the main discrepancy in knowledge between vapor-solvated and liquid-solvated brushes, and likely provide valuable insight into glass transitions in polymer brushes. Finally, sorption isotherms are an indication of equilibrium behavior only. In practical applications, the response time of the brush to a change in solvent composition may be important as well. Therefore, systematic exploration of the kinetics of brush swelling in different brush/vapor systems may be important in translating brush thermodynamics to design parameters.

Density profiles

The absorption behavior of polymer brushes can largely be described by bulk models, in which the overall composition of the brush is considered. However, solvent and polymer are not always evenly distributed throughout the brush, as the effect of chain stretching depends on the distance from the grafting plane. This variation in composition influences the interfacial properties of the polymer brush, making it highly relevant for surface functionalizations. In this section, we provide an overview of the literature that describes the density profiles for solvated polymer brushes. Next, we show how brushes in vapor may deviate from these profiles due to interfacial effects and incomplete solvation.

The physical properties of a solvated polymer brush depend not only on its composition, but also on the conformation of chains within the brush. In the preceding sections, we discussed mostly "box-like" descriptions of the brush, in which all chains are extended to the full brush height and the composition of the brush is homogeneous over its height in both good and poor solvents. Although such models are convenient and adequately predict some of the relevant scalings, [19, 45, 46] the assumption that all chains ends are located at the same distance from the substrate is unrealistic from an entropic perspective. In reality, chain conformations within a single brush may range from dense states close to the grafting plane to highly extended chains reaching all the way to the outer edge of the brush. Brushes at high grafting densities may still display step-like density profiles, as observed in both experiments [47] and

simulations [33, 48], since chains are sufficiently extended to describe the elastic contributions to the free energy by a mean-field argument. [44] Under moderate conditions, however, a more complex profile arises. Several self-consistent field studies have shown that the polymer concentration in a brush decays parabolically away from the grafting plane [44, 49, 50] i.e. $\phi_p(z) \sim C - z^2$, where C is a constant depending on the brush parameters. An approximation of this density profile is shown in orange in Figure 2.5. Additionally, in real systems, unconstrained chain ends near the outer edge of the brush create a short, Gaussian "tail" region far from the grafting surface. [51] Interestingly, this parabolic model retains the same height scaling of $h \sim \rho_g^{1/3} N$ as its box-like counterpart. Brushes in poor solvent retain their step-like density profile (dashed in Figure 2.5) in this description, since enthalpic and entropic contributions both favor the collapse of the polymer in this case. Interestingly, phase segregation is predicted to occur for polymers with a concentration dependent effective interaction (such as poly(N isopropylacrylamide) (PNIPAm)), at the transition between the parabolic and box-like phases. [52] This will results in a high density collapsed phase near the substrate and a low density swollen phase on top of it. [53] Yet, it has been difficult to confirm this experimentally.

The density profiles of polymer brushes in air may differ from ideal liquid-solvated brushes in many ways, however. For instance, the presence of a liquid-vapor interface may give rise to various boundary effects. When a boundary between a condensed phase and a gas or vacuum exists, molecules in the region near this boundary experience fewer intermolecular interactions than molecules in the bulk. In mixtures, this causes the species that experiences the weakest average interaction to migrate towards the surface, minimizing the energetic cost of the interface. Since interactions between two different species are symmetric, this is typically the component with the weaker self-interaction, i.e. the lower surface tension. Indeed, Sun et al. found results consistent with solvent enrichment at the liquid-air interface for neutron reflectivity (NR) measurements of polystyrene brushes in toluene vapor. [11] Furthermore, their experimental results and self-consistent field theory indicate that the polymer density profiles of these brushes are similar to the expected parabolic profiles for brushes in liquid, mainly deviating in the fact that the polymer density abruptly drops to zero near the free interface rather than decaying gradually. Another NR study on brushes of the weak polyelectrolyte poly(2-(dimethylamino)ethyl methacrylate) (PDMAEMA) in humid air by Galvin et al. showed similarly enhanced water concentrations near the air interface. [28] Dissipative particle dynamics simulations [54] and molecular dynamics simu-
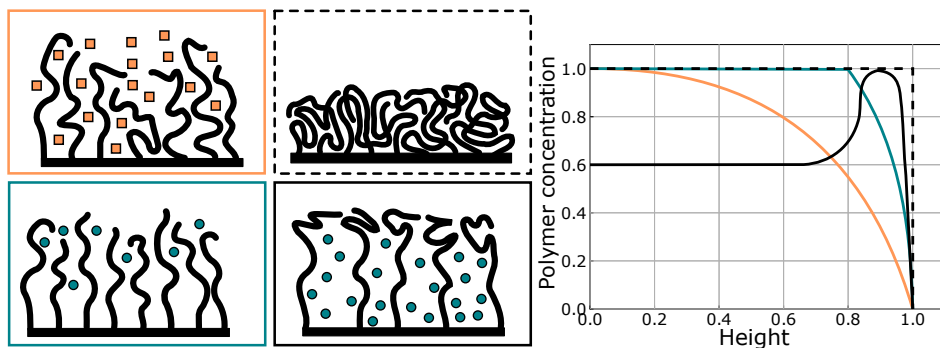
Figure 2.5: Polymer concentration against distance from the grafting plane, qualitatively represented for a number of the scenarios described in this section. Axes are normalized against the brush height and maximum polymer density for any given system, meaning that these should not be quantitatively compared. Orange: the density in a fully solvated neutral brush decays parabolically away from the grafting surface. Dashed: Dry and poorly solvated polymer brushes are completely collapsed, leading to a step-like density profile. Neglecting interfacial effects, this profile is also expected for non-grafted polymer films. Blue: Polymer brushes undersaturated with a good solvent maintain a constant density near the surface, but decay parabolically near the brush-air interface. [55] This is comparable to vapor-solvated systems below the saturation pressure. Black: the theoretical floating brush scenario, in which chains in an undersaturated polymer brush adsorb at the liquid-vapor interface.

lations [33] of chemically non-specific polymers also display this adsorption, indicating that it does not depend on any specific chemical effect.

Adsorption phenomena are not restricted to the solvent, however; many water-soluble polymers are surface-active at water-air interfaces due to their low surface tension tension relative to water. [56] Self-consistent field studies suggest that the free ends of grafted chains could similarly adsorb to the water-air interface, and that this in fact influences the wetting behavior of brushes. [57] However, to our knowledge, the existence of a "floating brush" (approximated by the black line in Figure 2.5), where a brush anchored to a solid substrate displays an enrichment in polymer at the liquid-air interface, has never been reported in experiment or simulation. Even in spin-coated polymer films, where polymer migration to the surface is not hindered by grafting, solvent-enriched layers have been observed at the polymer-air interface in experiment. [58, 59]

Finally, a good solvent vapor at low pressures will not necessarily condense in sufficient amounts to fully solvate the brush, resulting in partially swollen states. Goedel et al. expanded upon the analyses that yielded the parabolic brush profile to show that the density profiles of such intermediate states are truncated parabolas (shown in blue in Figure 2.5); that is, they display a constant polymer density near the grafting plane, but decay parabolically at large distances. [55] While this work does not explicitly consider vapors, the situation of a partially swollen brush appears thermodynamically similar to vapor solvation.

Outlook on Density Profile Characterization

Density profiles under liquid-solvated conditions have been thoroughly researched for neutral and charged polymer brushes in a variety of regimes. The principles that give rise to these profiles also apply to polymer brushes in air, suggesting that these results are relevant here as well. However, the effect of the brush-air interface is comparatively unexplored. The width of the interface is of particular interest, as this would inform calculations of the surface energy. Additionally, as Sun et al. point out, the shape of the brush-air interface influences surface fluctuations. [47] Another open question is the existence of the "floating brush" state described earlier in this section. Beyond theoretical curiosity, the floating brush state could lead to more thermally stable solvent binding, as the polymer-enriched layer would present a physical barrier to evaporation. Moreover, as a mechanically stable coating of surface-active polymer chains, the floating brush is likely to possess interesting wetting properties.

Vapor mixtures

Polymer brushes' responsive nature and ability to capture solvent molecules leads to diverse swelling behaviors in mixed solvent environments. We provide an overview of relevant research on polymer coatings in mixed vapors, and discuss the phenomena of co-solvency and co-non-solvency and their applicability to gaseous systems.

When a polymer brush is exposed to vapor mixtures, multiple effects can occur depending on the relative affinity of the vapor with the brush. Already for binary vapor mixtures, non-trivial swelling behavior can be observed. A coarse-grained molecular dynamics study by our group shows that, even in the absence of co-non-solvation, a mixture of two good solvent vapors may produce a range of enthalpy-driven absorption behaviors depending on the

vapor composition and energy of interaction between the brush and both solvents. [60] We identify preferential sorption of the better solvent whenever the two vapors are chemically distinct. In highly swollen, nearly saturated brushes, this leads to competition between the two solvents; at this point, increasing the polymer affinity of the preferred solvent causes very little additional swelling, but rather leads to the displacement of the secondary solvent out of the brush. Finally, when the affinity between the two solvents is stronger than the affinity of the secondary solvent for the brush, collaborative absorption may occur, in which the initial absorption of the preferred solvent creates a more favorable environment for the absorption of the secondary solvent. Figure 2.6 shows the the composition of a polymer brush in contact with a mixture of vapors under variation of the polymer-solvent interaction parameters, represented by the polymer-solvent interchange energy $W_{\mathrm{Pi}} = -\epsilon_{\mathrm{Pi}} + \frac{1}{2}(\epsilon_{\mathrm{ii}} + \epsilon_{\mathrm{PP}})$, with ϵ representing the energy of a single binary interaction, subscript P denoting the polymer, and subscript i indicating the solvent species. This quantity differs from the Flory-Huggins parameter χ only by a factor of z, the coordination number for particles in the solution. As a result, it is frequently convenient in describing molecular dynamics simulations, where the interaction energies are directly controllable, but the coordination number is not. Preferential absorption can be seen in the fact that A and B are not absorbed in equal measure when A and B are not chemically identical. Competitive absorption manifests as a decrease in B content at negative W_{PA} for the topmost two curves in 2.6b (meaning absorption of B decreases as the quality of the competing solvent is increased). Lastly, collaborative absorption is shown by the subtle increase in B fraction at negative W_{PA} for the curves with positive W_{PB} in 2.6b (indicating that, despite being a poor solvent, a small fraction of B is absorbed when A is a good solvent due to their miscibility).

Co-solvency, illustrated in the top half of Figure 2.7, is a phenomenon in which a mixture of two poor solvents may, as a whole, form a good solvent for a polymer. Although this effect is counterintuitive, it can be explained with mean-field models. [61–63] We refer the reader to the cited works for a comprehensive discussion of the thermodynamics, but we provide a qualitative argument. Approximating the solvent mixture as a single liquid yields an effective Flory-Huggins parameter $\chi_{\mathrm{P,L}} = \phi_A \chi_{\mathrm{P,A}} + \phi_B \chi_{\mathrm{P,B}} - \phi_A \phi_B \chi_{\mathrm{A,B}}$, where subscripts P, L, A and B indicate the polymer, solvent mixture, solvent A and solvent B respectively, and the volume fractions ϕ apply to the composition of the solvent mixture. The key feature here is that a small solvent particle gains significant translational entropy upon mixing, while this gain is negligible
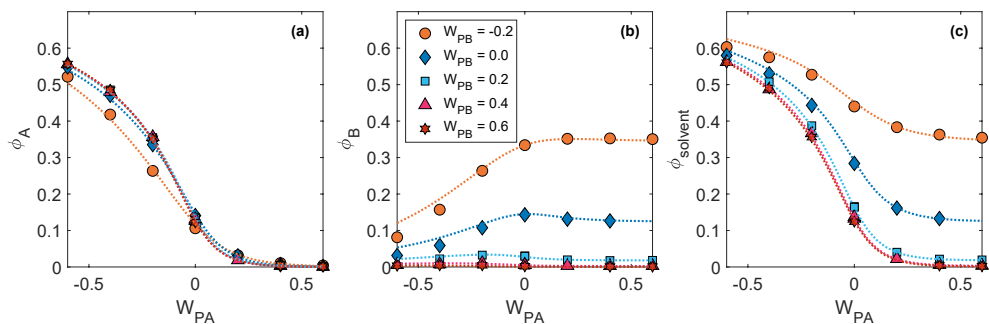
2

Figure 2.6: Composition of the polymer brush-vapor system described in ref. 60, consisting of a polymer brush in contact with a 50/50 mixture of two solvents. a) Volume fraction of solvent A in the brush, b) volume fraction of solvent B in the brush, and c) total solvent fraction in the brush as a function of the polymer-A interchange energy W_{PA} for a range of W_{PB} values. Markers indicate simulation results, dashed curves are theoretical predictions based on a ternary Flory-Huggins-like model. Reproduced from ref. 60. Copyright 2020 American Chemical Society.

for a large polymer coil. As a result, solvents with relatively high interaction energies may still be miscible (for $\chi_{A,B} < 2$), whereas only a weakly repulsive interaction is required for the solvent to form a poor medium for the polymer ($\chi_{P,A} > 0.5$ and $\chi_{P,B} > 0.5$.) In this range of interaction parameters, the individual solvents may interact with the polymer purely in order to minimize their contacts with each other, reducing their overall free energy. Co-solvency provides a way to switch the swelling state of a brush without fully replacing the solvent bulk, making it of interest for e.g. switchable adhesion applications. [64] Since co-solvency is driven by the enthalpy of exchanging solvent-cosolvent contacts for polymer-solvent and polymer-cosolvent contacts, it requires the presence of a solvent-rich phase for these solvent-cosolvent contacts to occur. As both solvents are individually poor, a polymer brush will not absorb a substantial fraction of solvent in a vapor environment, so solvent-cosolvent contacts are unlikely to be abundant within the brush. Poor solvents may still form a liquid adsorption layer on top of the brush when their surface tension is lower than that of the polymer, as discussed in section 2.2. However, this scenario is incompatible with the theory outlined in reference 61, which predicts full solubility of the polymer only when its cohesive energy density (a measure closely related to surface tension [65]) is intermediate between those of the two solvents. This suggests that substantial adsorption of both solvents

24
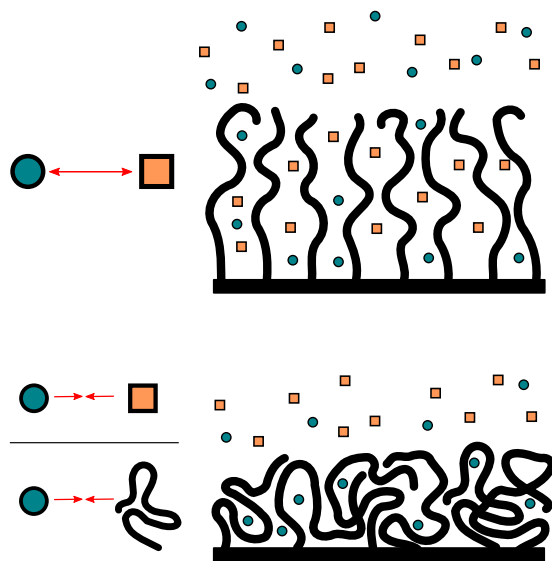
Figure 2.7: Schematic representation of co-solvation and co-non-solvation in polymer brushes. Top: co-solvency is driven by repulsive interactions between miscible poor solvents, causing them to swell the polymer brush. Bottom: Co-non-solvency causes the brush to collapse, usually containing a small amount of the minority solvent. While the exact mechanism remains to be clarified, it occurs mainly in systems with a strong preference of the polymer for one of the two solvents, or a strong interaction between the two solvents leading to avoidance of the polymer.

is incompatible with co-solvency, and seems to preclude co-solvation by vapors. We do point out that the work of Scott assumes a Hildebrand description of miscibility, which is best suited for apolar materials. Hence, vapor co-solvation in highly polar or otherwise strongly interacting systems may still be possible.

Co-non-solvency, counterpart to co-solvency, describes situations in which a mixture of two good solvents causes a polymer to collapse as if in a poor solvent. This scenario is shown in the bottom panel of Figure 2.7. PNIPAm-water-alcohol mixtures, which display an abrupt collapse and re-entrant swelling transition at low alcohol fractions, are the most well-known example of this phenomenon, and are often used as model systems. [66] Unlike co-solvency, co-non-solvency has not been conclusively explained, and the underlying mechanisms are a subject of active research. Some of the potential explanations focus

on the interaction between the two solvents: Liu et al. propose that co-non-solvency in the PNIPAm-water-alcohol system is caused by the composition-dependent formation of water-alcohol clusters, which have a weaker tendency to form hydrogen bonds than either of the pure solvents. [67] The stoichiometry of these clusters may also explain the asymmetric relation between solvent composition and solvent quality. A lattice model by Dudowicz et al. shows that two highly miscible, moderately good solvents can produce co-non-solvency by avoiding polymer-solvent contacts in favor of mixing between the two solvents. [62] Although this model does not account for solvent clustering and covers a limited parameter space, it agrees with reference 67 in attributing co-non-solvency primarily to solvent-solvent interactions. However, the majority of proposed mechanisms are centered around the polymer-solvent interactions. Tanaka et al. emphasize competition between solvents in forming hydrogen bonds with the polymer, and develop a model similar to competitive adsorption. [68] Their theory indeed predicts a minimum of bonded solvent molecules per polymer at intermediate solvent compositions. Mukherji et al. also take an adsorption-based approach to the co-non-solvency phenomenon, but without relying on any specific chemical interactions. Instead, they propose that a minority fraction of the preferred solvent may cause multiple monomers to adsorb to each solvent particle, thereby causing the collapse of the polymer, whereas larger amounts of the preferred solvent would simply solvate the polymer chain in its entirety. [69] This description was expanded to polymer brushes by Sommer, [70] and further tested in molecular dynamics simulations. [71] Rodríguez-Ropero et al. advance a model that is also based on preferential solvent binding, but propose that methanol stabilizes collapsed conformations of the PNIPAm chain entropically rather than enthalpically through chemistry-specific effects. [72] Later work in the same group suggests that preferential solvent binding is not required for co-non-solvency, supporting the claim that the co-non-solvency of the PNIPAm-water-alcohol system is chemistry-dependent. [73] Recent research tends to view solvent mixing and preferential solvation both as causes of the co-non-solvency phenomenon, rather than favoring one explanation over the other. [74] This is supported by theoretical work by Zhang et al., which shows that both these phenomena can be described under the same random phase approximation. [75]

The apparent mechanisms of co-non-solvency could, under suitable conditions, also apply to polymer brushes in gaseous environments. Mean-field solvent mixing, in which solvents prefer mixing over solvating the polymer, is the only scenario that seems unlikely, given the high polymer concentration in

a brush and the absence of a bulk solvent phase. Solvent clustering and preferential binding effects could plausibly occur in brushes in equilibrium with a vapor, although both are tied to specific compositions of the sorbed solvent; for preferential binding, the preferred solvent must be the minority component, whereas cluster formation restricts the composition of the sorbed solvent depending on the cluster stoichiometry. Hence, tuning of the vapor composition in addition to the polymer and solvent chemistry may be required to produce co-non-solvency. Recent experiments in the Müller-Buschbaum group do indeed show co-non-solvency for thin non-grafted films of a PNIPAm-based block copolymer, a PNIPAm analogue and polysulfobetaine in a mixed water-methanol atmosphere. [59, 76] While the films investigated in these experiments still swell relative to their dry state, their thickness at intermediate compositions is less than in either pure vapor, indicating a co-non-solvent effect.

Outlook on Mixed Vapors

As discussed in this section, binary solvent mixtures can cause counter-intuitive swelling responses already. While these responses are reasonably well-understood by now, there is little evidence of their occurrence in gaseous environments. While our qualitative arguments suggest that co-non-solvation by vapors is likely to exist, and co-solvation is not completely precluded, a more rigorous theoretical approach to extending liquid-based models could inform experimental research on these phenomena. Additionally, further experimental evidence of co-solvation and co-non-solvation by vapor would be of technological interest due to the possible use of vapors as a switching mechanism. Experimental studies on this subject may be complicated by differences in volatility between solvents, however. On the technical side, fine control of the vapor composition across a wide range of densities may be required. Additionally, the potential difference in volume fractions between the components of a mixed vapor may lead to different kinetics of sorption for each component, requiring careful monitoring to ensure an equilibrium state is reached. Finally, in many applications vapors will be composed of many more different components. It is probable that many of these components are poor solvents - for instance, dry air generally causes polymer brushes to collapse - and hence, sorption will be dominated by components for which the brush is selective or which are present at near-saturated concentrations. However, complex partitioning of minority components may occur as a result of collaborative absorption and the respective miscibilities of the many species present in such a system.

Mixed brushes

In this section, we discuss mixed polymer brushes: brushes consisting of two or more distinct types of polymer chains. Such brushes can form a range of different structures depending on solvent conditions, compatibility of the polymers, composition of the brush, and other parameters. [77] This results in switchability of the surface composition and structure, which provides additional avenues for control of surface properties. Here, we provide an outline of these structures and their responsiveness to solvent vapors.

Two polymer species grafted to a substrate at sufficient densities will form a brush just like a single species would. When both polymers are similar, i.e. they are miscible and have similar affinities for the substrate and the free interface, this simply results in a brush structure in which the two chain types are randomly intermixed. However, dissimilarities between chains lead to phase separation. When the polymers are compatible but differ in their affinity for the substrate or the environment outside the brush, the two polymer types will assume different conformations, and a layer enriched in one of the two polymers may form at the interface, as shown in Figure 2.8. [78–80] Zalakain et al. showed that rearrangements in mixed polystyrene/poly(methyl methacrylate) (abbreviated PS and PMMA respectively) brushes can be triggered by exposure to selective solvents, with acetic acid producing a PMMA-enriched top layer, and cyclohexane enhancing the PS content of the brush surface, although in both cases contact angle measurements suggest that the surface layer still contained chains of both species. A degree of selectivity was also observed for vapors of these solvents. [78] This selectivity is of interest for switchable surface functionalization and sensing applications. Klushin et al. point out that the presence of the other brush species turns the collapse-swelling transition of the polymer that swells in a given solvent from a continuous transition into a sharp one, enhancing the responsivity of the system, and present a self-consistent field theory of this phenomenon. [81] In order to optimize responsiveness for a single analyte, having a minority of chains of the responsive polymer, with a larger average chain length than the non-responsive polymer appears to be most favorable. [81, 82] Experimental work by Motornov et al. provides an interesting example of this responsivity in relation to gaseous environments specifically; in this study, a mixed poly(dimethyl siloxane)/ethoxylated poly(ethyleneimine) (abbreviated PDMS and EPEI respectively) brush was found to be hydrophilic when submerged in water, but hydrophobic in air even at high relative humidities. [83] This was attributed to the formation of a hydrophobic PDMS layer on top of hydrophilic EPEI clusters, which prevented spreading of water

drops on the surface even when EPEI chains penetrated through the PDMS shell underneath the drop. This contact line pinning phenomenon is specific to three-phase systems, and illustrates once again that brushes in gaseous environments display interesting properties beyond those that can be extrapolated from liquid-solvated brushes.
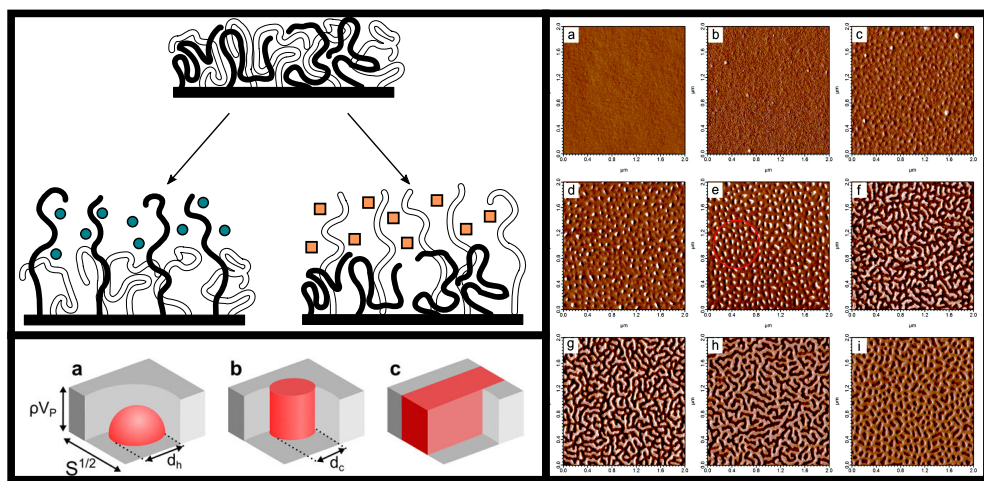
Figure 2.8: Phase segregation in mixed polymer brushes. Top left: Mixed polymer brushes may vertically separate when the surrounding medium is selective for either polymer species, altering the surface properties. Bottom left: Mixed brush systems may laterally segregate into a) hemispherical, b) cylindical and c) elongated stripe domains. Reprinted from ref. 84, with the permission of AIP Publishing. Right: atomic force microscopy (AFM) images of lateral phase separation in PS/PMMA brushes annealed under tetrahydrofuran vapor. PS content increases from 0 to 68% by volume from a to i. The red circle in e denotes a region of cylindrical domains that may be hexagonally ordered. Reproduced from ref. 85. Copyright 2012 American Chemical Society.

In addition to vertical separations resulting from collapse-swelling transitions of polymers, two incompatible polymer species in a brush may also phase-separate laterally. However, separation over large length scales is made impossible by the fact that the chains are anchored to a surface, leading to the formation of microdomains similar to those seen in block copolymer films. Self-consistent field studies and experiments both show that in binary brushes, these microdomains can take the form of a "ripple" phase, with extended highly directional domains, or hexagonally packed cylindrical or hemispheri-

cal domains (see Figure 2.8). [77, 86] Simocko et al. identify a conceptually similar, but more complex phase diagram for ternary mixed brushes. [87] Due to the ability to form regular features on nanometer scales, these structures are considered interesting for lithographic applications. [88] Switching from a disordered or vertically segregated state to a lateral microdomain state can generally be achieved by treatment with a solvent vapor that is nonselectively good for both polymers. [80, 85] Santer et al. observed persistence of the domain structure across multiple cycles of selective and nonselective solvent vapor treatment in a PS/PMMA system, describing this phenomenon as partial domain memory. [80] A followup study showed a far weaker memory effect for Y-shaped brushes, which were produced using a surface-anchored bifunctional initiator. This memory effect was attributed to variations in the local composition of grafted chains, which are largely eliminated by the use of these Y-polymers. [89] Eliminating this domain memory effect might enable the use of patterned brush surfaces to transport selectively adsorbed particles around under repeated patterning and depatterning by solvent cycling. Bao et al. investigated mixed brushes grown using a Y-shaped initiator on silica particles, tuning the grafting density of the brushes via the initiator/particle ratio. Microphase separation was found to become stronger with increasing grafting density, whereas the typical width of the ripple microphase decreased. [90] Finally, recent simulation studies in our group have shown that microphase-separated brushes display enhanced vapor sorption capacity and overall solvent affinity, as the polymer-polymer interfaces form a high-energy interface that readily adsorbs solvent vapors. [84, 91]

Outlook on Mixed Brushes

While mixed polymer brushes display a range of interesting properties, they share some of these with free or grafted coatings of copolymers, which may be easier to produce. Nonetheless, their mechanical stability and phenomena such as domain memory effects are of unique interest. Further research into the change of mixed brush conformations as a function of solvent conditions may be of interest, both to optimize brush architecture and chemistry for potential applications and to better understand the thermodynamic and kinetic effects of e.g. vapor annealing. However, producing mixed polymer brushes of high grafting densities for a wide variety of polymers remains nontrivial, especially for immiscible polymers. Identifying flexible and robust synthetic strategies for producing mixed brushes is another substantial open issue.

2.3 Applications

Sensing

The stimulus-responsive nature of polymer brushes makes them of great interest for a wide range of sensing applications. In this section, we discuss how solvent-absorbing brushes can be used to enable and improve sensing technologies for chemical detection in the gas phase specifically. We include both designs which use brushes to enhance the capabilities of a separate sensing platform and ones in which the brush response itself (directly or indirectly) measures the analyte concentration. Vapor sorption in polymer brushes can generate or amplify a sensor response in a variety of ways, some of which are illustrated in Figure 2.9.

Gravimetric Sensing

In gravimetric sensing techniques, the concentration of an analyte is typically measured by the shift in resonant frequency of a piezoelectric component as its mass changes with the adsorption of analyte. Grafting polymer brushes onto the resonating component in such a setup can increase the affinity between the solvent and the sensor surface, the selectivity towards the analyte, and the total sorption capacity. For example, McCaig et al. modified piezoelectric silicon nitride cantilevers with both grafted and drop-cast PMMA, and recorded the shift in resonant frequency of these cantilevers on exposure to various organic vapors. The response of the brush-coated cantilevers relative to the bare and drop-cast ones was enhanced substantially in polar vapors, which are generally compatible with PMMA, but was not altered significantly for apolar vapors. [2] This approach also applies to quartz crystal microbalance (QCM) setups, in which the resonant frequency of a piezoelectric quartz crystal is monitored. [32, 93, 94] Brush-enhanced QCM has been applied for a variety of polymer-solvent systems, with varying response kinetics and reversibility. High degrees of tunable selectivity are attainable by functionalizing the brushes with specific side groups. Kimura et al. demonstrated this by using metallophtalocyanines with different steric protecting groups, which resulted in different selecitivities towards various volatile organic compounds. [94]

Electronic Sensing

Brush-based compounds can also be used in electronic sensors. Typically, this is done by coating conductive particles with a polymer brush layer, so that electronic contact between particles becomes dependent on the swelling state

2
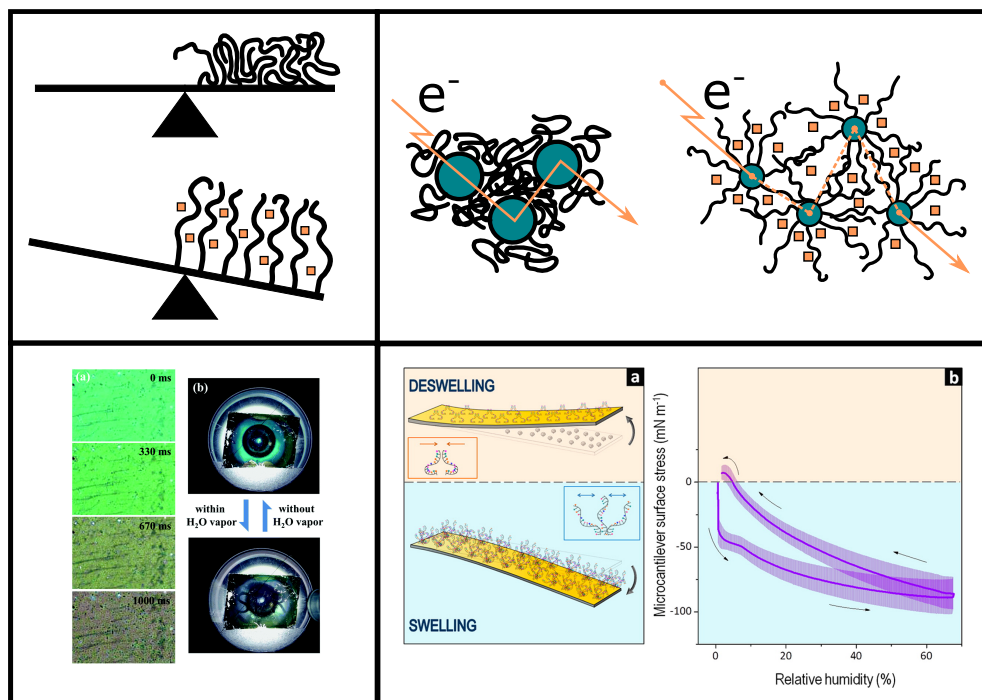
Figure 2.9: A variety of sensing methodologies incorporating polymer brushes. Top left: solvent vapor uptake by polymer brushes can be detected gravimetrically. Typically, these microscopic mass changes would be measured via the shift in resonant frequency of an oscillating system, such as in a QCM setup. Top right: The swelling of grafted polymers on conductive particles can break up conductive paths, altering the electric resistance of nanoparticle-brush composites. Bottom left: Swelling of polymer brushes can alter active length scales in optically active materials, leading to a change of color. Shown here: solvent uptake in polymer brushes on the bottom of silver nanovolcano arrays lead to a shift in color from light to dark green; reproduced from ref. 92 with permission from the Royal Society of Chemistry. Bottom right: swelling of grafted polymer chains or DNA strands increases lateral stresses within the brush, which can lead to bending of thin or soft substrates. Reproduced from ref. 41. Copyright 2014 American Chemical Society

of the brush. Dispersions or layers of such brush-coated particles will show increasing electric resistivity as the brush swells, creating another method of translating a brush response into a signal. For instance, Li et al. demonstrated that grafting polymer chains onto graphitic carbon nanofibers (GCNFs) enhanced the response of a GCNF/platinum interdigitated array electrode to various vapors by at least an order of magnitude relative to bare GCNFs on the same electrode. Moreover, this enhancement was found to increase with the polymer-solvent affinity, creating a degree of selectivity. [1] Wang et al. showed that the resistivity of dip-coated thin films of CB particles functionalized with polystyrene and poly(4-vinylpyridine) brushes increases strongly in the presence of good solvent vapors, as the swelling of the polymer disrupts the conductive network. [95] This response was found to be reversible for methanol vapor, with larger alcohols producing a residual resistivity. Previously, Chen and Tsubokawa demonstrated that a similar concept, in which CB particles were dispersed into a non-grafted polymer matrix, could also be improved for a range of good solvent vapors by surface functionalization of the CB with brushes. In this case, the brush coating increases the dispersibility of the particles by lowering the surface energy of the carbon black, and improves the response time and re-usability of the sensor material by preventing vapor molecules from binding directly to the carbon black surface. [96, 97]

Optical Sensing

Lastly, we highlight the use of polymer brushes in optical sensors, in which the solvent response of the brush alters the interaction between some part of the sensor and incident light. This is a rather diverse category, as most sensor designs under this umbrella are based on intrinsically optically active structures, in which a brush is used to vary the optically relevant dimension. Wei et al. grew multi-responsive polymer brushes on a gold substrate, and further coated this brush layer with a gold top layer to produce an optical cavity akin to an etalon. The size of this cavity depends on the thickness of the brush layer, and so the reflected wavelengths change as the brush responds to shifts in temperature, pH and relative humidity. [98] Wang et al. created optical responsiveness using a silver nanovolcano array, an optically active structure of open, truncated cones, [99] with a PNIPAm brush coating at the bottom of the nanovolcano cones. [92] Such nanovolcano arrays are monochromatic transmitters, in which the vapor swelling of the PNIPAm brush produced a shift in color by altering the effective depth of the cones. Another optical sensor design measures the deflection of a laser by a brush-coated substrate,

thereby detecting the bending of the substrate. For sufficiently thin or soft surfaces, a brush can relax the lateral excluded volume stresses associated with swelling by bending its substrate rather than by chain stretching. [100] This property was utilized by Domínguez et al., by creating films of grafted single-stranded DNA with specific sequences on gold microcantilevers. When exposed to complementary DNA fragments in solution, these grafted DNA strands hybridize to form double-stranded DNA, which is significantly more rigid than ssDNA. [41] This results in a void-filling swelling mechanism, with less variation of lateral stresses and hence a different bending response. [12] This has been proposed as a rapid and tunable detection technique for identifying pathogens or specific genetic sequences, such as the ones responsible for antibiotic resistance. [41, 101, 102]

Outlook on Sensing

The responsive and selective nature of brushes gives rise to a wide range of potential sensor designs. However, some challenges present themselves. In addition to the general issues of brush stability and scalable synthesis, the actual range of applications for brush-based sensors is limited by the analytes for which brushes can be made sufficiently selective. Chemical research to tailor polymers to specific target compounds could expand the applicability of brush-based sensing concepts. Additionally, fouling or interactions between common gas components could influence the sensing functionality, and may therefore be worth investigating.

Finally, some sensor designs for liquid environments may also work under gases. For instance, in one study, opal-like arrays of silicon nanoparticles coated with brushes containing hydrophobic and negatively charged blocks were shown to change in color in the presence of lysozyme proteins, due to the change in Bragg reflection wavelength as the brush swelling alters the periodicity of the structure. [103] While this was demonstrated in a liquid environment, a solvent vapor in air is from a thermodynamic perspective comparable to a minority component with strong polymer affinity in a poor background solvent, suggesting that concepts like this may extend to the gas phase as well.

Separations

Polymer brushes' potential for selective absorption has the potential to enhance various separation technologies. Additionally, hydrophilic polymer brushes have found use in forming conducting channels with applications for proton
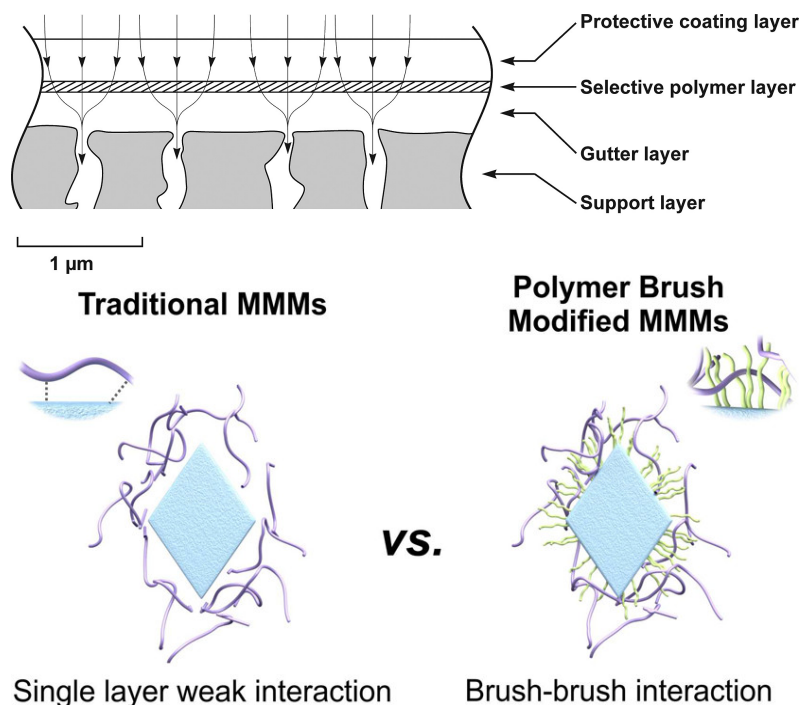
Figure 2.10: Incorporation of (grafted) polymers in membrane architectures. Top: Typical membrane architecture, consisting of a protective coating, a thin selective layer, and a porous, typically inorganic support. A "gutter layer" may interspersed to compatibilize the support and the selective layer. While we focus on the use of grafted polymer materials in the selective polymer layer, membrane properties can also be modified by anchoring polymer chains inside the porous support. Reproduced from ref. 104. Copyright 2017 American Chemical Society. Bottom: contrast between grafted and non-grafted mixed matrix membrane (MMM) structures. Usually, MMMs consist of separate inorganic particles incorporated in a polymer matrix. However, functionalizing the particle surface with a polymer brush can improve the compatibility of the surface and the polymer matrix, and prevent particle aggregation. Reproduced from ref. 105. Copyright 2018 American Chemical Society.

separation, or enhancing the formation of such channels in existing proton separation materials. In this section, we provide an overview of these applications and the role polymer brushes play in them.

Gas Separations

The most broadly relevant gas separations are between combinations of N_2, O_2, H_2, CO_2, CH_4 and He. Some notable combinations of these comprise air separation, natural gas sweetening, flue gas treatments, and hydrogen separation. [106–110] Membranes used in these separations classically consist of a thin, highly selective layer over a porous support material, which provides mechanical stability (see Figure 2.10). For sufficiently large pore sizes, surface functionalizations can also be applied to the inside of the pores in the support material. [111] Research on this class of polymer brush-based membranes has been reviewed by Keating et al. [112] Bruening et al. provide an overview of the synthesis and use of polyelectrolyte multilayers and polymer brushes for membrane applications, and conclude that their selectivity and compatibility with a range of supports makes polymer brushes an attractive class of materials for gas separations. [111] For example, Balachandra et al. investigated the performance of poly(ethylene glycol dimethacrylate) (PEGDMA) and poly(hydroxyethyl methacrylate) (PHEMA) brushes anchored from polyelectrolyte multilayers on porous alumina. [108] They report high CO_2 permeability and selectivities towards CO_2 for the PEGDMA-functionalized membranes, which is attributed to crosslinking of the PEGDMA brush (which favors the diffusion of small molecules) and high solubility of CO_2 in the brush through polar interactions with carbonyl groups in PEGDMA. PHEMA, on the other hand, did not display any significant selectivity. Upon functionalization with a perfluorinated side chain, however, the PHEMA-based membrane acquired CO_2 permeability comparable to the PEGDMA-functionalized membrane, albeit with lower selectivities towards CO_2. This suggests functionalized PHEMA layers with an appropriately selected side group may be of use for specialty separations. Grajales et al. show that membranes functionalized with brushes of poly(ethylene glycol methyl ether methacrylate) (PEGMEMA) polymers display enhanced CO_2/H_2 selectivity when PEGMEMA monomers with a variety of poly(ethylene glycol) (PEG) side chain lengths are incorporated. This dispersity of side chain lengths inhibits the crystallization of the brush, which would favor diffusion of the smaller H_2. [113] Aliyev et al. found that grafting PDMAEMA brushes to graphene oxide (GO) on a porous polyacrylonitrile support covered up pinhole defects in the GO layer and provided strong selectivity towards water vapor, enhancing membrane performance relative to a bare GO membrane. [114]

Mixed matrix membranes, in which the polymeric layer is loaded with filler materials such as zeolites or metal-organic frameworks (MOFs) may improve upon
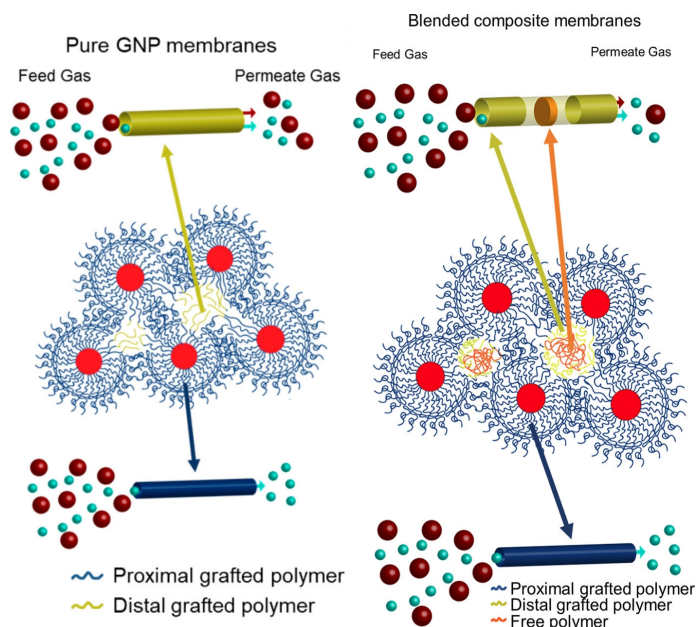
Figure 2.11: Inefficient packing of polymer chains in interstitial volumes reduces size-dependent selectivity in grafted nanoparticle membranes (left). Adding free polymer chains to this structure re-introduces a degree of size-based selectivity, dependent on the distribution and molecular weight of the free polymer. Adapted from ref. 115. Copyright 2020 American Chemical Society.

the properties of the pure polymeric membrane functionalizations described above, e.g. by acting as molecular sieves or selective adsorbents. [104, 116] However, such materials are faced with stability issues such as aggregation of filler particles. When this architecture is modified by replacing the free polymer matrix with a grafted polymer coating on the particle surface, the dispersibility of the particles is improved. [115, 117] Moreover, Bilchak et al. showed that membranes composed of grafted silica nanoparticles displayed increased free volume relative to the neat polymer matrix, since the packing of the spherical particle leaves interstitial volumes, resulting in increased permeability at the expense of selectivity, as illustrated in Figure 2.11. [117] Followup research showed that this free volume can be tuned through the addition of long free polymer chains which preferentially occupy the interstitial volume, reintroducing size-based selectivity to the membrane. [115] Experiments by Jeong et al. using poly(butyl methacrylate)-grafted particles show that high

grafting densities are required for increased gas permeability. [118] This is attributed to the formation of polymer bridges between particles at low grafting densities, either during polymerization or by penetration of polymer chains from one particle to the surface of another, which can result in inhomogeneous dispersion of the particles. Xin et al. found that brush functionalization with polystyrene-derived polymers improved the compatibility of various inclusions with a sulfonated poly(ether ether ketone) (SPEEK) matrix. [119–121] Additionally, they observed that pyridine-functionalized graft polymers enhance selectivity towards CO_2, [119, 120] presumably due to the chemical similarities to amines, which are highly effective at binding CO_2. [122] Wang et al. compared a mixed matrix membrane design of metal-organic framework particles in a polyimide matrix with a membrane architecture composed purely of brush-grafted MOF particles, and similarly found that both membrane performance and mechanical stability are enhanced by improvement of the particle-polymer interfacial interaction. At high MOF loading, however, the increased viscosity of the grafted polymer relative to the non-grafted matrix hinders the solution casting procedure employed in this work, resulting in deterioration of membrane properties. [105]

Proton Conduction

Polymeric membranes also find use in ion exchange membranes for energy applications, such as proton exchange membrane (PEM) fuel cells. In such fuel cells, hydrogen is catalytically oxidized at the anode, and the resulting protons diffuse through a membrane to react with oxygen and electrons at the cathode side. The archetypal polymer for proton exchange membranes is Nafion, a perfluorinated polymer with ether-linked sulfonated oligomer side chains, which phase-separates under humid conditions to form hydrophilic channels with a high density of sulfonate groups, which are suitable for selective proton transport. [123, 124] However, Nafion and similar perfluorinated polyelectrolytes are costly, require high humidity to function, and are only moderately stable mechanically. Farrukh et al. incorporated silica nanoparticles functionalized with grafted poly(monomethoxy oligo(ethylene glycol) methacrylate) (PMeOEGMA), a hygroscopic polymer. Small amounts (1 wt%) of these nanoparticle inclusions were found to enhance proton conductivity by up to an order of magnitude, with the largest improvements observed at low temperatures and humidities. [125] Niepceron et al. fabricated membranes of an inert fluoropolymer matrix with poly(styrene sulfonate)-grafted nanoparticle inclusions, and found that these composites displayed high proton

conductivities in addition to self-humidifying properties. [126] Most research on grafted polymers for ion exchange membranes focuses on non-fluorinated polymer sulfonates, however. Yameen et al. investigated membranes composed of polyacid brushes on macroporous silica, and found that these materials displayed proton conductivity approaching that of Nafion membranes and enhanced mechanical stability due to the presence of a solid scaffold. [123, 127] Incorporating hygroscopic PMeOEGMA blocks in the polymer brush in these same membranes reduced the temperature and relative humidity dependence of the proton conductivity, leading to high conductivity under a wide range of conditions. [128] Another research team performed several studies in which partially sulfonated polystyrene was grafted onto filler materials and dispersed these into a polymer matrix. This generally results in enhanced proton conductivity relative to the neat polymer. [129, 130] The improved conductivity is generally attributed to improved dispersibility of the filler and formation of conductive networks throughout the polymer matrix. [130] Zheng et al. investigated the effect of polymerization parameters on the conductivity of poly(2-acrylamido-2-methylpropane sulfonic acid) (PAMPS) brushes grafted to titanate nanotubes, and found non-monotonic dependencies on both grafting density and chain length. [131] Dong et al. studied a similar system, consisting of PAMPS brushes in aligned titanate nanotubes, and report that the PAMPS brush enhances proton conduction relative to the bare nanotube array. This enhancement is observed when nanotubes are partially or completely filled by the brush, suggesting that sulfonate groups near the nanotube wall have the largest impact on conductivity. [132] However, we point out that incomplete pore filling may have detrimental effects on selectivity.

Outlook on Separations

As described above, many brush-based solutions for separations have been proposed. Yet, we see room of improvement. A systematic theoretical study of the effects of brush characteristics (grafting density and polymer length) on the gas transport properties has not been performed so far and this might be key in optimizing the separation performance. Additionally, in some of the works discussed in this section, polymer brushes are used primarily to compatibilize inorganic components with the polymer matrix in a mixed matrix membrane architecture. In these cases, significant improvements can be made on a long-term stability and the prevention of particle aggregation. Extrapolating from existing works, the use of crosslinking functionalities to covalently bond particles to the matrix could be of interest here. While this would not necessarily

reduce the particle-polymer interfacial energy relative to non-bonded brush-bearing particles in the matrix, it would create additional physical barriers to particle aggregation and enforce matrix-particle contacts. In other cases, such as the majority of proton separation applications we describe, the grafted polymers qualitatively alter transport through the membrane. The directionality imposed by grafted polymer, the high density of specific binding sites, and transport along brush-air and brush-inorganic interfaces are all potential contributors to permeability and selectivity. Further research into the physical structure of membrane architectures containing grafted polymers could indicate which of these contributions are most significant, and how membrane architecture can be further optimized for this.

Adhesion and friction control

The unique structure and solvent-binding abilities of polymer brushes lead to interesting mechanical properties in addition to the previously discussed chemistry-oriented applications. In this section, we describe the friction and adhesion properties of polymer brushes, and outline how these responses are modified by the presence of solvent vapors. Additionally, we highlight experimental works that make use of these properties and theoretical approaches that investigate the specific effects of vapor solvation.

(Non-)Selective Adhesion

Adhesion is a surface property with clear practical applications: highly adhesive surface coatings could be used as glues, whereas low adhesion makes surfaces fouling-resistant and easy to clean. Adhesion is typically defined by the reduction in surface energy upon putting two surfaces together. Hence, surfaces that interact unfavorably with the background medium tend to be non-selectively adhesive. A classic polymeric example is the hydrophobic polymer PDMS, a commonly used material in microfluidics for biomedical applications, which is hindered by its tendency to non-specifically adsorb organic compounds in an aqueous environment. However, surfaces can also be tuned to interact strongly with specific materials through e.g. hydrogen bonding or supramolecular chemistry, leading to selective adhesion. Additionally, the mechanical properties and nonideality of a surface may influence the adhesive properties: soft materials may conform to the contacting surface, whereas surface roughness may increase or decrease the effective contact area for soft and hard countersurfaces respectively. Since the mechanical properties and surface energy of polymer

brushes vary with the chain conformation, which can be tuned and switched by a wide variety of parameters, polymer brushes are of great interest for modifying surface adhesion.

In many settings, preventing the adhesion of certain components to a surface is important. This includes precipitation of salts and other solids in industrial contexts, protein and cell adhesion in biomedical applications, and growth of both micro- and macroscopic organisms in marine environments. This is generally achieved by antifouling surface functionalizations. In a recent review on antifouling polymer surfaces, Maan et al. distinguish three forms of antifouling functionality: fouling resistance, in which adhesion of certain components is prevented, fouling release, in which foulants can weakly adhere to the surface but are easily removed by some external stimulus or force, and fouling-degrading, in which the material breaks down adsorbed foulants. [133] In this framework, hydrophilic polymer brushes are naturally fouling-resistant due to their high polymer density, internal osmotic pressure, [134] and the formation of a tightly bound water layer around the polymers. [135, 136] While linear PEG brushes are a simple and commonly applied example, [137] research into other polymers and brush architectures for antifouling is ongoing. Examples include the use of sugar-functionalized brushes to selectively promote and reduce bacterial adhesion [138] or zwitterionic brushes for general protein repulsion. [139] Variations in architecture can further enhance the coating properties. Wang et al. found that a bottlebrush coating of poly(N-vinylpyrrolidone) (PVP) attached to a PHEMA backbone was more effective at preventing protein adhesion to a gold surface than a linear PVP brush of the same thickness. [140] Morgese et al. investigated loop-type brushes, consisting of cyclic polymers anchored to a surface by a single point. [141] These loop brushes can accommodate higher areal densities of polymer than linear brushes, which could result in enhanced antifouling capacities. PDMS brushes have been identified as particularly effective antifouling coatings. [142–145] Even oils, that completely wet almost all substrates, easily roll off substrates coated with PDMS brushes. This has been attributed to the low surface energy of PDMS and intrinsic liquid state of these brushes.

Besides reducing unwanted adhesion, polymer brushes can also be used as general or targeted adhesives by presenting a high density of functional groups. Chaudhary et al. studied the adhesion of PDMS surfaces functionalized with poly(2-ethylhexyl acrylate) (P2EHA) brushes by recording force-distance curves with a sapphire probe. [146] While this functionalization did enhance the adhesion between the PDMS and the probe, a maximum in the adhesion as a

function of chain length was observed. This maximum was attributed to longer P2EHA chains entering into and stiffening the PDMS network. Nonetheless, the results for lower chain lengths illustrate the ability of hydrophobic polymers to function as dry adhesives. Supramolecular compounds based on multivalent host-guest interactions can function as a strong and selective adhesive, and are in many cases switchable. Lamping et al. have reported several examples of such supramolecular adhesives, in which the host and guest functionalities are attached to different brush coatings. [147, 148] In particular, a system based on the interaction between phenylboronic acid- and catechol-containing brushes was found to be strongly adhesive, water-resistant, and switchable by the addition of carbohydrates. [147] As illustrated in figure 2.12, once activated and placed together, these brushes performed well in weight tests.

Switching Adhesion

Finally, adhesion modification is compatible with the switchable behavior of polymer brushes. Synytska et al. synthesized copolymer brushes with randomly distributed (hydrophobic) PDMS and (hydrophilic) PEG side chains. [149] These brushes were found to display a degree of phase separation, resulting in an enrichment in PDMS at the brush-air interface under dry conditions, and an enrichment of PEG when submerged in water. Adhesion forces with both hydrophilic and hydrophobic probes were found to be nonlinear with the brush composition, with higher PEG content leading to higher adhesion to hydrophilic surfaces. However, PEG-rich systems fully submerged in water displayed low adhesion regardless of the probe, presumably due to a preference for PEG-water contacts.

Dissipation and Friction Mechanisms

In an idealized scenario, adhesion is thermodynamically reversible: the reduction in surface energy when putting two surfaces together should be equal to the energy required to separate them. However, in reality, separating the surfaces typically requires some additional energy. This phenomenon is called adhesion hysteresis, and is generally related to rearrangements in the material upon contact or separation. An intuitive example in soft materials is deformation to maintain contact with the countersurface, which dissipates additional energy. This adhesion hysteresis can be intuitively related to friction: an object moving over a surface is continuously making contact with the surface ahead of it, while separating from the surface behind it. With this in mind, we look
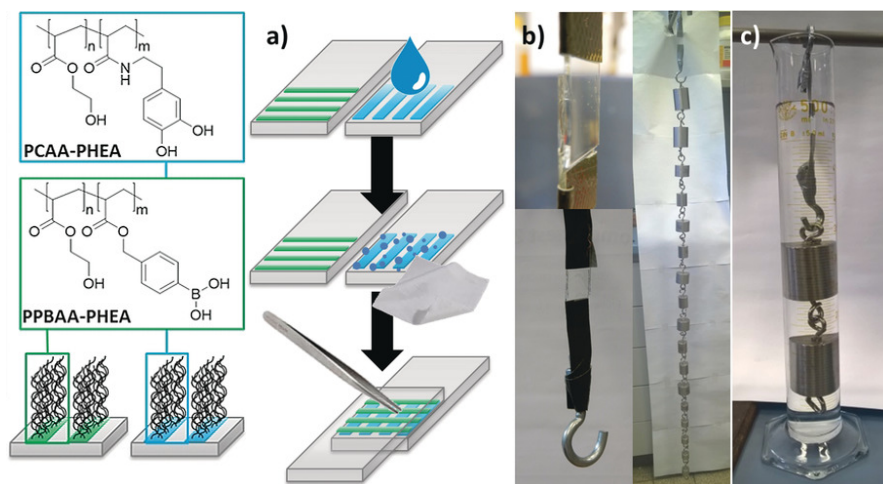
2

Figure 2.12: Polymer brushes can serve as an effective platform for supramolecular adhesives. Shown here are copolymers of phenylboronic acid acrylate (PPBAA) and catechol acrylamide (PCAA) with hydroxyethyl acrylate (PHEA). a) After preparation of the brush-coated surfaces, a drop of de-ionized water is placed on one of the surfaces, left to rest for 10 minutes and dried with tissue paper before placing the surfaces together for 30 minutes. This provides a favorable environment for the formation of dynamic covalent bonds between the boronic acid and catechol functionalities. [147] b) Close-up of adhering surfaces, and weight test using a chain of weights hanging on the glued surfaces. c) A similar weight test performed in water, indicating the water-resistant nature of the adhesive. Reproduced with permission from ref. 147. Copyright 2018 Wiley-VCH Verlag.

at the ways this phenomenon manifests in polymer brushes, and how this can be used in order to modify surface friction.

Although the two phenomena are somewhat different in origin, many of the properties that lend polymer brushes their low adhesion are also relevant to their lubricious properties. The internal osmotic pressure of the brush creates an opposing force to compression [154] and inclusions [134], reducing the degree to which a countersurface can be pressed into the brush, and consequently the contact area over which friction forces apply. Brush bilayers, contacts between two polymer brushes, can also serve as effective lubricants: while the osmotic pressure in two identical brushes is the same, the entropic cost of chain stretching limits brush interdigitation to a relatively narrow region
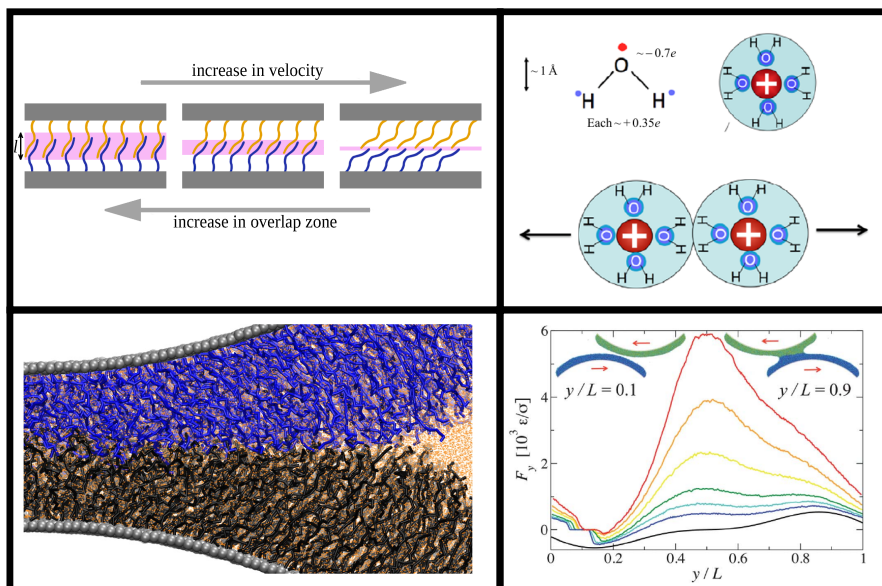
2

Figure 2.13: A selection of relevant mechanisms in friction and lubricity in polymer brush bilayers. Top left: Reduction of the interdigitation zone by chain tilting under shear. Reproduced from ref. 150, originally released under Creative Commons attribution (CC-BY) license. Top right: repulsion between hydration shells around solvated polymers. Reproduced from ref. 151, originally released under CC-BY license. Bottom left: chain tilting out of the point of contact between asperities. Reproduced from ref. 152. Copyright 2014 American Chemical Society. Bottom right: formation and movement of a meniscus between the brush-coated surfaces. Reproduced from ref. 153 with permission from the Royal Society of Chemistry.

near the center of the bilayer. [155] Since the interdigitation of chains in the contact area is an important source of adhesion hysteresis in brush bilayers, this helps reduce friction. Alternatively, this can be considered as a reduction in the effective contact area between the brush-covered surfaces. Moreover, the chains in a brush bilayer may tilt under shear, further reducing the width of the region where the brushes contact each other (see Figure 2.13, top left). [156]

Various types of dissipation mechanisms can determine the friction in brush bilayers in air, as was studied using molecular dynamics simulations. In these simulations, two opposing brush-coated cylinder sections are moved against each other in longitudinal, transverse and normal motion, simulating shear between

smooth surfaces, friction between colliding asperities, and compression. [153] Solvent molecules are included in the brushes, but no bulk solvent phase is present outside the brushes, meaning that these simulations are comparable to experiments in air at high relative humidity. The obtained friction scalings indicate that asperity collisions are qualitatively different from smooth-surface shearing, as transient interdigitation [157] of the polymer brushes becomes relevant in addition to steady-state interdigitation. Moreover, a meniscus forms between the two surfaces, creating adhesion hysteresis and thus friction as the point of contact moves over the cylindrical geometry and the meniscus changes shape. This phenomenon is particular to the system in air, and shows that friction between rough surfaces in humid air is qualitatively different from that in water. In a later study, the same authors studied similar systems containing two chemically distinct polymer brushes and two solvent types. It was found that for liquid-immersed systems, the curvature of the cylindrical surface allows chains to tilt away from the point of contact between the asperities, reducing interdigitation and thus friction. Similar behavior holds for systems "in air" when the two brushes are made immiscible, either by preferential absorption of immiscible solvents or by direct repulsion between the polymers. However, in miscible undersaturated systems, capillary contributions force the chains towards the contact and leading to increased friction. [152] Further simulations and experiments also support that dissipation is restricted when the opposing polymer brushes are immiscible, leading to lower friction. [10]

Lubricity

In addition to the various chain conformation and orientation effects discussed in the previous paragraphs, the interaction between polymer brushes and solvents contributes to the lubricity of swollen brushes, as demonstrated by Jacob Klein and coworkers in various works. Due to the aforementioned osmotic pressure, an organic solvent absorbed in a polymer brush resists squeeze-out even under high loads, and ensures the fluidity of the brush in the contact region. [158] Polyelectrolyte bilayers in water, however, display even stronger and more robust lubricity. [159] This has been attributed to a combination of increased osmotic pressure as a result of the presence of counterions, which would enhance the previously discussed effects, and enhanced repulsive interactions arising from the hydration shell around the charged polymer segments (see Figure 2.13. The hydration shell is tightly bound and stable, while remaining liquid even at short timescales due to the rapid exchange of water molecules between the hydration shell and the surrounding liquid. [151, 160]

2

Kobayashi et al. demonstrated low friction between a glass probe and a surface coated with the polyzwitterion poly(methacryloyl oxyethyl phosphoryl choline) (PMPC) in both water and humid air. Friction was found to decrease with relative humidity, and at high relative humidity (80%), the vapor-solvated system in fact displays lower friction that the liquid-solvated system. [8] This was attributed to the liquid-solvated chains being more extended, allowing them to form a larger contact area with the probe. Friction in liquid toluene, a poor solvent, was found to be comparatively high. This may be due to polymer chains adhering to the probe in order to reduce unfavorable PMPC-toluene contacts. When both the probe and the brush were functionalized with PMPC brushes, creating a bilayer scenario, similar trends were observed for the water and humid air cases. However, the system submerged in toluene displayed slightly lower friction than the system in liquid water. This was attributed to the reduced interdigitation between poorly solvated (hence collapsed) brushes. Followup studies including polycationic and polyanionic brushes in bilayer geometries found that the friction in these systems was lowest when submerged in water, although swelling by water vapors did reduce the friction relative to the dry state. [161, 162] It remains unclear why, out of the polymers discussed in these works, only PMPC displayed lower friction in humid air than in water, although the original authors point out the possibility of lubrication by an adsorbed water layer due to the superhydrophilic nature of PMPC. [161]

Strongly self-interacting hydrophobic polymers can also function as lubricants, depending on the intended countersurface. Bhairamadgi et al. present results on both friction and adhesion on polymer brush coatings, in which poly(ethyl methacrylate) and poly(2,2,2-trifluoroethyl methacrylate) are compared. In all cases, the fluorinated polymer displayed substantially lower adhesion and friction with a silica probe than its non-fluorinated counterpart, with the most pronounced differences for adhesion under humid conditions. [9] This was attributed primarily to the apolar, hydrophobic nature of the fluoropolymer, which reduces ab- and adsorption of ambient water, and hence prevents the formation of a water meniscus between the brush surface and the probe. Adhesion and friction were found to decrease with increasing molecular weight and grafting density of the brush, an observation consistent with the fact that the compressibility of the brush also tends to decrease with these parameters.

Switching Friction

A topic of technological interest for brushes in air is switchable friction. While we have already discussed the humidity dependence of friction behavior in var-
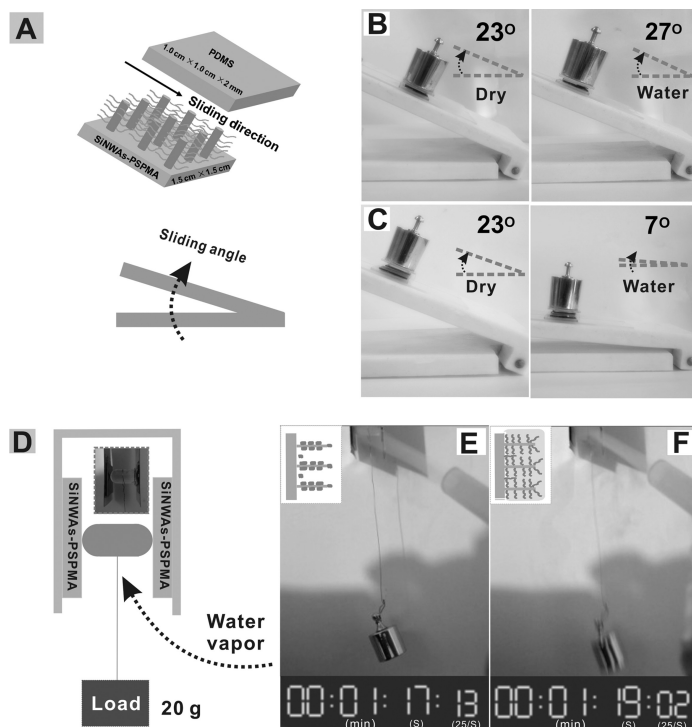
Figure 2.14: a) In ref. 163, the friction between a weighted PDMS surface and a PSPMA-functionalized silicon nanowire array (SiNWa) is tested by placing the system on an inclined plane and recording the angle at which the PDMS begins sliding. b) Sliding angle measurements in dry air and in the presence of water vapor for the bare silicon nanowire array, c) Sliding angle measurements for the PSPMA-functionalized SiNWa in dry air and in the presence of water vapor. The sliding angle in the presence of water vapor decreases significantly. d) Alternative testing setup, in which a piece of PDMS with an attached load is clamped between two PSPMA-functionalized SiNWa surfaces. e) and f) When water vapor is introduced to the system, the clamped PDMS quickly slides downward under gravity, indicating a rapid friction response. Reproduced with permission from ref. 163. Copyright 2014 Wiley-VCH Verlag.

ious brushes, a range of other switching mechanisms is available. For example, friction can be switched by changing the degree of interdigitation by external stimuli. [164] Moreover, Ma et al. demonstrated humidity-switchable friction of poly(sulfopropyl methacrylate) (PSPMA) brushes on a silicon nanowire array substrate (illustrated in figure 2.14, and showed that the collapse of the PSPMA brush by increasing the salt concentration ("salting out") can also be used to modify friction properties, with substantially increased friction for the salted-out brush. [163] The same study also demonstrated pH-dependent switching in poly(methacrylic acid) brushes. Liu et al. realized switchable friction in polymer brushes under humid (90% RH) air by grafting a PSPMA brush from a matrix containing photothermally responsive Fe_3O_4 particles. [165] Under near-infrared (NIR) irradiation, the thermogenic response of these particles resulted in the dehydration and collapse of the brush. This was paired with a change from low friction coefficients in the hydrated state, to high friction in the dehydrated state. Notably, rehydration upon switching off the NIR laser is rapid, on the order of seconds. Zeng et al. found that poly(allyloxy hydroxypropyl sulfonate) brushes in humid air can be reversibly collapsed using an external electric field. [166] In their collapsed state, these brushes display reduced friction relative to their extended state. While the friction coefficients reported in this work are comparatively high, the demonstration of electro-switchable friction is of particular technological relevance.

Outlook on Adhesion and Friction control

The general concepts underlying friction and adhesion in polymer brushes appear to be comparatively well-understood. As a result, many of the works reviewed here are focused on optimizing brush chemistry and architecture. However, the effects of relative humidity and the exact solvation state of the polymer will also impact friction and adhesion. As discussed in section 2.2, Goedel et al. showed that partially solvated brushes are parabolic (i.e. well-solvated) at the brush-air interface, but retain a constant density closer to the substrate. [55] As a result, the outer surface of the brush may be considerably solvated even when the bulk is dry, resulting in a non-linear effect of solvent uptake on the mechanical properties of the brush. Quantifying this will be of great interest for optimizing application conditions for brush-based adhesives and lubricants. Finally, due to the stresses inherently involved in mechanical applications, the stability of polymer brushes is a particular concern in friction control applications.

2

Wetting control

As highly tunable surfaces with potentially switchable properties, polymer brushes can be used for tuning a wide variety of surface interactions. Controlling the wetting behavior of drops and liquid films on surfaces is an example that is specific to three-phase systems, most notably surfaces in air. While non-grafted polymer coatings can effectively modify surface interactions, surface anchoring provides stability under highly solvated conditions. Here, we discuss how polymer brushes can be applied to control surface wetting, and how their properties can lead to non-classical wetting phenomena.

The classical description of partial wetting, i.e. drops on surfaces, is given by the Young equation $\gamma_{sv} \cos\theta + \gamma_{sl} - \gamma_{lv} = 0$, where the drop is considered as a spherical cap with a base angle of θ, γ_{ij} denotes the surface tension between phases i and j, and the subscripts s, l and v indicate the solid surface, the liquid and the surrounding vapor. When no value of θ satisfies this expression, either total wetting ($\theta = 0$) or complete dewetting ($\theta = 180$) occurs. This expression follows from a balance of lateral forces acting on the three-phase contact line. However, it assumes that the surface does not undergo any structural changes in response to wetting, and neglects the vertical component of the liquid-vapor surface tension under the assumption that the solid is perfectly rigid. Neither of these assumptions is necessarily valid for polymer brushes. Brushes may swell in the presence of the solvent, changing their volume, composition and entropic elasticity. Moreover, polymeric materials can be unusually soft. As a result, the vertical force applied by the liquid-vapor interface may deform the surface, pulling it upwards to form a "wetting ridge" near the three-phase contact line. In more extreme cases, the system may even deform on the length scale of the droplet, resulting in Neumann wetting. However, this has mostly been observed in extremely soft gels, rather than brushes. [167, 168]

Effects of Brush Parameters on Wetting State

One interesting aspect of wetting in polymer brushes is that only partial wetting is observed for many combinations of polymers and good solvents, when complete wetting might be expected based on classical arguments of solvation energy. Cohen Stuart et al. investigated this phenomenon through self-consistent field studies and experimental contact angle measurements, and propose an explanation based on the interaction between polymers and the liquid-air interface. Based on the surface activity of many water-soluble polymers, they suggest that the free end of polymer chains in the brush may adsorb

at the liquid-air interface that is formed by a droplet on the surface despite being in a good solvent. Since releasing the adsorbed chain from the surface would increase the interfacial energy, this creates a (local or global) minimum in the free energy at a finite contact angle, stabilizing the partial wetting state. [57]

The wetting behavior of polymer melts on brushes forms a noteworthy example of the non-classical wetting behavior of brushes. First, we discuss the case of chemically identical melts and brushes. Maas et al. studied this situation for a variety of grafting densities, grafted chain lengths and melt chain lengths using a scaling theory, self-consistent field calculations, and AFM imaging of a polystyrene melt/brush system. [169] On a substrate that is partially wet by the polymer melt, a low density of grafted chains (below the critical density for brush formation) induces a transition to complete wetting. This is the result of a tradeoff between the free energy of the grafted chains, which gain entropy and reduce their surface energy by interacting with the melt, and that of the melt polymers, which lose entropy as their movement and conformation are restricted by the presence of the surface. This complete wetting regime persists as grafting densities increase and the system becomes brush-like, as one might expect for a chemically identical surface and liquid. However, an upper grafting density exists at which the brush becomes too dense to accommodate the melt chains. At this point, the brush behaves approximately as an energetically neutral hard surface, which once again results in partial wetting by the melt, [170] a phenomenon known as autophobicity. The loss of entropy at the brush-melt interface had previously been reported by Reiter and Khanna. [171] Moreover, the lower and upper grafting density limits for complete wetting are expected to meet for very long melt chains, meaning that the melt will always partially wet the surface. However, this was not experimentally observed, which was attributed to metastability of the thick melt layer. In fact, a self-consistent field study by Matsen and Gardiner suggests that complete wetting may always be a metastable state. [172] While this is a difficult claim to test, X-ray reflectivity results for a polystyrene melt/brush system by Zhang et al. show an approximate quantitative match with this self-consistent field theory. [173]
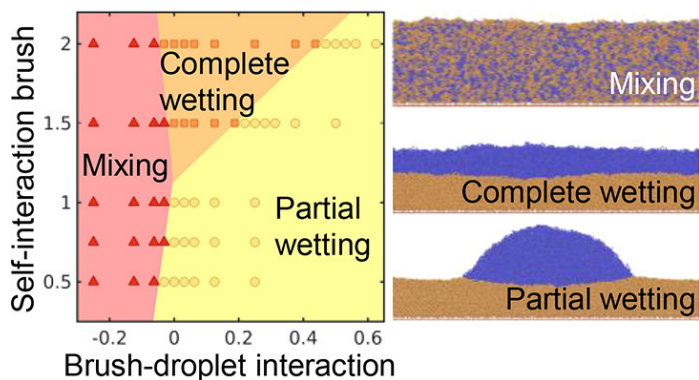
Figure 2.15: Phase diagram of wetting behavior for an oligomer droplet on a polymer brush as a function of the polymer self-attraction and the polymer-droplet interaction energy; the case of a chemically identical brush and drop is found on the vertical line at 0. Conventionally, mixing would be expected for all non-positive interaction energies, but an additional attraction is required due to autophobicity effects. Reproduced from ref. 174. Copyright 2019 American Chemical Society.

Mensink et al. investigated the case of chemically distinct melts on brushes through coarse-grained molecular dynamics simulations. [174, 175] This resulted in a phase diagram distinguishing partial wetting, complete wetting, and mixing of the melt and brush as a function of the brush-melt interchange energy (a quantity linear with the Flory-Huggins parameter, as discussed in section 2.2) and the brush self-interaction strength. While the general shape of the phase diagram (shown in Figure 2.15) was well described by a classical enthalpic approach, the exact position of phase boundaries deviated due to the negative excess entropy at the brush-melt interface. Moreover, entropic contributions result in significant deviations of the contact angle from Young's law in the partial wetting regime. [174] Transitions between partial wetting, complete wetting and mixing are also strongly influenced by the chain length of the melt polymers, with shorter chains favoring complete wetting and mixing. This is explained by the fact that shorter chains gain substantially more translational entropy from the additional accessible volume than longer chains. [175] Finally, for weak brush self-interactions, resulting in a mechanically soft brush, no transition to Neumann behavior was observed. This contrasts with similar simulations of polymeric drops on soft gels by Cao and Dobrynin, in which brush-drop contact angles decreased as the gel became softer and a Neumann regime was reached. [167]

Switching the Wetting State

As discussed in previous sections on the different applications, switchable surface properties can be produced by various types of brush chemistry and architecture, which can be utilized to switch the wetting state for brushes as well. For example, thermal switching can be achieved by lower critical solution temperature polymers such as PNIPAm, which is hydrophilic at room temperature but transitions to a hydrophobic state around 32°C. [176] Sun et al. employed PNIPAm brushes on rough surfaces to enhance this effect and create switchability between a superhydrophilic and superhydrophobic state. [177] Ionic strength and pH are another widely applicable switching mechanism. Fielding et al. demonstrated reversible wettability switching in brushes of several weak polybases, using protonation by HCl vapors as the switching mechanism. In their initial deprotonated state, these brushes are hydrophobic, and display correspondingly high water contact angles. Upon protonation by HCl, the brushes become charged and hydrophilic, displaying a moderately hydrophilic contact angle. Sun et al. [178] synthesized brushes containing both poly(methacrylic acid) (PMAA) and basic PDMAEMA in random copolymer, block copolymer, and "V-shaped" polymer architectures, with the latter indicating a PMAA block and a PDMAEMA block anchored to the substrate at the same point by a surface-reactive block in the middle of the chain. [179] After exposure to acidic or basic environments, resulting in protonation of the PDMAEMA block or deprotonation of the PMAA block respectively, these brushes displayed very low contact angles with aqueous solutions of the same pH as the switching solution. For approximately neutral pH, however, the copolymer is uncharged, and behaves hydrophobically. Demirci et al. produced polymer brushes of the ionic liquid 1-vinyl-3-buthylimidazolium bromide functionalized with cyclodextrin, a common host group in supramolecular chemistry. Anion exchange, in which the bromide was replaced with the highly cyclodextrin-compatible bis(trifluoromethane)sulfonimide ion, resulted in a switch from hydrophilic to hydrophobic wetting behavior. [180] This may be due to the tighter binding of counterions to the polymer chains via the host-guest interaction, weakening the ionic character of the brush.
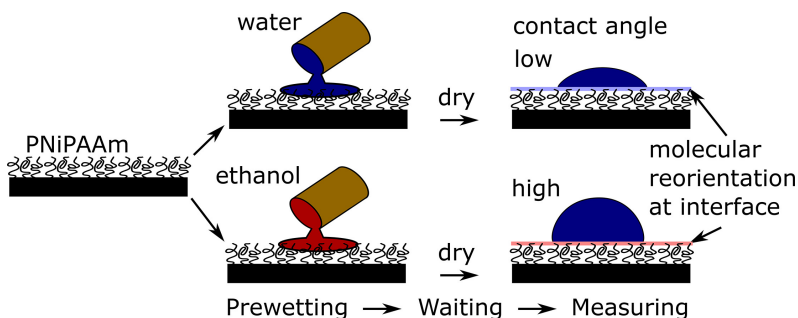
Figure 2.16: The prior wetting history of PNIPAm brushes has a persistent effect on the orientation of functional groups at the brush-air interface, resulting in differences in wetting behavior. Reproduced from ref. 181, with permission from Elsevier.

Schubotz et al. show not only switchability of the water contact angle on PNIPAm brushes by prior wetting with water or ethanol, but also observe a long-term memory effect. [181] As qualitatively illustrated in figure 2.16, pre-wetting with water results in a reduction of the water contact angle in the wetted area, whereas pre-wetting with ethanol increases the water contact angle, leading to a range of (advancing) contact angles from 25° to 65° on otherwise identical brush samples. This effect persisted after drying the brush and for periods of months. The memory effect is attributed to the rearrangement of PNIPAm at the surface in response to different solvent conditions, resulting in the exposure of either the amide side group or the alkane backbone. This rearrangement is confirmed by sum frequency generation spectroscopy.
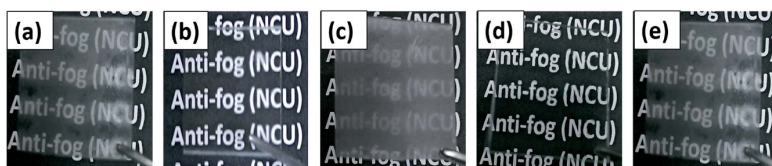

Figure 2.17: Antifogging properties of polyelectrolyte brushes. a) untreated glass; b) superhydrophilic (thin) PSBMA brush; c) hydrophilic (thick) PSPBA brush; d) superhydrophilic PSBVI brush; e) hydrophilic PSBVI brush. Reproduced from ref. 182 with permission from the Royal Society of Chemistry.

Anti-fogging and Anti-icing

An everyday application of wetting control is found in anti-fogging and anti-icing surfaces. The formation of small water droplets or ice crystals on surfaces can be a problem when the surfaces in question are e.g. glasses, windows or optical instruments. By scattering incident light, such drops or crystals reduce the light transmission and visibility through a surface. Interestingly, both hydrophobic [183] and hydrophilic [184] surfaces are suitable for anti-fogging applications, since hydrophobic surfaces repel water altogether and strongly hydrophilic ones favor complete wetting, leading to the formation of a continuous liquid film. Howarter and Youngblood combined self-cleaning and anti-fogging properties on one surface using a brush of PEG chains capped with perfluorinated alkane segments. These brushes rearrange to present PEG segments at their surface in an aqueous or humid environment, and fluorinated segments when in contact with organics, tested in this study with hexadecane. [185] Due to the low adhesion of hexadecane to the fluorinated surface and the hydrophilicity of PEG, the organic droplets could be removed from the surface by submersion in water. Ezzat and Huang investigated anti-fogging and anti-icing properties using poly(sulfobetaine methacrylate (PSBMA) and poly(sulfobetaine vinylimidazole) (PSBVI) brushes of different thicknesses. [182] Thin brush layers of these polyzwitterions were found to be more hydrophilic than thicker ones, an effect attributed to self-association of the ionic groups in the brush [186] and related to the anomalous swelling of sulfobetaine-functionalized polymers observed in ref. 28 (see section 2.2). Both of the superhydrophilic thin brushes were found to display strong anti-fogging and anti-icing properties, with the anti-fogging effect shown in Figure 2.17. The anti-icing properties of the thinner brushes were attributed to their low surface roughness, providing minimal nucleation points for nucleation of ice growth. [182] Anti-fogging and anti-icing have been observed in a variety of other polyelectrolyte and polyzwitterionic coatings due to their hydrophilic nature. [187, 188] It has also been suggested that bound water in the surface layer of brush coatings contributes to anti-icing by reducing the adhesion of ice on the brush surface. [189, 190]

Wetting Dynamics

The responsive character of brushes influences the dynamics of wetting as well. Shiomoto et al. studied wetting by water drops on a substrate patterned with hydrophilic PSPMA brush and hydrophobic fluoroalkylsilane monolayer stripes

using optical microscopy, dying the water and the PSPMA brush for contrast. They found that this setup also facilitates visualization of the precursor film, the microscopically thin layer that spreads ahead of the macroscopic contact line when a liquid wets a surface. [191] The spreading of the drop itself was found to follow a classical Tanner's law time scaling to within reasonable corrections. However, the precursor film dynamics displayed two different regimes: the exact time scaling exponent depends on the liquid volume at the start of the experiment, but always transitions to an exponent of 0.6 for longer times. This was suggested to mark the transition from an adiabatic precursor film, where spreading is accelerated by the conversion of potential to kinetic energy in the flattening of the liquid drop, to a diffusive precursor film, which spreads purely under surface forces. However, the diffusive spreading exponent still differs from the classical value of 0.5 for general surfaces. [192] The proposed mechanism underlying this is a combination of the large hydration energy of the brush driving wetting and energy dissipation by chain stretching slowing down the front. The precise origin of this scaling remains to be determined, however. Etha et al. used molecular dynamics to study a similar system, consisting of a brush wet by a drop of chemically identical oligomers. They identified a time scaling $r \sim t^{1/4}$ and an equilibrium drop radius of $r_\text{eq} \sim \rho_\text{g}^{-1/3}$, consistent with a scaling approach in which the capillary driving force is balanced by viscoelastic forces resulting from the drop-substrate interaction. [193] Moreover, they investigate the swelling dynamics of polymer chains as a function of grafting density via the brush height in the early stages of the wetting process, and find that the initial swelling response follows an approximate power law $h \sim t^\delta$, where the exponent δ is typically smaller than unity and decreases as the grafting density of the brush increases, resulting in the intuitive conclusion that denser brushes display a slower swelling response. Thiele and Hartmann developed a model for the spreading of a drop on a polymer brush, based on gradient dynamics on a free energy expression accounting for capillary effects, brush wetting and brush elasticity. [194] The dynamics are simplified to hydrodynamics within the drop, exchange of solvent between the brush and the drop, and diffusion within the brush, meaning that transport within the droplet and the brush are not coupled. The mesoscopic contact angles (Neumann angles at the approximate three-phase point) are found to evolve exponentially towards their equilibrium value, in accordance with other theoretical work, but show complex dynamics on short timescales as a result of the interplay between swelling, wetting and hydrodynamics.

Outlook on Wetting Control

Since wetting is inherently tied to surface energy, fundamental results and experimental possibilities are closely linked in this context. Improving our understanding of the structure and width of the brush-air interface could provide additional, non-chemical parameters for tuning wetting behavior. Moreover, sorption kinetics in polymer brushes are not thoroughly explored. The various works on wetting dynamics we discuss all clearly illustrate the relevance of the brush swelling kinetics, suggesting a need for further research. This could also help in determining the relative importance of brush swelling, diffusion through the brush and hydrodynamics in wetting dynamics, which would enable predictions of wetting dynamics in experimental systems.

2.4 Conclusion

In this chapter, we have provided an overview of the state of the art with respect to polymer brushes in air, and we identified promising future avenues of research. On the fundamental side, many important results for brushes in liquid appear to extend to brushes under vapors as well. However, some open questions specific to the gas phase remain. The structure of the brush-air interface and the associated surface energy are a particularly relevant example, as e.g. wetting behavior and mechanical properties of brush-functionalized surfaces will likely be dominated by the interfacial region of the brush. We anticipate that recently developed synthesis routes to fluorescently label brush polymers, [195, 196] can provide new insights on interfacial compositions for brushes in air. Additionally, predicting free volume within the brush is still a challenge. As illustrated by various results discussed in section 2.2 (for instance: refs. 12 and 36), free space within the brush alters the thermodynamics of vapor sorption and the brush response dramatically. This also touches on the topic of brush dynamics and kinetics: while the equilibrium behavior of polymer brushes is understood to a reasonable degree, effects such as solvent-induced glass transitions and vapor sorption kinetics have not been documented as thoroughly. Both of these topics are closely related to mobility and relaxation times of the brush, suggesting this as an avenue of further research. This is not only of great theoretical interest, as it relates to the ongoing research into polymeric glass transitions in general, but also of practical importance, since response times are at least as important as equilibrium behavior in switchability and sensing applications.

Despite the open fundamental questions, the works featured in the second half of this chapter show that useful and innovative applications of polymer brushes in air are already possible. Scaling these applications up beyond laboratory demonstrations remains a challenge, however. Novel techniques for applying polymer brush coatings are needed to make large-scale application feasible. Grafting-to methods remain somewhat restrictive with respect to brush architecture and grafting density, whereas the most common grafting-from strategies (surface-initiated radical polymerizations) usually require an oxygen-free environment. Additionally, both strategies only effectively utilize a small fraction of the monomer or polymer content of the reaction mixture. The use of e.g. oxygen-consuming additives [197] or filter paper-assisted surface-initiated Cu0-mediated polymerizations [188] could make grafting-from in air possible, with the added benefit that the polymerization naturally terminates once the oxygen consumer is exhausted. This could allow for control of the approximate chain length via the composition of the reaction mixture. Relatedly, brush coatings in practical settings will need to be stable under fluctuations in temperature and chemical environment, and possibly under mechanical stresses, all of which may be large depending on the intended application. Many anchoring strategies do not yet meet this criterion, leading to degrafting [198–201] even under relatively mild conditions in humid air. [32] While this issue is relatively well-known and research on stable anchoring strategies is ongoing, [202–204] further developments may be necessary to realize robust brush coatings.

Notwithstanding the remaining challenges, we are optimistic about the state of research on polymer brushes in air. Firstly, the works cited in this chapter clearly show the potential utility of brush-based technologies in the gas phase. Additionally, many of the fundamental questions we raise are closely related to outstanding questions in broader polymer (brush) research. We see this as indicative of the maturing of brush-in-air research, and are excited to see the further development of this subject.

Acknowledgements

2.5 References

[1] L. Li, J. Li, and C. M. Lukehart, "Graphitic carbon nanofiber-poly(acrylate) polymer brushes as gas sensors", Sens. Actuators, B **130**, 783 – 788 (2008), URL http://www.sciencedirect.com/science/article/pii/S0925400507008738.

[2] H. C. McCaig, E. Myers, N. S. Lewis, and M. L. Roukes, "Vapor sensing characteristics of nanoelectromechanical chemical sensors functionalized using surface-initiated polymerization", Nano Lett. **14**, 3728–3732 (2014), URL https://doi.org/10.1021/nl500475b, pMID: 24922358.

[3] Y. Wang, J. Chen, C. Zhu, B. Zhu, S. Jeong, Y. Yi, Y. Liu, J. Fiadorwu, P. He, and X. Ye, "Kinetically controlled self-assembly of binary polymer-grafted nanocrystals into ordered superstructures via solvent vapor annealing", Nano Lett. **21**, 5053–5059 (2021), URL https://doi.org/10.1021/acs.nanolett.1c00890, pMID: 34101469.

[4] R. Lundy, P. Yadav, N. Prochukhan, E. C. Giraud, T. F. O'Mahony, A. Selkirk, E. Mullen, J. Conway, M. Turner, S. Daniels, P. G. Mani-Gonzalez, M. Snelgrove, J. Bogan, C. McFeely, R. O'Connor, E. McGlynn, G. Hughes, C. Cummins, and M. A. Morris, "Precise definition of a "monolayer point" in polymer brush films for fabricating highly coherent tio2 thin films by vapor-phase infiltration", Langmuir **36**, 12394–12402 (2020), URL https://doi.org/10.1021/acs.langmuir.0c02512, pMID: 33021792.

[5] H. Yang, H. Zhu, M. M. R. M. Hendrix, N. J. H. G. M. Lousberg, G. de With, A. C. C. Esteves, and J. H. Xin, "Temperature-triggered collection and release of water from fogs by a sponge-like cotton fabric", Adv. Mater. (Weinheim, Ger.) **25**, 1150–1154 (2013), URL https://onlinelibrary.wiley.com/doi/abs/10.1002/adma.201204278.

[6] X. Liu, Y. Li, J. Hu, J. Jiao, and J. Li, "Smart moisture management and thermoregulation properties of stimuli-responsive cotton modified with polymer brushes", RSC Adv. **4**, 63691–63695 (2014), URL http://dx.doi.org/10.1039/C4RA11080C.

[7] M. Messerschmidt, A. Janke, F. Simon, C. Hanzelmann, T. Riske, M. Stamm, B. Raether, O. da Costa e Silva, and P. Uhlmann,

2

"Fluorocarbon-free dual-action textile finishes based on covalently attached thermoresponsive block copolymer brush coatings", ACS Appl. Mater. Interfaces **10**, 40088–40099 (2018), URL `https://doi.org/10.1021/acsami.8b11448`.

[8]   M. Kobayashi, Y. Terayama, N. Hosaka, M. Kaido, A. Suzuki, N. Yamada, N. Torikai, K. Ishihara, and A. Takahara, "Friction behavior of high-density poly(2-methacryloyloxyethyl phosphorylcholine) brush in aqueous media", Soft Matter **3**, 740–746 (2007), URL `http://dx.doi.org/10.1039/B615780G`.

[9]   N. S. Bhairamadgi, S. P. Pujari, F. A. M. Leermakers, C. J. M. van Rijn, and H. Zuilhof, "Adhesion and friction properties of polymer brushes: Fluoro versus nonfluoro polymer brushes at varying thickness", Langmuir **30**, 2068–2076 (2014), URL `https://doi.org/10.1021/la404915k`, pMID: 24555721.

[10]   S. De Beer, E. Kutnyanszky, P. M. Schön, G. J. Vancso, and M. H. Müser, "Solvent-induced immiscibility of polymer brushes eliminates dissipation channels", Nat. Commun. **5**, 3781 (2014).

[11]   L. Sun, B. Akgun, R. Hu, J. F. Browning, D. T. Wu, and M. D. Foster, "Scaling behavior and segment concentration profile of densely grafted polymer brushes swollen in vapor", Langmuir **32**, 5623–5628 (2016), URL `https://doi.org/10.1021/acs.langmuir.6b00845`, pMID: 27172089.

[12]   M. Wagman, S. Medalion, and Y. Rabin, "Anomalous swelling of polymer monolayers by water vapor", Macromolecules **45**, 9517–9521 (2012), URL `https://doi.org/10.1021/ma3018553`.

[13]   M. Ballauff and O. Borisov, "Polyelectrolyte brushes", Curr. Opin. Colloid Interface Sci. **11**, 316–323 (2006).

[14]   S. Das, M. Banik, G. Chen, S. Sinha, and R. Mukherjee, "Polyelectrolyte brushes: theory, modelling, synthesis and applications", Soft Matter **11**, 8550–8583 (2015).

[15]   E. van Andel, S. C. Lange, S. P. Pujari, E. J. Tijhaar, M. M. J. Smulders, H. F. J. Savelkoul, and H. Zuilhof, "Systematic comparison of zwitterionic and non-zwitterionic antifouling polymer brushes on a bead-based platform", Langmuir **35**, 1181–1191 (2019).

[16] S.-i. Yamamoto, J. Pietrasik, and K. Matyjaszewski, "Temperature- and ph-responsive dense copolymer brushes prepared by atrp", Macro- molecules **41**, 7013–7020 (2008).

[17] A. Chakrabarti, "Monte carlo study of pancake to brush transition", J. Chem. Phys. **100**, 631–635 (1994), URL https://doi.org/10.1063/1. 466925.

[18] W. J. Brittain and S. Minko, "A structural definition of polymer brushes", J. Polym. Sci., Part A: Polym. Chem. **45**, 3505–3512 (2007), URL https: //onlinelibrary.wiley.com/doi/abs/10.1002/pola.22180.

[19] T. Wu, K. Efimenko, and J. Genzer, "Combinatorial study of the mushroom-to-brush crossover in surface anchored polyacrylamide", J. Am. Chem. Soc. **124**, 9394–9395 (2002), URL https://doi.org/10. 1021/ja027412n, pMID: 12167033.

[20] We point out that these structures are not micelles by the typical defi- nition, since their formation does not require any variation of chemistry over the polymer chain. However, we adhere to the historic terminology.

[21] D. Williams, "Grafted polymers in bad solvents: octopus surface micelles", J. Phys. II **3**, 1313–1318 (1993), URL https://hal. archives-ouvertes.fr/jpa-00247908.

[22] B. Zdyrko and I. Luzinov, "Polymer brushes by the "grafting to" method", Macromol. Rapid Commun. **32**, 859–869 (2011), URL https: //onlinelibrary.wiley.com/doi/abs/10.1002/marc.201100162.

[23] J. O. Zoppe, N. C. Ataman, P. Mocny, J. Wang, J. Moraes, and H.-A. Klok, "Surface-initiated controlled radical polymerization: State-of-the- art, opportunities, and challenges in surface and interface engineering with polymer brushes", Chem. Rev. (Washington, DC, U. S.) **117**, 1105– 1318 (2017), URL https://doi.org/10.1021/acs.chemrev.6b00314, pMID: 28135076.

[24] S. Ma, X. Zhang, B. Yu, and F. Zhou, "Brushing up functional materials", NPG Asia Mater. **11**, 24 (2019).

[25] F. Brochard-Wyart and P. G. De Gennes, "Controlled swelling of polymer brushes", Macromol. Symp. **79**, 1–16 (1994), URL https: //onlinelibrary.wiley.com/doi/abs/10.1002/masy.19940790103.

[26] K. N. Jayachandran, P. R. Chatterji, and J. M. Prausnitz, "Vapor-liquid equilibria for solutions of brush poly(methyl methacrylate) in chloroform", Macromolecules **31**, 2375–2377 (1998), URL `https://doi.org/10.1021/ma971023+`.

[27] M. Biesalski and J. Rühe, "Swelling of a polyelectrolyte brush in humid air", Langmuir **16**, 1943–1950 (2000), URL `https://doi.org/10.1021/la990863+`.

[28] C. J. Galvin, M. D. Dimitriou, S. K. Satija, and J. Genzer, "Swelling of polyelectrolyte and polyzwitterion brushes by humid vapors", J. Am. Chem. Soc. **136**, 12737–12745 (2014), URL `https://doi.org/10.1021/ja5065334`, pMID: 25134061.

[29] C. J. Galvin and J. Genzer, "Swelling of hydrophilic polymer brushes by water and alcohol vapors", Macromolecules **49**, 4316–4329 (2016), URL `https://doi.org/10.1021/acs.macromol.6b00111`.

[30] S. V. Orski, R. J. Sheridan, E. P. Chan, and K. L. Beers, "Utilizing vapor swelling of surface-initiated polymer brushes to develop quantitative measurements of brush thermodynamics and grafting density", Polymer **72**, 471–478 (2015), URL `https://www.sciencedirect.com/science/article/pii/S0032386115004723`, macromolecular Engineering - Dedicated to Professor Krzysztof Matyjaszewski on the Occasion of his 65th Birthday.

[31] T. M. Birshtein and Y. V. Lyatskaya, "Theory of the collapse-stretching transition of a polymer brush in a mixed solvent", Macromolecules **27**, 1256–1266 (1994), URL `https://doi.org/10.1021/ma00083a028`.

[32] M. Brió Pérez, M. Cirelli, and S. de Beer, "Degrafting of polymer brushes by exposure to humid air", ACS Appl. Polym. Mater. **2**, 3039–3043 (2020), URL `https://doi.org/10.1021/acsapm.0c00474`.

[33] G. C. Ritsema van Eck, L. B. Veldscholte, J. H. W. H. Nijkamp, and S. de Beer, "Sorption characteristics of polymer brushes in equilibrium with solvent vapors", Macromolecules **53**, 8428–8437 (2020), URL `https://doi.org/10.1021/acs.macromol.0c01637`.

[34] P. Schroeder, "Über erstarrungs- und quellungserscheinungen von gelatine", Z. Phys. Chem., Stoechiom. Verwandtschaftsl. **45U**, 117 – 75 (1903).

[35] V. A. Davankov and A. V. Pastukhov, "Swelling of crosslinked polymers in liquids and vapors. rational explanation of thermodynamic paradoxes", Z. Phys. Chem. (Muenchen, Ger.) **228**, 691–710 (2014), URL `https://doi.org/10.1515/zpch-2013-0497`.

[36] A. Laschitsch, C. Bouchard, J. Habicht, M. Schimmel, J. Rühe, and D. Johannsmann, "Thickness dependence of the solvent-induced glass transition in polymer brushes", Macromolecules **32**, 1244–1251 (1999), URL `https://doi.org/10.1021/ma980743t`.

[37] S. Christau, S. Thurandt, Z. Yenice, and R. Von Klitzing, "Stimuli-responsive polyelectrolyte brushes as a matrix for the attachment of gold nanoparticles: The effect of brush thickness on particle distribution", Polymers (Basel, Switz.) **6**, 1877–1896 (2014), URL `https://www.mdpi.com/2073-4360/6/7/1877`.

[38] X. J. Zhao, Z. F. Gao, and Z. Y. Jiang, "A study of hcl gas adsorption/desorption properties of pnipam brushes", Macromol. Theory Simul. **24**, 460–467 (2015), URL `https://onlinelibrary.wiley.com/doi/abs/10.1002/mats.201500027`.

[39] S. Brunauer, L. S. Deming, W. E. Deming, and E. Teller, "On a theory of the van der waals adsorption of gases", J. Am. Chem. Soc. **62**, 1723–1732 (1940), URL `https://doi.org/10.1021/ja01864a025`.

[40] R. Koehler, R. Steitz, and R. von Klitzing, "About different types of water in swollen polyelectrolyte multilayers", Adv. Colloid Interface Sci. **207**, 325–331 (2014), URL `https://www.sciencedirect.com/science/article/pii/S0001868614000037`, special Issue: Helmuth Möhwald Honorary Issue.

[41] C. M. Domínguez, P. M. Kosaka, G. Mokry, V. Pini, O. Malvar, M. del Rey, D. Ramos, A. San Paulo, J. Tamayo, and M. Calleja, "Hydration induced stress on dna monolayers grafted on microcantilevers", Langmuir **30**, 10962–10969 (2014), URL `https://doi.org/10.1021/la501865h`, pMID: 25148575.

[42] X.-J. Zhao, Z.-F. Gao, and Z.-Y. Jiang, "A theoretical investigation on anomalous switching of single-stranded deoxyribonucleic acid (ssDNA) monolayers by water vapor", Chin. Phys. B **24**, 044701 (2015), URL `https://doi.org/10.1088/1674-1056/24/4/044701`.

[43] O. Löhmann, S. Micciulla, O. Soltwedel, E. Schneck, and R. von Klitzing, "Swelling behavior of composite systems: Mutual effects between polyelectrolyte brushes and multilayers", Macromolecules **51**, 2996–3005 (2018), URL `https://doi.org/10.1021/acs.macromol.8b00359`.

[44] S. T. Milner, T. A. Witten, and M. E. Cates, "Theory of the grafted polymer brush", Macromolecules **21**, 2610–2619 (1988), URL `https://doi.org/10.1021/ma00186a051`.

[45] B. Zhao and W. Brittain, "Polymer brushes: surface-immobilized macromolecules", Prog. Polym. Sci. **25**, 677–710 (2000), URL `https://www.sciencedirect.com/science/article/pii/S0079670000000125`.

[46] P. Auroy, L. Auvray, and L. Léger, "Characterization of the brush regime for grafted polymer layers at the solid-liquid interface", Phys. Rev. Lett. **66**, 719–722 (1991), URL `https://link.aps.org/doi/10.1103/PhysRevLett.66.719`.

[47] L. Sun, B. Akgun, S. Narayanan, Z. Jiang, and M. D. Foster, "Surface fluctuations of polymer brushes swollen in good solvent vapor", Macromolecules **49**, 7308–7313 (2016), URL `https://doi.org/10.1021/acs.macromol.6b01081`.

[48] I. Coluzza and J.-P. Hansen, "Transition from highly to fully stretched polymer brushes in good solvent", Phys. Rev. Lett. **100**, 016104 (2008), URL `https://link.aps.org/doi/10.1103/PhysRevLett.100.016104`.

[49] A. Skvortsov, I. Pavlushkov, A. Gorbunov, Y. Zhulina, O. Borisov, and V. Pryamitsyn, "Structure of densely grafted polymeric monolayers", Polym. Sci. U.S.S.R. **30**, 1706–1715 (1988), URL `https://www.sciencedirect.com/science/article/pii/0032395088903930`.

[50] S. T. Milner, "Polymer brushes", Science **251**, 905–914 (1991), URL `https://science.sciencemag.org/content/251/4996/905`.

[51] A. Karim, S. K. Satija, J. F. Douglas, J. F. Ankner, and L. J. Fetters, "Neutron reflectivity study of the density profile of a model end-grafted polymer brush: Influence of solvent quality", Phys. Rev. Lett. **73**, 3407–3410 (1994), URL `https://link.aps.org/doi/10.1103/PhysRevLett.73.3407`.

2

[52] A. Halperin, M. Kröger, and F. M. Winnik, "Poly(n-isopropylacrylamide) phase diagrams: Fifty years of research", Angew. Chem., Int. Ed. **54**, 15342–15367 (2015), URL https://onlinelibrary.wiley.com/doi/abs/10.1002/anie.201506663.

[53] M. Ballauff and O. V. Borisov, "Phase transitions in brushes of homopolymers", Polymer **98**, 402–408 (2016), URL https://www.sciencedirect.com/science/article/pii/S0032386116303810, special Issue: Polymer Brushes.

[54] R. A. Gumerov and I. I. Potemkin, "Swelling of Planar Polymer Brushes in Solvent Vapors", Polym. Sci., Ser. C **60**, 66–75 (2018).

[55] W. A. Goedel, P. Eibeck, and H. Xu, "Thermodynamics of a partially swollen polymer brush", Macromolecules **35**, 801–807 (2002), URL https://doi.org/10.1021/ma011197y.

[56] J. Lu, T. Su, R. Thomas, J. Penfold, and R. Richards, "The determination of segment density profiles of polyethylene oxide layers adsorbed at the air-water interface", Polymer **37**, 109–114 (1996), URL https://www.sciencedirect.com/science/article/pii/0032386196816053.

[57] M. A. Cohen Stuart, W. M. de Vos, and F. A. M. Leermakers, "Why surfaces modified by flexible polymers often have a finite contact angle for good solvents", Langmuir **22**, 1722–1728 (2006), URL https://doi.org/10.1021/la052720v, pMID: 16460097.

[58] L. P. Kreuzer, T. Widmann, N. Hohn, K. Wang, L. Bießmann, L. Peis, J.-F. Moulin, V. Hildebrand, A. Laschewsky, C. M. Papadakis, and P. Müller-Buschbaum, "Swelling and exchange behavior of poly(sulfobetaine)-based block copolymer thin films", Macromolecules **52**, 3486–3498 (2019), URL https://doi.org/10.1021/acs.macromol.9b00443.

[59] C. Geiger, J. Reitenbach, L. P. Kreuzer, T. Widmann, P. Wang, R. Cubitt, C. Henschel, A. Laschewsky, C. M. Papadakis, and P. Müller-Buschbaum, "Pmma-b-pnipam thin films display cononsolvency-driven response in mixed water/methanol vapors", Macromolecules **54**, 3517–3530 (2021), URL https://doi.org/10.1021/acs.macromol.1c00021.

[60] L. A. Smook, G. C. Ritsema van Eck, and S. de Beer, "Friends, foes, and favorites: Relative interactions determine how polymer brushes absorb

vapors of binary solvents", Macromolecules **53**, 10898–10906 (2020), URL https://doi.org/10.1021/acs.macromol.0c02228.

[61] R. L. Scott, "The Thermodynamics of High Polymer Solutions. IV. Phase Equilibria in the Ternary System: Polymer—Liquid 1—Liquid 2", J. Chem. Phys. **17**, 268–279 (1949), URL http://aip.scitation.org/doi/10.1063/1.1747238.

[62] J. Dudowicz, K. F. Freed, and J. F. Douglas, "Communication: Cosolvency and cononsolvency explained in terms of a Flory-Huggins type theory", J. Chem. Phys. 6 (2015).

[63] D. Mukherji, C. M. Marques, T. Stuehn, and K. Kremer, "Depleted depletion drives polymer swelling in poor solvent mixtures", Nat. Commun. **8**, 1374 (2017).

[64] Y. Yu, B. D. Kieviet, E. Kutnyanszky, G. J. Vancso, and S. de Beer, "Cosolvency-Induced Switching of the Adhesion between Poly(methyl methacrylate) Brushes", ACS Macro Lett. **4**, 75–79 (2015), URL https://pubs.acs.org/doi/10.1021/mz500775w.

[65] P. Becher, "The calculation of cohesive energy density from the surface tension of liquids", J. Colloid Interface Sci. **38**, 291–293 (1972), URL https://www.sciencedirect.com/science/article/pii/0021979772902457.

[66] H. Yong, E. Bittrich, P. Uhlmann, A. Fery, and J.-U. Sommer, "Cononsolvency transition of poly(n-isopropylacrylamide) brushes in a series of binary mixtures", Macromolecules **52**, 6285–6293 (2019), URL https://doi.org/10.1021/acs.macromol.9b01286.

[67] M. Liu, F. Bian, and F. Sheng, "FTIR study on molecular structure of poly(N-isopropylacrylamide) in mixed solvent of methanol and water", Eur. Polym. J. **41**, 283–291 (2005).

[68] F. Tanaka, T. Koga, and F. m. c. M. Winnik, "Temperature-responsive polymers in mixed solvents: Competitive hydrogen bonds cause cononsolvency", Phys. Rev. Lett. **101**, 028302 (2008), URL https://link.aps.org/doi/10.1103/PhysRevLett.101.028302.

[69] D. Mukherji, C. M. Marques, and K. Kremer, "Polymer collapse in miscible good solvents is a generic phenomenon driven by preferential adsorption", Nat. Commun. **5**, 4882 (2014).

[70] J.-U. Sommer, "Adsorption–attraction model for co-nonsolvency in polymer brushes", Macromolecules **50**, 2219–2228 (2017), URL `https://doi.org/10.1021/acs.macromol.6b02231`.

[71] A. Galuschko and J. U. Sommer, "Co-Nonsolvency Response of a Polymer Brush: A Molecular Dynamics Study", Macromolecules **52**, 4120–4130 (2019).

[72] F. Rodríguez-Ropero, T. Hajari, and N. F. Van Der Vegt, "Mechanism of Polymer Collapse in Miscible Good Solvents", J. Phys. Chem. B **119**, 15780–15788 (2015).

[73] S. Bharadwaj and N. F. A. van der Vegt, "Does preferential adsorption drive cononsolvency?", Macromolecules **52**, 4131–4138 (2019), URL `https://doi.org/10.1021/acs.macromol.9b00575`.

[74] H. Yong, H. Merlitz, A. Fery, and J.-U. Sommer, "Polymer Brushes and Gels in Competing Solvents: The Role of Different Interactions and Quantitative Predictions for Poly(N-isopropylacrylamide) in Alcohol–Water Mixtures", Macromolecules **53**, 2323–2335 (2020).

[75] X. Zhang, J. Zong, and D. Meng, "A unified understanding of the cononsolvency of polymers in binary solvent mixtures", Soft Matter **16**, 7789–7796 (2020).

[76] L. P. Kreuzer, C. Lindenmeir, C. Geiger, T. Widmann, V. Hildebrand, A. Laschewsky, C. M. Papadakis, and P. Müller-Buschbaum, "Poly(sulfobetaine) versus poly(n-isopropylmethacrylamide): Co-nonsolvency-type behavior of thin films in a water/methanol atmosphere", Macromolecules **54**, 1548–1556 (2021), URL `https://doi.org/10.1021/acs.macromol.0c02281`.

[77] S.-M. Hur, A. L. Frischknecht, D. L. Huber, and G. H. Fredrickson, "Self-consistent field simulations of self- and directed-assembly in a mixed polymer brush", Soft Matter **7**, 8776–8788 (2011), URL `http://dx.doi.org/10.1039/C1SM05747B`.

[78] I. Zalakain, N. Politakos, R. Fernandez, H. Etxeberria, J. A. Ramos, M. A. Corcuera, I. Mondragon, and A. Eceiza, "Morphology response by solvent and vapour annealing using polystyrene/poly(methyl methacrylate) brushes", Thin Solid Films **539**, 201–206 (2013), URL `https://www.sciencedirect.com/science/article/pii/S0040609013009279`.

[79] L. Wang, T. Zhong, X. Quan, and J. Zhou, "Solvent-responsiveness of PS–PEO binary mixed polymer brushes: a coarse-grained molecular dynamics study", Mol. Simul. **43**, 1322–1330 (2017), URL https://www.tandfonline.com/doi/full/10.1080/08927022.2017.1350662.

[80] S. Santer, A. Kopyshev, H.-K. Yang, and J. Rühe, "Local composition of nanophase-separated mixed polymer brushes", Macromolecules **39**, 3056–3064 (2006), URL https://doi.org/10.1021/ma060092y.

[81] L. I. Klushin, A. M. Skvortsov, A. A. Polotsky, S. Qi, and F. Schmid, "Sharp and Fast: Sensors and Switches Based on Polymer Brushes with Adsorption-Active Minority Chains", Phys. Rev. Lett. **113**, 068303 (2014), URL https://link.aps.org/doi/10.1103/PhysRevLett.113.068303.

[82] I. Bos, H. Merlitz, A. Rosenthal, P. Uhlmann, and J.-U. Sommer, "Design of binary polymer brushes with tuneable functionality", Soft Matter **14**, 7237–7245 (2018), URL http://xlink.rsc.org/?DOI=C8SM01108G.

[83] M. Motornov, R. Sheparovych, I. Tokarev, Y. Roiter, and S. Minko, "Nonwettable thin films from hybrid polymer brushes can be hydrophilic", Langmuir **23**, 13–19 (2007), URL https://doi.org/10.1021/la061737q, pMID: 17190478.

[84] L. A. Smook, G. C. Ritsema van Eck, and S. de Beer, "Vapor sorption in binary polymer brushes: The effect of the polymer–polymer interface", J. Chem. Phys. **155**, 054904 (2021).

[85] A. D. Price, S.-M. Hur, G. H. Fredrickson, A. L. Frischknecht, and D. L. Huber, "Exploring lateral microphase separation in mixed polymer brushes by experiment and self-consistent field theory simulations", Macromolecules **45**, 510–524 (2012), URL https://doi.org/10.1021/ma202542u.

[86] J. Wang and M. Müller, "Microphase Separation of Mixed Polymer Brushes: Dependence of the Morphology on Grafting Density, Composition, Chain-Length Asymmetry, Solvent Quality, and Selectivity", J. Phys. Chem. B **113**, 11384–11402 (2009), URL https://pubs.acs.org/doi/10.1021/jp903161j.

[87] C. K. Simocko, A. L. Frischknecht, and D. L. Huber, "Phase behavior of ternary polymer brushes", ACS Macro Lett. **5**, 149–153 (2016), URL `https://doi.org/10.1021/acsmacrolett.5b00792`.

[88] W. J. Durand, G. Blachut, M. J. Maher, S. Sirard, S. Tein, M. C. Carlson, Y. Asano, S. X. Zhou, A. P. Lane, C. M. Bates, C. J. Ellison, and C. G. Willson, "Design of high-χ block copolymers for lithography", J. Polym. Sci., Part A: Polym. Chem. **53**, 344–352 (2015), URL `https://onlinelibrary.wiley.com/doi/abs/10.1002/pola.27370`, _eprint: https://onlinelibrary.wiley.com/doi/pdf/10.1002/pola.27370.

[89] S. Santer, A. Kopyshev, J. Donges, J. Rühe, X. Jiang, B. Zhao, and M. Müller, "Memory of Surface Patterns in Mixed Polymer Brushes: Simulation and Experiment", Langmuir **23**, 279–285 (2007), URL `https://pubs.acs.org/doi/10.1021/la0629577`.

[90] C. Bao, S. Tang, J. M. Horton, X. Jiang, P. Tang, F. Qiu, L. Zhu, and B. Zhao, "Effect of overall grafting density on microphase separation of mixed homopolymer brushes synthesized from y-initiator-functionalized silica particles", Macromolecules **45**, 8027–8036 (2012), URL `https://doi.org/10.1021/ma301300k`.

[91] L. A. Smook, G. C. Ritsema van Eck, and S. de Beer, "Concentrating vapor traces with binary brushes of immiscible polymers", ACS Appl. Polym. Mater. **3**, 2336–2340 (2021), URL `https://doi.org/10.1021/acsapm.1c00321`.

[92] T. Wang, Y. Yu, D. Chen, S. Wang, X. Zhang, Y. Li, J. Zhang, and Y. Fu, "Naked eye plasmonic indicator with multi-responsive polymer brush as signal transducer and amplifier", Nanoscale **9**, 1925–1933 (2017), URL `http://dx.doi.org/10.1039/C6NR09631J`.

[93] M. Matsuguchi, K. Takaoka, and H. Kai, "Hcl gas adsorption/desorption properties of poly(n-isopropylacrylamide) brushes grafted onto quartz resonator for gas-sensing applications", Sens. Actuators, B **208**, 106–111 (2015), URL `https://www.sciencedirect.com/science/article/pii/S0925400514013495`.

[94] M. Kimura, M. Sugawara, S. Sato, T. Fukawa, and T. Mihara, "Volatile organic compound sensing by quartz crystal microbalances coated with nanostructured macromolecular metal complexes", Chem. - Asian J. **5**,

869–876 (2010), URL `https://onlinelibrary.wiley.com/doi/abs/10.1002/asia.200900333`.

[95] H. Wang, Y. Li, Y. Chen, M. Yuan, M. Yang, and W. Yuan, "Composites of carbon black functionalized with polymers as candidates for the detection of methanol vapor", React. Funct. Polym. **67**, 977–985 (2007), URL `https://www.sciencedirect.com/science/article/pii/S1381514807001071`.

[96] J. Chen and N. Tsubokawa, "A novel gas sensor from polymer-grafted carbon black: responsiveness of electric resistance of conducting composite from ldpe and pe-b-peo-grafted carbon black in various vapors", Polym. Adv. Technol. **11**, 101–107 (2000), URL `https://onlinelibrary.wiley.com/doi/abs/10.1002/1099-1581%28200003%2911%3A3%3C101%3A%3AAID-PAT950%3E3.0.CO%3B2-0`.

[97] J. Chen and N. Tsubokawa, "Novel gas sensor from polymer-grafted carbon black: Vapor response of electric resistance of conducting composites prepared from poly(ethylene-block-ethylene oxide)-grafted carbon black", J. Appl. Polym. Sci. **77**, 2437–2447 (2000).

[98] M. Wei, Y. Gao, and M. J. Serpe, "Polymer brush-based optical device with multiple responsivities", J. Mater. Chem. B **3**, 744–747 (2015), URL `http://dx.doi.org/10.1039/C4TB01950D`.

[99] B. Ai, Y. Yu, H. Möhwald, and G. Zhang, "Responsive monochromatic color display based on nanovolcano arrays", Adv. Opt. Mater. **1**, 724–731 (2013), URL `https://onlinelibrary.wiley.com/doi/abs/10.1002/adom.201300224`.

[100] M. Manav, P. Anilkumar, and A. S. Phani, "Mechanics of polymer brush based soft active materials– theory and experiments", J. Mech. Phys. Solids **121**, 296–312 (2018), URL `https://www.sciencedirect.com/science/article/pii/S0022509618303934`.

[101] C. M. Domínguez, P. M. Kosaka, A. Sotillo, J. Mingorance, J. Tamayo, and M. Calleja, "Label-free dna-based detection of mycobacterium tuberculosis and rifampicin resistance through hydration induced stress in microcantilevers", Anal. Chem. (Washington, DC, U. S.) **87**, 1494–1498 (2015), URL `https://doi.org/10.1021/ac504523f`, pMID: 25599922.

[102] C. M. Domínguez, D. Ramos, J. Mingorance, J. L. G. Fierro, J. Tamayo, and M. Calleja, "Direct detection of oxa-48 carbapenemase gene in lysate samples through changes in mechanical properties of dna monolayers upon hybridization", Anal. Chem. (Washington, DC, U. S.) **90**, 968–973 (2018), URL https://doi.org/10.1021/acs.analchem.7b04094, pMID: 29186953.

[103] W. Chen, K. J. Shea, M. Xue, L. Qiu, Y. Lan, and Z. Meng, "Self-assembly of the polymer brush-grafted silica colloidal array for recognition of proteins", Anal. Bioanal. Chem. **409**, 5319–5326 (2017), URL https://doi.org/10.1007/s00216-017-0477-5.

[104] M. Galizia, W. S. Chi, Z. P. Smith, T. C. Merkel, R. W. Baker, and B. D. Freeman, "*50th Anniversary Perspective*: Polymers and Mixed Matrix Membranes for Gas and Vapor Separation: A Review and Prospective Opportunities", Macromolecules **50**, 7809–7843 (2017), URL https://pubs.acs.org/doi/10.1021/acs.macromol.7b01718F.

[105] H. Wang, S. He, X. Qin, C. Li, and T. Li, "Interfacial engineering in metal–organic framework-based mixed matrix membranes using covalently grafted polyimide brushes", J. Am. Chem. Soc. **140**, 17203–17210 (2018), URL https://doi.org/10.1021/jacs.8b10138, pMID: 30433777.

[106] Y. Yampolskii, "Polymeric gas separation membranes", Macromolecules **45**, 3298–3311 (2012), URL https://doi.org/10.1021/ma300213b.

[107] L. M. Robeson, "The upper bound revisited", J. Membr. Sci. **320**, 390–400 (2008), URL https://www.sciencedirect.com/science/article/pii/S0376738808003347.

[108] A. M. Balachandra, G. L. Baker, and M. L. Bruening, "Preparation of composite membranes by atom transfer radical polymerization initiated from a porous support", J. Membr. Sci. **227**, 1–14 (2003), URL https://www.sciencedirect.com/science/article/pii/S0376738803003843.

[109] M.-A. Pizzoccaro-Zilamy, M. Drobek, E. Petit, C. Totée, G. Silly, G. Guerrero, M. G. Cowan, A. Ayral, and A. Julbe, "Initial steps toward the development of grafted ionic liquid membranes for the selective transport of co2", Ind. Eng. Chem. Res. **57**, 16027–16040 (2018).

[110] M. A. Pizzoccaro-Zilamy, S. M. Piña, B. Rebiere, C. Daniel, D. Farrusseng, M. Drobek, G. Silly, A. Julbe, and G. Guerrero, "Controlled grafting of dialkylphosphonate-based ionic liquids on γ-alumina: design of hybrid materials with high potential for co2 separation applications", RSC Adv. **9**, 19882–19894 (2019).

[111] M. L. Bruening, D. M. Dotzauer, P. Jain, L. Ouyang, and G. L. Baker, "Creation of functional membranes using polyelectrolyte multilayers and polymer brushes", Langmuir **24**, 7663–7673 (2008), URL `https://doi.org/10.1021/la800179z`, pMID: 18507420.

[112] J. J. Keating, J. Imbrogno, and G. Belfort, "Polymer brushes for membrane separations: A review", ACS Appl. Mater. Interfaces **8**, 28383–28399 (2016), URL `https://doi.org/10.1021/acsami.6b09068`, pMID: 27709877.

[113] S. T. Grajales, X. Dong, Y. Zheng, G. L. Baker, and M. L. Bruening, "Effects of Monomer Composition on CO_2-Selective Polymer Brush Membranes", Chem. Mater. **22**, 4026–4033 (2010), URL `https://pubs.acs.org/doi/10.1021/cm100740n`.

[114] E. Aliyev, S. Shishatskiy, C. Abetz, Y. J. Lee, S. Neumann, T. Emmler, and V. Filiz, "Si-atrp polymer-functionalized graphene oxide for water vapor separation", Adv. Mater. Interfaces **7**, 2000443 (2020), URL `https://onlinelibrary.wiley.com/doi/abs/10.1002/admi.202000443`.

[115] C. R. Bilchak, M. Jhalaria, Y. Huang, Z. Abbas, J. Midya, F. M. Benedetti, D. Parisi, W. Egger, M. Dickmann, M. Minelli, F. Doghieri, A. Nikoubashman, C. J. Durning, D. Vlassopoulos, J. Jestin, Z. P. Smith, B. C. Benicewicz, M. Rubinstein, L. Leibler, and S. K. Kumar, "Tuning selectivities in gas separation membranes based on polymer-grafted nanoparticles", ACS Nano **14**, 17174–17183 (2020), URL `https://doi.org/10.1021/acsnano.0c07049`, pMID: 33216546.

[116] G. Liu, V. Chernikova, Y. Liu, K. Zhang, Y. Belmabkhout, O. Shekhah, C. Zhang, S. Yi, M. Eddaoudi, and W. J. Koros, "Mixed matrix formulations with MOF molecular sieving for key energy-intensive separations", Nat. Mater. **17**, 283–289 (2018), URL `http://www.nature.com/articles/s41563-017-0013-1`.

[117] C. R. Bilchak, E. Buenning, M. Asai, K. Zhang, C. J. Durning, S. K. Kumar, Y. Huang, B. C. Benicewicz, D. W. Gidley, S. Cheng, A. P. Sokolov, M. Minelli, and F. Doghieri, "Polymer-Grafted Nanoparticle Membranes with Controllable Free Volume", Macromolecules **50**, 7111–7120 (2017), URL https://pubs.acs.org/doi/10.1021/acs.macromol.7b01428.

[118] S. P. Jeong, R. Kumar, A.-C. Genix, I. Popov, C. Li, S. M. Mahurin, X. Hu, W. Bras, I. Popovs, A. P. Sokolov, and V. Bocharova, "Improving gas selectivity in membranes using polymer-grafted silica nanoparticles", ACS Appl. Nano Mater. **4**, 5895–5903 (2021), URL https://doi.org/10.1021/acsanm.1c00803.

[119] Q. Xin, Y. Zhang, Y. Shi, H. Ye, L. Lin, X. Ding, Y. Zhang, H. Wu, and Z. Jiang, "Tuning the performance of co2 separation membranes by incorporating multifunctional modified silica microspheres into polymer matrix", J. Membr. Sci. **514**, 73–85 (2016), URL https://www.sciencedirect.com/science/article/pii/S0376738816302782.

[120] Q. Xin, H. Liu, Y. Zhang, H. Ye, S. Wang, L. Lin, X. Ding, B. Cheng, Y. Zhang, H. Wu, and Z. Jiang, "Widening co2-facilitated transport passageways in speek matrix using polymer brushes functionalized double-shelled organic submicrocapsules for efficient gas separation", J. Membr. Sci. **525**, 330–341 (2017), URL https://www.sciencedirect.com/science/article/pii/S0376738816315290.

[121] Q. Xin, F. Ma, L. Zhang, S. Wang, Y. Li, H. Ye, X. Ding, L. Lin, Y. Zhang, and X. Cao, "Interface engineering of mixed matrix membrane via co2-philic polymer brush functionalized graphene oxide nanosheets for efficient gas separation", J. Membr. Sci. **586**, 23–33 (2019), URL https://www.sciencedirect.com/science/article/pii/S0376738819303412.

[122] R. Vaidhyanathan, S. S. Iremonger, G. K. H. Shimizu, P. G. Boyd, S. Alavi, and T. K. Woo, "Direct observation and quantification of co₂ binding within an amine-functionalized nanoporous solid", Science **330**, 650–653 (2010), URL https://www.science.org/doi/abs/10.1126/science.1194237.

[123] B. Yameen, A. Kaltbeitzel, A. Langner, H. Duran, F. Müller, U. Gösele, O. Azzaroni, and W. Knoll, "Facile large-scale fabrication of proton

conducting channels", J. Am. Chem. Soc. **130**, 13140–13144 (2008), URL https://doi.org/10.1021/ja804683j, pMID: 18774817.

[124] D. A. Bussian, J. R. O'Dea, H. Metiu, and S. K. Buratto, "Nanoscale Current Imaging of the Conducting Channels in Proton Exchange Membrane Fuel Cells", Nano Lett. **7**, 227–232 (2007), URL https://pubs.acs.org/doi/10.1021/nl061170y.

[125] A. Farrukh, F. Ashraf, A. Kaltbeitzel, X. Ling, M. Wagner, H. Duran, A. Ghaffar, H. ur Rehman, S. H. Parekh, K. F. Domke, and B. Yameen, "Polymer brush functionalized sio2 nanoparticle based nafion nanocomposites: a novel avenue to low-humidity proton conducting membranes", Polym. Chem. **6**, 5782–5789 (2015), URL http://dx.doi.org/10.1039/C5PY00514K.

[126] F. Niepceron, B. Lafitte, H. Galiano, J. Bigarré, E. Nicol, and J.-F. Tassin, "Composite fuel cell membranes based on an inert polymer matrix and proton-conducting hybrid silica particles", J. Membr. Sci. **338**, 100–110 (2009), URL https://www.sciencedirect.com/science/article/pii/S0376738809002919.

[127] B. Yameen, A. Kaltbeitzel, G. Glasser, A. Langner, F. Müller, U. Gösele, W. Knoll, and O. Azzaroni, "Hybrid polymer-silicon proton conducting membranes via a pore-filling surface-initiated polymerization approach", ACS Appl. Mater. Interfaces **2**, 279–287 (2010), URL https://doi.org/10.1021/am900690x, pMID: 20356246.

[128] B. Yameen, A. Kaltbeitzel, A. Langer, F. Müller, U. Gösele, W. Knoll, and O. Azzaroni, "Highly proton-conducting self-humidifying microchannels generated by copolymer brushes on a scaffold", Angew. Chem., Int. Ed. **48**, 3124–3128 (2009), URL https://onlinelibrary.wiley.com/doi/abs/10.1002/anie.200805576.

[129] H. Bai, H. Zhang, Y. He, J. Liu, B. Zhang, and J. Wang, "Enhanced proton conduction of chitosan membrane enabled by halloysite nanotubes bearing sulfonate polyelectrolyte brushes", J. Membr. Sci. **454**, 220–232 (2014), URL https://www.sciencedirect.com/science/article/pii/S0376738813009587.

[130] L. Zhao, Y. Li, H. Zhang, W. Wu, J. Liu, and J. Wang, "Constructing proton-conductive highways within an ionomer membrane by embedding sulfonated polymer brush modified graphene oxide", J. Power

Sources **286**, 445–457 (2015), URL `https://www.sciencedirect.com/science/article/pii/S0378775315006448`.

[131] X. Zheng, K. Liu, Y. Huang, H. Tang, W. Tu, M. Pan, and H. Zhang, "Grafting distance and molecular weight dependent proton conduction of polymer electrolyte brushes", Eur. Polym. J. **64**, 93–100 (2015), URL `https://www.sciencedirect.com/science/article/pii/S0014305714004753`.

[132] Y. Dong, J. Feng, D. Lu, H. Zhang, M. Pan, and P. Fang, "Titanate nanotube array membranes filled with polyelectrolyte brushes for proton conduction", Eur. Polym. J. **88**, 183–190 (2017), URL `https://www.sciencedirect.com/science/article/pii/S0014305716317591`.

[133] A. M. C. Maan, A. H. Hofman, W. M. de Vos, and M. Kamperman, "Recent developments and practical feasibility of polymer-based antifouling coatings", Adv. Funct. Mater. **30**, 2000936 (2020), URL `https://onlinelibrary.wiley.com/doi/abs/10.1002/adfm.202000936`.

[134] S. de Beer, L. I. S. Mensink, and B. D. Kieviet, "Geometry-Dependent Insertion Forces on Particles in Swollen Polymer Brushes", Macromolecules **49**, 1070–1078 (2016), URL `https://pubs.acs.org/doi/10.1021/acs.macromol.5b01960`.

[135] H. Thérien-Aubin, L. Chen, and C. K. Ober, "Fouling-resistant polymer brush coatings", Polymer **52**, 5419–5425 (2011), URL `https://linkinghub.elsevier.com/retrieve/pii/S0032386111007580`.

[136] S. Chen, L. Li, C. Zhao, and J. Zheng, "Surface hydration: Principles and applications toward low-fouling/nonfouling biomaterials", Polymer **51**, 5283–5293 (2010), URL `https://www.sciencedirect.com/science/article/pii/S0032386110006968`.

[137] G. W. Greene, L. L. Martin, R. F. Tabor, A. Michalczyk, L. M. Ackland, and R. Horn, "Lubricin: A versatile, biological anti-adhesive with properties comparable to polyethylene glycol", Biomaterials **53**, 127–136 (2015), URL `https://www.sciencedirect.com/science/article/pii/S0142961215002161`.

[138] A. I. Lopez, A. Kumar, M. R. Planas, Y. Li, T. V. Nguyen, and C. Cai, "Biofunctionalization of silicone polymers using

poly(amidoamine) dendrimers and a mannose derivative for prolonged interference against pathogen colonization", Biomaterials **32**, 4336–4346 (2011), URL `https://www.sciencedirect.com/science/article/pii/S014296121100233X`.

[139] A. T. Nguyen, J. Baggerman, J. M. J. Paulusse, C. J. M. van Rijn, and H. Zuilhof, "Stable Protein-Repellent Zwitterionic Polymer Brushes Grafted from Silicon Nitride", Langmuir **27**, 2587–2594 (2011), URL `https://pubs.acs.org/doi/10.1021/la104657c`.

[140] P. Wang, Y. Dong, S. Zhang, W. Liu, Z. Wu, and H. Chen, "Protein-resistant properties of poly(N-vinylpyrrolidone)-modified gold surfaces: The advantage of bottle-brushes over linear brushes", Colloids Surf., B **177**, 448–453 (2019), URL `https://www.sciencedirect.com/science/article/pii/S0927776519301122`.

[141] G. Morgese, L. Trachsel, M. Romio, M. Divandari, S. N. Ramakrishna, and E. M. Benetti, "Topological Polymer Chemistry Enters Surface Science: Linear versus Cyclic Polymer Brushes", Angew. Chem., Int. Ed. **55**, 15583–15588 (2016), URL `https://onlinelibrary.wiley.com/doi/abs/10.1002/anie.201607309`, _eprint: https://onlinelibrary.wiley.com/doi/pdf/10.1002/anie.201607309.

[142] D. F. Cheng, C. Urata, M. Yagihashi, and A. Hozumi, "A statically oleophilic but dynamically oleophobic smooth nonperfluorinated surface", Angew. Chem., Int. Ed. **51**, 2956–2959 (2012), URL `https://onlinelibrary.wiley.com/doi/abs/10.1002/anie.201108800`.

[143] L. Wang and T. J. McCarthy, "Covalently attached liquids: Instant omniphobic surfaces with unprecedented repellency", Angew. Chem., Int. Ed. **55**, 244–248 (2016), URL `https://onlinelibrary.wiley.com/doi/abs/10.1002/anie.201509385`.

[144] S. Wooh and D. Vollmer, "Silicone brushes: Omniphobic surfaces with low sliding angles", Angew. Chem., Int. Ed. **55**, 6822–6824 (2016), URL `https://onlinelibrary.wiley.com/doi/abs/10.1002/anie.201511895`.

[145] J. Liu, Y. Sun, X. Zhou, X. Li, M. Kappl, W. Steffen, and H.-J. Butt, "One-step synthesis of a durable and liquid-repellent poly(dimethylsiloxane) coating", Adv. Mater. (Weinheim, Ger.) **33**,

2

2100237 (2021), URL `https://onlinelibrary.wiley.com/doi/abs/10.1002/adma.202100237`.

[146] O. J. Chaudhary, E. P. Calius, J. V. Kennedy, M. Dickinson, T. Loho, and J. Travas-Sejdic, "Bioinspired dry adhesive: Poly(dimethylsiloxane) grafted with poly(2-ethylhexyl acrylate) brushes", Eur. Polym. J. **68**, 432–440 (2015), URL `https://www.sciencedirect.com/science/article/pii/S0014305715002803`.

[147] S. Lamping, T. Otremba, and B. J. Ravoo, "Carbohydrate-responsive surface adhesion based on the dynamic covalent chemistry of phenyl-boronic acid- and catechol-containing polymer brushes", Angew. Chem., Int. Ed. **57**, 2474–2478 (2018), URL `https://onlinelibrary.wiley.com/doi/abs/10.1002/anie.201711529`.

[148] S. Lamping, L. Stricker, and B. J. Ravoo, "Responsive surface adhesion based on host–guest interaction of polymer brushes with cyclodextrins and arylazopyrazoles", Polym. Chem. **10**, 683–690 (2019), URL `http://dx.doi.org/10.1039/C8PY01496E`.

[149] A. Synytska, E. Svetushkina, D. Martina, C. Bellmann, F. Simon, L. Ionov, M. Stamm, and C. Creton, "Intelligent materials with adaptive adhesion properties based on comb-like polymer brushes", Langmuir **28**, 16444–16454 (2012).

[150] K. J. van der Weg, G. C. Ritsema van Eck, and S. de Beer, "Polymer brush friction in cylindrical geometries", Lubricants **7** (2019), URL `https://www.mdpi.com/2075-4442/7/10/84`, 84.

[151] J. Klein, "Hydration lubrication", Friction **1**, 1–23 (2013).

[152] S. de Beer and M. H. Müser, "Friction in (im-) miscible polymer brush systems and the role of transverse polymer tilting", Macromolecules **47**, 7666–7673 (2014), URL `https://doi.org/10.1021/ma501718b`.

[153] S. de Beer and M. H. Müser, "Alternative dissipation mechanisms and the effect of the solvent in friction between polymer brushes on rough surfaces", Soft Matter **9**, 7234–7241 (2013), URL `http://dx.doi.org/10.1039/C3SM50491C`.

[154] S. B. Abbott, W. M. de Vos, L. L. E. Mears, B. Cattoz, M. W. A. Skoda, R. Barker, R. M. Richardson, and S. W. Prescott, "Is Osmotic

Pressure Relevant in the Mechanical Confinement of a Polymer Brush?", Macromolecules **48**, 2224–2234 (2015), URL `https://pubs.acs.org/doi/10.1021/ma502246r`.

[155] A. Galuschko, L. Spirin, T. Kreer, A. Johner, C. Pastorino, J. Wittmer, and J. Baschnagel, "Frictional forces between strongly compressed, nonentangled polymer brushes: Molecular dynamics simulations and scaling theory", Langmuir **26**, 6418–6429 (2010), URL `https://doi.org/10.1021/la904119c`.

[156] T. Kreer, "Polymer-brush lubrication: a review of recent theoretical advances", Soft Matter **12**, 3479–3501 (2016), URL `http://xlink.rsc.org/?DOI=C5SM02919H`.

[157] W. J. Briels, "Transient forces in flowing soft matter", Soft Matter **5**, 4401–4411 (2009).

[158] J. Klein, E. Kumacheva, D. Mahalu, D. Perahia, and L. J. Fetters, "Reduction of frictional forces between solid surfaces bearing polymer brushes", Nature (London, U. K.) **370**, 634–636 (1994), URL `http://www.nature.com/articles/370634a0`.

[159] U. Raviv, S. Giasson, N. Kampf, J.-F. Gohy, R. Jérôme, and J. Klein, "Lubrication by charged polymers", Nature (London, U. K.) **425**, 163–165 (2003), URL `http://www.nature.com/articles/nature01970`.

[160] U. Raviv, S. Giasson, N. Kampf, J.-F. Gohy, R. Jérôme, and J. Klein, "Normal and Frictional Forces between Surfaces Bearing Polyelectrolyte Brushes", Langmuir **24**, 8678–8687 (2008), URL `https://pubs.acs.org/doi/10.1021/la7039724`.

[161] M. Kobayashi and A. Takahara, "Tribological properties of hydrophilic polymer brushes under wet conditions", Chem. Rec. **10**, 208–216 (2010), URL `https://onlinelibrary.wiley.com/doi/abs/10.1002/tcr.201000001`.

[162] M. Kobayashi, M. Terada, and A. Takahara, "Polyelectrolyte brushes: a novel stable lubrication system in aqueous conditions", Faraday Discuss. **156**, 403–412 (2012), URL `http://dx.doi.org/10.1039/C2FD00123C`.

[163] S. Ma, D. Wang, Y. Liang, B. Sun, S. N. Gorb, and F. Zhou, "Gecko-inspired but chemically switched friction and adhesion on nanofibrillar

surfaces", Small **11**, 1131–1137 (2015), URL `https://onlinelibrary.wiley.com/doi/abs/10.1002/smll.201402484`.

[164] S. de Beer, "Switchable friction using contacts of stimulus-responsive and nonresponding swollen polymer brushes", Langmuir **30**, 8085–8090 (2014).

[165] G. Liu, M. Cai, Y. Feng, X. Wang, F. Zhou, and W. Liu, "Photothermally actuated interfacial hydration for fast friction switch on hydrophilic polymer brush modified pdms sheet incorporated with fe3o4 nanoparticles", Chem. Commun. (Cambridge, U. K.) **52**, 3681–3683 (2016), URL `http://dx.doi.org/10.1039/C5CC09954D`.

[166] H. Zeng, Y. Zhang, S. Mao, H. Nakajima, and K. Uchiyama, "A reversibly electro-controllable polymer brush for electro-switchable friction", J. Mater. Chem. C **5**, 5877–5881 (2017), URL `http://dx.doi.org/10.1039/C7TC01624G`.

[167] Z. Cao and A. V. Dobrynin, "Polymeric droplets on soft surfaces: From neumann's triangle to young's law", Macromolecules **48**, 443–451 (2015), URL `https://doi.org/10.1021/ma501672p`.

[168] L. Lubbers, J. Weijs, L. Botto, S. Das, B. Andreotti, and J. Snoeijer, "Drops on soft solids: free energy and double transition of contact angles", J. Fluid Mech. **747**, R1 (2014), URL `https://www.cambridge.org/core/product/identifier/S0022112014001529/type/journal_article`.

[169] J. H. Maas, G. J. Fleer, F. A. M. Leermakers, and M. A. Cohen Stuart, "Wetting of a polymer brush by a chemically identical polymer melt: Phase diagram and film stability", Langmuir **18**, 8871–8880 (2002).

[170] F. A. M. Leermakers, L. J. M. Schlangen, and L. K. Koopal, "Critical Point Wetting for Binary Two-Phase Polymer-Solvent Mixtures on Solid Interfaces", Langmuir **13**, 5751–5755 (1997), URL `https://pubs.acs.org/doi/10.1021/la9702704`.

[171] G. Reiter and R. Khanna, "Negative excess interfacial entropy between free and end-grafted chemically identical polymers", Phys. Rev. Lett. **85**, 5599–5602 (2000), URL `https://link.aps.org/doi/10.1103/PhysRevLett.85.5599`.

[172] M. W. Matsen and J. M. Gardiner, "Autophobic dewetting of homopolymer on a brush and entropic attraction between opposing brushes in a homopolymer matrix", J. Chem. Phys. **115**, 2794–2804 (2001), URL `http://aip.scitation.org/doi/10.1063/1.1385557`.

[173] X. Zhang, F. K. Lee, and O. K. C. Tsui, "Wettability of end-grafted polymer brush by chemically identical polymer films", Macromolecules **41**, 8148–8151 (2008), URL `https://doi.org/10.1021/ma801549r`.

[174] L. I. S. Mensink, J. H. Snoeijer, and S. de Beer, "Wetting of polymer brushes by polymeric nanodroplets", Macromolecules **52**, 2015–2020 (2019), URL `https://doi.org/10.1021/acs.macromol.8b02409`.

[175] L. I. S. Mensink, S. de Beer, and J. H. Snoeijer, "The role of entropy in wetting of polymer brushes", Soft Matter **17**, 1368–1375 (2021), URL `http://dx.doi.org/10.1039/D0SM00156B`.

[176] H. G. Schild and D. A. Tirrell, "Microcalorimetric detection of lower critical solution temperatures in aqueous polymer solutions", J. Phys. Chem. **94**, 4352–4356 (1990), URL `https://pubs.acs.org/doi/10.1021/j100373a088`.

[177] T. Sun, G. Wang, L. Feng, B. Liu, Y. Ma, L. Jiang, and D. Zhu, "Reversible switching between superhydrophilicity and superhydrophobicity", Angew. Chem., Int. Ed. **43**, 357–360 (2004), URL `https://onlinelibrary.wiley.com/doi/abs/10.1002/anie.200352565`.

[178] Not to be confused with the Sun et al. mentioned earlier in this paragraph.

[179] W. Sun, S. Zhou, B. You, and L. Wu, "Polymer brush-functionalized surfaces with reversible, precisely controllable two-way responsive wettability", Macromolecules **46**, 7018–7026 (2013), URL `https://doi.org/10.1021/ma401416k`.

[180] S. Demirci, S. Kinali-Demirci, and B. VanVeller, "Controlled supramolecular complexation of cyclodextrin-functionalized polymeric ionic liquid brushes", ACS Appl. Polym. Mater. **2**, 751–757 (2020), URL `https://doi.org/10.1021/acsapm.9b01058`.

[181] S. Schubotz, C. Honnigfort, S. Nazari, A. Fery, J.-U. Sommer, P. Uhlmann, B. Braunschweig, and G. K. Auernhammer, "Memory effects in polymer brushes showing co-nonsolvency effects", Adv. Colloid Interface Sci. **294**, 102442 (2021), URL `https://www.sciencedirect.com/science/article/pii/S000186862100083X`.

[182] M. Ezzat and C.-J. Huang, "Zwitterionic polymer brush coatings with excellent anti-fog and anti-frost properties", RSC Adv. **6**, 61695–61702 (2016), URL `http://dx.doi.org/10.1039/C6RA12399F`.

[183] J. B. Boreyko and C. P. Collier, "Delayed frost growth on jumping-drop superhydrophobic surfaces", ACS Nano **7**, 1618–1627 (2013), URL `https://doi.org/10.1021/nn3055048`, pMID: 23286736.

[184] M. W. England, C. Urata, G. J. Dunderdale, and A. Hozumi, "Anti-fogging/self-healing properties of clay-containing transparent nanocomposite thin films", ACS Appl. Mater. Interfaces **8**, 4318–4322 (2016), URL `https://doi.org/10.1021/acsami.5b11961`, pMID: 26845075.

[185] J. Howarter and J. Youngblood, "Self-cleaning and anti-fog surfaces via stimuli-responsive polymer brushes", Adv. Mater. (Weinheim, Ger.) **19**, 3838–3843 (2007), URL `https://onlinelibrary.wiley.com/doi/abs/10.1002/adma.200700156`.

[186] O. Azzaroni, A. A. Brown, and W. T. S. Huck, "Ucst wetting transitions of polyzwitterionic brushes driven by self-association", Angew. Chem., Int. Ed. **45**, 1770–1774 (2006), URL `https://onlinelibrary.wiley.com/doi/abs/10.1002/anie.200503264`.

[187] A. S. Münch, S. Adam, T. Fritzsche, and P. Uhlmann, "Tuning of smart multifunctional polymer coatings made by zwitterionic phosphorylcholines", Adv. Mater. Interfaces **7**, 1901422 (2020), URL `https://onlinelibrary.wiley.com/doi/abs/10.1002/admi.201901422`.

[188] W. Li, W. Sheng, B. Li, and R. Jordan, "Surface grafting "band-aid" for "everyone": Filter paper-assisted surface-initiated polymerization in the presence of air", Angew. Chem., Int. Ed. **60**, 13621–13625 (2021), URL `https://onlinelibrary.wiley.com/doi/abs/10.1002/anie.202103182`.

[189] D. Chen, M. D. Gelenter, M. Hong, R. E. Cohen, and G. H. McKinley, "Icephobic surfaces induced by interfacial nonfrozen water", ACS

Appl. Mater. Interfaces **9**, 4202–4214 (2017), URL `https://doi.org/10.1021/acsami.6b13773`, pMID: 28054770.

[190] B. Liang, G. Zhang, Z. Zhong, Y. Huang, and Z. Su, "Superhydrophilic anti-icing coatings based on polyzwitterion brushes", Langmuir **35**, 1294–1301 (2019), URL `https://doi.org/10.1021/acs.langmuir.8b01009`.

[191] S. Shiomoto, K. Yamaguchi, and M. Kobayashi, "Time evolution of precursor thin film of water on polyelectrolyte brush", Langmuir **34**, 10276–10286 (2018), URL `https://doi.org/10.1021/acs.langmuir.8b02070`, pMID: 30102545.

[192] J. Joanny and P.-G. de Gennes, "Upward creep of a wetting fluid : a scaling analysis", J. Phys. (Paris) **47**, 121–127 (1986), URL `http://www.edpsciences.org/10.1051/jphys:01986004701012100`.

[193] S. A. Etha, P. R. Desai, H. S. Sachar, and S. Das, "Wetting dynamics on solvophilic, soft, porous, and responsive surfaces", Macromolecules **54**, 584–596 (2021), URL `https://doi.org/10.1021/acs.macromol.0c02234`.

[194] U. Thiele and S. Hartmann, "Gradient dynamics model for drops spreading on polymer brushes", Eur. Phys. J.: Spec. Top. **229**, 1819–1832 (2020).

[195] M. Kopeć, S. Tas, M. Cirelli, R. van der Pol, I. de Vries, G. J. Vancso, and S. de Beer, "Fluorescent patterns by selective grafting of a telechelic polymer", ACS Appl. Polym. Mater. **1**, 136–140 (2019).

[196] Q. A. Besford, H. Yong, H. Merlitz, A. J. Christofferson, J.-U. Sommer, P. Uhlmann, and A. Fery, "Fret-integrated polymer brushes for spatially resolved sensing of changes in polymer conformation", Angew. Chem., Int. Ed. **60**, 16600–16606 (2021).

[197] L. A. Navarro, A. E. Enciso, K. Matyjaszewski, and S. Zauscher, "Enzymatically degassed surface-initiated atom transfer radical polymerization with real-time monitoring", J. Am. Chem. Soc. **141**, 3100–3109 (2019).

[198] B. Liberelle and S. Giasson, "Chemical end-grafting of homogeneous polystyrene monolayers on mica and silica surfaces", Langmuir **23**, 9263–9270 (2007).

[199] S. Tugulu and H.-A. Klok, "Stability and nonfouling properties of poly(poly(ethylene glycol) methacrylate) brushes under cell culture conditions", Biomacromolecules **9**, 906–912 (2008).

[200] H.-A. Klok and J. Genzer, "Expanding the polymer mechanochemistry toolbox through surface-initiated polymerization", ACS Macro Lett. **4**, 636–639 (2015).

[201] M. Menzel, W.-L. Chen, K. Simancas, H. Xu, O. Prucker, C. K. Ober, and J. Rühe, "Entropic death of nonpatterned and nanopatterned polyelectrolyte brushes", J. Polym. Sci., Part A: Polym. Chem. **57**, 1283–1295 (2019).

[202] D. Paripovic and H.-A. Klok, "Improving the stability in aqueous media of polymer brushes grafted from silicon oxide substrates by surface-initiated atom transfer radical polymerization", Macromol. Chem. Phys. **212**, 950–958 (2011).

[203] M. Divandari, E. S. Dehghani, N. D. Spencer, S. N. Ramakrishna, and E. M. Benetti, "Understanding the effect of hydrophobic protecting blocks on the stability and biopassivity of polymer brushes in aqueous environments: A tiramisù for cell-culture applications", Polymer **98**, 470–480 (2016), special Issue: Polymer Brushes.

[204] Y. Yu, G. J. Vancso, and S. de Beer, "Substantially enhanced stability against degrafting of zwitterionic pmpc brushes by utilizing pgma-linked initiators", Eur. Polym. J. **89**, 221–229 (2017), URL `https://www.sciencedirect.com/science/article/pii/S0014305717300137`.

Chapter 3

Sorption Characteristics for Polymer Brushes in Equilibrium with Solvent Vapors[*]

Polymer brushes, coatings of polymers covalently end-grafted to a surface, have been proposed as a more stable alternative to traditional physisorbed coatings. However, when such coatings are applied in settings such as vapor sensing and gas separation technologies, their responsiveness to solvent vapors becomes an important consideration. It can be anticipated that the end-anchoring in polymer brushes reduces the translational entropy of the polymers and instead introduces an entropic penalty against stretching when vapor is absorbed.

Therefore, swelling can be expected to be diminished in brushes compared to non-grafted films. Here, we study the effect of the anchoring-constraint on vapor sorption in polymer coatings using coarse-grained molecular dynamics simulations as well as humidity-controlled ellipsometry on chemically identical polymer brushes and non-grafted films. We find a qualitative agreement between simulations and experiments, with both indicating that brushes certainly swell less than physisorbed films, although this effect is minor for common grafting densities. Our results imply that polymer brushes indeed hold great potential for the intended applications.

3.1 Introduction

In many experimental studies of vapor sorption in polymer brushes, the Flory-Huggins theory [1] for polymer-solvent mixtures is employed to model the solvent's volume fraction in the brush as a function of the relative vapor pressure. [2–5] By imposing that the solvent vapor is in chemical equilibrium with the solvent in the polymer-solvent mixture, a prediction of the brush composition is obtained. Although this theory is useful for describing qualitative trends, it fails to capture brush-specific effects. In its simplest form, application of the Flory-Huggins theory leads to the assumption of a homogeneous density of solvent throughout the brush. However, neutron reflectometry measurements of vapor-solvated brushes indicate that the brush density decreases as a function of the distance from the anchoring surface. [6] Another assumption in the basic Flory-Huggins model is that brush swelling is independent of the grafting density, while experimentally it is found that the swelling increases with decreasing grafting density. [7] A model that includes the entropic penalty for polymer stretching allows for predicting grafting density effects, even in a mean field approach. [7, 8] A third assumption in the basic Flory-Huggins model is that it accounts for the polymer-solvent interactions via a single Flory-Huggins parameter χ_{ps}. Thereby, interactions of polymers and solvent with air are assumed to be equal and interfacial effects are not captured in the model. Yet, neutron reflectometry measurements indicate the existence of a solvent-enriched layer at the brush-air interface, [4, 6] even though the authors of Ref. 4 considered their density variation to be a fitting artifact. Therefore, the question arises if the employment of a Flory-Huggins type model is appropriate for vapor-solvated brushes.

In this chapter we use molecular dynamics simulations to provide a detailed microscopic interpretation of solvent sorption for polymer brushes in equilibrium with solvent vapors for different interaction parameters, brush densities, and relative solvent pressures. We evaluate the polymer and solvent density profiles and discuss similarities and differences with the profiles for brushes in contact with liquids as well as experimental observations. Moreover, we compare the solvent fraction in our brushes to a modified Flory-Huggins model, to investigate the validity of Flory-Huggins type models for systems containing solvent vapors. Solvent adsorption at the brush-vapor interface is quantified across the parameter space of interaction energies as well and discussed in the context of predictions based on energetic arguments.
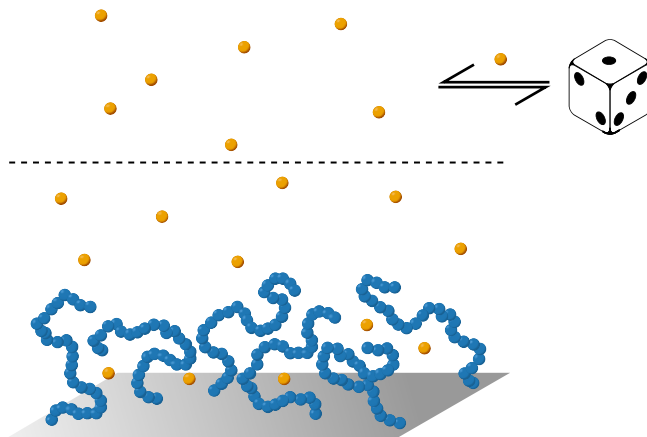
3.2 Model and Methods

Figure 3.1: Schematic of the simulation box. Monodisperse polymer chains of length (depicted: $N = 30$) are grafted to an atomic wall to form the brush. Above the brush, a vapor region periodically exchanges particles with a virtual reservoir through the GCMC procedure.

Solvent partitioning is investigated using coarse-grained molecular dynamics (MD) simulations of the brush-solvent system, alternated with grand-canonical Monte Carlo (GCMC) sweeps to maintain a constant solvent vapor pressure in a region above the brush. In this GCMC procedure, a set number of particle insertions and deletions is attempted and evaluated based on a Metropolis criterion. All simulations were performed using the MD package LAMMPS (Large-scale Atomic/Molecular Massively Parallel Simulator). [9]

A system is set up consisting of a rectangular box of dimensions 50 x 50 x 100 σ^* (x, y, z respectively) that is periodic in x and y. Polymer chains are represented by a freely-jointed bead-spring model based on the work of Kremer and Grest [10], and consist of $N = 30$, 60, or 100 beads each. These lengths are selected to limit computational costs while still producing the characteristic behaviors of polymers. [11, 12] We note that our brushes are perfectly monodisperse. Polydispersity can qualitatively alter density profiles, penetration [13] and absorptive properties. [14] Therefore, we anticipate that our results might change when polydispersity is introduced. A polymer brush

is created by 'grafting' chains to immobile particles positioned randomly in a plane at the bottom of the box ($z = 0$). The code used to generate the initial data comprising these polymer brush systems is available online. [15] Above the polymer brush at the top of the box, solvent particles are inserted/removed in a 20 σ thick slab according to the GCMC procedure outlined above, as illustrated in Figure 3.1. The background medium (air) is modeled implicitly. A system of low-density LJ particles in an implicit background is similar to simulations of brushes in contact with nanoparticles [16] or co(non)solvents, [17] except that our implicit background is a poor solvent for the brushes. Repulsive harmonic 'mathematical walls', with a spring constant of 100 $\epsilon\sigma^{-2*}$ are placed at the bottom and top of the box to prevent polymer and vapor particles leaving the system through the fixed boundary in z.

Non-bonded interactions in the system are described by a form of the well-known Lennard-Jones (LJ) potential

$$U_{\mathrm{LJ}}(r) = 4\epsilon\left(\left(\frac{\sigma}{r}\right)^{12} - \left(\frac{\sigma}{r}\right)^{6}\right), \tag{3.1}$$

where r represents the interparticle distance, ϵ is the depth of the potential well, and σ is the zero-crossing distance. The minimum occurs at $r_m = 2^{1/6}\sigma$. Specifically, the truncated and potential-shifted (SP) form of the Lennard-Jones potential is used

$$U_{\mathrm{LJ,SP}}(r) = \begin{cases} U_{\mathrm{LJ}}(r) - U_{\mathrm{LJ}}(r_\mathrm{c}) & \text{for } r \leq r_\mathrm{c} \\ 0 & \text{for } r > r_\mathrm{c} \end{cases}, \tag{3.2}$$

where r_c is the cutoff distance for the interaction. In this research, we use reduced Lennard-Jones units, meaning ϵ and σ are used as energy and length units for our system, respectively. Additionally, all particle masses are equal. All these interactions are truncated and potential-shifted to zero at 2.5 σ. Therefore, all interparticle interactions in our simulations are attractive at distances larger than 1 σ. Consecutive beads along a polymer backbone are bonded via a Finitely Extensible Non-linear Elastic (FENE) potential (Equation 3.3) combined with a Weeks-Chandler-Anderson (WCA) potential (Equation 3.4). The latter is equivalent to a LJ potential truncated at its minimum and shifted to zero at the cutoff, thereby making it purely repulsive. The total

---

*Where σ and ϵ refer to the length and energy unit (respectively) in the system of reduced Lennard-Jones units used in this chapter.

bonded potential is the sum of the FENE and WCA potentials (Equation 3.5).

$$U_{\text{FENE}}(r) = -0.5 K R_0^2 \ln\left(1 - \left(\frac{r}{R_0}\right)^2\right) \tag{3.3}$$

$$U_{\text{WCA}}(r) = \begin{cases} U_{\text{LJ}}(r) + \epsilon & \text{for } r \leq 2^{1/6} \\ 0 & \text{for } r > 2^{1/6} \end{cases} \tag{3.4}$$

$$U_{\text{bond}}(r) = U_{\text{WCA}}(r) + U_{\text{FENE}}(r) \tag{3.5}$$

In Equation 3.3, R_0 is the maximum bond length and K is a spring constant. In our simulations, K is set to 30 $\epsilon\sigma^{-2}$, R_0 is 1.5 σ, and ϵ and σ are equal to 1. These parameters, borrowed directly from the Kremer-Grest model [10], prevent bond crossing and other unphysical behaviors. This model evidently cannot account for various chemical specificities. In particular, effects of molecular geometry and directional interactions such as hydrogen bonding cannot be captured effectively by a Lennard-Jones-based model. Our results will therefore deviate somewhat from most experimental systems. However, that same generality makes this simulation setup particularly suitable for testing the applicability of the extended Flory-Huggins model to vapor sorption. The entire system is thermostatted to a temperature of 0.85 $\epsilon k_{\text{B}}^{-1}$ using a chain of three Nosé-Hoover thermostats (which ensures proper sampling of the canonical ensemble [18]) with a damping constant of 0.15 τ, where τ represents the reduced time unit derived from the Lennard-Jones potential. k_{B} is the Boltzmann constant, which we take to be unity, as the energy scale of the simulations is arbitrary. The temperature of 0.85 $\epsilon k_{\text{B}}^{-1}$ was determined to allow vapor-liquid coexistence for the solvent. The GCMC chemostat is active every 10000 timesteps, where it attempts 1000 solvent particle insertions/deletions. These values were empirically determined to result in a good balance between simulation performance and convergence speed.

The polymer system is first equilibrated by running a short minimization using the conjugate gradient method, followed by running dynamics for 10000 timesteps with a limit imposed on the maximum movement of a particle in one timestep of 1 σ and a Langevin thermostat with a damping parameter of 1000 τ. A second minimization is then performed. Finally, 200000 timesteps of more viscous Langevin dynamics are performed with a damping parameter of 100 τ and without the limit. This procedure is chosen to relax the system from the low-entropy initial state (fully-extended chains) as quickly and efficiently as possible. After the equilibration, a production run is started in which solvent particles are introduced into the system by enabling the GCMC mechanism.

The system is simulated for 60 million timesteps (900000 τ), as this ensures an equilibrated state and adequate signal-to-noise ratio for all simulation cases. LAMMPS input files, as well as a Python wrapper around LAMMPS are available online. [19]

For the equilibration, the LAMMPS default value for the timestep (0.005 τ) is used. For the production runs, the rRESPA multi-timescale integrator [20] is employed with an outer timestep of 0.015 τ and a 2-fold as short inner timestep. This results in non-bonded pair interactions being computed every 0.015 τ, but bonded interactions being computed every 0.0075 τ.

The depth of the energetic minimum of the polymer self-interaction (ϵ_{pp}) and of the polymer-solvent interaction (ϵ_{ps}) are both varied with the goal of identifying sorption behavior regimes of the vapor-solvated polymer brush system in the two-dimensional parameter space. We assume the ϵ values to represent general short-range interactions, and therefore do not account for combining rules in our selection of parameter space. For solvent self-interactions, we use the reference value of unity for ϵ. In our primary simulations, the GCMC chemostat maintains a solvent pressure of 0.0154 $\epsilon\sigma^{-3}$, corresponding to a relative pressure of $P/P_{\mathrm{sat}} \approx 0.73$. Simulations are performed for brush systems with average grafting densities of 0.34 σ^{-2} (in the case of $N = 30$), and 0.15 and 0.25 σ^{-2} (in the case of $N = 100$). These values are chosen so that the mean distance between polymers is significantly smaller (up to an order of magnitude) than the radius of gyration for a collapsed single chain. This ensures brush conditions in the full range of solvent conditions probed, and prevents the formation of octopus micelles [21] at poor solvent conditions, which was observed at lower grafting densities. Radii of the collapsed chains were determined through long single-chain simulations of free polymers with a poor implicit medium. Additionally, the solvent pressure is also varied from 0.0021 $\epsilon\sigma^{-3}$ to 0.0208 $\epsilon\sigma^{-3}$ (corresponding to relative pressures from 10% to 99%) at constant ϵ_{pp} and ϵ_{ps}.

The sorption behavior of the system is evaluated by analyzing density profiles of the polymer and the solvent over the z direction (averaged over x and y). During the simulation, these are dumped every 10000 timesteps (averaged over 100 timesteps equally spaced out since the previous frame). In order to ensure properly equilibrated results, the first 95% of all frames is discarded and only the last 5% is time-averaged for further processing. For the calculation of several physical quantities, definitions of spatial limits are required. First, the brush height is defined by the inflection point (point of maximum slope, as determined using a Savitzky-Golay filter) in the polymer density profile. Second, we define a outer limit for the adsorption layer by a (arbitrary) lower

threshold of 0.002 σ^{-4} in the solvent density gradient. Any solvent beyond this point is considered vapor bulk. To mitigate discretization errors in the determination of the limits described above, the density profiles are spatially interpolated 10x using a cubic spline interpolant prior to time-averaging. The amount of absorption (solvent inside the brush) is calculated as the integral of the solvent density profile up to the brush height, and similarly, the amount of adsorption is calculated as the integral of the solvent density profile from the brush height up to the adsorption layer end. The Python code that implements this procedure is available online. [22]

3.3   Theory

The interaction between solvents and grafted or adsorbed polymers is often described using the Flory-Huggins model of mixing. [23–25] The Flory-Huggins model is a lattice model, in which every particle is assumed to occupy exactly one site in a fully occupied lattice of arbitrary geometry. [26] Polymer beads and solvent particles are placed onto lattice sites randomly, respecting the requirement of connectivity along polymer backbones. Employing a mean-field assumption with respect to the composition of the system, the combinatorial entropy of placing the particles on the lattice can be determined, resulting in an entropy-of-mixing expression

$$\frac{\Delta S_{\mathrm{mix}}}{k_{\mathrm{B}}} = -(n_{\mathrm{s}} \ln \phi_{\mathrm{s}} + n_{\mathrm{p}} \ln \phi_{\mathrm{p}}), \tag{3.6}$$

with S being the entropy, n the number of molecules of a given species, ϕ the site fraction of a given species, and subscripts s and p denoting solvent and polymer respectively. Note that n_{p} represents the number of polymer chains, and so the number of polymer-occupied sites is $n_{\mathrm{p}}N$, with N the degree of polymerization. The energetic effects of mixing are treated by defining an interaction parameter

$$\chi = \frac{zW}{k_{\mathrm{B}}T}, \tag{3.7}$$

where z is the coordination number of the lattice, T is the temperature, and W is the energetic effect of forming a single solvent-polymer contact by eliminating solvent-solvent and polymer-polymer contacts, meaning that

$$W = -\epsilon_{\mathrm{ps}} + \frac{1}{2}(\epsilon_{\mathrm{ss}} + \epsilon_{\mathrm{pp}}) \tag{3.8}$$

under the assumption that the spacing of the Flory-Huggins lattice is determined exactly by the minimum of the Lennard-Jones potential. Hence, negative W indicates mixing is enthalpically favorable, although entropy-driven mixing may still be possible for positive W. We will refer to W as the relative affinity between polymer and solvent.

Using the aforementioned mean-field assumption for the polymer and solvent concentrations, this results in an energetic contribution of

$$\frac{U_{\text{mix}}}{k_{\text{B}}T} = \chi n_{\text{s}}\phi_{\text{p}},$$
(3.9)

and a total free energy of mixing of

$$\frac{F_{\text{mix}}}{k_{\text{B}}T} = n_{\text{s}}\ln\phi_{\text{s}} + n_{\text{p}}\ln\phi_{\text{p}} + \chi n_{\text{s}}\phi_{\text{p}}.$$
(3.10)

The model as outlined above does not account for grafting effects, however. First of all, grafting of the polymer chains removes their translational entropy, meaning that the second addend in Equation 3.10 should be eliminated. Additionally, grafted chains can swell only by extending, which incurs an entropic penalty. A mean-field elasticity term dependent on the height of the brush can be used to describe the entropic elasticity of polymer chains in the swollen brush. [7, 27] This requires $\rho_{\text{g}} << N^{2/3}$ (with ρ_{g} the grafting density of the brush in chains σ^{-2}), as this ensures that collapsed brush states do not display substantial lateral inhomogeneities [27]. Our primary simulations meet this condition by a factor of roughly 3.5. The introduction of this elasticity results in a new free energy expression

$$\frac{F_{\text{mix}}}{k_{\text{B}}T} = n_{\text{s}}\ln\phi_{\text{s}} + \chi n_{\text{s}}\phi_{\text{p}} + n_{\text{p}}\frac{3h^2}{2N},$$
(3.11)

with h being the height of the polymer brush. This amounts to an Alexander-de Gennes ansatz, [28, 29] in which all chain ends are located at the outer edge of the brush. Assuming the density of the swollen brush to be independent of its composition, the height of the brush becomes directly proportional to the number of particles per unit area. Per polymer chain, this may be expressed as

$$h \approx \frac{N\rho_{\text{g}}}{\phi_{\text{p}}}.$$
(3.12)

As a result the elasticity term can also be expressed in the form

$$n_{\text{p}}\frac{3N\rho_{\text{g}}^2}{2\phi_{\text{p}}^2}.$$
(3.13)

Taking the derivative of this elasticity-adjusted free energy expression with respect to the amount of absorbed solvent yields the chemical potential for solvent within the brush:

$$\frac{\mu_{\text{in}}}{k_{\text{B}}T} = \ln(1 - \phi_{\text{p}}) + \phi_{\text{p}} + \chi\phi_{\text{p}}^2 + \frac{3\rho_{\text{g}}^2}{\phi_{\text{p}}}. \tag{3.14}$$

Note that any direct dependence on N can be incorporated into a ϕ_{p} term, meaning that we expect to see a quantitatively similar relation between interaction parameters and bulk composition for different chain lengths. Although this is convenient for the current discussion, this prediction is limited to monodisperse systems, as it relies on the assumption that every polymer chain occupies the same volume.

At chemical equilibrium, the chemical potential for solvent inside the brush and for the solvent vapor phase are equal by definition. Ideally, the chemical potential of the bulk vapor is given by

$$\frac{\mu_{\text{out}}}{k_{\text{B}}T} = \ln\left(\frac{P}{P_{\text{sat}}}\right), \tag{3.15}$$

with P indicating the pressure of the vapor phase, and P_{sat} the saturation pressure of the vapor. We outline a procedure for determining P_{sat} of the simulated vapor in the Supporting Information, Section 1. Hence, the equilibrium absorption behavior of the brush is determined by

$$\ln\left(\frac{P}{P_{\text{sat}}}\right) = \ln(1 - \phi_{\text{p}}) + \phi_{\text{p}} + \chi\phi_{\text{p}}^2 + \frac{3\rho_{\text{g}}^2}{\phi_{\text{p}}}. \tag{3.16}$$

From this, we obtain dependencies of the brush swelling on several parameters. The absence of explicit dependencies on the individual interaction energies ϵ_{ss}, ϵ_{pp} and ϵ_{ps} indicates that we may expect identical sorption behavior for any combination of interaction energies that results in a given value of χ. It should be noted that this is reliant on the assumption that the system density and coordination number remain constant with this variation of interaction energies, however.

Since Flory-Huggins-derived models are primarily concerned with bulk composition, we may expect the greatest deviation from conventional theory at the brush-vapor interface. Both the structure and composition of the interface are not easily predicted. However, by describing the system as sharply-defined polymer, solvent and vapor layers, we can obtain a first approximation of

the adsorption behavior. In this idealized model, adsorption would be determined by the Hamaker constant for polymer and vapor interacting across the solvent layer. [30] Making use of combining rules, the Hamaker constant for such a three-phase system can be decomposed into the Hamaker constants for individual materials in vacuum as

$$A_{\mathrm{psv}} = \left(\sqrt{A_{\mathrm{pp}}} - \sqrt{A_{\mathrm{ss}}}\right)\left(\sqrt{A_{\mathrm{vv}}} - \sqrt{A_{\mathrm{ss}}}\right),\qquad(3.17)$$

with A the Hamaker constant and the subscript v denoting vapor. If this combined Hamaker constant is negative, the net interaction between the polymer-solvent and solvent-vapor interfaces is repulsive, meaning that the formation of an adsorption layer is energetically favorable. A_{ii}, with i an arbitrary component, is typically positive, and is negligible for gases. Hence, the second term on the right-hand-side of Equation 3.17 will always be negative for the systems under consideration, and the sign of A_{psv} is determined by the first term. Under the simplifying assumption that the polymer and solvent phases are entirely incompressible (i.e. their density is independent of their self-affinity), A_{pp} and A_{ss} become directly proportional to ϵ_{pp} and ϵ_{ss}. As a result, we may expect adsorption for $\epsilon_{\mathrm{pp}} > \epsilon_{\mathrm{ss}}$. Note, however, that this approach implicitly assumes no absorption of solvent, and makes use of the same mixing rules we explicitly disregard in our parameter selection.

3.4   Results and Discussion

In this section, we will first discuss the effects of the individual interaction energies ϵ_{pp} and ϵ_{ps} on sorption behavior, based on density profiles extracted from our simulations. We also discuss the effect of the relative polymer-solvent affinity W, and relate this to the Flory-Huggins theory. Next, we show results across the same parameter space for different brush densities and compare brush density effects to theory. Finally, we show the effect of the relative vapor pressure on absorption for selected interaction energies, at chain lengths of $N = 30, 60, 100$. Data underlying all figures are available online free of charge. [31]

It is typical to discuss interactions in polymeric systems in terms of a second virial coefficient, as seen in related work by Mukherji et al. [32] and Opferman et al. [33] We express our results in terms of W and various ϵ, since this research is restricted to particles of a single size. A model for the general case would have to make use of such a virial coefficient in order to account for particle size effects.
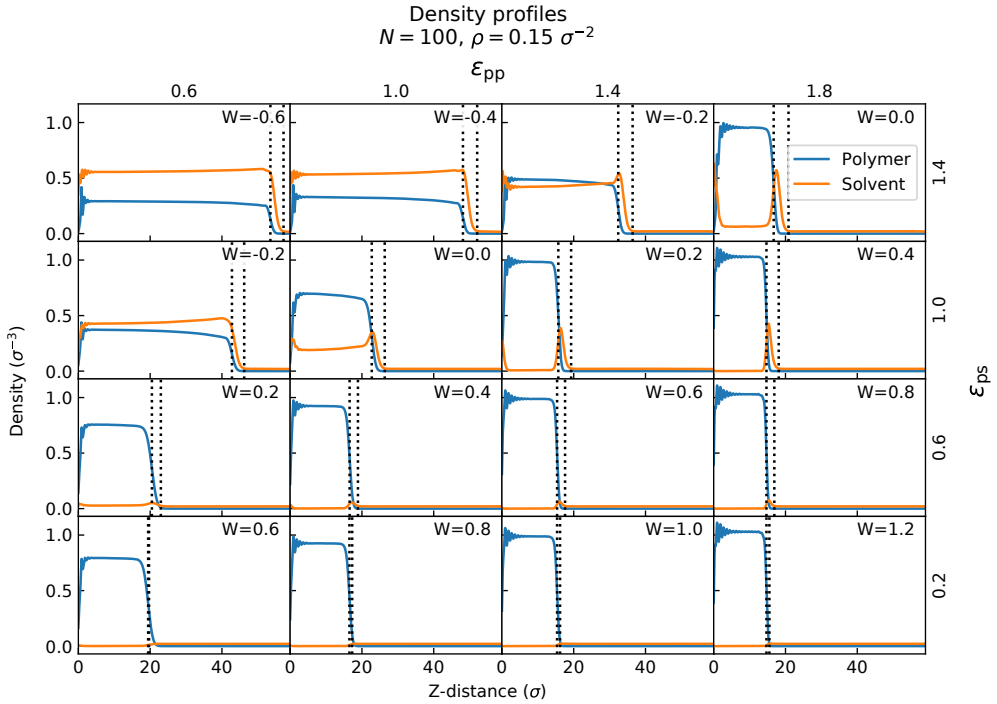
Figure 3.2: Density profiles of polymer (blue) and solvent (orange) for a 4x4 grid of ϵ_{pp} and ϵ_{ps} values, at $N = 100$ and $\rho = 0.15\ \sigma^{-2}$. The dotted lines indicate the limits of the adsorption layer as defined by the top of the polymer brush and the top of the adsorbed solvent layer respectively.

Effect of Brush and Solvent Affinities

The density profiles obtained for a 4x4 grid in ϵ_{pp}, ϵ_{ps} parameter space are shown in Figure 3.2. Each of the 16 graphs shows the density profiles (number density vs z-distance) of the polymer (blue) and solvent (orange) particles in the brush system. The polymer brush height is indicated by the first dotted vertical line. The second dotted line indicates the outer edge of the adsorption layer.

Immediately visible is absorption in the top-left corner of Figure 3.2 (low ϵ_{pp}, high ϵ_{ps}) indicated by the elevated concentration of solvent within the brush. In contrast, in the top-right corner (high ϵ_{pp}, high ϵ_{ps}), solvent uptake is dominated by adsorption, as shown by the peaks in solvent density near the brush surface. Little sorption of any kind occurs at the lower part of the figure (low ϵ_{ps}). Note that adsorption and absorption are not mutually exclusive, as

evidenced by the coexistence of bulk absorption with a solvent density peak at the interface at several points (e.g. $\epsilon_{\mathrm{pp}} = \epsilon_{\mathrm{ps}} = 1.4$).

In the absorption regime (top left of Figure 3.2), we observe solvent uptake coupled with strong swelling of the brush, as well as the formation of a solvent layer on top of the brush. Taking the dry brush height at a given ϵ_{pp} as reference, we find swelling ratios of over 2 for the most swollen systems. This is comparable to experimentally determined swelling ratios, which range up to approximately 2 for poly(methyl methacrylate) [7], modified poly(2-(dimethylamino)ethyl methacrylate) [5] and poly(2-methacryloyloxyethyl phosphorylcholine) [34] brushes under good solvent vapors. Polymer density profiles decay only very slightly as a function of the distance from the surface, then fall off dramatically in a narrow interfacial region. This behavior qualitatively resembles the results of a self-consistent field model by Sun et al. [6] This model predicts polymer brushes under a vapor atmosphere to assume a density profile similar to the classical parabolic field, [35, 36] but with a more sharply defined interface. Furthermore, solvent densities in these highly swollen systems are generally high and constant throughout the brush. This suggests that the attraction between polymer and solvent leads to condensation of the vapor. The occurrence of absorption for these parameter combinations matches a simple picture based on the interchange energy between bulk phases. As the insertion of a solvent particle into the brush leads to the displacement of polymer-polymer interactions, the polymer-solvent affinity must be greater than the average of the polymer and solvent self-affinities for absorption to occur.

As we move to the top-right corner of the figure, we observe primarily adsorption, as the strong polymer self-affinity largely precludes solvent absorption; the interior of the polymer brush contains little to no solvent, but a solvent layer still covers the surface of the brush. Translational entropy of the solvent leads to some penetration of solvent into the brush, but chain stretching into the solvent layer is precluded by the associated entropic penalty. As a result, the brush density profile falls off rather sharply near the interface in this regime. The fact that an adsorption layer of solvent can form for a wide range of interaction parameters is notable. Liquid adsorption on polymer brushes is of great practical interest, as e.g. the lubricious properties of brushes result in significant part from the formation of a stable liquid layer on top of the brush. [24, 37] We also find an enrichment in solvent near the grafting plane in a number of these systems. Since the grafting plane truncates the brush bulk, it creates a second interfacial region. We may therefore expect the component

that interacts less strongly with the bulk to accumulate at the grafting plane. The adsorption of solvent to the grafting plane is further favored by the fact that the solvent monomers do not lose any conformational entropy near the grafting plane, unlike the polymer chains.

Finally, the bottom profiles (low ϵ_{ps}) exhibit little sorption at all. W values in this regime are positive or zero, and solvent absorption carries an entropic penalty through chain stretching. As previously discussed, we would still expect adsorption for the cases where $\epsilon_{pp} > \epsilon_{ss}$, as this results in a negative value of the two-interface Hamaker constant. However, ϵ_{ps} is also less than $k_B T = 0.85$, meaning that the thermal motion of the solvent particles will dominate over the polymer-solvent attraction. A stable adsorption layer cannot be formed as a result. For $\epsilon_{ps} = 0.6$ and $\epsilon_{pp} = 0.6$, the small adsorption appears to be inside the brush. However, examination of the snapshots indicate that the solvent resides to a large extend in valleys of the rough brush surface, instead of inside the brush.
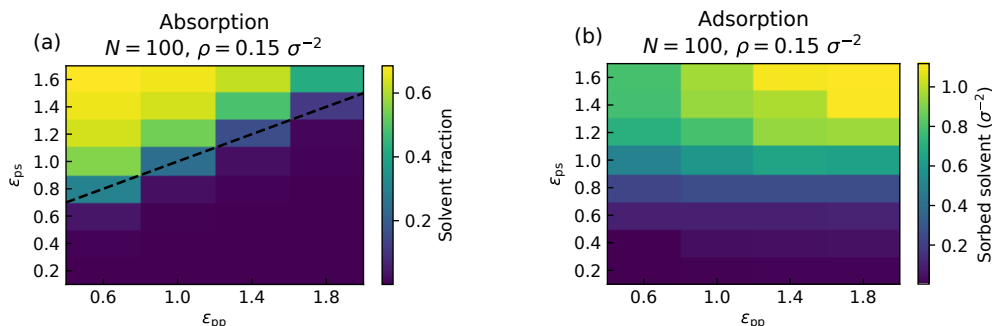
Figure 3.3: Heatmaps of the amount of absorption (solvent fraction) **(a)** and adsorption (integrated solvent density) **(b)** at $N = 100$ and $\rho = 0.15\ \sigma^{-2}$. The dashed line in the absorption heatmap denotes the locus where $W = 0$.

Figure 3.3 **(a)** and **(b)** show heatmaps of the solvent fraction inside the brush and the integrated excess solvent density outside of the brush respectively, over $\epsilon_{pp}, \epsilon_{ps}$ space covered by our simulations. From Figure 3.3 it is clear that both adsorption and absorption vary with ϵ_{pp} as well as ϵ_{ps}.

Absorption appears approximately constant along lines of slope $1/2$. Since the solvent self-affinity for these systems is fixed, this corresponds to constant W. This indicates that mixing behavior is determined by the relative polymer-solvent affinity, and may follow Flory-Huggins theory. We discuss this point in more detail further on.

In the diagram for adsorption, a sharp increase in adsorption is clearly visible between $\epsilon_{\mathrm{ps}} = 0.8$ and $\epsilon_{\mathrm{ps}} = 1$, corresponding to the requirement that $\epsilon_{\mathrm{ps}} > k_{\mathrm{B}}T$. Adsorption increases with ϵ_{pp}, matching our previous argument based on the Hamaker constant. More intuitively, this behavior can also be explained as a density effect. For strong polymer self-affinities, the attraction between beads leads to relatively dense, contracted brush profiles. As a result, the density of attractive interactions a solvent particle near the interface experiences will increase with ϵ_{pp}, rendering adsorption more favorable energetically. Moreover, for lower ϵ_{ps}, solvent absorption increases, such that polymer density in the top of the brush reduces even further.

At high ϵ_{ps}, some degree of solvent adsorption persists even when $\epsilon_{\mathrm{pp}} < \epsilon_{\mathrm{ss}}$, contradicting our expectations based on the two-interface Hamaker constant. The observation of an enhanced solvent density in the top of the brush for highly swollen brushes, is consistent with experimental observations. [4, 6] Yet, it appears to clash with self-consistent field theory by Cohen Stuart et al., [38] which indicates the possibility of chain segments adsorbing at the brush-air interface for low ϵ_{pp}. We attribute the absence of a polymer-enriched phase at the interface to the relatively high entropic penalty for chain stretching, which arises from the relatively short chain length and high grafting density we employ in our simulations. This is supported by polymer and solvent density profiles for $N = 30$, presented in the SI (Section 3). In these profiles, the difference between solvent densities in the brush bulk and at the interface is more pronounced than for $N = 100$, suggesting that the finite extensibility of the polymer chains does indeed limit polymer adsorption at the interface.

Figure 3.4 presents the same information as Figure 3.3 **(a)**, but in the form of solvent fraction against W, which represents the energetic effect of forming a single polymer-solvent contact at the expense of the polymer and solvent bulk interactions. Conventionally, W is expected to be directly proportional to χ (see Equation 3.7). For all values of ϵ_{pp}, the transition from a collapsed brush to a swollen one occurs in the same range of W values, with higher ϵ_{pp} showing less absorption in the intermediate range. For all ϵ_{pp}, absorption is observed for positive W already, where interaction energies alone are not sufficient to result in mixing. This indicates that the increase in translational entropy for our solvent beads is higher than the entropic penalty for polymer stretching upon mixing these concentrations. The opposite is often observed for brushes in contact with polymer melts, [39–41] because melt-polymers gain less translational entropy than solvent molecules upon mixing.

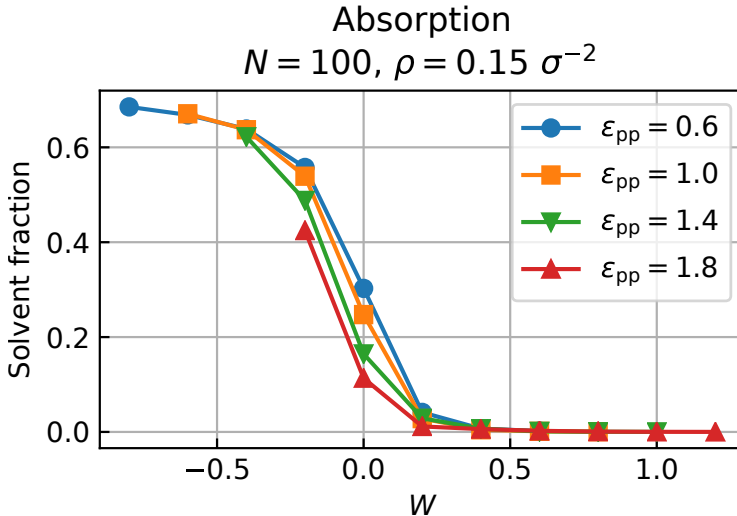The relatively minor difference in the transition W is remarkable, as the relative

Figure 3.4: Absorption (solvent fraction) plotted against the relative affinity W for several values of ϵ_{pp}, at $N = 100$ and $\rho = 0.15$. The lines connecting markers are meant to guide the eye.

affinity is defined between two dense bulk phases. No liquid solvent bulk phase is present in our simulations, however. In a simple view of the system, this would lead us to expect a negligible effective value for ϵ_{ss} due to the low density of the vapor phase, and a free energy of mixing dependent on the composition of the interface. We speculate that vapor absorption in polymer brushes is a two-step process, in which particles are first adsorbed to form a dense (multi-)layer, which subsequently diffuses into the polymer phase.

Despite qualitative similarities, the absorption behavior for different ϵ_{pp} in Figure 3.4 varies quantitatively at intermediate values of W. Specifically, systems with a low polymer self-affinity absorb more solvent. This is possibly because dry brushes at high self-affinity are denser than their low ϵ_{pp} counterparts (see Figure 3.2, bottom row). If free volume is present in the dry brush, the free site may be replaced with a solvent particle at no cost of combinatorial entropy and without increasing the brush stretching. Hence, a brush that contains free volume in its dry state incurs a smaller entropic penalty for absorbing moderate amounts of solvent. This also matches the fact that solvent fractions appear to tend towards a common plateau value again at very negative W. This does represent a breakdown of the assumption that the polymer phase is incompressible, which we have used so far. In the context of the extended

Flory-Huggins model, this would have two consequences: with a change of the interparticle distance, the effective strength of interactions between neighboring particles would also change, and the coordination number (z in Equation 3.7) in the fluid would no longer be constant. The latter in particular could have a substantial impact on the system behavior. The former is of less concern, as the ϵ values we choose remain linearly related to the actual interaction.

A dependence of the coordination number on ϵ_{pp} would provide an intuitively attractive explanation for the difference in absorption across the transition shown in Figure 3.4. However, if this were the case, we would expect to see equal solvent fractions for all systems at $W = 0$, since this corresponds to a χ value of 0 regardless of the coordination number. While it is plausible that z would vary with ϵ_{pp}, we consider it unlikely that this would be the sole cause of the variation in absorption. We also note that the shape of the absorption curves appears to vary, suggesting either a nonlinear relation between ϵ_{pp} and the effective interaction parameter, or a dependence on ϵ_{ps} as well as ϵ_{pp}. In SI Section 4, we display calculated χ values based on the solvent fraction for each point in Figure 3.4.

Effect of Grafting Density
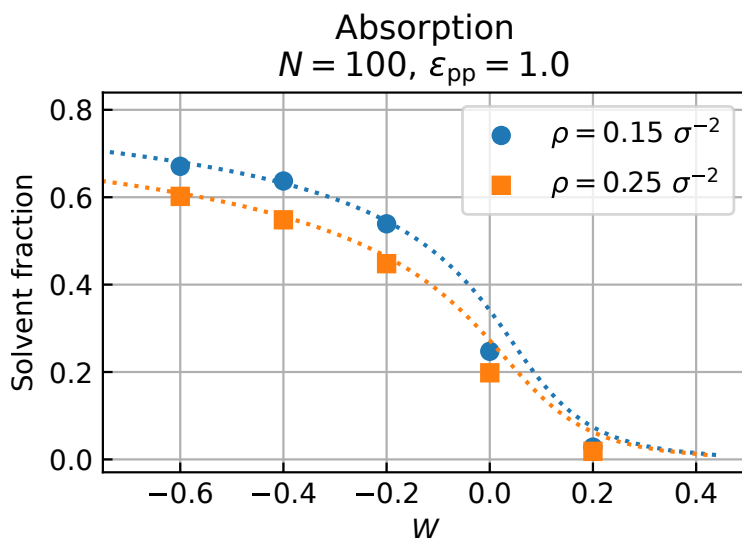
Figure 3.5: Absorption (solvent fraction) plotted against the relative affinity W for two different grafting densities at $N = 100$ and $\epsilon_{\mathrm{pp}} = 1.0$. The dotted curves correspond to theoretical predictions.

Figure 3.5 displays the amount of absorbed solvent as a function of W for two different values of the grafting density. Theoretical curves were obtained by rearranging Equation 3.16 to isolate χ. A linear relation between χ and W was obtained through a least-squares fit for the calculated χ of all points of $\epsilon_{\mathrm{pp}} = 1.0$ in Figure 3.4. As we discussed already W and the effective χ may not be directly proportional. [42] Yet, we consider this approach more informative than ad-hoc adjustments. As the relative affinity becomes positive, both curves tend towards zero absorption. For strongly negative values of W, solvent fractions at both grafting densities tend towards a plateau value, as the brush becomes saturated with solvent. These plateau values must decrease with grafting density for a given chain length, as the maximum volume available to the brush depends only on the chain length. Below these plateau values, the brush of lower grafting density still takes up more solvent. This matches the extended Flory-Huggins model: the elasticity contribution to the free energy (Equation 3.11) is quadratic in h, and h is directly proportional to the number of particles under the assumption that the brush-solvent system is incompressible. Hence the chemical potential for solvent particles in the brush will be more positive in a more extended brush, i.e. the one of higher grafting density (all else remaining equal).

Effect of Relative Vapor Pressure

Solvent fractions in the brush as a function of the relative solvent pressure are depicted in Figure 3.6 for three different polymer chain lengths at $\epsilon_{\mathrm{pp}} = 0.6$, $\epsilon_{\mathrm{ps}} = 1.0$. We obtain an expected pressure-composition relation for by exponentiating Equation 3.16, resulting in

$$\frac{P}{P_{\mathrm{sat}}} = (1 - \phi_{\mathrm{p}}) \exp\left(\phi_{\mathrm{p}} + \chi\phi_{\mathrm{p}}^2 + \frac{3\sigma^2}{\phi_{\mathrm{p}}}\right). \tag{3.18}$$

We realize that ϕ_{p} results from the imposed $\frac{P}{P_{\mathrm{sat}}}$. Yet, we express $\frac{P}{P_{\mathrm{sat}}}$ in terms of ϕ_{p} rather than vice versa because the resulting expression is more convenient to work with. In experiments and simulations, the relative solvent pressure will generally be the independent variable, and the model discussed thus far depends on the vapor phase being unaffected by the brush composition. In a traditional Flory-Huggins description, ϕ_{p} would go to zero as $\frac{P}{P_{\mathrm{sat}}}$ approaches unity. However, this causes the elasticity term $\frac{3\sigma^2}{\phi_{\mathrm{p}}}$ to diverge, and we obtain a finite ϕ_{p} when $\frac{P}{P_{\mathrm{sat}}} = 1$. The theoretical curves displayed correspond to a χ parameter of -1.7, which was determined based on a least-square fit of the
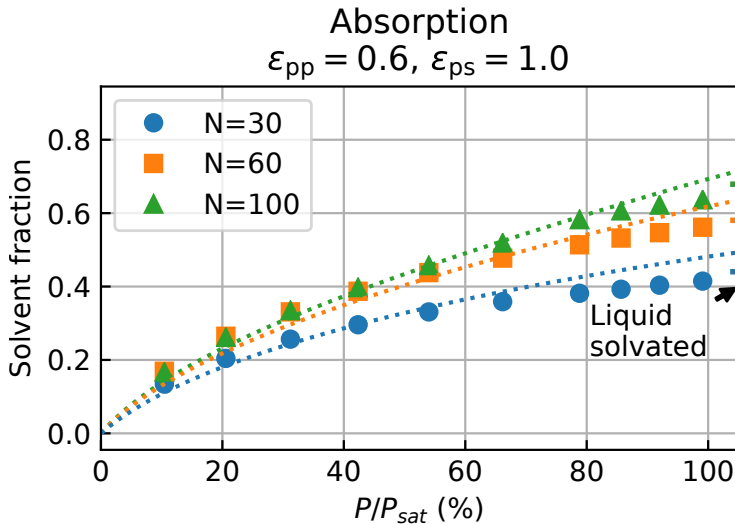
Figure 3.6: Absorption (solvent fraction) plotted against the relative solvent vapor pressure for different chain lengths, at $\epsilon_{\rm pp} = 0.6$ and $\epsilon_{\rm ps} = 1.0$. The grafting densities used are $\rho = 0.34$, 0.21, and 0.15 σ^{-2} respectively (for increasing N). The dotted curves correspond to theoretical predictions for $\chi = -1.7$.

data for $N = 100$. In accordance with the extended Flory-Huggins model, we find that the solvent fraction increases non-linearly with the relative solvent pressure, and reaches a plateau value at high $\frac{P}{P_{\rm sat}}$. This indicates that the presence of the brush cannot cause the condensation of a macroscopic solvent layer. For low values of $\frac{P}{P_{\rm sat}}$, the expected absorption curves closely match the observed absorption behavior. At higher relative pressures, however, the solvent fraction as extracted from our simulations levels off more than expected. This may once again be an effect of finite chain extensibility. Absorption behavior is qualitatively the same for all cases, but varies quantitatively with the chain length. This can be attributed to the difference in grafting density between systems, as the absorption behavior described by Equation 3.18 does not depend directly on the polymer chain length.

Experimental results show typical curves of absorption against pressure to be convex, [2–5, 8, 43] as opposed to the concave relations we obtain from both theory and simulations. This difference in shape of the absorption curve is a consequence of the large negative value of χ and the high grafting density of the brush. For positive χ, the extended Flory-Huggins model does indeed predict

the absorption curve to be convex. Predicted pressure-composition relations for a range of values are presented in Section 5 of the SI. Flory-Huggins parameters for well-solvated polymers are typically close to 0.5, although small negative values of χ are experimentally attainable. [44] This suggests that it may be possible to realize such concave-downward absorption curves experimentally for a highly attractive solvent-brush combination at high grafting densities. As such a system would retain large amounts of solvent even at low partial solvent pressures, this could increase the longevity and robustness of specific brush-solvent systems in air.

3.5 Conclusions

Solvent ab- and adsorption for polymer brushes in chemical equilibrium with solvent vapor have been investigated for a range of interaction parameters, brush densities and relative solvent pressures. The density for brushes and solvents for vapor-solvated systems are different from the density profiles for liquid-solvated systems. Moreover, adsorption films with an enhanced solvent density can be observed. Via analysis of the solvent fraction in the brushes, we find that a Flory-Huggins model that incorporates an entropic penalty for stretching brush-polymers describes highly swollen systems at different grafting densities well, but appears to overestimate absorption for high relative solvent pressures and in the onset of absorption. Variation of interaction parameters indicates that the effective value of χ depends on individual interaction parameters even in the absence of chemical specificity. This is a departure from the classical definition of the Flory-Huggins parameter as a function of the interchange energy between two components. The occurrence of adsorption is predicted qualitatively by the classical Hamaker theory, independently of the absorption behavior. However, some nonidealities are seen as a result of differences in the composition of the brush-air interface and the finite length of the simulated polymers. To further improve Flory-Huggins type models, chain conformations and free volume in the brush as a function of the interaction energies should be investigated.

Acknowledgements

3.6   Supporting Information

Determination of P_{sat} for LJ fluid

The thermodynamic properties of a LJ fluid are very sensitive to the exact truncation and shifting method used. As we were unable to find any values for P_{sat} in the conditions employed in our simulations, we determined the saturation pressure using MD.

For a vapor in equilibrium with the corresponding liquid phase, the pressure is constant and equal to the saturation pressure of the fluid. Hence, for any system in which vapor and liquid coexist at equilibrium, the pressure should be independent of the overall density. We make use of this well-known property by simulating vapor-liquid systems of various overall densities, and determining the pressure of the bulk phases.

Cubic simulation boxes with periodic boundary conditions, containing $N = 10000$ particles each, are used to determine the saturation pressure. The overall number density ρ of particles is varied by changing the simulation box volume, so that the length of the box in any dimension is equal to $\left(\frac{N}{\rho}\right)^{1/3}$. Simulations are performed at $\rho = 0.037, 0.050, 0.63, 0.075, 0.088, 0.100, 0.113, 0.125 \ \sigma^{-3}$, which all fall within the coexistence region. In all cases, temperature is kept at $T = 0.85$ using a chain of 3 Nosé-Hoover thermostats with a time constant of $0.5 \ \tau$. These simulations are run for 1 million timesteps with a timestep of $\Delta t = 0.005 \ \tau$ while pressure profiles are sampled.

At these densities, the system will assume a slab geometry along any of the three dimensions. This is a result of the periodicity of the boundaries, which eliminates the slab surface along two of the three dimensions. As a result, for a range of values of ρ, the interfacial area for the slab geometry is less than that of a spherical droplet of equal volume. However, the bulk pressure of

either phase should not be affected by the shape of the interface. We make use of this by introducing the particles to the simulation box in a slab along the x, y plane. This results in orientation of the equilibrium slab along said plane, allowing us to take pressure profiles along z only. However, as a result of the scale of our simulations, interfacial contributions to the total pressure are significant. To determine the bulk pressure, we only take into account points for which the absolute density gradient lies below a certain threshold value (see Figure 3.7).

Performing this construction for every ρ gives a value for saturation pressure of the LJ fluid of $P_{\text{sat}} = 0.021 \ \epsilon\sigma^{-3}$ (see Figure 3.8).
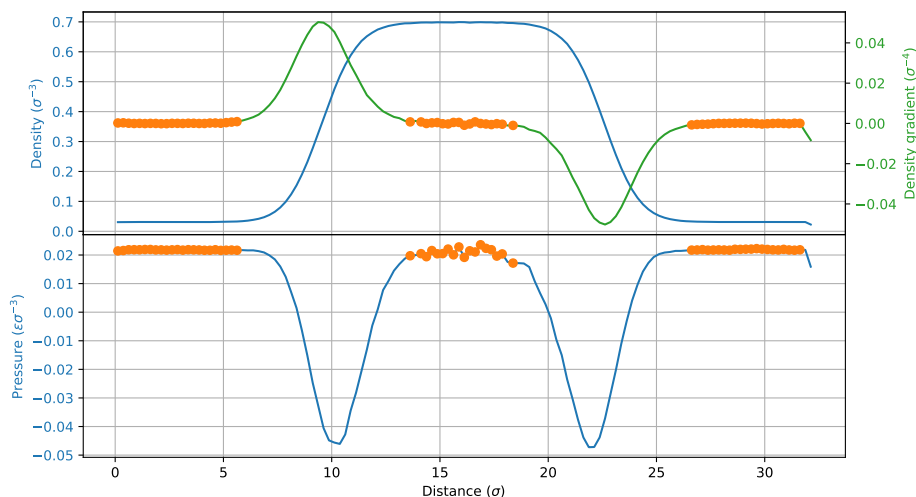
Figure 3.7: Density (top) and pressure (bottom) profiles for $\rho = 0.3 \ \sigma^{-3}$. The orange points indicate the bulk phases.
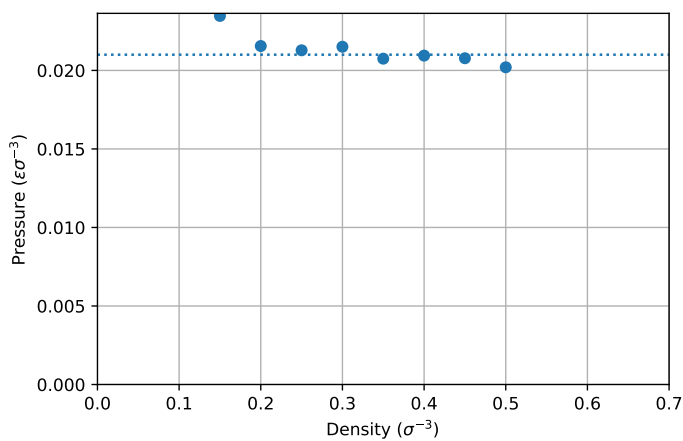
Figure 3.8: Mean pressure in the bulk of both phases as a function of overall density. The first point is considered an outlier due to instability of the interface.

Relation between P and P_{res} in GCMC

The GCMC mechanism maintains a virtual reservoir, of which the chemical potential (μ) or pressure (of a virtual ideal gas) is imposed.

In LAMMPS' implementation of this mechanism (`fix gcmc`), the desired pressure of the virtual reservoir can be specified. However, the caveat is that the chemical potential of this reservoir is calculated using the ideal gas equation-of-state:

$$\mu_{\text{res}} = k_{\text{B}}T \ln \left(\frac{P_{\text{res}} \Lambda^3}{k_{\text{B}}T} \right) \tag{3.19}$$

Grand-canonical Monte Carlo aims to equalize the chemical potential of the solvent in the simulation box with that of the virtual reservoir by particle insertions/deletions.

However, the real solvent in the simulation box is a Lennard-Jones fluid, which non-ideality is significant at the conditions used in our system. This causes the actual pressure in the box at equilibrium with the virtual reservoir to deviate from the requested reservoir pressure because an ideal gas was assumed for the latter.

Because the relation between P and P_{res} is not trivially derived from first principles, a 'calibration curve' was constructed by measuring the actual solvent pressure P in an empty box as function of the requested reservoir pressure P_{res}. This is shown in Figure 3.9. Note that P_{res} in this context can be regarded as the effective fugacity of the Lennard-Jones fluid in our simulation.

The points in the vapor phase are well fitted by a quadratic function, which is used to estimate the fugacity.
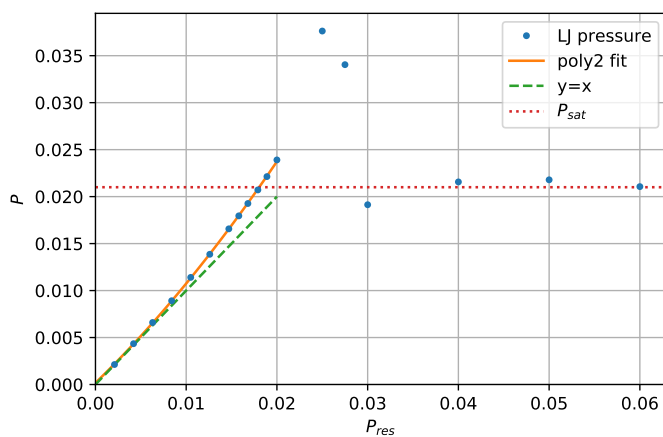
Figure 3.9: P v P_{res} for Lennard-Jones fluid cut-off at $r_{\text{c}} = 2.5\,\sigma$ with quadratic fit (orange curve). The red dotted horizontal line denotes the saturation pressure (P_{sat}) of the fluid. Note that some metastable (supersaturated) state exist at pressures above P_{sat} before it condenses to a liquid.
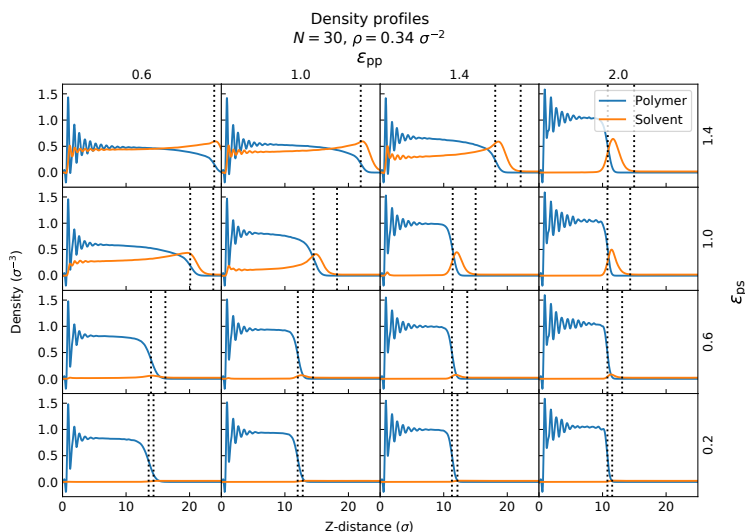
Density profiles, $N = 30$

Figure 3.10: Density profiles of polymer (blue) and solvent (orange) for a 4x4 grid of ϵ_{pp} and ϵ_{ps} values, at $N = 30$ and $\rho = 0.34\ \sigma^{-2}$. The dotted lines indicate the top of the polymer brush and the top of the adsorbed solvent layer respectively.
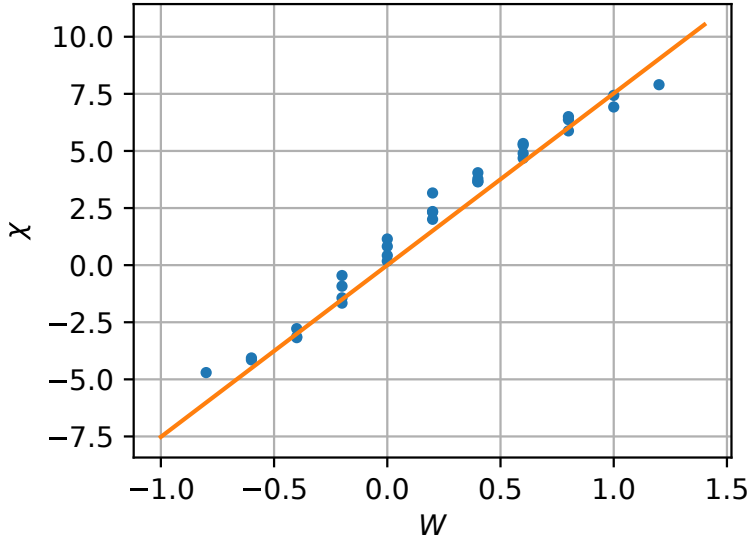
Effective χ values from simulation data

Figure 3.11: Calculated values of χ as a function of the interchange energy W for all points in the $\epsilon_{\text{pp}}, \epsilon_{\text{ps}}$ space investigated.

In Figure 3.11, we show calculated values of χ based on the solvent fractions found in our primary simulations. We obtain these values by isolating χ from the balance of chemical potential (equation 16 of the main work), resulting in

$$\chi = -\phi_{\text{p}}^{-2}\left(\ln(1-\phi_{\text{p}}) + \phi_{\text{p}} + \frac{3\sigma^2}{\phi_{\text{p}}} - \ln\left(\frac{P}{P_{\text{sat}}}\right)\right). \qquad (3.20)$$

We stress that this is purely a method of calculating the χ value that would result in a given brush composition; χ is a property of the brush-solvent combination, and cannot be modified via the polymer fraction. Note that, although points appear to fall near a single line, variation between ϵ_{pp} values at the same W is significant. This is further indication that the extended Flory-Huggins model is quantitatively inexact for these systems.

Predicted absorption for various χ, $\sigma = 0.15$
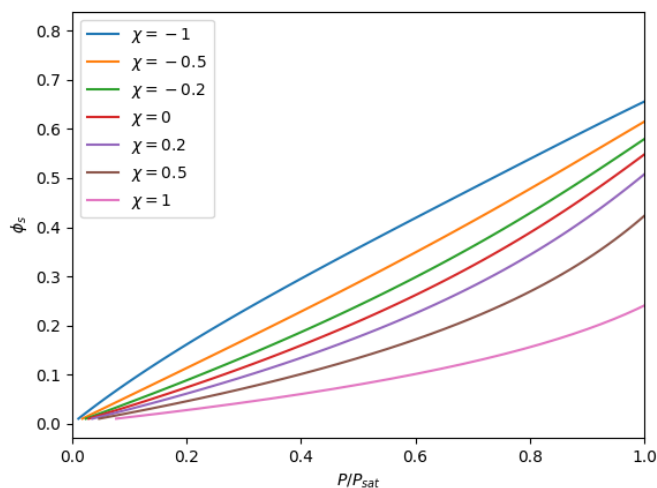

Figure 3.12: Predicted brush composition against relative solvent pressure for values of the Flory-Huggins parameter ranging from -1 to 1. Note in particular the shift from the typical convex curve at positive χ towards the eventual concave form at $\chi = -1$.

3.7 References

[1] P. J. Flory, *Principles of polymer chemistry* (Cornell University Press, Ithaca) (1953).

[2] A. Laschitsch, C. Bouchard, J. Habicht, M. Schimmel, J. Rühe, and D. Johannsmann, "Thickness dependence of the solvent-induced glass transition in polymer brushes", Macromolecules **32**, 1244–1251 (1999).

[3] M. Biesalski and J. Rühe, "Swelling of a polyelectrolyte brush in humid air", Langmuir **16**, 1943–1950 (2000).

[4] C. J. Galvin, M. D. Dimitriou, S. K. Satija, and J. Genzer, "Swelling of polyelectrolyte and polyzwitterion brushes by humid vapors", Journal of the American Chemical Society **136**, 12737–12745 (2014).

[5]   C. J. Galvin and J. Genzer, "Swelling of hydrophilic polymer brushes by water and alcohol vapors", Macromolecules **49**, 4316–4329 (2016).

[6]   L. Sun, B. Akgun, R. Hu, J. F. Browning, D. T. Wu, and M. D. Foster, "Scaling behavior and segment concentration profile of densely grafted polymer brushes swollen in vapor", Langmuir **32**, 5623–5628 (2016).

[7]   S. V. Orski, R. J. Sheridan, E. P. Chan, and K. L. Beers, "Utilizing vapor swelling of surface-initiated polymer brushes to develop quantitative measurements of brush thermodynamics and grafting density", Polymer **72**, 471 – 478 (2015).

[8]   K. N. Jayachandran, P. R. Chatterji, and J. M. Pausnitz, "Vapor-liquid equilibria for solutions of brush poly(methyl methacrylate) in chloroform", Macromolecules **31**, 2375–2377 (1998).

[9]   S. Plimpton, "Fast parallel algorithms for short-range molecular dynamics", Journal of Computational Physics **117**, 1 (1995).

[10] K. Kremer and G. S. Grest, "Dynamics of entangled linear polymer melts: A molecular-dynamics simulation", The Journal of Chemical Physics **92**, 5057 (1990), URL `http://scitation.aip.org/content/aip/journal/jcp/92/8/10.1063/1.458541`.

[11] S. de Beer, E. Kutnyanszky, P. M. Schön, G. J. Vancso, and M. H. Müser, "Solvent induced immiscibility of polymer brushes eliminates dissipation channels", Nat. Commun. **5**, 3781 (2014).

[12] M. K. Singh, P. Ilg, R. M. Espinosa-Marzal, M. Kröger, and N. D. Spencer, "Polymer brushes under shear: Molecular dynamics simulations compared to experiments", Langmuir **31**, 4798–4805 (2015).

[13] L. I. Klushin, A. M. Skvortsov, S. Qi, T. Kreer, and F. Schmid, "Polydispersity effects on interpenetration in compressed brushes", Macromolecules **52**, 1810–1820 (2019).

[14] W. M. de Vos, F. A. M. Leermakers, A. de Keizer, J. M. Kleijn, and M. A. Cohen Stuart, "Interaction of particles with a polydisperse brush: A self-consistent-field analysis", Macromolecules **42**, 5881–5891 (2009).

[15] L. B. Veldscholte, "Mdbrushgenerators", (2020).

3

[16] M. G. Opferman, R. D. Coalson, D. Jasnow, and A. Zilman, "Morphology of polymer brushes infiltrated by attractive nanoinclusions of various sizes", Langmuir **29**, 8584–8591 (2013), URL https://doi.org/10.1021/la4013922.

[17] A. Galuschko and J.-U. Sommer, "Co-nonsolvency response of a polymer brush: A molecular dynamics study", Macromolecules **52**, 4120–4130 (2019).

[18] E. Braun, S. M. Moosavi, and B. Smit, "Anomalous effects of velocity rescaling algorithms: The flying ice cube effect revisited", Journal of Chemical Theory and Computation **14**, 5262–5272 (2018).

[19] L. B. Veldscholte, "Spivhb", (2020).

[20] M. Tuckerman, B. J. Berne, and G. J. Martyna, "Reversible multiple time scale molecular dynamics", The Journal of Chemical Physics **97**, 1990–2001 (1992).

[21] D.R.M. Williams, "Grafted polymers in bad solvents: octopus surface micelles", J. Phys. II France **3**, 1313–1318 (1993), URL https://doi.org/10.1051/jp2:1993202.

[22] L. B. Veldscholte, "Mdbrushanalysis", (2020).

[23] D. Mukherji, C. M. Marques, and K. Kremer, "Smart responsive polymers: Fundamentals and design principles", Annual Review of Condensed Matter Physics **11**, 271–299 (2020), URL https://doi.org/10.1146/annurev-conmatphys-031119-050618.

[24] G.-W. Yang, G.-P. Wu, X. Chen, S. Xiong, C. G. Arges, S. Ji, P. F. Nealey, X.-B. Lu, D. J. Darensbourg, and Z.-K. Xu, "Directed self-assembly of polystyrene-b-poly(propylene carbonate) on chemical patterns via thermal annealing for next generation lithography", Nano Letters **17**, 1233–1239 (2017), URL https://doi.org/10.1021/acs.nanolett.6b05059.

[25] R. A. Gumerov, A. M. Rumyantsev, A. A. Rudov, A. Pich, W. Richtering, M. Möller, and I. I. Potemkin, "Mixing of two immiscible liquids within the polymer microgel adsorbed at their interface", ACS Macro Letters **5**, 612–616 (2016), URL https://doi.org/10.1021/acsmacrolett.6b00149.

[26] P. J. Flory, "Thermodynamics of high polymer solutions", J. Chem. Phys. **10**, 51 (1942).

[27] T. M. Birshtein and Y. V. Lyatskaya, "Theory of the collapse-stretching transition of a polymer brush in a mixed solvent", Macromolecules **27**, 1256–1266 (1994).

[28] S. Alexander, "Adsorption of chain molecules with a polar head a scaling description", J. Phys.-Paris **38**, 983 (1977).

[29] P. De Gennes, "Scaling theory of polymer adsorption", Journal de Physique **37**, 1445–1452 (1976), URL https://hal.archives-ouvertes.fr/jpa-00208546.

[30] J. N. Israelachvili, *Intermolecular and Surface Forces* (Academic Press, Elsevier, USA) (2011).

[31] L. B. Veldscholte, "Sorption characteristics for polymer brushes in equilibrium with solvent vapors: dataset", (2020), URL https://dx.doi.org/10.4121/uuid:f31d3b2b-1a75-43fb-a85e-c4c7e730c329.

[32] D. Mukherji, C. M. Marques, T. Stuehn, and K. Kremer, "Depleted depletion drives polymer swelling in poor solvent mixtures", Nature Communications **8** (2017).

[33] M. G. Opferman, R. D. Coalson, D. Jasnow, and A. Zilman, "Morphological control of grafted polymer films via attraction to small nanoparticle inclusions", Phys. Rev. E **86**, 031806 (2012).

[34] M. Brió Pérez, M. Cirelli, and S. de Beer, "Degrafting of polymer brushes by exposure to humid air", ACS Applied Polymer Materials **2**, 3039–3043 (2020).

[35] S. T. Milner, T. A. Witten, and M. E. Cates, "Theory of the grafted polymer brush", Macromolecules **21**, 2610 (1988).

[36] S. T. Milner, "Polymer brushes", Science **251**, 905 (1991).

[37] J. Klein, "Hydration lubrication", Friction **1**, 1–23 (2013), URL https://doi.org/10.1007/s40544-013-0001-7.

[38] M. A. Cohen Stuart, W. M. de Vos, and F. A. M. Leermakers, "Why surfaces modified by flexible polymers often have a finite contact angle for good solvents", Langmuir **22**, 1722–1728 (2006), URL https://doi.org/10.1021/la052720v.

[39] J. H. Maas, G. J. Fleer, F. A. M. Leermakers, and M. A. Cohen Stuart, "Wetting of a polymer brush by a chemically identical polymer melt: Phase diagram and film stability", Langmuir **18**, 8871–8880 (2002).

[40] C. Pastorino, K. Binder, T. Kreer, and M. Müller, "Static and dynamic properties of the interface between a polymer brush and a melt of identical chains", The Journal of Chemical Physics **124**, 064902 (2006).

[41] L. I. S. Mensink, J. H. Snoeijer, and S. de Beer, "Wetting of polymer brushes by polymeric nanodroplets", Macromolecules **52**, 2015–2020 (2019).

[42] W. Zhang, E. D. Gomez, and S. T. Milner, "Predicting flory-huggins χ from simulations", Phys. Rev. Lett. **119**, 017801 (2017).

[43] O. Rodríguez, F. Fornasiero, A. Arce, C. J. Radke, and J. M. Prausnitz, "Solubilities and diffusivities of water vapor in poly(methylmethacrylate), poly(2-hydroxyethylmethacrylate), poly(n-vinyl-2-pyrrolidone) and poly(acrylonitrile)", Polymer **44**, 6323 – 6333 (2003).

[44] K. Milczewska, A. Voelkel, and K. Piędzia, "Interactions in peg/aerosil® and pla/aerosil® composites described by igc-determined flory-huggins χ_{23} parameter", J. Polym. Res. **21** (2014).

Chapter 4

Vapor Swelling of Polymer Brushes Compared to Non-Grafted Films[*]

Polymer brushes, coatings of polymers covalently end-grafted to a surface, have been proposed as a more stable alternative to traditional physisorbed coatings. However, when such coatings are applied in settings such as vapor sensing and gas separation technologies, their responsiveness to solvent vapors becomes an important consideration. It can be anticipated that the end-anchoring in polymer brushes reduces the translational entropy of the polymers and instead introduces an entropic penalty against stretching when vapor is absorbed. Therefore, swelling can be expected to be diminished in brushes compared to nongrafted films. Here, we study the effect of the anchoring-constraint on vapor sorption in polymer coatings using coarse-grained molecular dynamics simulations as well as humidity-controlled ellipsometry on chemically identical polymer brushes and nongrafted films. We find a qualitative agreement between simulations and experiments, with both indicating that brushes certainly swell less than physisorbed films, although this effect is minor for common grafting densities. Our results imply that polymer brushes indeed hold great potential for the intended applications.

4.1 Introduction

In this chapter, we employ molecular dynamics simulations and humidity-controlled ellipsometry to address the question how end-anchoring of polymer chains to a surface affects the swelling properties of the coating. The systems being studied are illustrated in figure 1. From a theoretical perspective, one can expect that the constraint of end-anchoring the polymers will reduce the vapor sorption of brushes compared to non-grafted films. The end-anchored polymers in a brush incur an entropic penalty when absorbing the vapor, as they must stretch to accommodate the solvent. Thus, they will resist vapor sorption. In contrast, non-grafted chains can rearrange to accommodate solvent in all three dimensions. This leads to a much smaller increase in end-to-end distance, which determines the entropic penalty. Moreover, unbound polymers can gain translational entropy upon absorbing the solvent. Therefore, the expectation is that physisorbed polymer films will swell more than polymer brushes. Yet, it is not clear how significant this effect will be. Experimentally, it has been challenging to study the effect of end-anchoring alone, because it is difficult to keep the coating thickness [1], molar mass, and dispersity [2] constant between coatings of different structure. We address this difficulty by hydrolyzing the polymer-surface bonds in some of our polymer brush samples, resulting in non-grafted films of identical molecular weight and dispersity. Additionally, we study vapor sorption using molecular dynamics (MD) simulations, in which all relevant parameters can be set to isolate the effect of surface-grafting the polymers.

In the following, we will first present a theoretical description for vapor solvation of polymer coatings, based on the classical Flory Huggins model [3]. Next, we will compare the model to MD simulations of coatings that are exposed to vapors at a constant relative vapor pressure using a grand canonical Monte Carlo (GCMC) procedure. To do so, we build on a simulation procedure recently developed in our group [4]. Finally, we augment these MD results with experiments in which the swelling of brushes and chemically-identical degrafted films are compared.

4.2 Theory

The interaction between solvent and polymers can be described by a mean-field model, based on the Flory-Huggins theory of mixing [3]. This model has been shown to successfully describe the vapor-sorption in brushes for one- [4] and
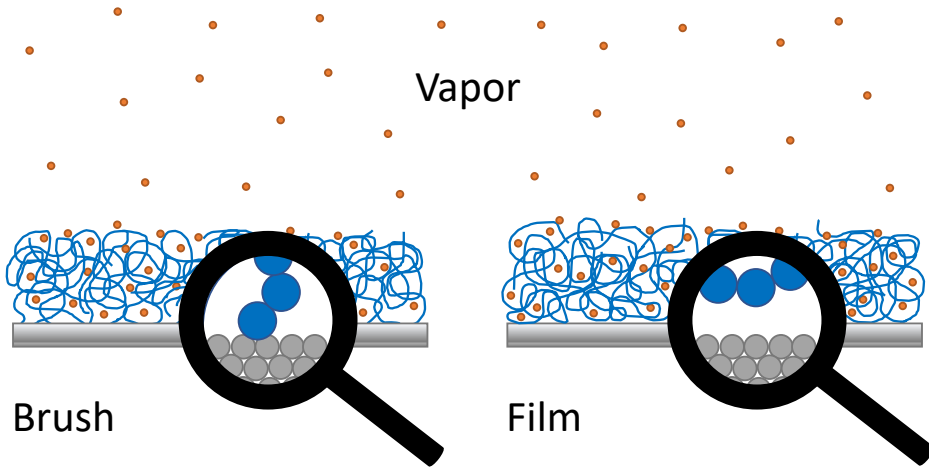
Figure 4.1: Sketch of the two types of systems that are being studied. Polymer brushes (left) and polymer films (right) are kept in equilibrium with a vapor at a constant chemical potential.

two-component [5] solvents. In the model, chemical equilibrium between the solvent vapor and the solvent in the polymer layer is assumed, such that a relation between relative vapor pressure and the solvent volume fraction in the coating can be found. In this section we will derive two distinct equations for brushes and physisorbed films in contact with solvent vapors and we will discuss the differences. We consider interactions that are short-ranged relative to the film thickness, so that interactions with the substrate do not influence bulk swelling behavior.

In the Flory-Huggins theory, a solution is described as a lattice of arbitrary but fixed geometry. In the simplest form of the model, the lattice is fully occupied and each polymer bead or solvent particle occupies exactly one lattice site. This amounts to assuming a constant density for the polymer solution. Particles are distributed over the lattice randomly, in such a way that particles along a polymer backbone are connected. Using a mean-field assumption for the local composition of the solution, a free energy of mixing

$$\frac{F_{\text{mix,f}}}{k_B T} = n_{\text{s,f}} \ln \phi_{\text{s,f}} + n_p \ln \phi_{\text{p,f}} + \chi n_{\text{s,f}} \phi_{\text{p,f}} \tag{4.1}$$

can be derived, in which the first two addends represent the combinatorial entropy of mixing, and the third represents the enthalpy of mixing relative to

the pure bulk solvent and polymer. Here, n is the number of molecules and ϕ the site fraction of polymer (denoted with subscript p) or solvent (denoted with subscript s), k_B is the Boltzmann constant and T the temperature. χ is the well-known Flory-Huggins parameter, which in the ideal theoretical case represents the interchange energy per site between bulk phases of the polymer and solvent. An additional subscript f is appended to all quantities to indicate that this expression describes the non-grafted film, in contrast to the polymer brush (denoted in later equations by subscript b).

The free energy expression described above cannot be used for polymer brushes, since it does not take grafting effects into account. Since chains in a polymer brush are anchored to the surface, they do not possess any translational entropy. The second term in Equation 4.1, which results from the translational freedom gained by the polymer upon solvation, should therefore be eliminated. Moreover, an additional term to include the entropic penalty of stretching of the polymer chains perpendicular to the surface must be added [6]. This results in a free energy expression for the brush:

$$\frac{F_{\text{mix,b}}}{k_B T} = n_{\text{s,b}} \ln \phi_{\text{s,b}} + \chi n_{\text{s,b}} \phi_{\text{p,b}} + n_{\text{p}} \frac{3h^2}{2N} \tag{4.2}$$

where N is the degree of polymerization, and h is the brush height, expressed in monomer lengths. The last term in this expression can be rewritten by assuming a uniform brush density. This means that the height of the brush is proportional to the total number of particles per unit area:

$$h \propto \frac{N\rho_g}{\phi_{\text{p,b}}} \tag{4.3}$$

where ρ_g is the grafting density; the number of chains per unit area. Substituting this expression for h in the free energy expression gives:

$$\frac{F_{\text{mix,b}}}{k_B T} = n_{\text{s,b}} \ln \phi_{\text{s,b}} + \chi n_{\text{s,b}} \phi_{\text{p,b}} + n_{\text{p}} \frac{3N\rho_g^2}{2\phi_{\text{p,b}}^2}. \tag{4.4}$$

Due to this additional force opposing solvent uptake, we expect polymer brushes to absorb less solvent vapor than non-grafted films. This difference should be most pronounced at high solvent uptake (i.e. low $\phi_{\text{p,b}}$), where the stretching term rapidly increases.

We obtain predicted sorption isotherms for both the brush and the non-grafted film by taking the derivatives of the free energy expressions with respect to n_s, which amounts to the chemical potential for solvent in the system. Assuming

the solvent vapor outside the coating to be an ideal gas, for which the chemical potential is given by

$$\frac{\mu_{\text{out}}}{k_{\text{B}}T} = \ln\left(\frac{P}{P_{\text{sat}}}\right),$$ (4.5)

we obtain equilibrium conditions by equating the chemical potential of solvent inside and outside the coating. The resulting relations between vapor pressure and solvent uptake are

$$\ln\left(\frac{P}{P_{\text{sat}}}\right) = \ln(1 - \phi_{\text{p,f}}) + (1 - \frac{1}{N})\phi_{\text{p,f}} + \chi\phi_{\text{p,f}}^2$$ (4.6)

for the non-grafted film, and

$$\ln\left(\frac{P}{P_{\text{sat}}}\right) = \ln(1 - \phi_{\text{p,b}}) + \phi_{\text{p,b}} + \chi\phi_{\text{p,b}}^2 + \frac{3\rho_{\text{g}}^2}{\phi_{\text{p,b}}}$$ (4.7)

for the polymer brush. While real gases typically deviate from ideality at high concentrations, this only influences the chemical potential of vapor outside the coating, and so comparisons between brushes and films at any given pressure should remain valid.

The expressions derived above give the shape of the sorption isotherm for any fixed value of χ. We may also relate the solvent fraction to a swelling ratio, which is more experimentally accessible, via the relation

$$\frac{h}{h_{\text{dry}}} = \frac{1}{(1 - \phi_{\text{s}})}.$$ (4.8)

This relation applies for any definition of the brush height that scales linearly with the total mass per unit area. Figure 4.2 displays the swelling ratio of a non-grafted film and polymer brushes of various grafting densities in an athermal solvent as predicted by this model. These isotherms show reduced sorption in polymer brushes relative to non-grafted films. Since the entropic penalty of stretching the polymer chains increases with the grafting density, solvent absorption is expected to decrease with the grafting density. To test if brushes indeed absorb less solvent than films, we have set up molecular dynamics simulations as explained in the next section.

4.3 Model and methods

Simulations

We investigate the sorption behavior of polymer brushes and films using an alternating molecular dynamics (MD) and grand-canonical Monte Carlo (GCMC)

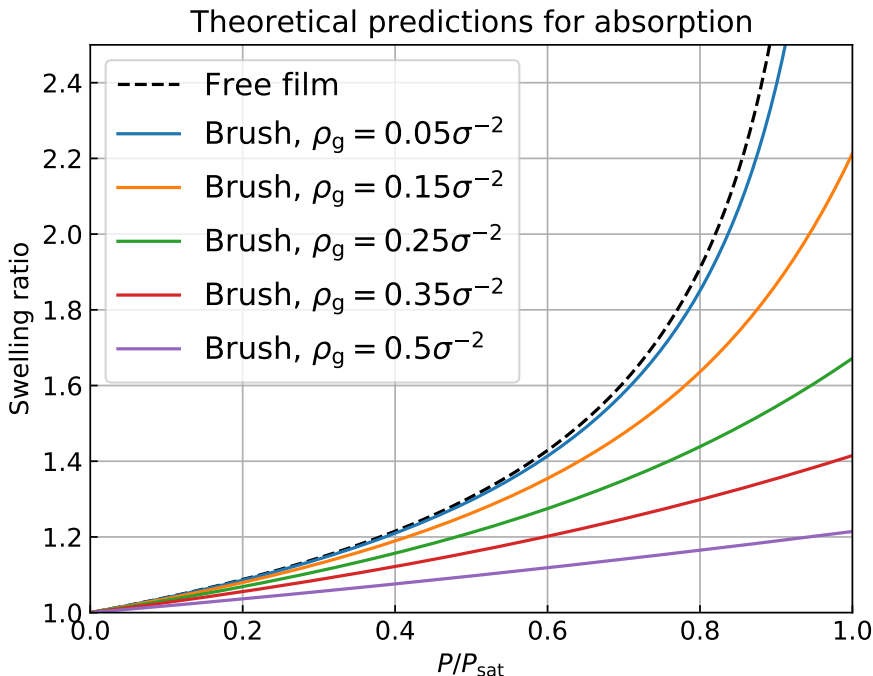## Theoretical predictions for absorption

Figure 4.2: Theoretical predictions for the swelling of the coatings as a function of vapor pressure according to Flory-Huggins theory for film and brush with different grafting densities and $\chi = 0$ and $N = 100$.

procedure, previously described in ref. 4. In this combined procedure, the molecular dynamics simulations model the evolution of the polymer-vapor system. Periodic GCMC sweeps maintain a constant chemical potential of the solvent vapor in a region above the brush. All simulations are performed using the LAMMPS package [7].

We describe our system in the system of reduced units derived from the Lennard-Jones (LJ) potential. Units of length (σ) and energy (ϵ) are derived from the zero-crossing distance and potential well depth of a reference LJ potential. A detailed discussion of the potentials used in our simulations can be found in the Supporting Information.

Our simulations consist of a box of 30 $\sigma \times$ 30 $\sigma \times$ 111 σ in x, y, z with periodic boundary conditions in the x and y dimensions. This box is closed off at the top in z by a mathematical wall, which imposes a strong ($100\ \epsilon\sigma^{-2}$) harmonic

repulsion on particles within 1 σ of the box edge. At the bottom of the box in z, the system is similarly bounded by a 9-3 LJ potential, which effectively models a perfectly flat, homogeneous wall of LJ particles. The potential well depth ϵ_{93} and the zero-crossing distance σ are set to 1, and the potential is cut off at a distance of 2.5 σ.

Simulated coatings are set up in a similar manner, so results are maximally comparable between brushes and non-grafted films. 135 polymer chains with chain length $N = 100$ are placed above the wall, amounting to an areal density of 0.15 chain σ^{-2}. This density ensures that the mean gyration radius of a polymer chain in the globule state is larger than the mean distance between polymers, meaning that chains in the grafted system will always experience excluded volume interactions. These polymer chains are represented by a freely-jointed bead-spring model, based on the coarse-grained model introduced by Kremer and Grest [8]. All interparticle interactions are truncated at 2.5σ, resulting in attractive interactions from the potential minimum up to the cutoff distance. This results in a poor implicit medium, representing the fact that air is an unfavorable medium for polymers. We assume that the LJ potentials we use represent arbitrary short-ranged interactions. Hence, we do not account for combining rules in our parameter selection. For most interactions, we simply use $\epsilon = 1$. However, we vary the polymer-solvent interaction strength ϵ_{ps} over a range from 0.7 to 1.4 (at constant $\epsilon_{\mathrm{pp}} = 1$), and the polymer self-interaction ϵ_{pp} from 0.8 to 1.2 (at constant $\epsilon_{\mathrm{ps}} = 1$).

A GCMC region of 40 σ in z, spanning the whole width of the box, is defined near the top of the box. This region exchanges vapor particles with a virtual atmosphere through the aforementioned GCMC procedure, in which particle insertions and deletions are evaluated according to a Metropolis criterion. GCMC sweeps are performed every 10000 timesteps, with 1000 attempted insertions and deletions per sweep.

This system is initially set up with the polymer chains in a fully extended configuration. In this initial state, each chain is attached by one end to an extra, "frozen" particle near the wall through a finitely extensible non-linearly elastic (FENE) bond. While the resulting configuration is brush-like, it also prevents the unequilibrated polymers from detaching from the surface in the free film case. This system is equilibrated first by energy minimization through the conjugate gradient method. This is followed by 10000 timesteps of dynamics, during which a maximum particle velocity of 1 σ per timestep is imposed. The system is thermostatted by a Langevin thermostat with a damping parameter of 1000 τ (LJ-derived time units) during this run. Afterwards, a second

minimization and 500000 more timesteps of dynamics are performed. During this second run, the damping parameter of the thermostat is set to 100 τ and no velocity limit is applied. In this way, we relax the polymer chains from their initial, extended state to a more entropically realistic one, while ensuring they remain at the surface. At this point, we change the thermostat to a chain of 3 Nosé-Hoover thermostats (which accurately samples the canonical ensemble [9]) and integrate the system for another one million timesteps at an LJ temperature of 0.85. This temperature has been previously verified to allow vapor-liquid coexistence for our vapor parameters. [10] We use the resulting system as the initial state for our polymer brush simulations. The initial configuration for the polymer film simulations is produced by deleting the previously introduced frozen particles, and allowing the system to re-equilibrate for another 1 million timesteps. Next, we perform production runs of 20 million timesteps with the aforementioned GCMC procedure, using the same thermostat. Both the equilibration and the production runs use a two-level rRespa integrator, [11] with an outer timestep of 0.015 τ and an inner timestep length of 0.0075 τ. Non-bonded pair interactions are computed in the outer timestep, while bonded interactions are computed in the inner timestep. These simulations are performed separately for all different combinations of ϵ_{pp} and ϵ_{ps} values. Additionally, sorption isotherms are obtained for $\epsilon_{\text{pp}} = 0.9, \epsilon_{\text{ps}} = 1.0, 1.4$ by changing the chemical potential of the virtual reservoir in the GCMC procedure (and hence the relative solvent pressure P/P_{sat}).

For all runs, density profiles of monomer and solvent particles are collected over the last 4 million timesteps of the simulation, to ensure an equilibrated solvent distribution. We verify that systems are equilibrated by ensuring that the density profiles no longer meaningfully change between the beginning and end of this collection period. In these profiles, we define the brush height as the inflection point of the brush density profile. Absorption is quantified by integrating the solvent concentration from 5 σ above the grafting plane up to the brush height, to exclude possible effects of the mathematical wall. Adsorption is defined by integrating the solvent concentration from the brush height up to the boundary of the solvent layer. We define this boundary as the point where the gradient of the solvent density reaches 0.002. This value is empirically determined to exclude fluctuations in the vapor bulk, while including almost all condensed solvent in the adsorption layer.

Experiments

Materials

Copper (I) bromide (CuBr, Merck, $\geq 98\%$) is purified in glacial acetic acid by continuous stirring until the suspension solution was pale white. After that, the acetic acid is removed, followed by multiple washing cycles with ethanol. Next, the resulting powder is dried in a vacuum oven (room temperature, overnight). 3-sulfopropyl methacrylate potassium salt (SPMAK, 98%), (3-aminopropyl)triethoxysilane (APTES, 98%), α-bromoisobutyryl bromide (BiBB, 98%), 2,2'-bipyridyl ($\geq 98\%$), triethylamine (TEA, $\geq 98\%$) and ethyl α-bromoisobutyrate (EBiB, $\geq 98\%$) were purchased from Merck and used as received. Methanol (ACS reagent) and toluene (ACS reagent) were purchased from Biosolve and used as received. MilliQ water was purified from a MilliQ Advantage A10 purification system (Millipore, Billerica, Ma, USA)

Synthesis of silane-anchored PSPMAK brushes

The followed synthetic route on the grafting of PSPMAK brushes from silicon substrates is explained with detail in Ref.12. Briefly, (3-aminopropyl)triethoxysilane is deposited by means of chemical vapor deposition on piranha-cleaned substrates, followed by the grafting of α-bromoisobutyryl bromide initiators. Afterwards, PSPMAK brushes are synthesized by means of Surface-Initiated Atom Transfer Radical Polymerization (SI-ATRP).

To determine an estimate of the grafting density of our brushes, we perform parallel experiments in which we simultaneously grow brushes in solution and from surfaces by the addition of a sacrificial initiator, ethyl α-bromoisobutyrate (EBiB). Based on the monomer conversion, measured by ^{1}H-NMR, and the initiator concentration in solution, we obtain an estimated molecular weight of 46.6 kDa for brushes around 15 nm in thickness. This corresponds to an approximate chain density of $0.15\,\text{nm}^{-2}$. Although polymerization in solution and from the surface may produce differences in chain length [13] and polydispersity [14], we take this as an order-of-magnitude indication that the surface grafting is sufficiently dense to form a brush. This is also supported by AFM imaging (figure S7), where the high chain density and overall layer uniformity can be visualized.

Films by degrafting brushes

Non-grafted films that are maximally comparable (in terms of thickness, molecular weight, and molecular weight distribution) to the brushes are produced by taking brushes and exposing them to saturated water vapor for an extended period. This reliably degrafts the brushes, without dissolving and removing the polymer from the substrate [15].

The brush samples were stored in an air-tight glass container containing a layer of liquid water for at least 8 weeks, without allowing them to come in contact with the liquid water, after which they are used as-is. Degrafting of the brushes was verified by Atomic Force Microscopy (AFM) imaging of additional samples (not used in subsequent swelling experiments) in their initial state and after degrafting and rinsing with water and ethanol; after the degrafting and rinsing procedure, only sporadic, thin patches of polymeric material remained, indicating that a large majority of polymer chains had in fact been degrafted and subsequently rinsed off. Considering its low surface coverage and thickness relative to the pristine coatings, we are confident that the remaining fraction of polymer could not cause brush-like behavior in the free coatings. AFM images and height profiles are shown in Supporting Information, Chapter4/figures S7 and S8.

Humidity-controlled ellipsometry

The humidity-dependent swelling response of the samples was characterized using a J.A. Woollam M-2000X spectroscopic ellipsometer with 5 mL heated liquid cell (J.A. Woollam) connected to an OpenHumidistat [16] humidity controller. The cell's heating feature was not used.

Closed-loop control over the humidity of an air stream is provided by the humidistat. Since it is not feasible to fit a humidity sensor (for feedback) in the ellipsometer's liquid cell, it is used with an universal pre-chamber containing the humidity sensor. The outlet of this pre-chamber is connected to the liquid cell of the ellipsometer.

Ellipsometry measurements were performed at wavelengths between 350 nm to 1000 nm, at an angle of incidence of 75°, in in-situ mode, which acquires data continuously over time. At the same time, the humidity setpoint on the humidistat is scanned in steps of 10 percent-point from 10% to 60%, and in steps of 5 percent-point from 60% to 90%. This procedure is chosen for better resolution and equilibration at higher humidity values because the swelling response of the films and brushes is highly super-linear. Every humidity

setpoint is held stable for 100 s. Since degrafting of PSPMA brushes in high humidity occurs on a timescale of days, [15] we do not expect substantial degrafting during these measurements.

The ellipsometric data were fitted to a model composed of a Si substrate, a 1 nm native oxide layer, and a Cauchy layer with (uniaxial) optical anisotropy. The thickness and Cauchy A_{xy}, A_z, B_{xy}, and B_z coefficients are fitted. Higher-order coefficients are not used, and our samples were assumed to be optically transparent over the measured wavelength range. Thickness non-uniformity (slight variation of the layer thickness within the measurement spot) is included in the model, and the amount is fitted. Though ellipsometry measurements of brushes in liquid can benefit from explicitly incorporating density gradients over the height of the layer using a graded model, [17, 18] we have shown in an earlier publication that the quality of the fit does not improve enough to justify complicating the fitting model in this way for vapor-solvated brush systems. [19]

The resulting thickness-over-time data were related to the humidity-over-time data from the humidistat. The two independently-measured timeseries are aligned in time using cross-correlation to determine the time delay, and interpolated at common time points. Next, the data is filtered to where the humidity is stable, and for each group of thickness-over-time for constant humidity, an exponential function (Equation 4.9) is fitted to extract the asymptote (h_{eq}), using the time constant τ as a fitting parameter. This way, the equilibrium thickness can be estimated even when swelling has not been able to reach full equilibrium within the allowed time.

$$h(t) = h_{eq} \left(1 - \exp \left(-\frac{t - t_0}{\tau} \right) \right)$$

(4.9)

The aforementioned procedure is performed for each in-situ ellipsometry measurement set. In total, 4 brush and 4 film samples were measured in duplo. The resulting thicknesses are converted to swelling ratios (by dividing by the dry height) and all data for the brushes and films are combined, to yield aggregated average swelling ratios as function of humidity and corresponding confidence intervals for brushes and for films.

4.4   Results and discussion

In this section, we first discuss the simulation results, starting with density profiles over a range of relative vapor pressures for grafted and non-grafted
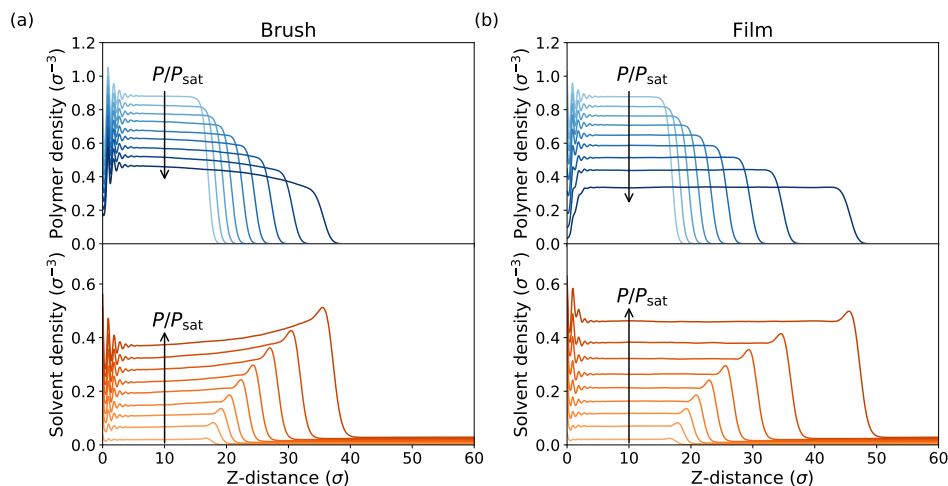
Figure 4.3: Density profiles of polymer (blue) and solvent (orange) of the brush (a) and film (b) for different vapor pressures and $\epsilon_{ps} = 1.0$, $\epsilon_{pp} = 0.9$. From light to dark, the vapor pressures associated with the lines in the graphs are: $P/P_{sat} = 4.9\%$, 15.7%, 26.1%, 36.4%, 48.4%, 60.3%, 72.7%, 85.6%, 99.1%.

coatings at fixed interaction energies. Next, we present the swelling ratio as a function of solvent pressure for both brushes and non-grafted films, for two different values of the polymer-solvent interaction strength. Finally, we will discuss the experimental results, where we obtained humidity-dependent swelling ratios for brushes and films.

Simulated vapor swelling

The density profiles of polymer and solvent as a function of relative vapor pressure are shown in Figure 4.3. These density profiles are obtained at interaction parameters $\epsilon_{ps} = 1.0$ and $\epsilon_{pp} = 0.9$. In all systems, slight density oscillations appear near the grafting surface, reflecting the formation of layers in the fluid near the wall. Although this layering is amplified by the perfectly flat mathematical wall, it is not unphysical, [20] and has in fact been observed experimentally. [21] The shape of the density profiles differs significantly between the free film and the brush, particularly at higher solvent pressures. Under these circumstances, the density profile of the brush resembles the parabolic one predicted by classical scaling theories, [22, 23] although neutron reflectometry studies show that the density of vapor-solvated brushes decays more

steeply at the outer edge of the brush. [24] The parabolic profile manifests only at high vapor pressures, since it requires the brush to be highly solvated. Additionally, the polymer-solvent interactions in these systems are highly favorable, translating to negative values of χ. These strong interactions may reduce the impact of entropic contributions on the profile shape, compared to more moderate interaction strengths. The free film, on the other hand, retains a single bulk composition in the entire layer at any given P/P_{sat}. At the highest P/P_{sat} values of 72.7 %, 85.6%, and 99.1 %, the film swells significantly more than the brush.

Brush swelling ratios for $\epsilon_{\text{pp}} = 0.9$ and $\epsilon_{\text{ps}} = 1.0, 1.4$ are shown as a function of P/P_{sat} in Figure 4.4a. Although excluded volume parameters more rigorously describe solvation behavior, [25] the pairwise interaction energies can be considered equivalent assuming the density of the solution does not change drastically. [26] These swelling ratios are obtained from solvent and polymer fractions in the brush using Equation 4.8, for easy comparison to the Flory-Huggins model. Since the total density of the coatings varies only slightly over the studied range of interaction parameters and humidities (see Supporting Information, Fig. S1-S5), we expect this to be an accurate indication of brush swelling.

We once again observe that the swelling ratios for the brush and the non-grafted system diverge at higher solvent pressures. For the brush, we find a convex swelling curve at $\epsilon_{\text{ps}} = 1.0$, shifting to a concave shape at $\epsilon_{\text{ps}} = 1.4$. This qualitative change can be explained as a shift from sorption driven by the entropic gain of the solvent entering the polymer layer, to a rapidly saturating maximization of polymer-solvent contacts, driven by enthalpy. [10] The non-grafted film behaves very similarly to the polymer brush at low solvent pressures, and swells slightly more than the brush at high P/P_{sat} values.

In the limit of vapor saturation, we would expect the condensation of a macroscopic solvent layer, turning the non-grafted film into a dilute polymer solution (cf. Figure 4.2). However, our model overestimates the sorption at high P/P_{sat} significantly, and we find strong but finite swelling even for near-saturated vapors. Since the Flory-Huggins theory considers only bulk solutions, it seems likely that this overestimation is due to some interfacial effect. For instance, the polymer chains possess less translational entropy than the solvent particles. This also means they may lose less entropy in the presence of the wall, which would favor finite swelling. Alternatively, the discrepancy may have dynamic origins. Even if the dissolution of the polymer film is thermodynamically favorable, entanglements between chains could plausibly prevent polymers

from leaving the layer and slow this process down beyond the timescale of our simulations. In addition to absorption, we observe adsorption of solvent onto the surface of the polymer layer. The amount of solvent per unit area outside the polymer bulk, indicative of adsorption, is shown in Figure 4.4b. The amount of adsorbed solvent increases with the solvent pressure in all cases, and does not differ strongly between the brush and the non-grafted film at low pressures. Near saturation, however, more solvent appears to adsorb onto the brush, especially in the $\epsilon_{ps} = 1.4$ case. Whether adsorption occurs is mainly defined by the difference in self-affinity (and by extension surface tension) between the polymer and solvent. The amount of solvent adsorbed is also influenced by attractive polymer-solvent interactions, however. [4] This may explain the difference in adsorption between polymer brushes and non-grafted films: since the brush contains less solvent than the non-grafted film, a higher concentration of polymer is available at the brush surface. Since the polymer-solvent interaction is stronger than the solvent self-affinity, the higher polymer concentration favors adsorption of solvent onto the brush surface.

Humidity-dependent swelling of poly(SPMA)

In Figure 4.5, the swelling of poly(SPMA) brushes and films as a function of the humidity, as measured by ellipsometry, are presented. These swelling curves represent aggregated average results for four polymer brush samples and four non-grafted film samples. Both films and brushes display limited swelling at low humidities, and the swelling curves are virtually identical up to 50% relative humidity. At higher humidities, both swelling plots display a concave-upward shape, which is commonly observed for polymer swelling experiments in moderately favorable solvent vapors. [2, 27–29] Although factors such as polydispersity could cause deviations from the idealized brushes studied in our simulations, [30, 31] the measured isotherms agree approximately with the simulated $\epsilon_{ps} = 1.0$ case shown in Figure 4.4a. A significant difference in swelling between the non-grafted films and brushes appears at higher humidity values, with films displaying more relative swelling. This finding also agrees with our theoretical and simulation results. At the highest measured humidity value of 90 %, the films swell ~1.7x on average, while the average swelling ratio of brushes does not exceed ~1.5 at that humidity.

The finding that polymer brushes display reduced swelling appears to contradict previous experimental results. McCaig et al. studied the responsiveness to organic vapors of gold-coated silicon nitride nanocantilevers functionalized with drop-cast poly(methyl methacrylate) (PMMA) and PMMA brushes. [1]
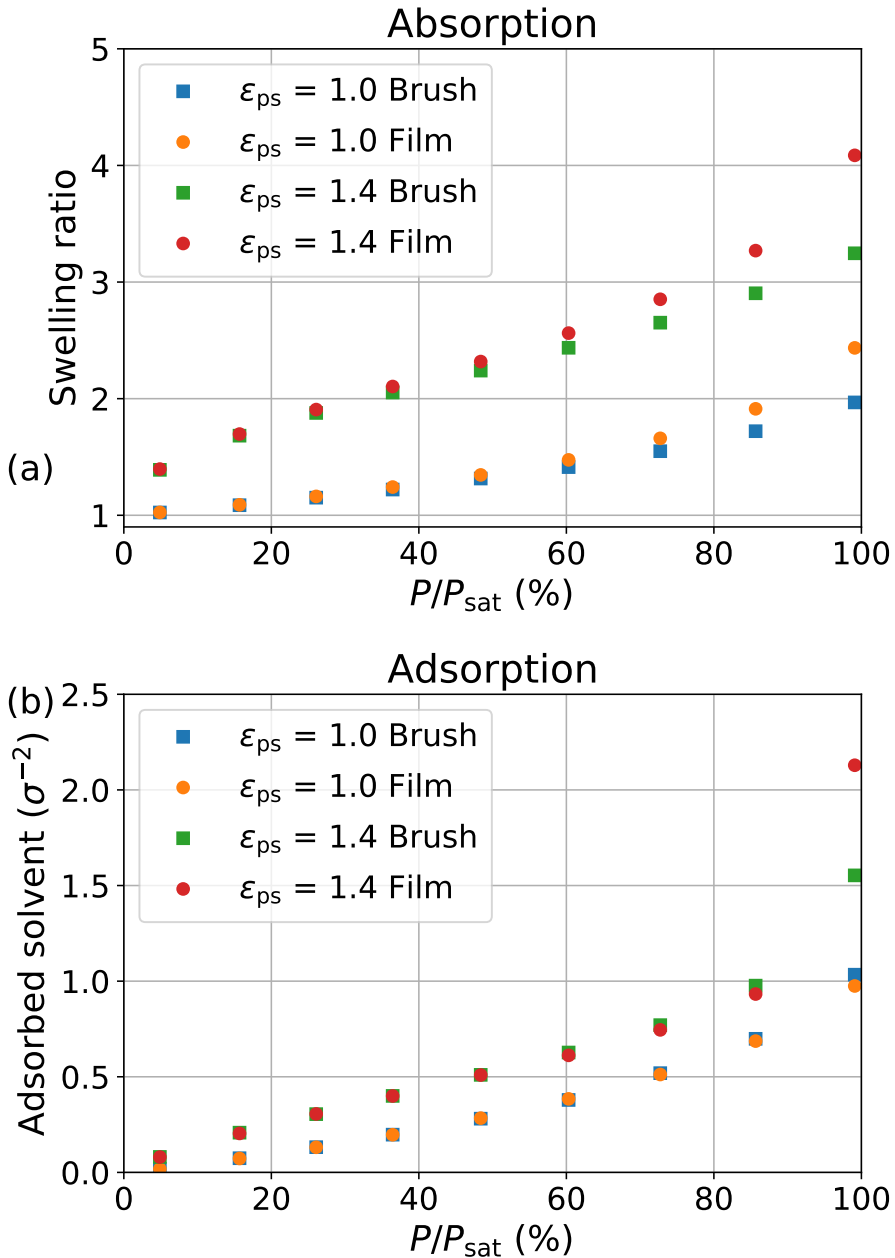
Figure 4.4: Swelling ratios (a) and amount of adsorbed solvent (b) at varying solvent pressure. Results are presented for the brush and film at $\epsilon_{pp} = 0.9$ and different ϵ_{ps} values.
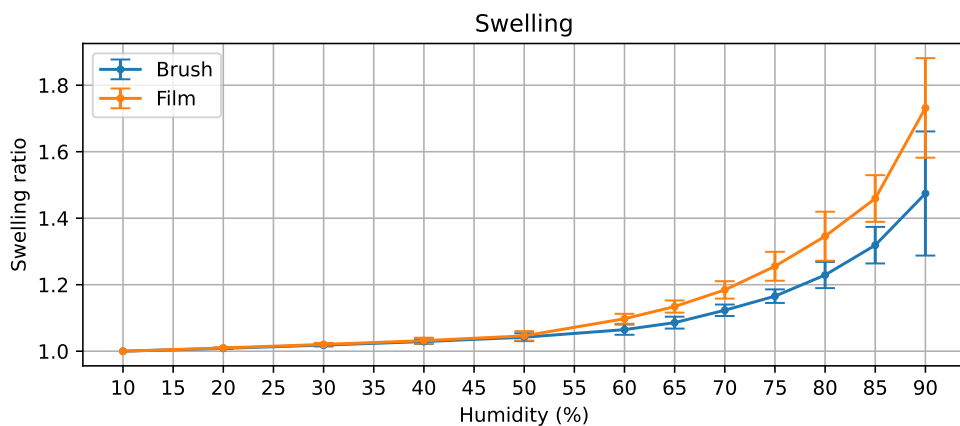
Figure 4.5: Average swelling behavior of brushes compared to films as measured by humidity-controlled ellipsometry. The lines connecting markers are meant to guide the eye. The error bars denote 95% confidence intervals.

When exposed to polar solvent vapors, brush-coated cantilevers displayed significantly increased frequency shifts compared to bare sensors and cantilevers with drop-cast films. However, the authors themselves point out that neither the mass uptake nor the swelling of the polymer film directly correlates with the sensor response. Moreover, synthesis procedures and film heights for the drop-cast films and the polymer brushes differed significantly. Similarly, Galvin and Genzer report higher swelling factors and correspondingly lower χ parameters for brushes in a spectrometric ellipsometry study of poly(2-(dimethylamino)ethyl methacrylate) (PDMAEMA) and PDMAEMA-derived films. [2] However, this study explicitly does not control for chain length or polydispersity. Galvin and Genzer also point out the possibility that the orientation of chains in the polymer brush, which is predominantly normal to the grafting surface, facilitates the formation of diffusion channels for vapor to enter the brush. Finally, they note that their experiments were carried out near the glass transition temperature of bulk PDMAEMA, which further complicates the interpretation of the results. For both of these studies, it is clear that a direct comparison of swelling in brushes and films is simply outside the scope of the work. Hence, we do not think our findings truly conflict with these previous results.

We also note that the optical anisotropy in brushes behaves differently from that in films. We found that films tend to become optically more isotropic with

swelling, while brushes do not. This matches our expectations: the optical anisotropy is related to the preferred alignment of chains. [32] Chains in films may be 'frozen' in an anisotropic state after fast drying processes, but become more mobile when solvated by water vapor. In contrast, the grafting of chains in the brushes precludes isotropic orientation even when solvated.

4.5 Conclusions

In this chapter, we have investigated and compared the swelling behavior of grafted and non-grafted polymer films in (water) vapor, incorporating theory, MD simulations and experiments. Non-grafted films in these experiments were prepared by degrafting of polymer brushes, ensuring good comparability between the two. Simulation results and experiments both indicate that a polymer brush swells less than the equivalent non-grafted film at all relative humidities, as a result of the constraints imposed by surface-anchoring. We relate these results to a modified Flory-Huggins model, which includes an entropic penalty for stretching of the grafted polymer. This model adequately describes the absorption isotherms obtained from molecular dynamics simulations, and qualitatively matches experimental results. However, the model overestimates the difference in swelling between polymer brushes and non-grafted films at high humidity. These results further support the potential of polymer brushes for sensing and separation technologies in the gas phase.

Acknowledgements

4.6 Supporting Information

Total particle density (as a function of interaction parameters)
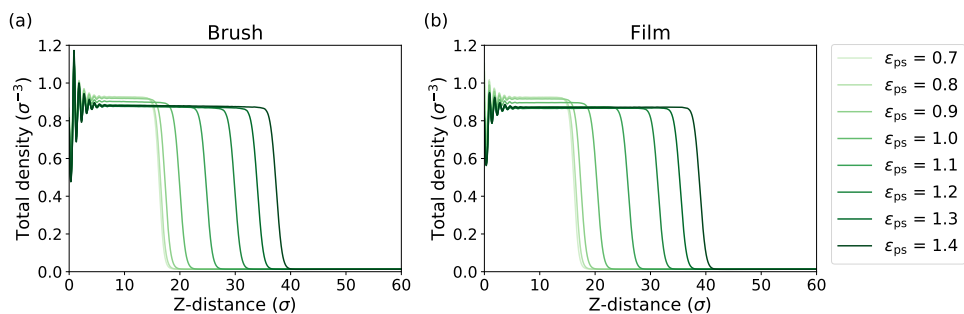
Figure 4.6: Profiles of the total density for ϵ_{ps} ranging from 0.7 to 1.4 and $\epsilon_{\mathrm{pp}} = 1.0$, $P/P_{\mathrm{sat}} = 50\%$.
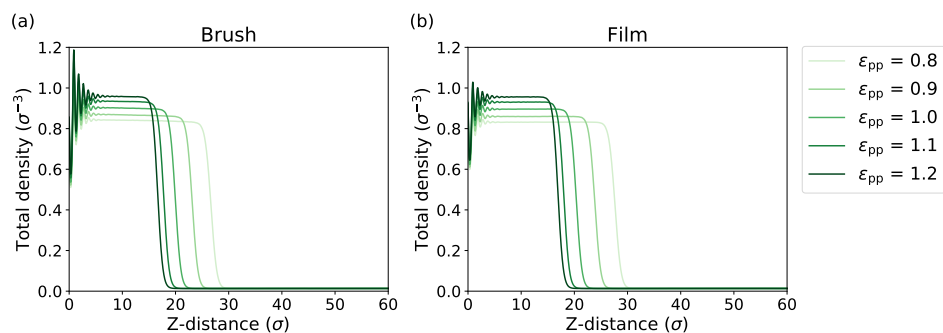
Figure 4.7: Profiles of the total density for ϵ_{pp} ranging from 0.8 to 1.2 and $\epsilon_{\mathrm{ps}} = 1.0$, $P/P_{\mathrm{sat}} = 50\%$.
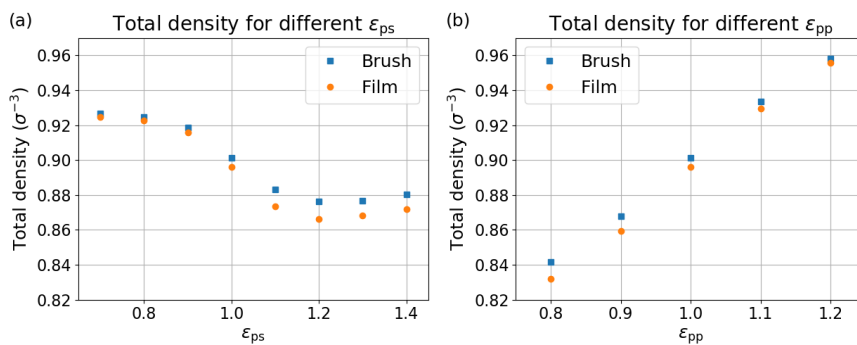
Figure 4.8: Total density at $z = 10\sigma$ for $P/P_{\text{sat}} = 50\%$ under variation of the polymer-solvent and polymer self- interaction energies.

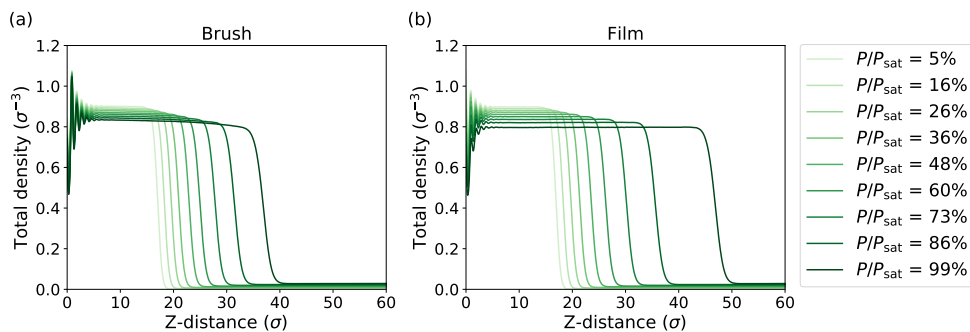## Total density as a function of P/P_{sat}

Figure 4.9: Profiles of the total particle density at different values of solvent activity for $\epsilon_{\text{ps}} = 1.0$, $\epsilon_{\text{pp}} = 0.9$.
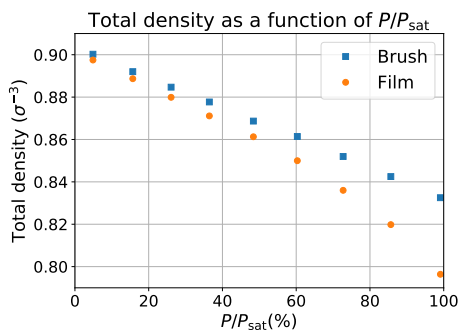

Figure 4.10: Total density at $z = 10\sigma$ vs P

Relation between simulation parameters and χ

From simulation results, we can obtain an effective χ value by rearranging equations 6 and 7 of the main work as:

$$\chi_{\mathrm{b}} = -\frac{1}{\phi_{\mathrm{p,b}}^2}\left(\ln(1 - \phi_{\mathrm{p,b}}) + \phi_{\mathrm{p,b}} + \frac{3\sigma^2}{\phi_{\mathrm{p,b}}} - \ln(\frac{P}{P_{\mathrm{sat}}})\right) \qquad (4.10)$$

for the brush, and

$$\chi_{\mathrm{l}} = -\frac{1}{\phi_{\mathrm{p,l}}^2}\left(\ln(1 - \phi_{\mathrm{p,l}}) + (1 - \frac{1}{N})\phi_{\mathrm{p,l}} - \ln(\frac{P}{P_{\mathrm{sat}}})\right) \qquad (4.11)$$

for the non-grafted film.
From a theoretical perspective, we can translate the interaction parameters $\epsilon_{\mathrm{pp}}, \epsilon_{\mathrm{ps}}$ and ϵ_{ss} to a pairwise interchange energy

$$W = -\epsilon_{\mathrm{ps}} + \frac{1}{2}\left(\epsilon_{\mathrm{pp}} + \epsilon_{\mathrm{ss}}\right). \qquad (4.12)$$

This quantity is related to χ by

$$\chi = \frac{zW}{k_{\mathrm{B}}T}, \qquad (4.13)$$

where z is the coordination number for particles in the solution. For constant density of the solution, this implies a linear relation between χ and W. Figure 6 displays χ values recovered from simulations at $P/P_{\mathrm{sat}} = 50\%$ as well as the best linear fit through the origin. While the simulation results do display the expected linear trend, the obtained χ values are consistently higher than expected. This further indicates that the Flory-Huggins description performs adequately, but overestimates polymer swelling in these systems.
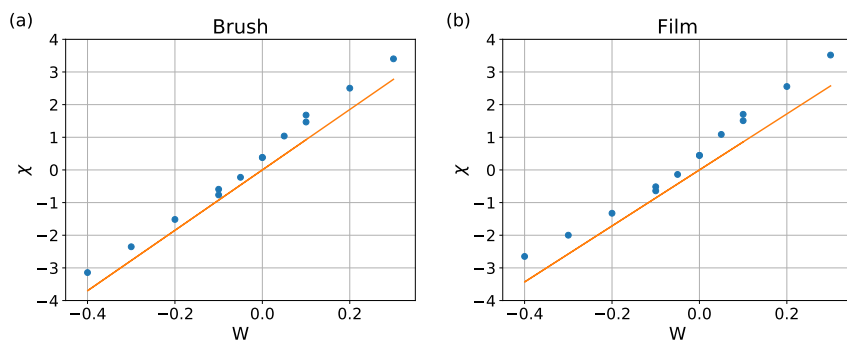
Figure 4.11: Effective values of the Flory-Huggins parameter as a function of the interchange energy W defined by simulation parameters, for (a) our polymer brush simulations and (b) our non-grafted film simulations.

Details of simulation potentials

Our simulations model polymeric behaviour through the Kremer-Grest bead-spring model [8], a set of interaction potentials that reproduce typical polymer dynamics and prevent certain unphysical behaviors such as bond-crossing. Non-bonded particles in the system interact through the well-known Lennard-Jones potential. The LJ potential is defined as

$$U_{\text{LJ}}(r) = 4\epsilon \left(\left(\frac{\sigma}{r} \right)^{12} - \left(\frac{\sigma}{r} \right)^{6} \right), \tag{4.14}$$

with r being the distance between a given particle pair, ϵ the value of the potential in its minimum, and σ the distance at which the potential crosses zero. This form includes an asymptotically decreasing long-range component, however. To maintain a computationally tractable system, we utilize the truncated and potential-shifted (SP) form:

$$U_{\text{LJ,SP}}(r) = \begin{cases} U_{\text{LJ}}(r) - U_{\text{LJ}}(r_{\text{c}}) & \text{for } r \leq r_{\text{c}} \\ 0 & \text{for } r > r_{\text{c}} \end{cases}, \tag{4.15}$$

where r_{c} is the cutoff distance for the interaction.

Particles along a polymer backbone are connected by the combination of a Weeks-Chandler-Anderson (WCA) potential (equivalent to an LJ potential cut off in the minimum at $2^{1/6}\sigma$) and a finitely extensible non-linear elastic (FENE) potential. Hence, the total form of the bonded potential is

$$U_{\text{FENE}}(r) = -0.5 K R_0^2 \ln \left(1 - \left(\frac{r}{R_0} \right)^2 \right) \tag{4.16}$$

$$U_{\text{WCA}}(r) = \begin{cases} U_{\text{LJ}}(r) + \epsilon & \text{for } r \leq 2^{1/6} \\ 0 & \text{for } r > 2^{1/6} \end{cases} \tag{4.17}$$

$$U_{\text{bond}}(r) = U_{\text{WCA}}(r) + U_{\text{FENE}}(r). \tag{4.18}$$

In these expressions, r is once again the interparticle distance, K is a spring constant, and R_0 is the maximum bond length. In the Kremer-Grest model, $K = 30$, $R_0 = 1.5$, $\epsilon = 1$ and $\sigma = 1$ are used in the combined bond potential. The 9-3 LJ potential we use to represent the substrate takes the form

$$U_{93}(r) = \epsilon_{93} \left(\frac{2}{15} \left(\frac{\sigma}{r} \right)^9 - \left(\frac{\sigma}{r} \right)^3 \right). \tag{4.19}$$

This follows from the classical 12-6 LJ potential, integrated over a half-space of particles. It should be noted that ϵ_{93} does not directly equate to the ϵ of an individual interaction, although they are similar in magnitude.

Confirmation of degrafting

We checked for degrafting of the brushes using AFM measurements on separate brush samples. These samples were produced in the same batch as the ones used in the primary ellipsometry measurements, and left to degraft in the same vessel. Brush heights were checked prior to degrafting by scratching the surface with a steel needle, rinsing the surface with water and ethanol, then measuring the step height at the scratch. Corresponding height profiles and images are shown in figure 4.12.
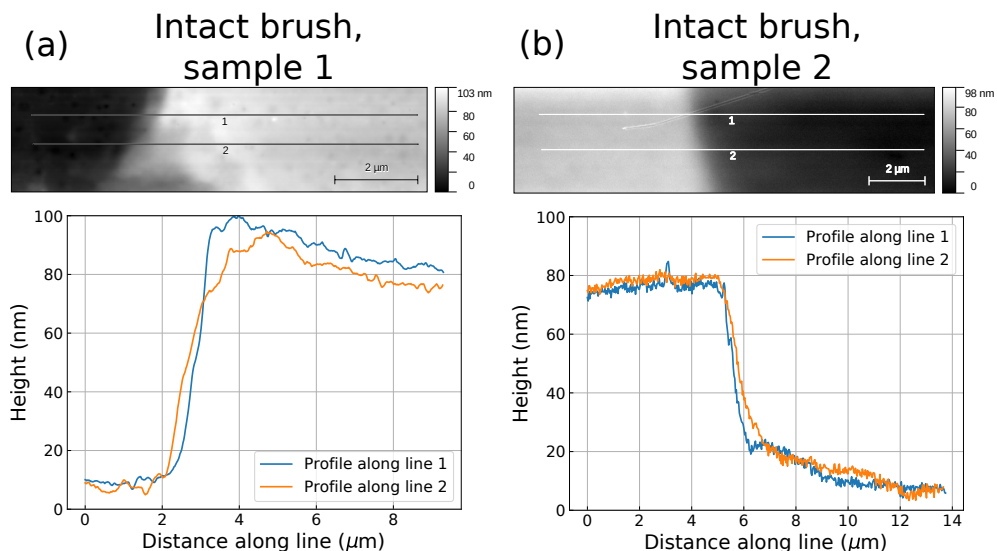

Figure 4.12: AFM height data and profiles across the edge of a scratch in the brush for two different brush samples.

After the degrafting period, one sample was again rinsed with water and ethanol, then measured. No scratch could be visually identified at this time, and surface features consisted mostly of irregular aggregates 20-30 nm in height. Height profiles and images are shown in figure 4.13. Since brushes are typically stable under normal rinsing and drying, we take this as indication that the degrafting procedure is succesful.
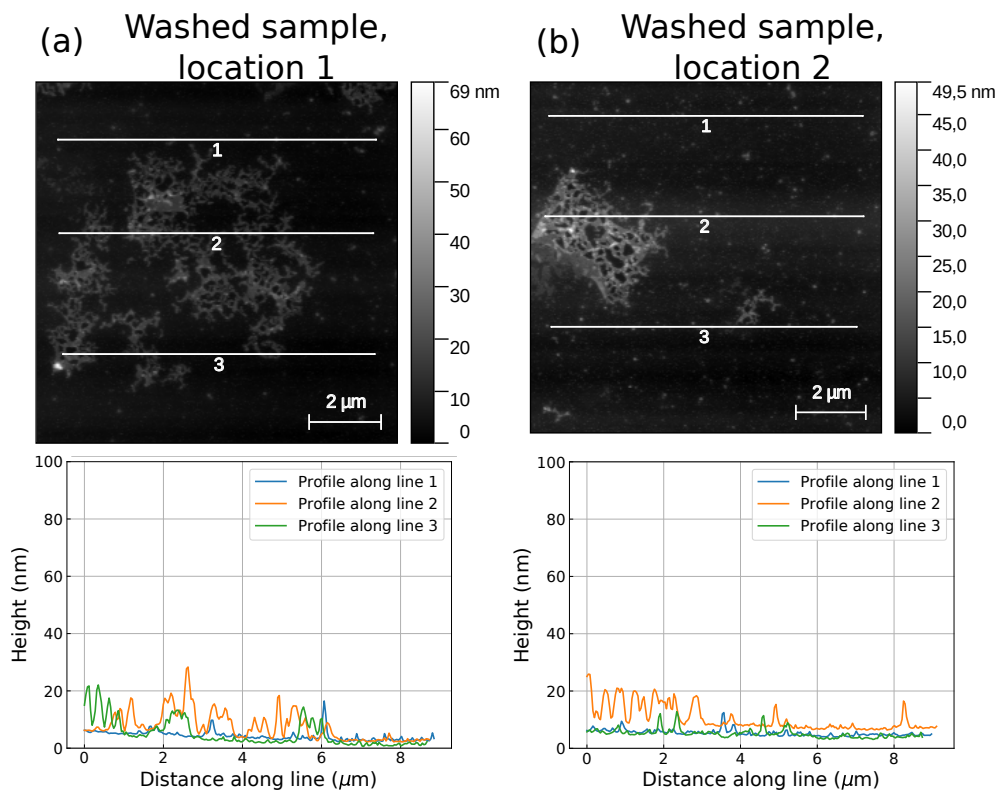
Figure 4.13: AFM height data and profiles of two spots on a brush sample after degrafting in saturated water vapor and rinsing.
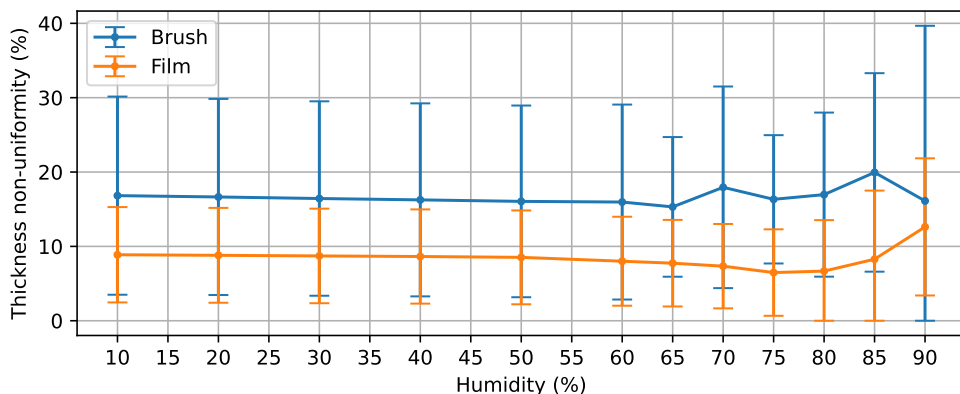
Thickness non-uniformity

Figure 4.14: Average fitted thickness non-uniformity (with 95% confidence intervals) for brushes and films as a function of humidity.

4.7 References

[1] H. C. McCaig, E. Myers, N. S. Lewis, and M. L. Roukes, "Vapor sensing characteristics of nanoelectromechanical chemical sensors functionalized using surface-initiated polymerization", Nano Letters **14**, 3728–3732 (2014).

[2] C. J. Galvin and J. Genzer, "Swelling of hydrophilic polymer brushes by water and alcohol vapors", Macromolecules **49**, 4316–4329 (2016).

[3] P. J. Flory, *Principles of polymer chemistry* (Cornell University Press, Ithaca) (1953).

[4] G. C. Ritsema van Eck, L. B. Veldscholte, J. H. W. H. Nijkamp, and S. de Beer, "Sorption characteristics of polymer brushes in equilibrium with solvent vapors", Macromolecules **53**, 8428–8437 (2020).

[5] L. A. Smook, G. C. Ritsema van Eck, and S. de Beer, "Friends, foes, and favorites: Relative interactions determine how polymer brushes absorb vapors of binary solvents", Macromolecules **53**, 10898–10906 (2020).

[6] T. M. Birshtein and Y. V. Lyatskaya, "Theory of the collapse-stretching transition of a polymer brush in a mixed solvent", Macromolecules **27**, 1256–1266 (1994).

[7] A. P. Thompson, H. M. Aktulga, R. Berger, D. S. Bolintineanu, W. Michael Brown, P. S. Crozier, P. J. in 't Veld, A. Kohlmeyer, S. G. Moore, T. D. Nguyen, R. Shan, M. Stevens, J. Tranchida, C. Trott, and S. J. Plimpton, "LAMMPS - a flexible simulation tool for particle-based materials modeling at the atomic, meso, and continuum scales", 108171 (2021).

[8] K. Kremer and G. S. Grest, "Dynamics of entangled linear polymer melts: A molecular-dynamics simulation", The Journal of Chemical Physics **92**, 5057–5086 (1990).

[9] E. Braun, S. M. Moosavi, and B. Smit, "Anomalous effects of velocity rescaling algorithms: The flying ice cube effect revisited", Journal of Chemical Theory and Computation **14**, 5262–5272 (2018).

[10] G. C. Ritsema van Eck, L. Chiappisi, and S. de Beer, "Fundamentals and applications of polymer brushes in air", ACS Applied Polymer Materials **4**, 3062–3087 (2022).

[11] M. Tuckerman, B. J. Berne, and G. J. Martyna, "Reversible multiple time scale molecular dynamics", The Journal of Chemical Physics **97**, 1990–2001 (1992).

[12] Y. Yu, M. Cirelli, P. Li, Z. Ding, Y. Yin, Y. Yuan, S. De Beer, G. J. Vancso, and S. Zhang, "Enhanced stability of poly (3-sulfopropyl methacrylate potassium) brushes coated on artificial implants in combatting bacterial infections", Industrial & Engineering Chemistry Research **58**, 21459–21465 (2019).

[13] J. O. Zoppe, N. C. Ataman, P. Mocny, J. Wang, J. Moraes, and H.-A. Klok, "Surface-initiated controlled radical polymerization: state-of-the-art, opportunities, and challenges in surface and interface engineering with polymer brushes", Chemical reviews **117**, 1105–1318 (2017).

[14] R. R. Patil, S. Turgman-Cohen, J. Šrogl, D. Kiserow, and J. Genzer, "On-demand degrafting and the study of molecular weight and grafting density of poly (methyl methacrylate) brushes on flat silica substrates", Langmuir **31**, 2372–2381 (2015).

4

[15] M. Brió Pérez, M. Cirelli, and S. de Beer, "Degrafting of polymer brushes by exposure to humid air", ACS Applied Polymer Materials **2**, 3039–3043 (2020).

[16] L. B. Veldscholte and S. de Beer, "OpenHumidistat: Humidity-controlled experiments for everyone", HardwareX **11**, e00288 (2022).

[17] E. S. Kooij, X. Sui, M. A. Hempenius, H. J. W. Zandvliet, and G. J. Vancso, "Probing the thermal collapse of poly(n-isopropylacrylamide) grafts by quantitative in situ ellipsometry", The Journal of Physical Chemistry B **116**, 9261–9268 (2012).

[18] Y. Yu, M. Cirelli, B. D. Kieviet, E. S. Kooij, G. J. Vancso, and S. de Beer, "Tunable friction by employment of co-non-solvency of pnipam brushes", Polymer **102**, 372–378 (2016), URL `https://www.sciencedirect.com/science/article/pii/S0032386116306863`, polymers at Interfaces: Probing Mechanics and Interactions by Atomic Force Microscopy.

[19] R. J. Horst, M. Brió Pérez, R. Cohen, M. Cirelli, P. S. Dueñas Robles, M. G. Elshof, A. Andreski, M. A. Hempenius, N. E. Benes, C. Damen, and S. de Beer, "Swelling of poly(methyl acrylate) brushes in acetone vapor", Langmuir **36**, 12053–12060 (2020).

[20] I. Snook and W. van Megen, "Structure of dense liquids at solid interfaces", The Journal of Chemical Physics **70**, 3099–3105 (1979), URL `https://doi.org/10.1063/1.437798`.

[21] H. Mo, G. Evmenenko, and P. Dutta, "Ordering of liquid squalane near a solid surface", Chemical Physics Letters **415**, 106–109 (2005).

[22] S. T. Milner, T. A. Witten, and M. E. Cates, "Theory of the grafted polymer brush", Macromolecules **21**, 2610–2619 (1988).

[23] S. T. Milner, "Polymer brushes", Science **251**, 905–914 (1991).

[24] L. Sun, B. Akgun, R. Hu, J. F. Browning, D. T. Wu, and M. D. Foster, "Scaling Behavior and Segment Concentration Profile of Densely Grafted Polymer Brushes Swollen in Vapor", Langmuir **32**, 5623–5628 (2016).

[25] M. Rubinstein and R. Colby, *Polymer Physics* (Oxford University Press, Oxford) (2003).

[26] D. Mukherji, C. M. Marques, T. Stuehn, and K. Kremer, "Depleted depletion drives polymer swelling in poor solvent mixtures", Nature Communications **8**, 1374 (2017), URL `http://dx.doi.org/10.1038/s41467-017-01520-5`.

[27] M. Biesalski and J. Rühe, "Swelling of a polyelectrolyte brush in humid air", Langmuir **16**, 1943–1950 (2000).

[28] C. J. Galvin, M. D. Dimitriou, S. K. Satija, and J. Genzer, "Swelling of polyelectrolyte and polyzwitterion brushes by humid vapors", Journal of the American Chemical Society **136**, 12737–12745 (2014).

[29] S. Christau, S. Thurandt, Z. Yenice, and R. Von Klitzing, "Stimuli-responsive polyelectrolyte brushes as a matrix for the attachment of gold nanoparticles: The effect of brush thickness on particle distribution", Polymers (Basel, Switz.) **6**, 1877–1896 (2014), URL `https://www.mdpi.com/2073-4360/6/7/1877`.

[30] W. M. de Vos and F. A. Leermakers, "Modeling the structure of a polydisperse polymer brush", Polymer **50**, 305–316 (2009).

[31] A. Galuschko and J.-U. Sommer, "Co-nonsolvency response of a polymer brush: A molecular dynamics study", Macromolecules **52**, 4120–4130 (2019).

[32] B. T. Koziara, K. Nijmeijer, and N. E. Benes, "Optical anisotropy, molecular orientations, and internal stresses in thin sulfonated poly(ether ether ketone) films", Journal of Materials Science **50**, 3031–3040 (2015).

Chapter 5

Enhanced vapor sorption in block and random copolymer brushes*

Polymer brushes in gaseous environments absorb and adsorb vapors of favorable solvents, which makes them potentially relevant for sensing applications and separation technologies. Though significant amounts of vapor are sorbed in homopolymer brushes at high vapor pressures, at low vapor pressures sorption remains limited. In this work, we vary the structure of two-component polymer brushes and investigate the enhancement in vapor sorption at different relative vapor pressures compared to homopolymer brushes. We perform molecular dynamics simulations on two-component block and random copolymer brushes and investigate the influence of monomer miscibility and formation of high-energy interfaces between immiscible monomers on vapor sorption. Additionally, we present absorption isotherms of pure homopolymer, mixed binary brush and 2-block, 4-block, and random copolymer brushes. Based on these isotherms, we finally show that random copolymer brushes absorb more vapor than any other architecture investigated thus far. Random brushes display enhanced sorption at both high and low vapor pressures, with the largest enhancement in sorption at low vapor pressures.

5.1 Introduction

While early research focused on applying polymer brushes in liquid, it was recently recognized that brushes can be employed broadly in air as well. [1] For example, lubricants, [2] vapor sensors, [3, 4] moisture harvesters [5] or gas separation technologies [6, 7] can benefit from brush functionalization, because the brushes can absorb vapor from the air. For most of these applications it is important that vapor sorption in the brush is maximized. However, this is difficult to achieve, especially at low vapor pressures.

The reason for the typical low absorption at low vapor pressures can be understood as follows. The amount of vapor absorbing in a brush is strongly affected by the vapor pressure [8–14] and the isotherm describing this can be determined by an extended version of the Flory-Huggins theory, [15, 16] as proposed by Birshstein and Lyatskaya. [17] The exact shape of these isotherms depends on the brush parameters (grafting density and chain length) and the solvent quality. However, in most experiments the isotherms are observed to be concave-upward, [8–14] with minimal absorption at low vapor pressures and a strong increase in absorption only near the saturation pressure of the vapor. This means that at low vapor concentrations, vapor sorption in brushes is typically very limited, unless alternative strategies are being employed.

In a recent publication, we have shown that vapor sorption at low concentrations can be strongly increased by utilising binary brushes composed of immiscible polymers (A and B). [18] These immiscible polymers can phase separate in nano-domains and excess vapor adsorbs at the high-energy polymer-polymer interface. This can, depending on the brush characteristics, [19] result in the sorption at low concentrations being even a factor 10 higher compared to sorption in homopolymer brushes. The best performance was observed for high density brushes with equal fractions of A and B polymers. Yet, these binary brushes are difficult to obtain synthetically. [20] Brushes with equal A-B fractions can be obtained by triblock copolymers, which are grafted by their middle block to the substrate to form y-shaped binary polymer structures. [21, 22] However, due to steric hindrance, the grafting density for these structures will be rather low. And while high density binary brushes can be obtained by grafting-from strategies, [23] for example from mixed monolayers with initiators for two different polymerization reactions [24] which allows for the consecutive polymerization of the A and B polymers, it is difficult to obtain equal fractions of both polymers in these systems. Therefore, we need polymer brush systems with two components that introduce high-energy interfaces and are easy to synthesize.

Block copolymers of incompatible polymers are promising candidates for producing high-energy interfaces in brushes with relative ease. Coatings of incompatible block copolymers have been extensively researched for their ability to spontaneously phase-separate into nanometer-scale domains, which finds potential applications in lithography. [25] Block and random copolymers of poly(styrene-*co*-(methyl methacrylate)), an archetypical incompatible copolymer, can be synthesized by a variety of methods including living anionic polymerization, [26, 27] nitroxide-mediated radical polymerization, [26, 27] and click reactions between end-functionalized homopolymers. [28] Many of these polymerization methods can also be initiated from functionalized surfaces, [23, 29] making the synthesis of high-density brushes of incompatible copolymers feasible. Additionally, extremely incompatible ("high-χ") block copolymers are an active topic of research. [30, 31]

To explore the feasibility of copolymer systems for vapor sorption, we employ molecular dynamics simulations to study the sorption enhancement of 2-block, 4-block and random copolymer brushes relative to a pure homopolymer brush. Additionally, we vary the interaction between the monomer species, and investigate how this influences phase separation and sorption in the brush. Finally, we vary the solvent vapor concentration to obtain absorption isotherms for all the aforementioned structures, as well as the previously studied mixed homopolymer brushes.

5.2 Models and Methods

To study the solvent distribution in a variety of binary polymer brush systems, we use coarse-grained molecular dynamics simulations. Such coarse-grained simulations are suitable for studying general scalings and trends in materials and microscopic systems, such as polymers [32] or functional brushes [2, 33, 34] and gels [35]. In this work, we simulate a variety of polymer brushes under implicit poor solvent conditions to model the conditions in dry air, and we expose them to an explicit good solvent to simulate the sorption of a solvent vapor.

We create Kremer-Grest polymer brushes by grafting the polymers to the substrate via an anchoring point ($z=0$). Monomer beads are stacked on top of each other perpendicular to the grafting surface. While a pure brush consists of a single monomer type, binary brushes consist of two immiscible monomer types: monomer A (dark, purple, near grafting plane) and monomer B (light, blue) (see Fig. 5.1). Besides a homopolymer brush (Fig. 5.1**a**), three different
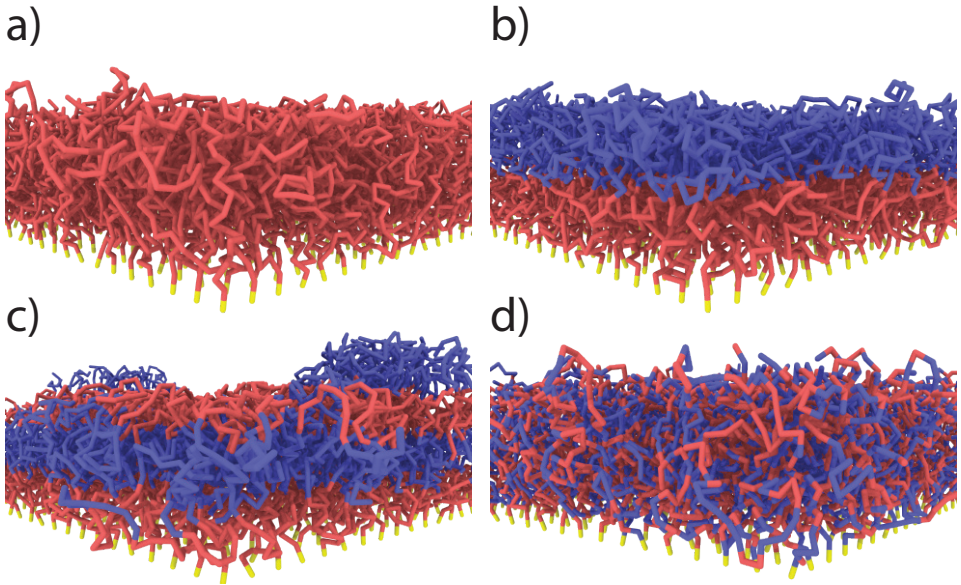
Figure 5.1: Illustrations of: a) Pure homopolymer brush, b) 2-Block brush, c) 4-Block brush, d) Random brush.

mixed brushes are created with a chain length of 32 beads: a 2-block copolymer brush (Fig. 5.1**b**), a 4-block copolymer brush (Fig. 5.1**c**), and a random copolymer brush (Fig. 5.1**d**). In each brush, monomer A is grafted closer to the grafting surface, and the length of block segments is equal. In other words, in a 2-block brush, we build two blocks of monomer A and monomer B each consisting of 16 monomers. Similarly, in a 4-block (ABAB) each of the four blocks consists of 8 monomers. Finally, the random brush is created by randomly substituting 50 % of monomers of a homopolymer brush by the other monomer type. Grafting density is kept constant in all brushes at 0.25 σ^{-2} (critical grafting density $\rho_{g,*} = 0.1263\sigma^{-2}$). The modeled system consists of a rectangular box $40 \times 40 \times 80$ σ^3 in the x, y, and z directions, respectively, with a periodic boundary condition in the x and y-direction and a fixed boundary condition in z-direction. The fixed boundary conditions in z are enforced by a repulsive harmonic wall potential whose spring constant is set to 100 $\epsilon\sigma^{-2}$ to prevent vapor and polymer particles from escaping from the simulation box.

Interactions between the particles in the system are described by two different potentials for bonded and non-bonded particles. The Lennard-Jones (LJ) potential (equation 5.1) is used to simulate non-bonded interactions, where U

148

is the potential, ϵ the depth of the potential well, r the distance between two particles, and σ the zero-crossing distance. [36, 37]

$$U_{\mathrm{LJ}} = 4\epsilon \left[\left(\frac{\sigma}{r} \right)^{12} - \left(\frac{\sigma}{r} \right)^{6} \right] \tag{5.1}$$

$$U_{\mathrm{LJ,PS}}(r) = \begin{cases} U_{\mathrm{LJ}}(r) - U_{\mathrm{LJ}}(r_{\mathrm{c}}) & \text{for } r \leq r_{\mathrm{c}} \\ 0 & \text{for } r > r_{\mathrm{c}} \end{cases} \tag{5.2}$$

The expression has an energetic minimum at $r = 2^{\frac{1}{6}}\sigma$. The specific form of the LJ potential used in our simulations is truncated and potential shifted (PS): where r_c is the cut-off (here $r_{\mathrm{c}} = 2.5\sigma$). By varying ϵ, the depth of the energy well in the LJ potential is changed. Thus, the strength of the interactions between polymer-polymer ($\epsilon_{\mathrm{pp}} = \epsilon_{\mathrm{aa}} = \epsilon_{\mathrm{bb}}$), monomer A - monomer B, (ϵ_{ab}), solvent-solvent (ϵ_{ss}), and polymer-solvent ($\epsilon_{\mathrm{ps}} = \epsilon_{\mathrm{as}} = \epsilon_{\mathrm{bs}}$) can all be changed individually. Here the subscripts refer to the particle type: a - monomer type A, b - monomer type B, p - any monomer type, s - solvent/vapor. Since all particles in our system are the same size, we use ϵ for particle-particle interactions. If the particles were not the same size, we would have to account for the particle size effect in terms of the virial coefficient. [38]

The bonded interactions are modeled by combining finite extensible nonlinear elastic (FENE) and Weeks-Chandler-Anderson (WCA) potential (Equation 5.3). Bonded interations are described by the sum of both the FENE and WCA potential (Equation 5.5). [36, 37].

$$U_{\mathrm{FENE}} = -0.5 K R_0^2 \ln \left[1 - \left(\frac{r}{R_0} \right)^2 \right] \tag{5.3}$$

$$U_{\mathrm{WCA}}(r) = \begin{cases} U_{\mathrm{LJ}}(r) + \epsilon & \text{for } r \leq 2^{1/6} \\ 0 & \text{for } r > 2^{1/6} \end{cases} \tag{5.4}$$

$$U_{\mathrm{bond}} = U_{\mathrm{FENE}} + U_{\mathrm{WCA}} \tag{5.5}$$

Here, K is the spring constant and R_0 the maximum bond length. In the simulations the parameters are set to $K = 30\epsilon\sigma^{-2}$, $R_0 = 1.5\ \sigma$, $\epsilon = 1$ and $\sigma = 1$. These values prevent the polymer chains from crossing each other and nonphysical behavior related to chain dynamics is prevented. [36, 37]

The timesteps between the Grand Canonical Monte Carlo (GCMC) steps (described later) are simulated in the canonical ensemble (NVT). The system is thermostatted to a temperature of 0.85 $\epsilon k_{\mathrm{B}}^{-1}$ by a chain of three Nosé-Hoover thermostats and the damping constant τ_{d} is set to 0.15τ, where τ is a reduced unit for time. We use the rRESPA multi-scale integrator [39] to allow the use of different timesteps for different interactions to speed up time integration. The time steps were chosen to be 0.0075 and 0.015 τ for the bonded interactions and the non-bonded interactions, respectively. All simulations are performed in LAMMPS. [40]

Each simulation consists of three steps: energy minimization, equilibration and production. First, we use an energy minimization on the artificial system so that the equilibration starts at a low-energy state. Then, we equilibrate the system in two steps. In the first step, a short NVT run ($5*10^4$ time steps) is computed where particle displacements are limited, and then a longer run ($5*10^5$ time steps) is performed where this limitation is lifted. We confirm that equilibrium is reached by observing that polymer density profiles no longer change with time. After the equilibrium is reached, we start the production run ($3*10^6$ time steps) where the vapor is introduced to the system via GCMC method (constant μVT) [16, 18]. During this production run, particle density profiles and snapshots are generated. A particle density profile normal to the grafting plane is computed every 10^5 timesteps by averaging over the final 100 configurations of this window at intervals of 100 timesteps. Snapshots are visualized in OVITO [41].

In our GCMC simulation set-up, the algorithm attempts to insert or remove vapor particles from a virtual reservoir into the simulation box every 10^4 steps. The insertions and deletions are evaluated using the Metropolis criterion. Since the GCMC assumes ideal gas behavior while the LJ vapor in the box shows non-ideal behavior, we compensate for this non-ideality using previously found correlations between the imposed and actual vapor pressure in the simulation. [16]

Similar to previous work, [16] we use the inflection point of the total polymer density profile (A + B) as a measure for the height of a polymer brush. Next, we integrate the density profiles below the brush height to find the solvent and polymer content in the brush, which are then converted into a solvent fraction. Any solvent above the brush height, including the adsorption film, is excluded from consideration so that interfacial effects between brush and vapor do not affect our solvent fraction.

We perform three sets of simulations.

1. Brush architecture. To see the effect of the polymer architecture, we expose a pure, 2-block, 4-block and random brush to an explicit good solvent and determine the local solvent fraction for each of them. Here, we set ϵ_{ab} to 0.4, ϵ_{pp} to 1, ϵ_{ss} to 1, and ϵ_{ps} to 1. Under these conditions, the solvent does not have any preference for a certain monomer type and the different polymers are expected to separate into different phases. [19] These simulations are performed at a constant relative pressure $P/P_{sat} \approx 0.619$. Based on these simulations, we determine which brush sorbs the most solvent.

2. Interfacial effect. To find the effect of the interface on vapor sorption, we use the same interaction strengths and vapor pressure as in the first set, except we vary the polymer cross-interaction ϵ_{ab}. Varying this cross-interaction shows how unfavorable interfaces affect the solvent fraction (ϕ_s) in the brush.

3. Absorption isotherms. To investigate the sorption behavior at different vapor pressures, we use the interaction parameters of the first set of simulations and vary the vapor pressure in order to generate absorption isotherms for all two-component brushes as well as a homopolymer brush with similar chain length and grafting density.

5.3   Results and Discussion

In this section, we present the results of the simulations described above. First, we discuss the effect of the copolymer architecture on the structure of the polymer brushes, and the uptake and distribution of solvent throughout the different systems. Next, we show how the solvent uptake depends on the interfacial energy between polymer phases, by presenting simulation results at different values of the interaction strength between the two monomer species. Finally, we present absorption isotherms for brushes of various copolymer architectures, as well as mixed homopolymer brushes. These results are compared to the pure homopolymer brush to identify the most promising structures and conditions for enhanced vapor sorption using copolymer brushes.
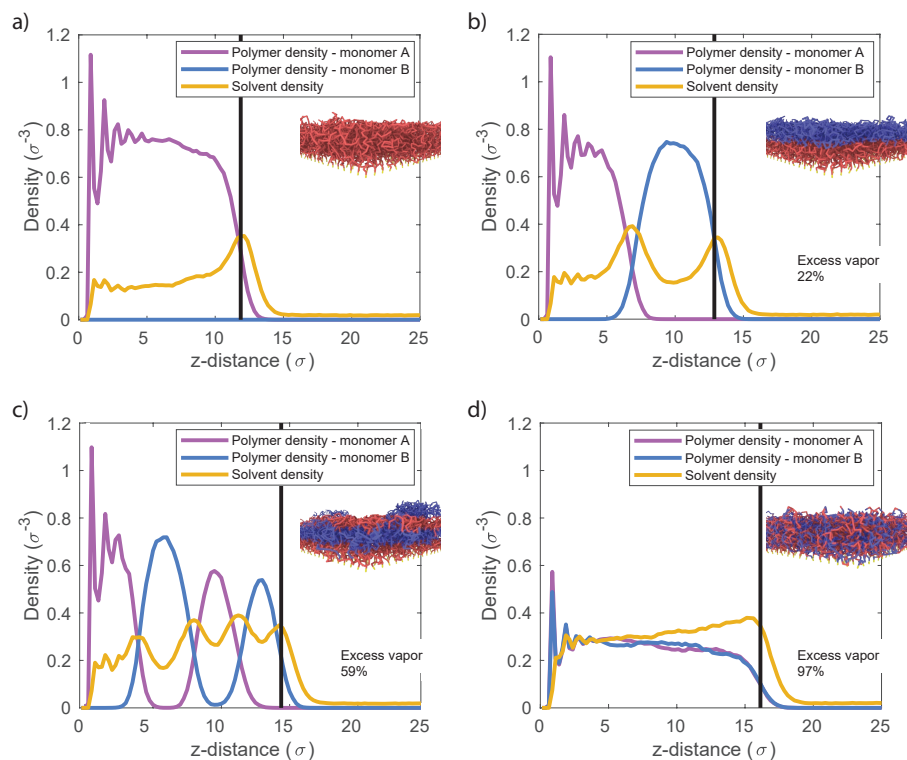
Figure 5.2: Monomer A (purple), Monomer B (blue) and Solvent (yellow) density profiles where the black vertical line represents the brush height. Excess vapor accumulates at unfavorable interfaces between immiscible blocks. a) Pure homopolymer brush, b) 2-block brush, c) 4-Block brush, d) Random brush. In all simulations we use $\epsilon_{ab} = 0.4$, $\epsilon_{aa} = \epsilon_{bb} = \epsilon_{as} = \epsilon_{bs} = \epsilon_{ss} = 1$

Interfacial effect

Enhanced vapor sorption in mixed polymer brushes is caused by vapor uptake at high-energy interfaces between the polymeric phases. [19] We therefore expect that the distribution of the different species will be critical to understand vapor sorption in our block copolymer systems as well. In Figure 5.2, we plot the concentration of monomer type A (purple), monomer type B (blue) and the solvent (yellow) as a function of the distance from the grafting plane for the pure, 2-block, 4-block and random copolymer brushes. In these systems, $\epsilon_{ab} = 0.4$, and the pressure of the solvent vapor corresponds to 62% of the saturation pressure. Since $\epsilon_{ab} < \epsilon_{pp}$, contacts between the two polymer species are unfavorable. In the block copolymer brushes (Fig. 5.2b and 5.2c), these unfavorable interactions result in vertical phase separation, which is in line with earlier simulations of diblock copolymer brushes. [42, 43] This vertical structure can be seen in the density profiles as well-defined peaks in the concentration of monomer species A (purple) and B (blue). The surface-anchored section of the block copolymer chains consists of Monomer A, which forms the layer closest to the substrate as a result. In this system, where the monomer species are immiscible, the interfaces between the different polymer layers are narrow and sharply defined. However, upon increasing ϵ_{ab}, the area of the overlap region becomes larger and larger with the increasing miscibility, as is shown in Fig. 1 of the Supporting Information. In the random copolymer case (Fig. 5.2d), the monomer species cannot phase-separate effectively on a large scale, and their distribution over the brush height is the same.

The distribution of solvent throughout the polymer brushes clearly shows enhanced sorption at interfaces. The yellow profile in Fig. 5.2 shows the solvent concentration as a function of the distance from the grafting plane. In the homopolymer brush, we find a near-constant concentration deeper in the brush, with a peak in the solvent content at the brush-vapor interface. This indicates the formation of an adsorption layer. For a 2-block brush, we observe two maxima in the solvent density. In addition to the adsorption layer at the brush-vapor interface, we find a second maximum inside the brush at the transition from the A to the B block (at $z = 6\sigma$). This sorption enhancement is a direct result of the incompatibility of the two monomer types, which leads to the formation of a high-energy interface in the dry brush. Solvent adsorption in this region reduces the number of unfavorable A-B contacts, thereby lowering the energy of the interface. An alternative but equivalent interpretation is that the local cohesive energy density in the brush is reduced by the weak A-B contacts, leading to an increased A-B interfacial tension. Since solvent-A and

153

solvent-B interfacial tensions are zero (the solvent is perfectly miscible with either polymer species), drawing solvent to the A-B interfaces then minimizes the system's interfacial energy.

The 4-block brush system behaves similarly to the 2-block system, with maxima in the solvent density at all A-B interfaces. The solvent uptake in random copolymer brushes does not display such well-defined maxima. Since there are no phase separated regions in this system, the solvent density is distributed approximately evenly over the brush height. However, the unfavorable contacts between the polymer segments reduce the average polymer self-affinity compared to the homopolymer case. As a result, the random brush extends further from the surface than the homopolymer brush, and contains significantly more solvent.

Based on these results, we conclude that all systems adsorb vapor at the brush-air interface, and absorb vapor in the bulk of the brush. In the two-component systems (block and random brushes), we also find enhanced adsorption wherever the two monomer species come into contact. Sorption as a result of A-B contacts is denoted as "excess vapor" in Fig. 5.2. At $P/P_{\mathrm{sat}} = 0.619$, the 2-block brush contains 22% excess solvent, and the 4-block brush contains 59% excess solvent relative to the homopolymer brush as a result of the additional adsorbing interfaces. Lastly, the random brush contains 97% excess adsorbed vapor. These results further support that the extra sorption is driven by A-B contacts in general, rather than the presence of large-scale A-B interfaces. An additional confirmation for this conclusion is Fig. SI3 where we show vapor sorption behaviour of an alternating polymer brush, which shows similar sorption to the random brush.

Monomer affinity effect

The interfacial energy between the polymeric species depends on the interaction strength between the two monomer types. Hence, we expect this interaction strength to influence the sorption at the polymer-polymer interfaces. In the simulations discussed so far, we set the cross-interaction between the monomer species as $\epsilon_{\mathrm{ab}} = 0.4$, and the self-interaction for both monomer species as $\epsilon_{\mathrm{pp}} = 1$. Because $\epsilon_{\mathrm{ab}} < \epsilon_{\mathrm{pp}}$, the different monomers are immiscible and all two-component brushes self-assemble in such a way to minimize A-B contacts. Here, we present simulation results for which we vary the miscibility of the monomer species, by changing ϵ_{ab}. Fig. 5.3 depicts solvent density profiles for $\epsilon_{\mathrm{ab}} = 0.4$, 0.7, and 1.0 in 2-block (Fig. 5.3**a**), 4-block (Fig. 5.3**b**) and random copolymer brushes (Fig. 5.3**c**) with all other parameters unchanged.
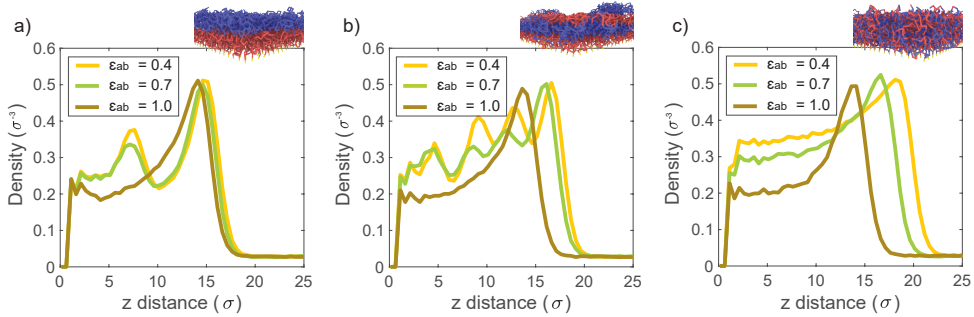
Figure 5.3: Solvent density profiles at different cross-interaction strengths (ϵ_{ab}) for: a) 2-Block brush, b) 4-Block brush, c) Random brush. At low ϵ_{ab} brushes phase separate and excess vapor gets adsorbed at the unfavorable interfaces. Thus, solvent density profiles contain the equal number of peaks to the number of blocks. In a random brush, there is no clear block interface, however, more solvent is sorbed when cross-interactions are unfavorable (at low ϵ_{ab}). In all simulations we keep $\epsilon_{aa} = \epsilon_{bb} = \epsilon_{as} = \epsilon_{bs} = \epsilon_{ss} = 1$ and only vary ϵ_{ab}.

When $\epsilon_{ab} = \epsilon_{pp} = 1$, the monomer species are functionally identical. In this limit, all systems behave like the homopolymer brush, and we find the same solvent distribution in all cases. For $\epsilon_{ab} = 0.4$ and 0.7, where the monomers are poorly miscible, the solvent density profiles once again display maxima inside the block copolymer brushes. The presence of these maxima indicates the presence of the high-energy interfaces between monomer species, which are the result of vertical phase separation in the brush. In the random copolymer brush, where phase separation is not possible, the solvent profile only shows a local maximum at the brush-air interface. With decreasing ϵ_{ab}, sorption in the brush increases, as polymer-solvent contacts become more favorable over monomer cross-interactions.
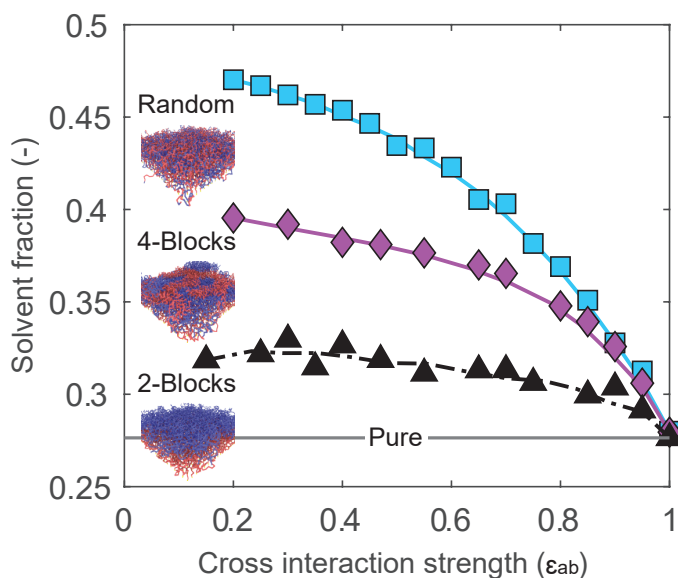
Figure 5.4: At low monomer cross-interaction strengths (ϵ_{ab}), the solvent fraction in the brush is large. When monomers start to mix, at high ϵ_{ab}, the enhanced sorption effect disappears for all two-component brushes. For a 2-block brush, dashed line is used to indicate fluctuations in solvent fractions. In all simulations we keep $\epsilon_{aa} = \epsilon_{bb} = \epsilon_{as} = \epsilon_{bs} = \epsilon_{ss} = 1$ and only vary ϵ_{ab}.

The cross-interaction strength affects the amount of absorbed solvent in the brush. Fig. 5.4 displays the solvent volume fraction in the brush as a function of ϵ_{ab} for block and random copolymer systems. As previously, at $\epsilon_{ab} = 1$ all systems are effectively homopolymer brushes, and absorb the same amount of solvent. In all systems, reducing the miscibility of the monomers through ϵ_{ab} leads to an increase in solvent uptake. The solvent uptake appears to increase monotonously with decreasing ϵ_{ab}, trending towards some saturation value at low ϵ_{ab}. The random copolymer brush absorbs the most solvent, followed by the 4-block brush and the 2-block brush, with the largest differences for highly immiscible systems. This is consistent with the expected behavior: sorption is driven by the unfavorable interaction between monomers, and increases with the number of contacts between the two monomer species.
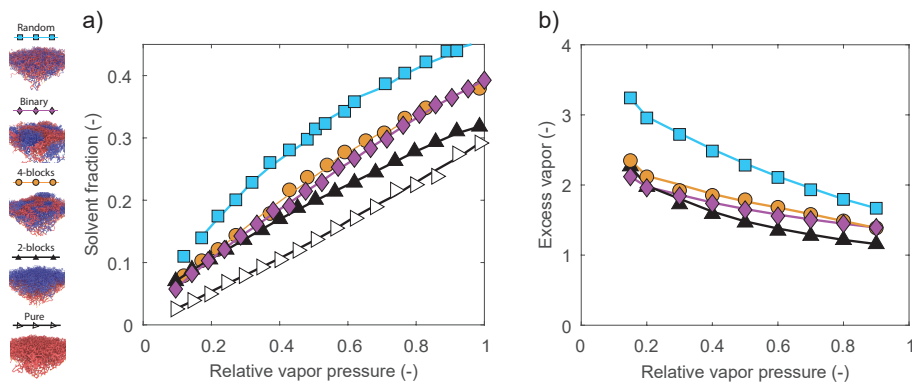
Isotherms

Figure 5.5: a) Absorption isotherms of random, mixed - binary, 4-block, 2-block and pure homopolymer brushes. All isotherms appear concave-downward, apart from the convex-upward shape of a pure homopolymer brush . b) Excess vapor sorbed at different relative vapor pressure in structurally distinct polymer brushes compared to the pure homopolymer brush. The random brush shows significant sorption enhancement at low relative vapor pressures. In all simulations we use $\epsilon_{ab} = 0.4$, $\epsilon_{aa} = \epsilon_{bb} = \epsilon_{as} = \epsilon_{bs} = \epsilon_{ss} = 1$.

In the last set of simulations, we vary the pressure of the solvent vapor and investigate the sorption behavior of pure, mixed binary, 2-block, 4-block and random brushes. The mixed binary brush system consists of equal fractions of homopolymers consisting of each monomer species, and is investigated for comparison to previous work. [18, 19] We consider the solvent fraction as a function of the relative solvent pressure, which we define as the solvent pressure normalized by the saturation pressure of the vapor. In Fig. 5.5**a**, we display the resulting isotherms, with the relative solvent pressure on the horizontal axis and the solvent fraction in the brush on the vertical axis. For the pure polymer brush, we find a convex-upward isotherm, which is consistent with typical experimental results. [8, 10, 44] However, for all two-component systems, we find a concave-upward isotherm. In previous simulation work, [16] we have found that this concave-upward isotherm occurs for very strong polymer-solvent interactions. Although uncommon, this type of isotherm is also observed experimentally in extremely hydrophilic systems, such as polyelectrolytes or densely hydrogen-bonding systems. [11, 13] The shift in isotherm shape is driven entirely by the net repulsion between the monomers,

as the interaction between the solvent and the two monomer species is the same. We once again find that the sorption depends on the number of A-B monomer contacts, with the random brush absorbing the most solvent out of the two-component systems, the mixed and 4-block brushes absorbing similar, intermediate amounts, and the 2-block brush absorbing the least.

We point out that we likely underestimate the sorption in the 4-block brush at low relative pressures. Under dry conditions, inhomogeneous patches of polymer B make up the topmost layer of the brush, making it impossible to define a single thickness for the whole polymer layer. To obtain a well-defined result, we do not include this topmost block when integrating the density profiles to obtain a solvent fraction.

Fig. 5.5**b** displays the same data, normalized by the solvent uptake in the pure brush. This gives us an enhancement factor relative to the homopolymer case. While all two-component brushes display a sorption enhancement by at least 1.5 times over the full range of relative pressures, the enhancement is largest at low relative pressures. Here, the random brush shows a particularly strong enhancement. This suggests that random copolymer brushes may be interesting for sensing applications, where it is often necessary to detect some minority component at a low concentration and pressure. This pressure-dependent enhancement may be explained by the fact that increasing relative pressures drive sorption in the polymer bulk as well as at the interfaces. The number of A-B contacts at the polymer-polymer interfaces therefore decreases with increasing relative pressure, as some fraction of the monomers in the interfacial region is displaced by solvent. This reduction in A-B contacts also reduces the interfacial energy that leads to enhanced sorption, leading to the observed trend.

5.4 Conclusions

Unfavorable interactions between monomers enhance the amount of vapor that a polymer brush can adsorb. These unfavorable interactions can be introduced by grafting the different types of polymers to the same surface to form a mixed brush. However, it is difficult to synthesize a mixed polymer brush system with optimal conditions. Therefore, we investigated polymer brushes made of block and random copolymers of which the different monomers have an unfavorable interaction with each other. We compared four different systems: a single-component (pure) homopolymer brush, a 2-block copolymer brush, a 4-block copolymer brush, and a random copolymer brush.

With molecular dynamics simulations, we make observations that lead to the following three conclusions. First, all copolymer systems show an enhanced adsorption of vapor at the interfaces between AB block in the case of the block copolymer brushes or throughout the brush in the case of the random copolymer brush. Thus, block and random copolymers efficiently introduce strongly adsorbing interfaces between different monomer types in the brush. Second, when varying the cross-interaction strength, we observe that the brushes with more AB-interactions have a higher vapor sorption: AB-interactions drive vapor sorption in two-component brushes. Finally, the adsorption isotherms of two-component brushes are concave downward, while the isotherm of the pure brush is concave upward. Hence, two-component brushes show an enhanced adsorption, especially at low vapor pressures; the block-copolymer brushes absorb $2\times$ as much vapor as a pure brush and the random copolymer brush $3\times$ as much. This enhancement makes these brushes good candidates for novel sensing and separation technologies where target molecules are present at low concentrations.

5.5 Expanded theory and outlook

The research presented in this chapter and references 18 and 19 shows that vapor absorption can be enhanced by creating energetically unfavorable interfaces within a polymer brush. However, our simulation work is limited to cases where the polymer species are identical, except for their cross-interaction. Also, we only consider the case of a single vapor. Here, a qualitative discussion based on a Flory-Huggins-like argument will be provided, in order to clarify the effect of the interface in more complex cases.

Partitioning

Assuming that the density of the brush only weakly depends on its local composition, we can simply describe the partitioning of an absorbed species in the brush by mean interaction energies. A solvent particle immersed in bulk polymer A would simply experience the polymer-solvent interaction ϵ_{as} with each of its neighbours. Moving this particle from the bulk of A to the middle of the A-B interface would remove half of those solvent-A contacts and replace them with solvent-B contacts. Additionally, moving the particle would displace a proportional number of A-B contacts at the interface, while making room for A-A contacts in the bulk. Hence, the energy of adsorbing a solvent

particle at the polymer-polymer interface will be

$$\Delta W_{\mathrm{A}\to\mathrm{I}} \propto \epsilon_{\mathrm{ab}} + \epsilon_{\mathrm{as}} - (\epsilon_{\mathrm{aa}} + \epsilon_{\mathrm{bs}})^{\dagger}. \qquad (5.6)$$

If this quantity is negative, absorption at the polymer-polymer interface is favored over absorption in the bulk. This is a fairly intuitive result; favorable interactions between polymer and solvent or between the two polymer species favor bulk absorption, whereas a strong self-interaction of the polymer or a favorable interaction between the solvent and the other polymer drives solvent to the interface. However, this only leads to adsorption at the interface if this condition is met for both polymers. Rearranging equation 5.6, we may express the condition for adsorption from A as $\epsilon_{\mathrm{aa}} - \epsilon_{\mathrm{ab}} > \epsilon_{\mathrm{as}} - \epsilon_{\mathrm{bs}}$ and likewise for B as $\epsilon_{\mathrm{bb}} - \epsilon_{\mathrm{ab}} < \epsilon_{\mathrm{as}} - \epsilon_{\mathrm{bs}}$, so that we find the full condition for adsorption

$$(\epsilon_{\mathrm{aa}} - \epsilon_{\mathrm{ab}}) > (\epsilon_{\mathrm{as}} - \epsilon_{\mathrm{bs}}) > (\epsilon_{\mathrm{bb}} - \epsilon_{\mathrm{ab}}). \qquad (5.7)$$

Under a Berthelot combining rule ($\epsilon_{\mathrm{ij}} = \sqrt{\epsilon_{\mathrm{ii}}\epsilon_{\mathrm{jj}}}$, typically used for systems dominated by Van der Waals interactions), this simplifies to the classical result that adsorption occurs when the solvents cohesive energy density is intermediate between those of the polymers. However, in sensing or separation applications, the difference between polymer-solvent affinities should be as small as possible; otherwise, the improved bulk absorption in a single-species brush of the more favorable polymer might be preferable. This would require that ϵ_{aa} and ϵ_{bb} are similar, resulting in relatively miscible polymers and weakening the sorption enhancement at the interface. Fortunately, this trade-off may be circumvented in systems with more specific noncovalent interactions. When the polymer-solvent interactions are dominated by e.g. hydrogen bonding, they become less dependent on the other interaction energies, which would make similar solvent absorption in two poorly miscible polymers possible. While this restricts the available chemistries somewhat, many compounds of interest are hydrogen bond donors or acceptors. Therefore, interfacial sorption enhancement may prove practically applicable even if it is not universal.

Specificity

In the immiscible brush systems described in this chapter, vapor absorption is driven in part by the reduction of unfavorable A-B contacts. Since this contribution does not depend on the nature of the solvent, this allows absorption of a

---

†Interchanging all As and Bs, this expression also describes the same process starting in the bulk polymer B.

broader range of species relative to a single-species brush. To demonstrate this, we derive an effective Flory-Huggins parameter for solvent in an interfacial mixed polymer phase. The generic expression for the Flory-Huggins parameter in a two-component system is

$$\frac{\chi_{\text{ps}}}{z} = \frac{\epsilon_{\text{pp}} + \epsilon_{\text{ss}} - 2\epsilon_{\text{ps}}}{2}. \tag{5.8}$$

Using a mean-field assumption for the composition of the mixed polymer phase, we can replace the interaction parameters for the polymer with those for the mixed polymer phase. We replace ϵ_{pp} with $f_{\text{a}}^2\epsilon_{\text{aa}} + 2f_{\text{a}}f_{\text{b}}\epsilon_{\text{ab}} + f_{\text{b}}^2\epsilon_{\text{bb}}$, where f_{i} is the volume fraction of species i in the dry polymer brush. Similarly, ϵ_{ps} becomes $f_{\text{a}}\epsilon_{\text{as}} + f_{\text{b}}\epsilon_{\text{bs}}$ in the mixed polymer case, resulting in

$$\frac{\chi_{\text{abs}}}{z} = \frac{f_{\text{a}}^2\epsilon_{\text{aa}} + 2f_{\text{a}}f_{\text{b}}\epsilon_{\text{ab}} + f_{\text{b}}^2\epsilon_{\text{bb}} + \epsilon_{\text{ss}} - 2(f_{\text{a}}\epsilon_{\text{as}} + f_{\text{b}}\epsilon_{\text{bs}})}{2}. \tag{5.9}$$

Under the simplifying assumptions used for the simulations in this chapter, $\epsilon_{\text{aa}} = \epsilon_{\text{bb}} = \epsilon_{\text{pp}}$ and $\epsilon_{\text{as}} = \epsilon_{\text{bs}} = \epsilon_{\text{ps}}$, and assuming $f_{\text{a}} = f_{\text{b}} = \frac{1}{2}$ over the interfacial region, we obtain

$$\frac{\chi_{\text{abs}}}{z} = \frac{\frac{1}{2}(\epsilon_{\text{pp}} + \epsilon_{\text{ab}}) + \epsilon_{\text{ss}} - 2\epsilon_{\text{ps}}}{2}. \tag{5.10}$$

This means the effective polymer-solvent Flory-Huggins parameter in the interfacial region is shifted by $\frac{1}{2}(\epsilon_{\text{ab}} - \epsilon_{\text{pp}})$, which must be nonpositive for immiscible polymers. Therefore adsorption at the interface becomes more favorable for all solvents, regardless of their interaction with the polymers. This is not necessarily a problem for potential applications; capturing a wide range of compounds may be desirable in sensors, for instance. However, the absolute effect of the interaction is largest for near-saturated vapors or liquids, as is illustrated by the isotherms in figure 5.5a. This may be detrimental when specific trace compounds in a mixture are targeted.

Acknowledgements

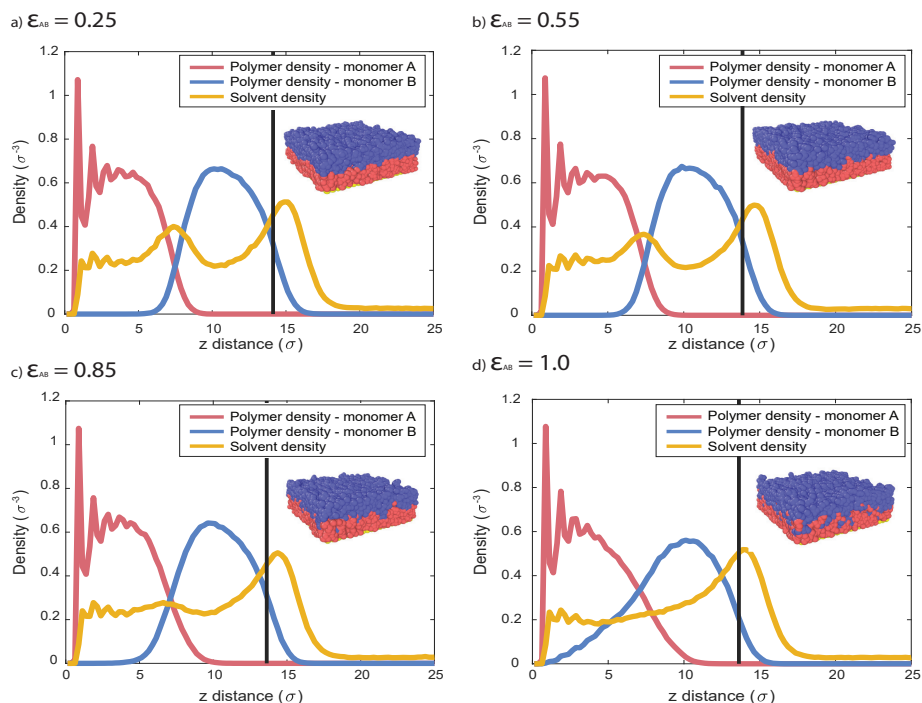## 5.6 Supporting Information

Difference in sorption upon changing ϵ_{ab}

Figure 5.6: Monomer A (purple), monomer B (blue) and solvent (yellow) density profiles at different monomer cross-interaction strengths (ϵ_{ab}). At ϵ_{ab} = 1, the peak correlated to excess solvent disappears due to the mixing of monomers (SI1d). In all simulations we keep $\epsilon_{pp} = \epsilon_{ss} = \epsilon_{ps} = 1$.

Alternating brush

We perform additional simulations of an alternating brush (-A-B-A-B-) to investigate the enhanced sorption effect. Even though the alternating brush contains the most A-B interfacial contacts, it does not sorb considerably more vapor than a random brush. To show this, we plot solvent density profiles at ϵ_{ab} = 0.4, 0,7 and 1.0 of an alternating and random brush in Fig. 5.7. Qualitatively, solvent profiles are similar in shape and area. Quantitatively, the difference of solvent sorbed is 0.6 % at ϵ_{ab} = 0.4, 0.4 % at ϵ_{ab} = 0.7, and 0.5 % at at ϵ_{ab} = 1.0. These values are obtained by integrating the areas below the solvent profiles. Therefore, we conclude that there is a negligible difference in vapor sorption between an alternating and random brush.
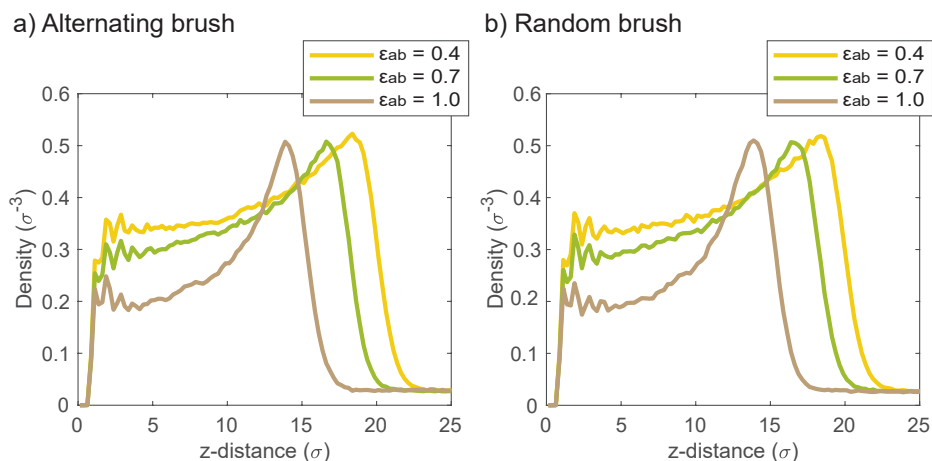

Figure 5.7: Solvent density profiles at different ϵ_{ab} of a) an alternating brush, and b) a random brush. Other particle-particle interactions are kept constant ($\epsilon_{pp} = \epsilon_{ps} = \epsilon_{ss} = 1$).

The same particle-particle interactions - the same polymer density profiles

We perform simulations of a pure homopolymer brush and a 2-block brush while maintaining all particle-particle interactions to be 1. When simulating a pure homopolymer brush this means: $\epsilon_{pp} = \epsilon_{ps} = \epsilon_{ss} = 1$. When simulating a 2-block brush, this means: $\epsilon_{ab} = \epsilon_{pp} = \epsilon_{ps} = \epsilon_{ss} = 1$. We observe that the pure brush density profile overlaps with the sum of 2-block brush density profile (sum polymer density A and polymer density B). The polymer density profiles are identical since the particle interactions are identical, as shown in Figure 5.8.
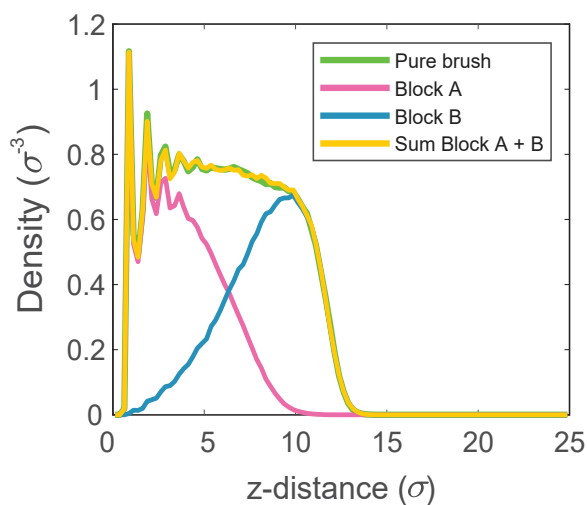

Figure 5.8: Polymer density profile of a pure homopolymer brush (green) and a sum of density profiles in a 2-block brush, A + B, shown in yellow. The profiles are identical since all particle-particle interactions are identical. $\epsilon_{xx} = 1$

5.7   References

[1]   G. C. Ritsema van Eck, L. Chiappisi, and S. de Beer, "Fundamentals and applications of polymer brushes in air", ACS Applied Polymer Materials **4**, 3062–3087 (2022).

[2] S. de Beer, E. Kutnyanszky, P. M. Schön, G. J. Vancso, and M. H. Müser, "Solvent induced immiscibility of polymer brushes eliminates dissipation channels", Nat. Commun. **5**, 3781 (2014).

[3] H. C. McCaig, E. Myers, N. S. Lewis, and M. L. Roukes, "Vapor sensing characteristics of nanoelectromechanical chemical sensors functionalized using surface-initiated polymerization", Nano Lett. **14**, 3728–3732 (2014), URL https://doi.org/10.1021/nl500475b.

[4] T. Wang, Y. Yu, D. Chen, S. Wang, X. Zhang, Y. Li, J. Zhang, and Y. Fu, "Naked eye plasmonic indicator with multi-responsive polymer brush as signal transducer and amplifier", Nanoscale **9**, 1925–1933 (2017), URL http://dx.doi.org/10.1039/C6NR09631J.

[5] H. Yang, H. Zhu, M. M. R. M. Hendrix, N. J. H. G. M. Lousberg, G. de With, A. C. C. Esteves, and J. H. Xin, "Temperature-triggered collection and release of water from fogs by a sponge-like cotton fabric", Adv. Mater. (Weinheim, Ger.) **25**, 1150–1154 (2013), URL https://onlinelibrary.wiley.com/doi/abs/10.1002/adma.201204278.

[6] M. A. Pizzoccaro-Zilamy, S. M. Piña, B. Rebiere, C. Daniel, D. Farrusseng, M. Drobek, G. Silly, A. Julbe, and G. Guerrero, "Controlled grafting of dialkylphosphonate-based ionic liquids on γ-alumina: design of hybrid materials with high potential for co2 separation applications", RSC Adv. **9**, 19882–19894 (2019).

[7] C. R. Bilchak, M. Jhalaria, Y. Huang, Z. Abbas, J. Midya, F. M. Benedetti, D. Parisi, W. Egger, M. Dickmann, M. Minelli, F. Doghieri, A. Nikoubashman, C. J. Durning, D. Vlassopoulos, J. Jestin, Z. P. Smith, B. C. Benicewicz, M. Rubinstein, L. Leibler, and S. K. Kumar, "Tuning selectivities in gas separation membranes based on polymer-grafted nanoparticles", ACS Nano **14**, 17174–17183 (2020), URL https://doi.org/10.1021/acsnano.0c07049.

[8] M. Biesalski and J. Rühe, "Swelling of a polyelectrolyte brush in humid air", Langmuir **16**, 1943–1950 (2000), URL https://doi.org/10.1021/la990863+.

[9] C. J. Galvin, M. D. Dimitriou, S. K. Satija, and J. Genzer, "Swelling of polyelectrolyte and polyzwitterion brushes by humid vapors", Journal of the American Chemical Society **136**, 12737–12745 (2014), URL https://doi.org/10.1021/ja5065334.

[10] S. Christau, S. Thurandt, Z. Yenice, and R. Von Klitzing, "Stimuli-responsive polyelectrolyte brushes as a matrix for the attachment of gold nanoparticles: The effect of brush thickness on particle distribution", Polymers **6**, 1877–1896 (2014), URL `https://www.mdpi.com/2073-4360/6/7/1877`.

[11] X. J. Zhao, Z. F. Gao, and Z. Y. Jiang, "A study of hcl gas adsorption/desorption properties of pnipam brushes", Macromolecular Theory and Simulations **24**, 460–467 (2015), URL `https://onlinelibrary.wiley.com/doi/abs/10.1002/mats.201500027`.

[12] S. V. Orski, R. J. Sheridan, E. P. Chan, and K. L. Beers, "Utilizing vapor swelling of surface-initiated polymer brushes to develop quantitative measurements of brush thermodynamics and grafting density", Polymer **72**, 471–478 (2015), URL `https://www.sciencedirect.com/science/article/pii/S0032386115004723`.

[13] C. J. Galvin and J. Genzer, "Swelling of hydrophilic polymer brushes by water and alcohol vapors", Macromolecules **49**, 4316–4329 (2016), URL `https://doi.org/10.1021/acs.macromol.6b00111`.

[14] M. Brió Pérez, M. Cirelli, and S. de Beer, "Degrafting of polymer brushes by exposure to humid air", ACS Applied Polymer Materials **2**, 3039–3043 (2020), URL `https://doi.org/10.1021/acsapm.0c00474`.

[15] S. V. Orski, R. J. Sheridan, E. P. Chan, and K. L. Beers, "Utilizing vapor swelling of surface-initiated polymer brushes to develop quantitative measurements of brush thermodynamics and grafting density", Polymer **72**, 471 – 478 (2015).

[16] G. C. Ritsema van Eck, L. B. Veldscholte, J. H. W. H. Nijkamp, and S. de Beer, "Sorption characteristics of polymer brushes in equilibrium with solvent vapors", Macromolecules **53**, 8428–8437 (2020), URL `https://doi.org/10.1021/acs.macromol.0c01637`.

[17] T. M. Birshtein and Y. V. Lyatskaya, "Theory of the collapse-stretching transition of a polymer brush in a mixed solvent", Macromolecules **27**, 1256–1266 (1994).

[18] L. A. Smook, G. C. Ritsema van Eck, and S. de Beer, "Concentrating vapor traces with binary brushes of immiscible polymers", ACS Applied Polymer

Materials **3**, 2336–2340 (2021), URL https://doi.org/10.1021/acsapm.1c00321.

[19] L. A. Smook, G. C. Ritsema van Eck, and S. de Beer, "Vapor sorption in binary polymer brushes: The effect of the polymer–polymer interface", The Journal of Chemical Physics **155**, 054904 (2021).

[20] M. Li and C. W. Pester, "Mixed polymer brushes for "smart" surfaces", Polymers **12**, 1553 (2020), URL https://www.mdpi.com/2073-4360/12/7/1553.

[21] D. Julthongpiput, Y.-H. Lin, J. Teng, E. R. Zubarev, and V. V. Tsukruk, "Y-shaped polymer brushes: Nanoscale switchable surfaces", Langmuir **19**, 7832–7836 (2003), URL https://doi.org/10.1021/la035007j.

[22] C. Tonhauser, A. A. Golriz, C. Moers, R. Klein, H.-J. Butt, and H. Frey, "Stimuli-responsive y-shaped polymer brushes based on junction-point-reactive block copolymers", Advanced Materials **24**, 5559–5563 (2012), URL https://onlinelibrary.wiley.com/doi/abs/10.1002/adma.201202105.

[23] J. O. Zoppe, N. C. Ataman, P. Mocny, J. Wang, J. Moraes, and H.-A. Klok, "Surface-initiated controlled radical polymerization: State-of-the-art, opportunities, and challenges in surface and interface engineering with polymer brushes", Chemical Reviews **117**, 1105–1318 (2017), URL https://doi.org/10.1021/acs.chemrev.6b00314, pMID: 28135076.

[24] X. Sui, S. Zapotoczny, E. M. Benetti, M. Memesa, M. A. Hempenius, and G. J. Vancso, "Grafting mixed responsive brushes of poly(n-isopropylacrylamide) and poly(methacrylic acid) from gold by selective initiation", Polym. Chem. **2**, 879–884 (2011), URL http://dx.doi.org/10.1039/C0PY00393J.

[25] L. Wan, R. Ruiz, H. Gao, K. C. Patel, T. R. Albrecht, J. Yin, J. Kim, Y. Cao, and G. Lin, "The limits of lamellae-forming ps-b-pmma block copolymers for lithography", ACS Nano **9**, 7506–7514 (2015), URL https://doi.org/10.1021/acsnano.5b02613, pMID: 26046475.

[26] W. Lee, S. Park, Y. Kim, V. Sethuraman, N. Rebello, V. Ganesan, and D. Y. Ryu, "Effect of grafting density of random copolymer brushes on perpendicular alignment in ps-b-pmma thin films", Macromolecules

50, 5858–5866 (2017), URL `https://doi.org/10.1021/acs.macromol.7b00133`.

[27] S. Ham, C. Shin, E. Kim, D. Y. Ryu, U. Jeong, T. P. Russell, and C. J. Hawker, "Microdomain orientation of ps-b-pmma by controlled interfacial interactions", Macromolecules **41**, 6431–6437 (2008), URL `https://doi.org/10.1021/ma8007338`.

[28] J. Lee, K. Lee, J. Park, J. K. Kim, and T. Chang, "Characterization and fractionation of PS-b-PMMA diblock copolymer synthesized via click chemistry", Polymer **80**, 46–51 (2015), URL `https://www.sciencedirect.com/science/article/pii/S0032386115303189`.

[29] C. Liu, F. Cheng, B. Liu, D. Gao, G. Cheng, C. Li, H. Wang, and W. He, "Versatile, oxygen-insensitive surface-initiated anionic polymerization to prepare functional polymer brushes in aqueous solutions", Langmuir **38**, 1001–1010 (2022), URL `https://doi.org/10.1021/acs.langmuir.1c02416`, pMID: 34949091.

[30] C. Sinturel, F. S. Bates, and M. A. Hillmyer, "High χ–low n block polymers: How far can we go?", ACS Macro Letters **4**, 1044–1050 (2015), URL `https://doi.org/10.1021/acsmacrolett.5b00472`.

[31] W. J. Durand, G. Blachut, M. J. Maher, S. Sirard, S. Tein, M. C. Carlson, Y. Asano, S. X. Zhou, A. P. Lane, C. M. Bates, C. J. Ellison, and C. G. Willson, "Design of high-χ block copolymers for lithography", Journal of Polymer Science Part A: Polymer Chemistry **53**, 344–352 (2015), URL `https://onlinelibrary.wiley.com/doi/abs/10.1002/pola.27370`, _eprint: https://onlinelibrary.wiley.com/doi/pdf/10.1002/pola.27370.

[32] D. Mukherji, C. M. Marques, T. Stuehn, and K. Kremer, "Depleted depletion drives polymer swelling in poor solvent mixtures", Nature Communications **8**, 1374 (2017), URL `http://dx.doi.org/10.1038/s41467-017-01520-5`.

[33] A. Galuschko, L. Spirin, T. Kreer, A. Johner, C. Pastorino, J. Wittmer, and J. Baschnagel, "Frictional forces between strongly compressed, nonentangled polymer brushes: Molecular dynamics simulations and scaling theory", Langmuir **26**, 6418–6429 (2010).

[34] M. K. Singh, P. Ilg, R. M. Espinosa-Marzal, M. Kröger, and N. D. Spencer, "Polymer brushes under shear: Molecular dynamics simulations compared to experiments", Langmuir **31**, 4798–4805 (2015).

[35] H. Yong, H. Merlitz, A. Fery, and J.-U. Sommer, "Polymer brushes and gels in competing solvents: The role of different interactions and quantitative predictions for poly(n-isopropylacrylamide) in alcohol–water mixtures", Macromolecules **53**, 2323–2335 (2020).

[36] G. S. Grest and K. Kremer, "Molecular dynamics simulation for polymers in the presence of a heat bath", Phys. Rev. A **33**, 3628–3631 (1986), URL `https://link.aps.org/doi/10.1103/PhysRevA.33.3628`.

[37] K. Kremer and G. S. Grest, "Dynamics of entangled linear polymer melts: A molecular-dynamics simulation", The Journal of Chemical Physics **92**, 5057–5086 (1990).

[38] D. Mukherji, C. M. Marques, T. Stuehn, *et al.*, "Depleted depletion drives polymer swelling in poor solvent mixtures", Nat Commun **8**, 1374 (2017), URL `https://doi.org/10.1038/s41467-017-01520-5`.

[39] M. Tuckerman, B. J. Berne, and G. J. Martyna, "Reversible multiple time scale molecular dynamics", The Journal of Chemical Physics **97**, 1990–2001 (1992), URL `https://doi.org/10.1063/1.463137`.

[40] A. P. Thompson, H. M. Aktulga, R. Berger, D. S. Bolintineanu, W. M. Brown, P. S. Crozier, P. J. in 't Veld, A. Kohlmeyer, S. G. Moore, T. D. Nguyen, R. Shan, M. J. Stevens, J. Tranchida, C. Trott, and S. J. Plimpton, "LAMMPS - a flexible simulation tool for particle-based materials modeling at the atomic, meso, and continuum scales", Comp. Phys. Comm. **271**, 108171 (2022).

[41] A. Stukowski, "Visualization and analysis of atomistic simulation data with ovito-the open visualization tool", Modelling and Simulation in Materials Science and Engineering **18**, 015012 (2010).

[42] T.-Y. Kim, G. R. Kang, M. Kim, V. Thapar, and S.-M. Hur, "Full parameter space exploration of microphase separation of block copolymer brushes within a single simulation framework", Mol. Syst. Des. Eng. **6**, 1087–1097 (2021), URL `http://dx.doi.org/10.1039/D1ME00126D`.

5

[43] J. Wang and M. Müller, "Microphase separation of diblock copolymer brushes in selective solvents: Single-chain-in-mean-field simulations and integral geometry analysis", Macromolecules **42**, 2251–2264 (2009).

[44] A. Laschitsch, C. Bouchard, J. Habicht, M. Schimmel, J. Rühe, and D. Johannsmann, "Thickness dependence of the solvent-induced glass transition in polymer brushes", Macromolecules **32**, 1244–1251 (1999), URL `https://doi.org/10.1021/ma980743t`.

Chapter 6

Exploratory investigation of Schroeder's Paradox[*]

It is an open question why polymer gels are sometimes found to absorb more solvent from a liquid than they do from the corresponding saturated vapor. This chapter describes an exploratory study of this phenomenon, which is known as Schroeder's paradox. We describe an experiment in which the paradox is identified in a crosslinked poly(hydroxyethyl methacrylate)-water system. Next, we present a simulation study that reproduces the phenomenon in a series of microscopic gels. Our results suggest that the paradox is not explained by the difference in surface tension between gel-liquid and gel-vapor interfaces, and indicate several potential directions for further research.

6.1 Introduction

In 1903, von Schroeder reported that a sample of gelatin swelled more when immersed in liquid water than when placed in saturated water vapor. [1]†
This is unexpected from a thermodynamic perspective: since a liquid and a saturated vapor are in equilibrium with one another, they would be expected to equilibrate with a third phase in the same way. Von Schroeder's result sparked contemporary discussion, [2, 3] but no broadly accepted interpretation of the effect was found. As a result, this phenomenon has become known as Schroeder's paradox. In the last two decades, Schroeder's paradox has once again drawn significant attention, this time from the membrane research community. [4] Nafion, a family of sulfonated perfluoropolymers commonly used in proton exchange membranes, appears to displays a Schroeder effect [5, 6] which may influence moisture buildup in proton exchange membrane fuel cells (PEMFCs). Since these PEMFCs only operate optimally under a limited range of water content, understanding this particular case of the Schroeder phenomenon is technologically important. This has led to a new wave of research focusing on the paradox in relation to the particular properties of Nafion. However, the effect also remains interesting from a fundamental point of view, and is not exclusive to Nafion or even to charged systems. [1, 7]

In this chapter, we will give an overview of fundamental research into Schroeder's paradox, and present a simulative and experimental exploration of the phenomenon. First, we present a selection of proposed explanations of Schroeder's paradox with emphasis on the more broadly applicable hypotheses. To identify and test the most likely of these hypotheses, we present a simulation study on the swelling behavior of gels in liquids and saturated vapors under a range of polymer-solvent interactions, gel sizes, and gel architectures. The swelling behavior and structure of the swollen gels are respectively quantified by the radius of the gel and the radial distribution functions for polymer and solvent particles, centered on polymer particles. In addition, we present a swelling experiment on poly(hydroxyethyl methacrylate) (PHEMA) gels in water and water vapor, in which we quantify the swelling of the gels by mass uptake. Finally, we discuss how the outcomes of these studies relate to the various hypotheses on Schroeder's paradox.

---

†In German; for those who prefer to read English, W.D. Bancroft provides a partial translation in ref. 2

6.2 Background

At the core of Schroeder's paradox is an apparent disequilibrium between two states that should be in equilibrium: A gel swollen in liquid and one swollen in saturated vapor equilibrate at different compositions, and switching the solvent environment between these states will cause the gel to swell or deswell to the corresponding composition. [1, 2] The repeatability of this process suggests that the transition between these equilibrium states is a strictly reversible process, which is not permitted by the second law. Research of the last two decades, often motivated by PEMFC applications, also associates the paradox with a difference in permeability and proton conductivity and sometimes uses these quantities as an indication of a Schroeder effect. [4, 8] There are two broad categories of hypotheses that attempt to explain the paradox: those based on equilibrium thermodynamics, and those that ascribe the effect to some non-equilibrium effect such as a metastability or history dependence of the gel structure. While theories relating to the dynamics or kinetics of swelling could explain the existence of two apparent equilibrium states, the (near-)reversible transition between the two swollen states poses a challenge to this type of explanation.

Purely thermodynamic descriptions typically propose some free energy model under which multiple equilibrium compositions for the swollen gel exist, or in which some novel term creates a difference between vapor and liquid solvation. The work of Vallieres et al. [7] is noteworthy in this category because it does not require any new free energy terms. Rather, it shows that the commonly used Flory-Rehner description of gel swelling [9] produces a Van der Waals loop (an equilibrium condition with multiple roots) for some combinations of gel structure and polymer-solvent interaction parameter. This is similar to the separation into a polymer-rich phase and a solvent-rich phase of free polymer chains in a poor solvent. While this is a simple and elegant explanation for the existence of multiple equilibrium compositions, its applicability is limited; the Van der Waals loop only occurs in poor solvent conditions, and the Flory-Rehner model is a mean-field description which cannot account for porosity or inhomogeneity. Since Nafion in water forms a two-phase structure, [10, 11] this model does not describe one of the most studied systems in which the Schroeder effect occurs. If the Van der Waals loop is preserved when accounting for these phenomena, a more sophisticated form of this model might still be applicable. Davankov and Pastukhov present experiments suggesting that the energy landscape in between the saturated vapor and liquid equilibrium conditions may be extremely flat, based on the absorption of microdroplets

deposited on swollen gel beads in saturated vapor conditions. [12] While this would explain the reversible transition between the two swelling states, it raises new questions instead. For instance, it is unclear why a singular equilibrium degree of swelling in liquid would still exist in the absence of both energetic barriers and transport limitations.

Thermodynamic explanations of the Schroeder effect often propose some additional free energy contribution that depends on the environment outside the gel. Such explanations are typically targeted at Nafion and its specific properties. Choi and Datta propose a model for the swelling of Nafion in which the swollen material develops a porous structure, which exposes water-filled pores to the environment. [13] In a saturated vapor environment, this creates a curved water-air interface, with an associated Laplace pressure that works against the swelling pressure of the gel. This interface does not exist in the liquid-immersed case, leading to a difference in swelling behavior. Other authors have, however, pointed out that this open pore structure may not be stable. [5, 7] Freger also presents an argument based on a Laplace pressure, but associates this pressure with micelle-like aggregates of polar or ionic side groups within the polymer matrix. [5] Requiring equal chemical potential between these aggregates and the hydrophilic groups on the outer surface of the gel makes the size of the water-rich aggregates strongly dependent on the surface tension between the gel and the external environment, resulting in a large difference in swelling between saturated vapor and liquid environments.

In contrast to the explanations above, Onishi, Prausnitz and Newman state that Schroeder's paradox in Nafion is purely a consequence of the thermal history of the polymer, and disappears when the liquid- and vapor-swollen gels are sufficiently pretreated. [8] Since this pretreatment process involves boiling the Nafion membrane in dilute hydrogen peroxide and sulfuric acid and drying it under vacuum, it seems possible that this pretreatment itself could impose a particular morphology, for instance by forming a particular pore structure during vacuum drying. Thus, while these results indicate that Schroeder's paradox depends on the morphology of the polymer phase as well as its chemistry, they do not exclude the possibility of a thermodynamic Schroeder effect for some gel morphology.

6.3 Experiments

Materials

Ethylene glycol dimethacrylate (EGDMA, >98%), tetramethylethylenediamine (TEMED, >99%), hydroxyethyl methacrylate (HEMA, >99%) and Ammonium persulfate (APS, >98%) were obtained from Merck and used as received. MilliQ water was obtained from a Millipore system. Ethanol (technical grade) was obtained from Boom.

Synthesis

A reaction solution was prepared in a glass vial by combining 5.63 μL (4.36 mg) of TEMED, 908 μL of HEMA (975 mg, 7.5 mmol) and 17.7 μL of EGDMA (18.6 mg, 0.0375 mmol) in 600 μL of milliQ water. This solution was stirred, then transferred to a 50 mL Falcon centrifuge tube and purged with nitrogen for 10 minutes. In another vial, 10.75 mg of APS was dissolved in 600 μL of milliQ water, and also stirred and purged with nitrogen for 10 minutes. The APS solution was then added to the reaction solution to start a free radical polymerization initiated by the APS/TEMED couple. The reaction mixture was briefly mixed with a vortex mixer, after which the centrifuge tube was placed on a rolling bench at 10 rpm for 24 hours. This procedure was repeated to produce two gels. We arbitrarily designate these gel 1 and gel 2.

After rolling, the centrifuge tubes were opened and the gels were gently detached from the tube walls with a clean spatula. The gels were then washed to remove any unconverted monomer and other reactants. In each washing step, any previous solvent was discarded and the tube was filled with either water or ethanol, then placed on the rolling bench at 10 rpm for 24 hours. In this way, the gels were washed twice with milliQ water, once with ethanol, then once with milliQ water again. After removing the water, the gels were cut into three pieces each with a scalpel; while the pieces of each gel were not equal in size, care was taken to divide the both gels in roughly the same way. The gel fragments were then returned to the tubes and freeze-dried by immersing the centrifuge tubes in liquid nitrogen, then placing the tubes in a container under vacuum for approx. 72 hours. These freeze-dried gel fragments were used as the starting state for the swelling experiment.

In order to verify that any unreacted monomer was removed in the washing step, an FTIR spectrum of a small piece of gel 1 was recorded on a Bruker ALPHA II spectrometer. Comparing this spectrum, shown in figure 6.1, to

a reference spectrum of HEMA monomer [14], most features match up as expected. For instance, the strong peaks near 1200 cm^{-1} and 1700 cm^{-1}, which likely correspond to the C-O single and double bond stretching, are present in both spectra. A broad O-H stretching peak around 3300 cm^{-1} is also found in both spectra; while this peak is expected for HEMA or its polymer, it is less specific, since it also corresponds to water or ethanol. Regardless, these spectra indicate that HEMA is incorporated into the gel as expected. On the other hand the minor peak at 1600 cm^{-1}, which is attributed to the C-C double bond, [15] is not observed. This indicates that the unconverted monomer is successfully removed by washing.
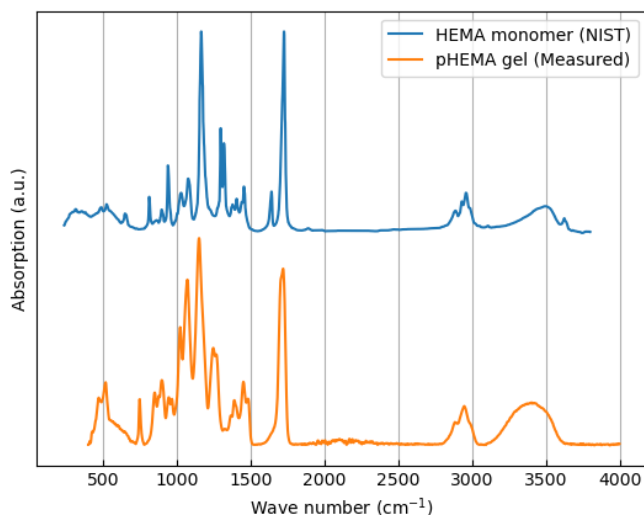

Figure 6.1: Dispersive IR spectrum of HEMA monomer (NIST) [14] and FTIR spectrum of pHEMA gel (measured).

Swelling experiment

A simple experiment was designed and conducted to test the occurrence of Schroeder's paradox in the pHEMA gels. In the experimental design, the main considerations were to keep the treatment of liquid- and vapor-swollen gels as similar as possible, and minimize perturbation of the gels by temperature changes or ambient air exposure. The freeze-dried gel fragments were individually weighed to obtain their dry weight m_0; the dry weights for all gel

Table 6.1: Initial and final dry weight of the gel samples used in the swelling experiment.

	m_0 (g)	m_{final}
Liquid-swollen, gel 1	0.44494	0.44111
Liquid-swollen, gel 2	0.48928	0.48829
Vapor-swollen, gel 1	0.30137	0.30335
Vapor-swollen, gel 2	0.31006	0.31074
Additional tests, gel 2	0.18714	-

samples used are listed in table 6.1. Then, from each gel one fragment was selected to be swollen in liquid and one fragment was selected to be swollen in vapor, so that the gels used in each phase were of roughly equal weight. Gel samples were swollen in liquid by placing them each in a separate clean beaker filled with milliQ water, which was covered with parafilm. For vapor swelling, each gel was placed in a plastic dish, which was set on a platform above a layer of water inside a sealed chamber, with each gel in a different chamber. These beakers and chambers were left in a fume hood to equilbrate. An UEMON UMTS-TH01 temperature and humidity sensor was placed in the fume hood to monitor the ambient conditions. This found a near-constant temperature of 20.5 ± 0.1 °C, and an ambient humidity of 43 ± 5%. The same sensor was later placed in one of the chambers used for vapor swelling to check whether saturation was reached. After an equilibration period of 72 hours, the sensor reported a constant relative humidity >99%. Although it has been noted that even small deviations from saturation in the vapor can cause a noticeable difference in swelling, [16] we assume this indicates saturation. After the experiment, gels used in the primary swelling experiment were freeze-dried in the same way as previously described, and weighed again to check for degradation. The final dry weights are also reported in table 6.1. All changes in dry weight over the course of the experiment are <1% of the total weight; we attribute the apparent mass gain of some of the samples to general experimental error.

The swollen gels were periodically weighed in order to determine the mass of the absorbed water. To limit ambient air exposure and minimize error, measurements were performed following a fixed procedure. First, a dry, empty beaker (the "weighing beaker") with a parafilm cover was placed on a balance, which was then tared. The vapor-swollen gels were removed from the sealed chamber inside the plastic dish, after which the chamber was closed again

Table 6.2: Weight over time of a liquid-swollen gel, left uncovered under ambient conditions.

	Weight (g)	Swelling ratio (-)
Dry	0.18714	1
Liquid-swollen (t = 0)	0.38741	2.0702
t = 1 min	0.38706	2.0683
t = 2 min	0.38665	2.0661
t = 3 min	0.38624	2.0639
t = 4 min	0.38585	2.0618
t = 5 min	0.38547	2.0598

and the gel was quickly transferred from the dish into the weighing beaker with a spatula. The liquid-swollen gels were taken out of the water with a spatula, quickly blotted with a Kimtech Precision wipe to remove excess water, and placed into the weighing beaker. The parafilm cover was drawn over the weighing beaker to limit water loss to evaporation. Then, the covered weighing beaker was weighed to obtain the weight of the swollen gel m_{sw}. The gel was placed back into its swelling environment, and the beaker was weighed again to find the weight of residual water m_{res} left behind by the gel. This procedure was repeated in its entirety for each gel to be weighed. The measured weight of the gel was considered to be $m_{gel} = m_{sw} - m_{res}$. The swelling ratio is defined as m_{gel}/m_0.

To check whether evaporation during the weighing process might influence the results, one of the gel fragments not used in the primary experiment was immersed in milliQ water for 72 hours. It was then weighed as described above, with the difference that the beaker was left uncovered on the balance for 5 minutes, during which the weight of the gel was recorded every minute. The weight of the gel over this period is listed in table 6.2. While a continuous decrease in weight was observed, this decrease was on the order of 1% of the dry gel weight over 5 minutes. Since the weighing procedure generally involves less than a minute of ambient air exposure, we take this as indication that water losses to evaporation will not qualitatively change our results.

Finally, the sample used in the evaporation test was also used to investigate the transition between the liquid-swollen and vapor-swollen state. After the evaporation measurements, in its still liquid-swollen state, it was placed in a saturated vapor environment as described above. It was kept in this environment for most of the swelling experiment, and transferred to a beaker of water

again near the end of the experiment. During this period, it was weighed at the same times as the other gel samples.

Results and discussion

The swelling over time of our gel samples is plotted in figure 6.2. The liquid-swollen gels each absorbed around 80-85% of their dry weight in water (corresponding to a swelling ratio of 1.8-1.85), and did not show any clear trend or large fluctuations in weight once this degree of swelling was reached. The vapor-swollen gels, in contrast, only absorb around 30% of their dry weight in water, indicating the presence of a Schroeder effect. As far as we are aware, this is the first time a Schroeder effect has been reported for the pHEMA-water system. The liquid-immersed samples swell relatively quickly, with one sample attaining its apparent equilibrium composition within two days, and the other lagging slightly but still equilibrating within 5 days. The vapor-swollen gels were somewhat slower to reach their final degree of swelling, and displayed larger differences in swelling rate than the liquid-swollen samples. The behavior of sample 1 is as expected, swelling monotonously and reaching a plateau value around the measurement at 9 days, somewhat slower than the samples in liquid. Sample 2, however, follows the same trajectory initially, but appears to lose weight and settle at a lower degree of swelling, before abruptly swelling to the same extent as the other sample near the end of the experiment. While it is possible that this lower plateau value indicates some metastable state, it seems more likely that the chamber for this gel was not properly sealed, creating an unsaturated vapor environment during parts of the experiment.
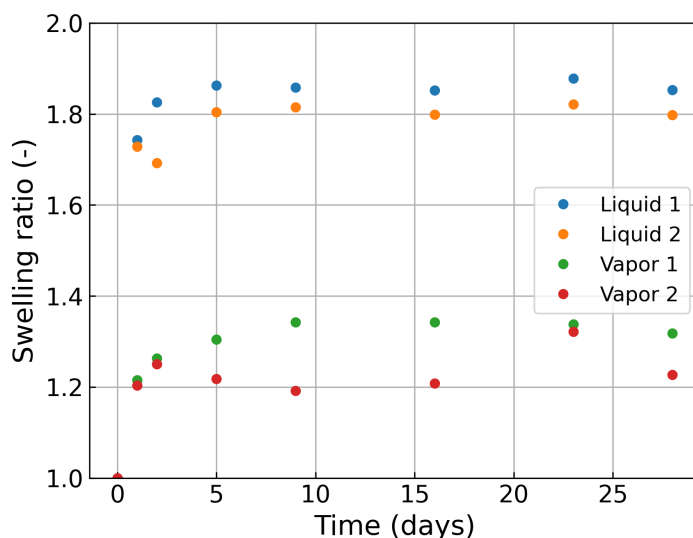
179

Figure 6.2: Swelling ratio over time for all gels kept in a constant environment. A swelling ratio of 1 corresponds to a completely dry gel.

Figure 2 shows the degree of swelling for the additional sample, which was transferred from liquid to vapor and back again over the course of the experiment. The mean swelling ratios at steady state (from the measurement at 9 days onwards) of the samples in the primary swelling experiment are also shown for comparison. The additional sample attains a swelling ratio of 1.90, which is marginally higher than that of the samples used in the primary experiment. After being transferred to a saturated vapor environment, it slowly deswells until reaching a swelling ratio of 1.28, comparable to other vapor-swollen samples. Transferring it to liquid again causes it to swell to its previous weight again. The fact that we find two different steady states that only appear to be stable in the corresponding environment is informative. Assuming vapor saturation is indeed achieved in the experiment, this result challenges the Van der Waals loop hypothesis set out in ref. 7: if vapor and liquid swelling are described by a single isotherm with multiple equilibrium compositions, we would expect either composition to be stable in both environments. Moreover, the fact that the gel readily transitions to a different composition suggests that there are no major thermodynamic barriers separating the two states. Therefore, it also seems unlikely that the transition we observe is between two equilibria on a single isotherm; if this were the case, we would also expect a gel kept in

a steady environment to occasionally pass from one equilibrium composition to another. Thus, the swelling and deswelling of the gel in this experiment cannot be explained by equilibrium thermodynamics alone without accounting for differences between liquid and vapor solvation. Since the interface between the gel and its environment is rather different in liquid and in vapor, it seems plausible that interfacial or capillary effects provide the energetic contribution distinguishing the two swelling equilibria. We investigate these possibilities in an exploratory simulation study in the next section.
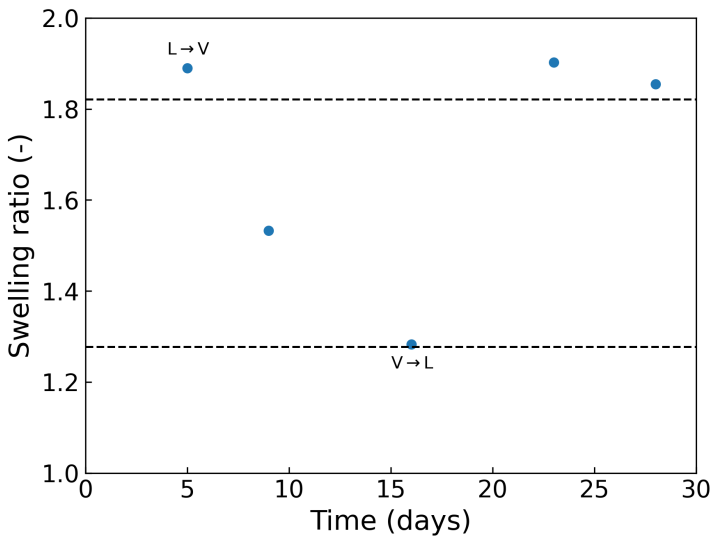
Figure 6.3: Swelling ratio of a gel under changes in solvation environment. Mean steady-state values from the primary experiment are shown as dashed horizontal lines. Annotations indicate that the gel was transferred to a different environment *after* the annotated measurement.

6.4 Simulation Study

Theory

The simplest possible scenario is that the Schroeder effect is caused by the difference in surface tension between the vapor-gel interface and the liquid-gel interface, which would produce a larger energetic penalty for swelling in vapor than in liquid. While it is unlikely that this describes our macroscopic

experiments, in which the surface to volume ratio of the gels is small, we will be simulating microscopic systems. To define a basic hypothesis, we will derive a simple energetic description of gel swelling including an interfacial contribution. Our approach resembles the Flory-Rehner description [9], although we make use of some known results to simplify the derivation.

We assume the entropy of mixing for the solvent and the enthalpy of mixing between polymer and solvent are described by Flory-Huggins terms, so that

$$\frac{\Delta E_{\text{FH}}}{k_{\text{B}}T} = n_{\text{s}} \ln \phi_{\text{s}} + \chi n_{\text{s}} \phi_{\text{p}}. \tag{6.1}$$

Next, we associate the swelling of the gel with a penalty to the configurational entropy of the polymer chains. Assuming random-walk behavior for the chains, their configurational entropy depends on their end-to-end distance as $\frac{3}{2} k_{\text{B}} T \frac{R^2_{\text{end-to-end}}}{Na^2}$, with N the number of monomers in the chain and a the length of a monomer. We set a to 1, since our simulations allow us to use the monomer size as a length scale, and decompose $R^2_{\text{end-to-end}}$ into orthogonal components $R^2_{\text{x}} + R^2_{\text{y}} + R^2_{\text{z}}$. To derive the energetic effect of swelling the gel, we use an affine network assumption, i.e. we assume that a linear extension of the gel by λ in any direction stretches all chains in the network by λ in the same direction. Thus, the end-to-end vector for a chain in a deformed gel becomes $(\lambda_{\text{x}} R_{\text{x,0}})^2 + (\lambda_{\text{y}} R_{\text{y,0}})^2 + (\lambda_{\text{z}} R_{\text{z,0}})^2$, with the subscript 0 denoting the measures of the undeformed chain. Assuming our gel is isotropically deformed by swelling, this simplifies to $\lambda^2 (R^2_{\text{x,0}} + R^2_{\text{y,0}} + R^2_{\text{z,0}}) = (\lambda R_{\text{end-to-end,0}})^2$. Thus, we obtain the gel elasticity contribution as the difference between the deformed and undeformed states

$$\frac{\Delta S_{el}}{k_{\text{B}}T} = S_\lambda - S_0 = -\frac{3n}{2} \frac{(\lambda^2 - 1) R^2_{\text{end-to-end,0}}}{N}, \tag{6.2}$$

with n the number of chains in the gel. Assuming an ideal polymer chain, the end-to-end distance of a chain scales with $\sqrt{N}$ giving (down to a prefactor)

$$\frac{\Delta S_{el}}{k_{\text{B}}T} = -\frac{3n}{2} (\lambda^2 - 1). \tag{6.3}$$

Next, we estimate the effect of the surface energy of the interface the gel and its environment. We may assume the surface area of the gel to scale with the square of its radius (or some other linear dimension). Thus, we find

$$\frac{\Delta E_{\text{int}}}{k_{\text{B}}T} = \gamma(R^2 - R_0^2) = \gamma((\lambda R_0)^2 - R_0^2) = \gamma(\lambda^2 - 1)R_0^2, \tag{6.4}$$

where γ is the surface tension between the gel and its environment, by the same logic as previously. Combining all these terms gives a total expression

$$\frac{\Delta E_{\text{FH}} + \Delta E_{\text{int}} - \Delta S_{\text{el}}}{k_{\text{B}}T} = n_{\text{s}} \ln \phi_{\text{s}} + \chi n_{\text{s}} \phi_{\text{p}} + \frac{3n}{2}(\lambda^2 - 1) + \gamma(\lambda^2 - 1)R_0^2. \quad (6.5)$$

Via the swelling ratio $\frac{1}{\phi_{\text{p}}} = \frac{V}{V_0} = \lambda^3$, we relate the λ terms to typical Flory-Huggins language, and combine them. Additionally, we relate n to R_0 by the assumption that all chains in the gel occupy the same volume $V_{\text{c},0}$ in the dry state. Thus, we substitute $n = \frac{R_0^3}{V_{\text{c},0}}$, giving

$$\frac{\Delta G}{k_{\text{B}}T} = n_{\text{s}} \ln \phi_{\text{s}} + \chi n_{\text{s}} \phi_{\text{p}} + (\gamma R_0^2 + \frac{3R_0^3}{2V_{\text{c},0}})(\phi_{\text{p}}^{-2/3} - 1). \quad (6.6)$$

This supports our qualitative expectations:

- Since γ will always be larger in vapor than in liquid as long as the liquid actually swells the polymer, gels in vapor should swell less than in liquid.

- A more favorable polymer-solvent interaction will increase the cohesive energy density of the swollen gel, leading to a larger γ in vapor. On the other hand, an attractive polymer-solvent interaction creates more favorable interactions at the interface, leading to a lower γ in liquid. Therefore, we expect differences between vapor and liquid swelling to become larger in better solvents.

- Elastic and interfacial effects both oppose the swelling of the gel

- Both the elastic and the interfacial contribution increase with the dry radius of the gel, although the interfacial effect scales with the surface area of the gel and the elastic effect scales with its volume. The crossover from an interface-dominated to a bulk-dominated regime would depend on the relative magnitudes of γ and R_0, although the several prefactors we have neglected in this analysis make it difficult to give an exact prediction.

For any quantitative use of this expression, it should be noted that γ itself is dependent on the composition of the swollen gel.

Simulation design

To further investigate Schroeder's paradox, we employ coarse-grained molecular dynamics simulations of gels in different environments. By using simulations, we ensure that all our gels are perfectly identical, and obtain convenient access to information on the state of the gel. All simulations are run in LAMMPS, [17] and visualized using Ovito. [18]

By simulating the swelling of gels of different sizes, we can test whether any Schroeder effect we observe is related to the surface tension between the swollen gel and its environment. Since our systems are fairly small, their surface to volume ratio is strongly size-dependent; thus, if the Schroeder effect is simply caused by surface tension, we would expect it to be largest in the smaller systems. Additionally, we vary the polymer-solvent interaction strength between 1 and 2 in increments of 0.25 ϵk_B^{-1}, which changes both the driving force for swelling and the surface energy of the gel. This should also influence the swelling of the gel, although the effect will likely be more complex.

As in previous chapters, polymer chains are simulated by a Kremer-Grest bead-spring model. [19] This means non-bonded interactions within the chain are described by a truncated and shifted Lennard-Jones potential

$$U_{\mathrm{LJ,SP}}(r) = \begin{cases} 4\epsilon \left(\left(\left(\frac{\sigma}{r} \right)^{12} - \left(\frac{\sigma}{r} \right)^6 \right) - \left(\left(\frac{\sigma}{r_c} \right)^{12} - \left(\frac{\sigma}{r_c} \right)^6 \right) \right) & \text{for } r \leq r_{\mathrm{c}} \\ 0 & \text{for } r > r_{\mathrm{c}} \end{cases},$$
(6.7)

where ϵ defines the depth of the potential minimum, σ is the zero-crossing distance of the potential, r is the interparticle distance, and r_{c} is a cutoff length past which the potential is zero. Bonded interactions are described by the sum of a repulsive Weeks-Chandler-Andersen potential, which is equivalent to equation 6.7 with $r_c = 2^{1/6}$, and an attractive finitely extensible non-linearly elastic (FENE) potential

$$U_{\mathrm{FENE}}(r) = -0.5KR_0^2 \ln \left(1 - \left(\frac{r}{R_0} \right)^2 \right).$$
(6.8)

Here, K is a spring constant, and R_0 sets the maximum bond length. Following the original work of Kremer and Grest [19], we set K to 30 $\epsilon\sigma^{-2}$, R_0 to 1.5, and ϵ and σ to 1. Non-bonded interactions outside the polymer are also described by equation 6.7. For all interactions, σ is set to 1 and r_c is set to 2.5; ϵ is set to 1 for solvent-solvent and polymer-polymer interactions, and is varied between simulations for polymer-solvent interactions. All production runs use

a timestep of $0.015\,\tau$, where τ is the Lennard-Jones reduced unit of time. In the production runs, a rRESPA multiscale integrator was used to compute bonded interactions twice and non-bonded interactions once every full timestep.

Data files describing highly regular gels with tetrafunctional crosslinks are set up using a purpose-built Python code which places crosslink particles on the points of a diamond cubic lattice, and then constructs polymer chains of 30 beads between each crosslink and its nearest neighbours. The resulting structure for a single cell is illustrated in figure 6.4 This ensures that all crosslinks in the gel are equally saturated, with no large loops or dangling segments. Cubic systems with 1, 2, 3 and 4 of these diamond cubic cells to a side (totaling 1, 8, 27 and 64 cells) were set up in this way. Additional simulations were run with variations of the 2 and 3-cell system, in which all polymer segments with free chain ends had been removed.

These gel structures are first relaxed through energy minimization by the conjugate gradient method. Next, we run NVE dynamics for 100.000 timesteps of 0.005τ with a maximum particle displacement of 0.1 σ in a timestep, thermostatted to a temperature of $1\epsilon k_{\mathrm{B}}^{-1}$ by a Langevin thermostat with a damping parameter of 1000τ. The energy minimization is then repeated, and we run the same NVE dynamics again for 300.000 timesteps. At the end of this procedure, all gels were relaxed into a dense, spherical globule. This was the starting point for our production runs.
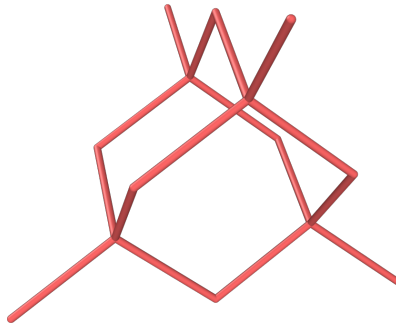

Figure 6.4: Crosslinks in our gels are connected according to a diamond cubic, a three-dimensional structure in which all points are connected to four neighbors (if tiled over the full space). This is a visualization of a single-cell gel in a fully stretched state. Note that the polymer chains are not rigid; in a dynamic simulation, this cell will collapse into a more compact and chaotic globule.

To set up the liquid-solvated systems, a fully periodic, cubic simulation box

was used. The box was scaled to have sides of $8.4 \cdot Rg_0$ in length, where Rg_0 was the radius of the polymer globule in σ after the initial relaxation. $375 \cdot Rg_0{}^3$ solvent particles were then placed into the simulation box in a cubic region of $6 \cdot Rg_0$ per side, in which a spherical cavity of $1.5 \cdot Rg_0$ in radius was left around the center of the gel. This procedure was empirically found to produce a bulk liquid phase that comes into contact with the gel, as well as a bubble of vapor, ensuring vapor-liquid coexistence.

The simulation box for vapor-solvated systems was set up as a rectangular prism with sides of $16.7 \cdot Rg_0$ in length in the x direction and sides $8.5 \cdot Rg_0$ in y and z. The box is periodic in y and z, but bounded in x by a 9-3 Lennard-Jones potential. This potential takes the form

$$E = \epsilon_{93} \left(\frac{2}{15} \left(\frac{\sigma_{93}}{r} \right)^9 - \left(\frac{\sigma_{93}}{r} \right)^3 \right) \tag{6.9}$$

up to a cutoff length r_c, and effectively simulates the presence of a smooth, dense wall of LJ particles. In this simulation, we set ϵ_{93} and σ_{93} to 1 and r_c to 2.5. On either side of the box, a region spanning $4.7 \cdot Rg_0$ away from the wall in the x-direction and covering the entire y,z plane was defined. In each of these regions, $200 \cdot Rg_0{}^3$ solvent particles were placed to create two large reservoirs of liquid. By evaporation of the liquid, a saturated vapor environment is produced during the simulations. Simulation snapshots of equilibrated simulation boxes are shown in figure 6.5.

After the simulation setup and addition of the solvent, the system is once again relaxed by energy minimization. Next, we run 500.000 timesteps of NVE dynamics with a maximum displacement of 0.1 σ per timestep again. This run is thermostatted to a temperature of 0.85 ϵk_B^{-1} by a Langevin thermostat with a damping parameter of 100 τ. During this relaxation and in the further production runs, the gel is kept centered in the simulation box by a harmonic restoring force acting on its center of mass with a spring constant of 50 $\epsilon\sigma^{-1}$. Finally, we perform 7.5 milion timesteps of production runs, in which the system is thermostatted to a temperature of 0.85 ϵk_B^{-1} by a chain of three Nosé-Hoover thermostats. This temperature was selected to allow vapor-liquid coexistence in the LJ fluid.

Results and discussion

For our primary simulations, we used the radius of gyration (mean second moment about the center of mass) of the gel as an indication of its size. We
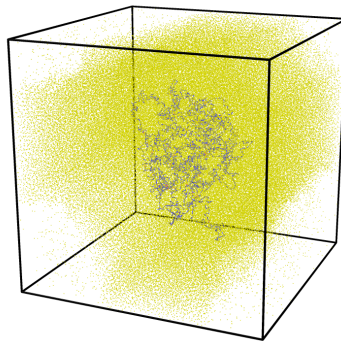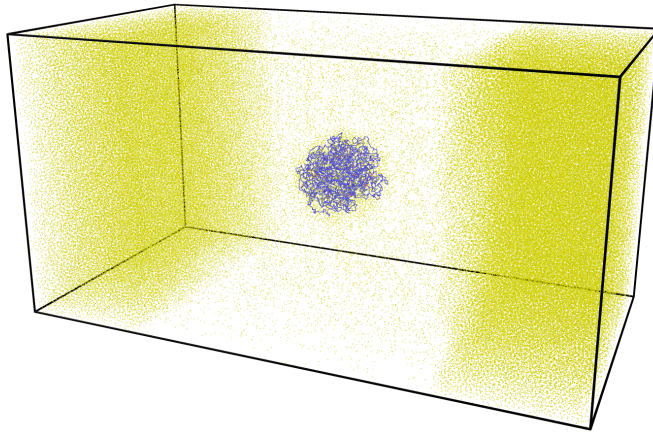
Figure 6.5: Simulation snapshots of typical vapor- and liquid-solvated systems (top and bottom respectively). Solvent particles (yellow) are represented smaller than they actually are in order to make the gel (blue) visible.
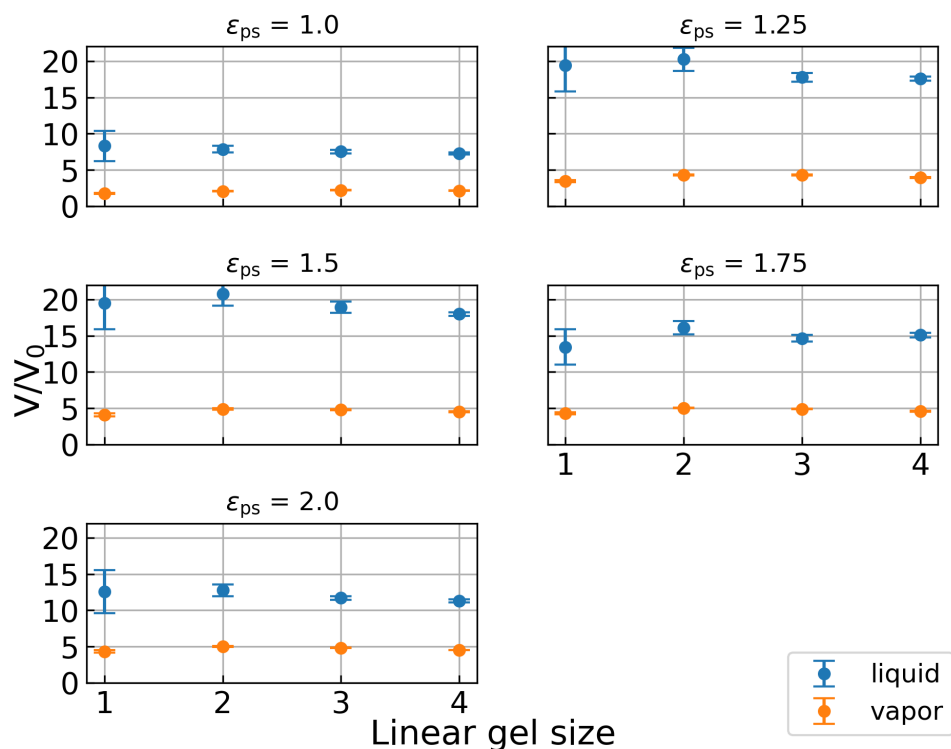
Figure 6.6: Time-averaged swelling ratios at different polymer-solvent interaction energies, plotted against gel size.

compute approximate swelling ratios of the gel as $\frac{V}{V_0} = \left(\frac{Rg}{Rg_0}\right)^3$. Output was recorded every 1000 timesteps, averaged over every 10th timestep in this period. We plot time averaged swelling ratios over the last 2.5 million timesteps of the production run against the approximate linear dimension of the gel (the number of diamond cubic cells per dimension in the initial gel setup) in figure 6.6. Error bars represent the standard deviation of the swelling ratio. We find a substantial Schroeder effect in all systems; the swelling ratio of the vapor-swollen gels ranges from around 2 for the weakest polymer-solvent interaction ($\epsilon_{ps} = 1$) to 4 or 5 for stronger interactions, whereas the swelling ratio in liquid ranges from around 8 up to 20. Moreover, we do not see the expected size dependence of the swelling ratios; the smallest vapor-swollen gels swell marginally less than larger gels, but any system of $2 \times 2 \times 2$ cells or more displays nearly the same swelling behavior. Swelling ratios in liquid also remain constant or perhaps decrease slightly as the size of the gel increases; as a
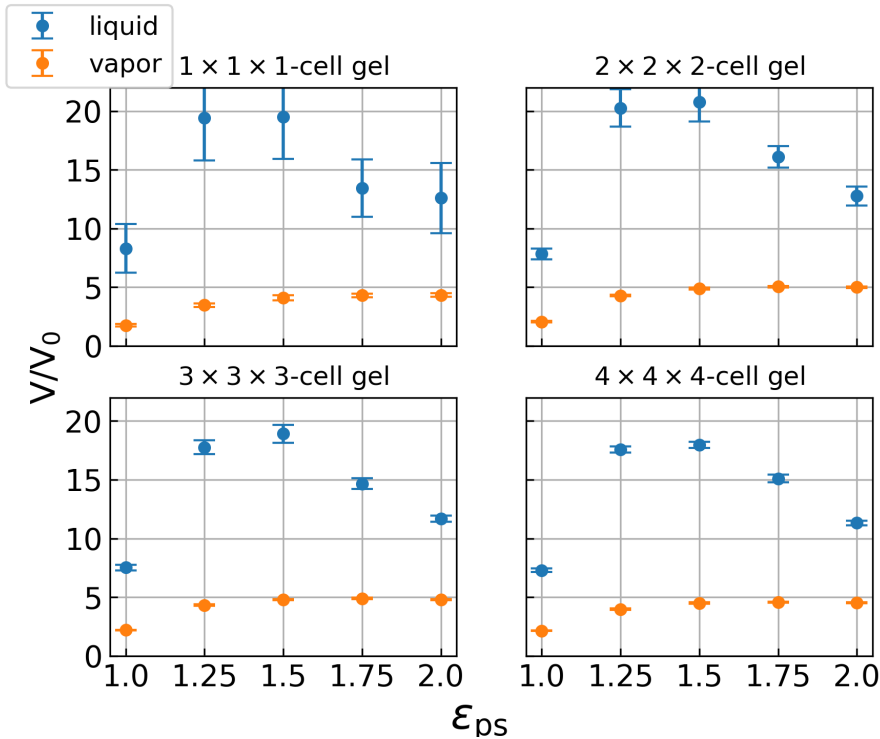
Figure 6.7: Time-averaged swelling ratios of each gel, plotted against polymer-solvent interaction energy.

result, the Schroeder effect might be slightly stronger in small systems, but the dependence is significantly weaker than expected. Visualizing the same data as a function of ϵ_{ps} in figure 6.7 shows another surprising outcome: the swelling ratio in liquid depends non-monotonically on the polymer-solvent interaction, passing through a maximum near $\epsilon_{ps} = 1.5$. No obvious explanation for this effect presents itself; while the limited extensibility of the polymer chains could explain why the swelling ratio might plateau at high ϵ_{ps}, the fact that it decreases again is not accounted for. Finally, we note that the standard deviation of the swelling ratio does strongly depend on the gel size, and is largest in the smaller gels. This is an expected result, as small systems are more susceptible to fluctuations.

Iterating on these results, we also ran simulations of $2 \times 2 \times 2$ and $3 \times 3 \times 3$-cell gels that were 'pruned' by removing all chains with free ends. The goal of this was to mitigate the effect of these free chains at the outer surface of the
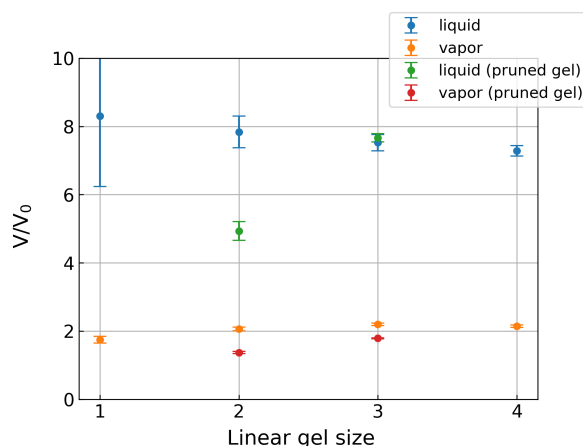
Figure 6.8: Time-averaged swelling ratios of regular and pruned gels at $\epsilon_{\mathrm{ps}} = 1.0$, plotted against gel size.

gel: in liquid, they would likely form a more extended, highly solvated outer layer, whereas in vapor they would remain in the spherical gel globule under the influence of the gel-vapor surface tension. Additionally, we output radial density profiles of polymer and solvent particles in these simulations, showing the concentration of either species as a function of distance from the gel. This may provide a more robust indication of the swelling of the gel: the radius of gyration is a good indicator of volumetric swelling as long as our gels remain approximately spherical and are roughly homogeneous in composition. While asphericity of the gel remains a concern, density profiles provide information on the distribution of solvent. These simulations were run at $\epsilon_{\mathrm{ps}} = 1.0$ in order to avoid the unexplained nonmonotonic effect of the interaction parameter.

Insofar as we can draw conclusions from these four data points, the behavior of the pruned gels falls closer to our expectations than our other results. Swelling ratios are generally lower than those in non-pruned gels, and the size dependence of the swelling ratio appears more pronounced. The large jump in swelling ratio in the liquid-solvated systems is surprising, although it is possible that relatively free loops still exist at the surface of the pruned gel. The exact conformation of such loops could influence the apparent degree of swelling in a similar way as free chain ends.

The density profiles, shown in figure 6.9, are more informative. First, the density profiles for the gels in liquid have a rather long tail. This tail is seen to a lesser degree for polymer brushes in liquid [20], and there results from

the unconstrained configurations of polymer segments near the surface. Long loops at the gel surface might cause a similar effect here.

The density profiles in vapor display a distinct peak just outside the surface of the gel. This peak indicates the presence of liquid solvent on the gel surface. Considering that the density at the peak nearly matches that of the bulk liquid solvent, this is almost certainly an adsorption layer. We also observed an adsorption layer on a polymer brush with the same interaction parameters in **chapter 3**. The presence of the adsorption layer may have a significant impact on the swelling behavior of the gel. The adsorption layer obviously alters the composition of the gel-vapor interface, and may thereby change its interfacial energy (although in the particular case $\epsilon_{ps} = 1$ this does not have any enthalpic effect). Additionally, swelling the gel while maintaining the adsorption layer requires the condensation of extra solvent proportional to the surface area created. It seems plausible that this could slow down the swelling of the gel considerably or create metastable states.
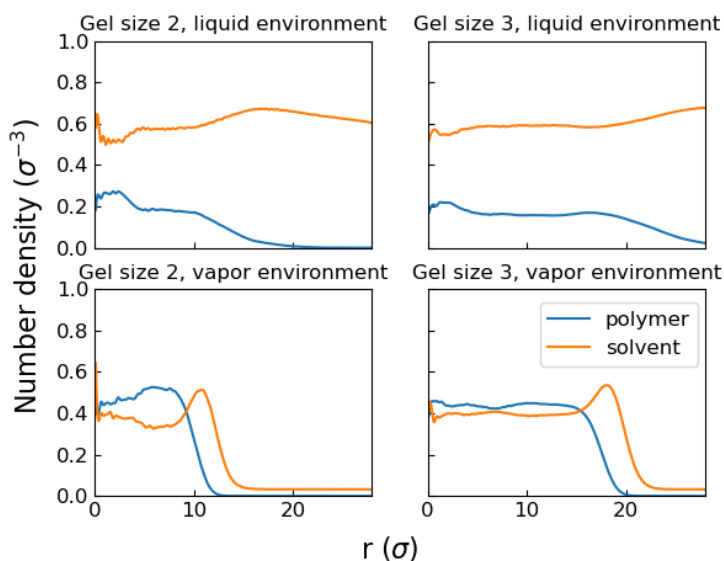

Figure 6.9: Number density of polymer and solvent particles against distance from the center of the gel.

6.5 Conclusion and recommendations

This exploration of Schroeder's paradox has been successful in identifying avenues for further research. First of all, in the course of this study, the Schroeder effect has been remarkably easy to reproduce. This may simply indicate that it is hard to maintain an exactly saturated environment in an experimental setting. Taking our results at face value, however, we have identified pHEMA/water as a new system that displays Schroeder's paradox. The pHEMA gels absorbed considerably more liquid water than saturated vapor, and readily changed their swelling state when transferred from liquid to vapor or vice versa. These observations are consistent with other reports of the effect. Combined with the fact that we did not see large fluctuations in the degree of swelling of gels left in either environment, these findings challenge thermodynamic descriptions that describe liquid and vapor swelling as multiple equilibria on a single isotherm.

The fact that we observed the paradox in the first polymer investigated suggests that it might not be a particularly rare phenomenon, and it could be productive to survey polymers with similar properties (e.g. hydrogen bond acceptors or weakly hydrophilic side groups) for a Schroeder effect as well. Varying the structure of the gel while keeping the same chemistry may also be interesting. For instance, varying the crosslink density of a material with a known Schroeder effect could provide information on the role of gel elasticity. Repeating the experiment with a controlled radical polymerization method could similarly be of interest: since the longest chains would typically contribute the most to the extensibility of the gel, changing the chain length distribution should alter its mechanical properties. This would also make the gel more homogeneous, which could prevent the formation of internal voids or water pockets that would introduce capillary effects. Along this same line, identifying a non-destructive way to image the swollen gels would provide valuable information on their internal structure, which would allow for a better description of potential internal capillary effects. Finally, the experimental results were produced with available materials. It would be good to simply reproduce the experiment with a more sophisticated setup, particularly with a vapor environment in which saturation can be better ensured and measured.

On the simulation side, we observed a Schroeder effect in a wide range of small gels in highly favorable solvent environments. While surface effects are relatively strong in such small systems and could create a difference between vapor and liquid swelling, the effects we observed largely did not follow the expected scalings for a simple surface energy effect. Early followup simulations

suggest that the apparent Schroeder effect is enlarged by free chain ends at the surface of the gel, and show a distinct adsorption layer on the surface of the vapor-swollen gel. The role of this adsorption layer is probably worth investigating in future simulations. Examining histograms of the gel radius or related quantities and computing Boltzmann weights to produce an energy landscape could identify metastabilities and confirm that our systems are truly in an steady state. Further simulations should also use systems without free chain ends to reduce noise, and use radial or spherical profiles as output to work around the inhomogeneity and possible asphericity of the gel. Monitoring stresses and pressures within the system in more detail will be both informative and methodologically important. This would help quantify the effect of surface tension, for instance. Additionally, this could help in verifying that the solvent phases in our simulations are behaving as expected; i.e. that the vapor is saturated and the liquid is not compressed. Considering that the possibility of actual non-equilibrium is an obvious pitfall in studies of the Schroeder effect, and the difficulty of explaining some of our results, the time needed to make the radial stress computation in LAMMPS work would likely be well spent. On the theoretical side, the long tail to the density profile of the liquid-swollen gels suggests that they might be too small and too solvated to consider them as a single gel phase. While this would not translate to the macroscopic, such small gels might be better considered as polymeric solutes and described by an appropriate scaling theory.

In summary, reproductions and methodological improvements would be especially important in this area of research, since the requirement of a completely saturated vapor leaves any test of the effect very susceptible to error. With this caution in mind, however, our results suggest Schroeder's paradox may be more common than previously thought, and indicate interfacial effects and the dynamics of vapor condensation as possible directions for further research.

Acknowledgements

6.6 References

[1] P. Schroeder, "Über erstarrungs- und quellungserscheinungen von gelatine", Zeitschrift für Physikalische Chemie **45U**, 117 – 75 (1903).

[2] W. D. Bancroft, "The action of water vapor on gelatine", The Journal of Physical Chemistry **16**, 395–406 (1912), URL `https://doi.org/10.1021/j150131a004`.

[3] L. K. Wolff and E. H. Büchner, "Über das von schroedersche paradoxon", Zeitschrift für Physikalische Chemie **89U**, 271–280 (1914), URL `https://doi.org/10.1515/zpch-1914-8922`.

[4] L. Chen, Y. Chen, and W.-Q. Tao, "Schroeder's paradox in proton exchange membrane fuel cells: A review", Renewable and Sustainable Energy Reviews **173**, 113050 (2023), URL `https://linkinghub.elsevier.com/retrieve/pii/S1364032122009315`.

[5] V. Freger, "Hydration of Ionomers and Schroeder's Paradox in Nafion", The Journal of Physical Chemistry B **113**, 24–36 (2009), URL `https://pubs.acs.org/doi/10.1021/jp806326a`.

[6] C. M. Gates and J. Newman, "Equilibrium and diffusion of methanol and water in a nafion 117 membrane", AIChE Journal **46**, 2076–2085 (2000), URL `https://aiche.onlinelibrary.wiley.com/doi/abs/10.1002/aic.690461018`.

[7] C. Vallieres, D. Winkelmann, D. Roizard, E. Favre, P. Scharfer, and M. Kind, "On Schroeder's paradox", Journal of Membrane Science **278**, 357–364 (2006), URL `https://www.sciencedirect.com/science/article/pii/S0376738805008276`.

[8] L. M. Onishi, J. M. Prausnitz, and J. Newman, "Water-Nafion Equilibria. Absence of Schroeder's Paradox", The Journal of Physical Chemistry B **111**, 10166–10173 (2007), URL `https://pubs.acs.org/doi/10.1021/jp073242v`.

[9] P. J. Flory and J. Rehner, John, "Statistical Mechanics of Cross-Linked Polymer Networks II. Swelling", The Journal of Chemical Physics **11**, 521–526 (1943), URL `https://doi.org/10.1063/1.1723792`.

[10] J. A. Elliott and S. J. Paddison, "Modelling of morphology and proton transport in pfsa membranes", Phys. Chem. Chem. Phys. **9**, 2602–2618 (2007), URL `http://dx.doi.org/10.1039/B701234A`.

[11] W. Y. Hsu and T. D. Gierke, "Ion transport and clustering in nafion perfluorinated membranes", Journal of Membrane Science **13**, 307–326

(1983), URL `https://www.sciencedirect.com/science/article/pii/S037673880081563X`.

[12] V. A. Davankov and A. V. Pastukhov, "Paradoxes of thermodynamics of swelling equilibria of polymers in liquids and vapors", The Journal of Physical Chemistry B **115**, 15188–15195 (2011), URL `https://doi.org/10.1021/jp208209c`, pMID: 22077346.

[13] P. Choi and R. Datta, "Sorption in proton-exchange membranes: An explanation of schroeder's paradox", Journal of The Electrochemical Society **150**, E601 (2003), URL `https://dx.doi.org/10.1149/1.1623495`.

[14] NIST Mass Spectrometry Data Center, William E. Wallace, director, *NIST Chemistry WebBook, NIST Standard Reference Database Number 69, Eds. P.J. Linstrom and W.G. Mallard*, chapter Infrared spectra (National Institute of Standards and Technology, Gaithersburg MD, 20899), retrieved January 17th 2024.

[15] E. Vargün and A. Usanmaz, "Degradation of poly(2-hydroxyethyl methacrylate) obtained by radiation in aqueous solution", Journal of Macromolecular Science, Part A **47**, 882–891 (2010), URL `https://doi.org/10.1080/10601325.2010.501304`.

[16] S. Jeck, P. Scharfer, and M. Kind, "Absence of Schroeder's paradox: Experimental evidence for water-swollen Nafion® membranes", Journal of Membrane Science **373**, 74–79 (2011), URL `https://www.sciencedirect.com/science/article/pii/S0376738811001566`.

[17] A. P. Thompson, H. M. Aktulga, R. Berger, D. S. Bolintineanu, W. M. Brown, P. S. Crozier, P. J. in 't Veld, A. Kohlmeyer, S. G. Moore, T. D. Nguyen, R. Shan, M. J. Stevens, J. Tranchida, C. Trott, and S. J. Plimpton, "LAMMPS - a flexible simulation tool for particle-based materials modeling at the atomic, meso, and continuum scales", Comp. Phys. Comm. **271**, 108171 (2022).

[18] A. Stukowski, "Visualization and analysis of atomistic simulation data with ovito-the open visualization tool", Modelling and Simulation in Materials Science and Engineering **18**, 015012 (2010).

[19] K. Kremer and G. S. Grest, "Dynamics of entangled linear polymer melts: A molecular-dynamics simulation", The Journal of Chemical Physics **92**,

6

5057 (1990), URL `http://scitation.aip.org/content/aip/journal/jcp/92/8/10.1063/1.458541`.

[20] L. Sun, B. Akgun, R. Hu, J. F. Browning, D. T. Wu, and M. D. Foster, "Scaling behavior and segment concentration profile of densely grafted polymer brushes swollen in vapor", Langmuir **32**, 5623–5628 (2016), URL `https://doi.org/10.1021/acs.langmuir.6b00845`, pMID: 27172089.

Summary

Polymer brushes are a class of coatings consisting of end-anchored polymer chains. These brushes can be synthesized by chemically bonding entire polymer chains to a surface, or by growing the chains from initiating groups on the surface. Since they are strongly bound to the surface, brush coatings contain a high concentration of polymer even when immersed in a favorable solvent. This leads to a high osmotic pressure in the brush, which produces a range of technologically interesting properties. Proposed applications for brushes include fouling-resistant layers, surfaces with low friction and adhesion, and coatings that would increase the selectivity and absorption capacity of sensors and separation processes. Additionally, polymer molecules are generally responsive to changes in their environment, and retain this property in brush form. Polymer brushes can therefore also be employed as "smart" materials, whose properties can be switched on demand or made dependent on environmental conditions. While early polymer brush research focused on brushes in liquid environments, the use of polymer brushes in air or solvent vapors has also become a topic of interest in the last decades. Experimental studies have shown that many of the interesting properties of polymer brushes in liquid also extend to brushes in solvent vapor. However, fundamental research into vapor swelling of brushes is relatively limited. In this thesis, the validity of several simple but previously untested assumptions is examined using coarse-grained molecular dynamics simulations as the primary tool.

Chapter 1 briefly introduces the concept of polymer brushes and their relevance. **Chapter 2** provides an extensive literature review and discusses the state of the art of brush-in-air research. The first half of this review covers fundamental topics. First, the origin of polymer brushes and the energetic contributions that determine their behavior are introduced. Next, we discuss the sorption isotherms and density profiles of polymer brushes in vapors, and the effect of mixed vapors or complex brush architectures on swelling behavior. For each of these topics, we provide a general overview, highlight specific cases

of interest, and identify relevant open questions. In the second half of this chapter, we discuss application-focused research on polymer brushes in four fields: sensing, separations, friction and adhesion, and wetting. Examples of the use of brushes in each of these cases are explained, and we discuss how open fundamental questions relate to these applications. In **chapter 3**, we test whether the vapor swelling of polymer brushes is appropriately described by Flory-Huggins-like theories. We use a modified Flory-Huggins model by Birshtein and Lyatskaya, which was originally developed for brushes in mixed solvents. The predictions of this model are compared to the results of coarse-grained molecular dynamics simulations of the swelling process. We find that the modified Flory-Huggins model provides an appropriate qualitative description of vapor swelling, and identify general conditions for vapor absorption and for the formation of an adsorption layer. **Chapter 4** compares the swelling behavior of brushes in vapor to that of non-anchored polymer films. Since the anchored chains in a brush need to extend to absorb solvent, theories such as the one in **chapter 3** predict a polymer brush to swell less than a non-anchored coating of the same chains under identical circumstances. This was tested experimentally by allowing polymer brushes with a hydrolyzable anchoring group to de-graft in a humid environment, producing non-anchored films with the exact same chain length distribution as the polymer brushes. The swelling of these brushes and films was then measured by ellipsometry in a humidity-controlled environment. Additionally, coarse-grained molecular dynamics simulations of brushes and free films were performed. Both the experiments and the simulations support the prediction that brushes display reduced swelling compared to free polymer films. In **chapter 5**, we investigate the vapor swelling of polymer brushes that contain two poorly miscible polymer species in various chain architectures. As expected, we find that swelling increases with the number of unfavorable polymer-polymer contacts. Interestingly, the swelling enhancement in the mixed brush is largest at low vapor concentrations, making mixed polymer brushes potentially interesting for sensing applications. Finally, **chapter 6** presents exploratory research into Schroeder's paradox, a discrepancy between the swelling of gels by a saturated vapor and the corresponding liquid that has not been conclusively explained. Experimentally, we find that macroscopic samples of chemically crosslinked poly(hydroxyethyl methacrylate) produced by free radical polymerization do indeed display this discrepancy. Additionally, these samples change their degree of swelling acccordingly when moved from the liquid to the saturated vapor or vice versa. We also reproduce the effect in a (microscopic) simu-

lated system, in the absence of chemical details. These results suggest that Schroeder's paradox may be a more common phenomenon than previously thought, and allow us to exclude a hypothesis based on a Van der Waals loop in the swelling isotherm.

Samenvatting

Polymeerborstels zijn een type coatings die bestaan uit polymeerketens, waarvan het uiteinde aan een oppervlak geankerd is. Deze borstels kunnen worden gesynthetiseerd door volledige polymeerketens chemisch aan het oppervlak te binden, of door de ketens vanaf initiatorgroepen aan het oppervlak te laten groeien. Doordat ze sterk aan het oppervlak gebonden zijn bevatten borstel-coatings een hoge concentratie aan polymeren, zelfs wanneer ze ondergedompeld zijn in een gunstig solvent. Dit leidt tot een hoge osmotische druk, die de polymeerborstels een aantal technologisch interessante eigenschappen verleent. Beoogde toepassingen van borstel-coatings omvatten bijvoorbeeld vuilafstotende lagen, oppervlakken met lage wrijving en adhesie, en coatings die de selectiviteit en opnamecapaciteit van sensoren en scheidingsprocessen zouden kunnen verbeteren. Bovendien reageren polymeermoleculen in het algemeen sterk in veranderingen in hun omgeving, en dat geldt ook voor polymeerborstels. Hierdoor kunnen polymeerborstels ook worden ingezet als "slimme" materialen, waarvan de eigenschappen op commando of afhankelijk van de omgeving kunnen veranderen.

Hoewel de nadruk in vroeg onderzoek naar polymeerborstels lag op vloeibare omgevingen, is het gebruik van polymeerborstels in gassen en dampen in de laatste decennia ook een actief onderzoeksveld geworden. Experimenten hebben uitgewezen dat veel van de nuttige eigenschappen van polymeerborstels in vloeistof ook aanwezig zijn in borstels in solventdampen. Er is echter betrekkelijk weinig fundamenteel onderzoek naar het zwellen van polymeerborstels door dampen gedaan. In dit proefschrift wordt de geldigheid van een aantal simpele maar tot dusver ongetoetste aannames onderzocht, met *molecular dynamics* simulaties als primaire methode.

Hoofdstuk 1 leidt het concept en de relevantie van polymeerborstels kort in. **Hoofdstuk 2** biedt een uitgebreid literatuuroverzicht en bespreekt de stand van zaken in het onderzoek naar borstels in lucht. De eerste helft van dit overzicht gaat over fundamentele onderwerpen. Allereerst worden de

oorsprong van polymeerborstels en de energetische bijdragen die hun unieke gedrag bepalen geintroduceerd. Hierna bespreken we de sorptie-isothermen en dichtheidsprofielen van polymeerborstels in dampen, en het effect van gemengde dampen en complexe borstel-architecturen op het zwellingsgedrag van de borstel. Voor elk van deze onderwerpen geven we een algemeen overzicht, lichten we specifieke interessante gevallen uit, en wijzen we op belangrijke open vragen. De tweede helft van dit hoofdstuk gaat over toepassingsgericht onderzoek naar polymeerborstels in vier velden: sensoren, scheidingsprocessen, wrijving en adhesie, en het controleren van *wetting* (het gedrag van druppels en vloeistoflagen op een oppervlak). We lichten voorbeelden van het gebruik van polymeerborstels in deze toepassingen toe, en bespreken hoe openstaande fundamentele vragen samenhangen met deze toepassingen. In **hoofdstuk 3** wordt onderzocht of het opzwellen van polymeerborstels door dampen afdoende wordt beschreven door een Flory-Huggins-achtige theorie. We gebruiken een aangepast Flory-Huggins-model, dat oorspronkelijk door Birshtein and Lyatskaya is ontwikkeld voor polymeerborstels in gemengde solventen. De voorspellingen van dit model worden vergeleken met de resultaten van *coarse-grained molecular dynamics*-simulaties van het zwellingsproces. We concluderen dat het aangepaste Flory-Huggins-model een adequate kwalitatieve beschrijving van de damp-opname geeft, en stellen vereisten voor damp-opname en het vormen van een adsorptielaag vast. In **hoofdstuk 4** vergelijken we het opzwellen van borstels in dampen met het gedrag van ongeankerde polymeerlagen. Omdat de geankerde polymeerketens in een borstel zich moeten uitstrekken om solvent op te nemen, voorspellen theorieën zoals die in **hoofdstuk 3** dat een polymeerborstel minder op zal zwellen dan een ongeankerde coating van dezelfde ketens onder gelijke omstandigheden. Dit wordt experimenteel getest door polymeerborstels met een hydrolyzeerbare ankergroep in een vochtige omgeving los te laten komen van het oppervlak, waardoor we ongeankerde lagen met exact dezelfde ketenlengteverdeling als onze polymeerborstels verkrijgen. Het opzwellen van deze borstels en lagen is gemeten door middel van ellipsometrie in een omgeving met gecontroleerde luchtvochtigheid. Hiernaast zijn *molecular dynamics*-simulaties van borstels en vrije polymeerlagen gedaan. Zowel de experimenten als de simulaties ondersteunen de voorspelling dat polymeerborstels minder opzwellen dan vrije polymeerlagen. In **hoofdstuk 5**, onderzoeken we het opzwellen van polymeerborstels die twee slecht mengbare polymeersoorten in verschillende ketenstructuren bevatten. Zoals verwacht concluderen we dat de zwelling van de borstel toeneemt met het aantal ongunstige polymeer-polymeer contacten. Opmerkelijk genoeg is deze

toename het grootst bij lage dampconcentraties, waardoor deze gemengde borstels van belang zouden kunnen zijn voor sensortoepassingen. Tot slot beschrijft **hoofdstuk 6** een verkennend onderzoek naar de paradox van Schroeder, een tot op heden onverklaard verschil tussen het opzwellen van gels in verzadigde dampen en in de bijbehorende vloeistof. Experimenteel blijkt dat macroscopische monsters van chemisch gecrosslinkt poly(hydroxyethylmethacrylaat) uit vrije radicaalpolymerizatie dit verschil inderdaad vertonen. Daarnaast verandert de mate van opzwellen wanneer deze gels van de vloeistof naar de verzadigde damp of vice versa verplaatst worden. Dit effect lijkt reproduceerbaar in een (microscopisch) gesimuleerd systeem, vrij van chemische details. Deze resultaten suggereren dat de paradox van Schroeder wellicht algemener is dan tot dusver gedacht werd, en dat dit effect waarschijnlijk niet veroorzaakt wordt door een Van der Waals-lus in de absorptie-isotherm.

Acknowledgements

This thesis is the culmination of four years of research. Here, at the end of it, I want to thank all the people who contributed to this work, and accompanied me on this academic journey.

First of all, I am grateful to my promotors Sissi and Jacco. Sissi: I first walked into your office eight years ago when I was in search of a bachelor thesis assignment. Your enthusiasm for polymer physics turned out to be infectious, and I have enjoyed working with you for my bachelor, master and now my doctoral thesis. Over the course of the project, you have granted me a lot of freedom, but provided support and guidance when it was needed. Your patience and respect for your students has made for a great working environment, and I feel that I have learned a lot from you both in terms of research and of general outlook. Where Sissi was an energizing influence, Jacco helped keep things on track with the occasional reality check. Jacco, I have appreciated your helpful and interested supervision, and the different physical perspectives you contributed.

Next, I want to thank my paranymphs and friends Lars and Koen. We started our Ph.D. research around the same time, and shared a lot of coffee breaks over the last four years. Celebrating, complaining and philosophizing together has been a great enrichment, and you two have made this whole journey a lot more enjoyable. Lars has also been one of my closest collaborators and my constant office neighbor. Thank you for all the sparring, brainstorming and the LAMMPS "problem" assessment forms.

The Functional Polymer Surfaces group, also known as Team Sissi, also has my thanks. The group meetings have always been enjoyable, constructive and productive, and every one of you has contributed to that. The extracurricular activities such as ice skating, pub quizzes, dinners and spicy food tastings were also great fun. While my thanks extend to all the current and former team members and students, I particularly want to highlight Maria, Sander, Esli, Leon, Erik, Paloma and Andriy here. My Ph.D. would not have been the same

Scientific output

Publications

- **2023:**

  Hybrid Ceramic Nanofiltration Membranes Prepared by Impregnation and Solid-State Grafting of Organophosphonic Acids
  Nikos Kyriakou, Elmar Boorsma, Gert-Jan Aardema, **Guido C. Ritsema van Eck**, Martin Drobek, Sissi de Beer, Arian Nijmeijer, Louis Winnubst, Marie-Alix Pizzoccaro-Zillamy
  Journal of Membrane Science 687 (2023), 122041

- **2022:**

  Vapor Swelling of Polymer Brushes Compared to Nongrafted Films
  Guido C. Ritsema van Eck, Ellen M. Kiens, Lars B. Veldscholte, Maria Brió Pérez, Sissi de Beer
  Langmuir 2022, 38, 45, 13763-13770

  Enhanced Vapor Sorption in Block and Random Copolymer Brushes
  Ivona Glišić, **Guido C. Ritsema van Eck**, Leon A. Smook, Sissi de Beer
  Soft Matter, 2022, 18, 8398-8405

  Fundamentals and Applications of Polymer Brushes in Air
  Guido C. Ritsema van Eck, Leonardo Chiappisi, Sissi de Beer
  ACS Appl. Polym. Mater. 2022, 4, 5, 3062-3087

- **2021:**

  Vapor Sorption in Binary Polymer Brushes
  Leon A. Smook, **Guido C. Ritsema van Eck**, Sissi de Beer
  J. Chem. Phys. 155, 054904 (2021)

- **2021 (continued):**
  Concentrating Vapor Traces with Binary Brushes of Immiscible Polymers
  Leon A. Smook, **Guido C. Ritsema van Eck**, Sissi de Beer
  ACS Appl. Polym. Mater. 2021, 3, 2336-2340

- **2020:**
  Friends, Foes, and Favorites: Relative Interactions Determine How Polymer Brushes Absorb Vapors of Binary Solvents
  Leon A. Smook, **Guido C. Ritsema van Eck**, Sissi de Beer
  Macromolecules 2020, 53, 10898-10906

  Sorption Characteristics of Polymer Brushes in Equilibrium with Solvent Vapors
  Guido C. Ritsema van Eck, Lars B. Veldscholte, Sissi de Beer
  Macromolecules 2020, 53, 8428-8437

- **2019:**
  Polymer Brush Friction in Cylindrical Geometries
  Karel J. van der Weg, **Guido C. Ritsema van Eck**, Sissi de Beer
  Lubricants, 7, 84